Untersuchungen zu Struktur-Aktivitätsbeziehungen und zum Wirkmechanismus der Melleolid-Antibiotika

Dissertation

zur Erlangung des akademischen Grades

„doctor rerum naturalium“ (Dr. rer. nat.)

vorgelegt dem Rat der Fakultät für Biowissenschaften
der Friedrich-Schiller-Universität Jena

von Dipl.-Pharm. Maximilian Dörfer,

geboren am 15.09.1989
in Gera

Tag der Einreichung: 12.12.2019

Gutachter: Prof. Dr. Dirk Hoffmeister
Friedrich-Schiller-Universität, Jena

Prof. Dr. Oliver Werz
Friedrich-Schiller-Universität, Jena

Prof. Dr. Gabriele M. König
Rheinische Friedrich-Wilhelms-Universität, Bonn

Tag der Disputation: 15.07.2020

FÜR MEINE FAMILIE

Inhaltsverzeichnis

1. Einleitung

1.1. Die Gattung *Armillaria*

Die Basidiomyceten (Ständerpilze) sind mit ca. 30000 Arten die größte Klasse der Pilze. Ihr Hauptmerkmal ist ein Sporenständer (Basidiophor), welcher die Basidiosporen beherbergt. Die Basidiomyceten-Gattung *Armillaria,* zu der auch der honiggelbe Hallimasch (*Armillaria mellea*) gehört, zählt weltweit ca. 40 Arten in fast allen Klimazonen, vom Regenwald bis hin zum borealen Nadelwald (Baumgartner et al., 2011; Hood, 1991; Shaw und Kile, 1991).

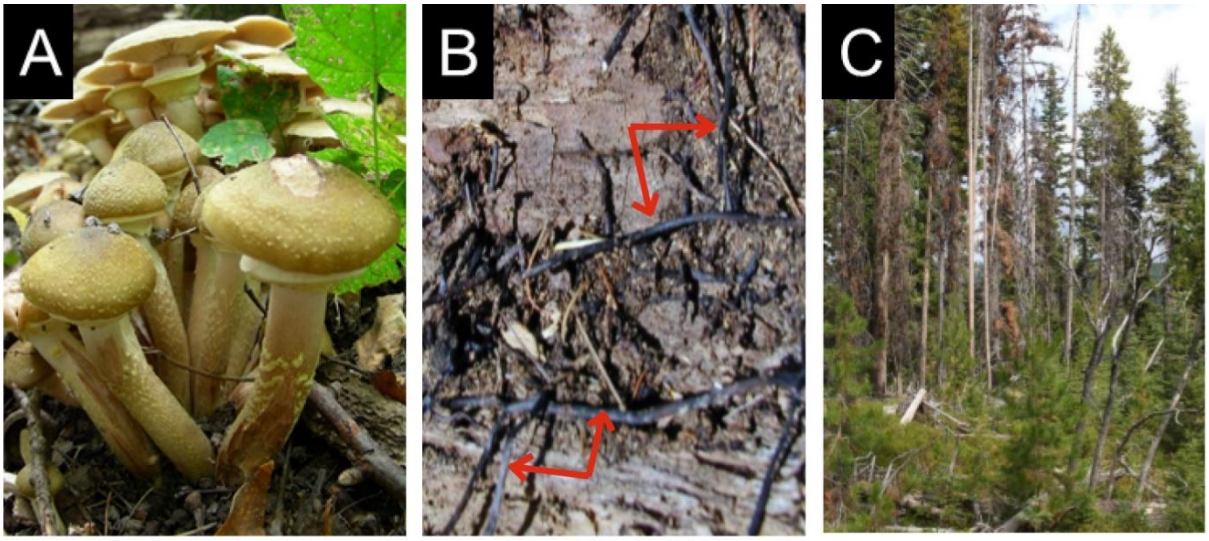

Abbildung 1. *A* Fruchtkörper von *A. mellea*. (Dirk Hoffmeister Big Woods State Park, Nerstrand, Minnesota) **B Rhizomorphe von *A. mellea*.** (Schmitt und Tatum, 2008) **C von *A. mellea* infiziertes Waldareal.** (Schmitt und Tatum, 2008)

Bereits im späten 19. Jahrhundert war *A. mellea* als Pflanzenpathogen bekannt (Smith, 1894). Heute sind Vertreter der Gattung *Armillaria* nicht nur als ökologisch wertvolle Saprophyten, sondern auch parasitische Besiedler von über 500 verschiedenen Nadel- und Obstgehölzen bekannt (Raabe, 1962; Williams und Wargo, 1989). Der Hallimasch zählt in unseren Breiten neben dem Borkenkäfer zu den prominentesten Forstschädlingen (Petercord et al., 2009).

Doch was macht die Gattung *Armillaria* so erfolgreich in seiner Ausbreitung?
Zunächst ermöglichen Rhizomorphen (siehe Abbildung 1 B), eine mit pflanzlichen Wurzeln vergleichbare morphologische Differenzierungsform des Myzels, die Erschließung neuer Lebensräume (Lamour et al., 2007). Die 1 - 3 mm dicken Gebilde sind in der äußeren Schicht stark melanisiert und somit gut vor äußeren Einflüssen wie oxidativen Effekten oder UV-Strahlung geschützt (Ribera et al., 2019). Die Rhizomorphen eigen sich somit bestens für den Transport von Wasser oder Nährstoffen über weite Strecken (Boddy et al., 2009), dienen aber auch als Überdauerungsorgan und zur Erschließung neuer Lebensräume.
Das größte Lebewesen der Welt, ein Vertreter der *Armillaria ostoyae*, besiedelt im US-Bundesstaat Oregon aktuell eine Fläche von ca. 9,6 km² über ein dicht verzweigtes Netzwerk

aus Rhizomorphen und Mycel (Schmitt und Tatum, 2008). Mit einem Alter von 1900 bis zu 8650 Jahren ist es eines der ältesten Lebewesen auf unserem Planeten (Ferguson et al., 2003). Ein weiterer, ca. 2500 Jahre alter Vertreter, *Armillaria gallica,* besiedelt in Michigan eine Fläche von 3,7 km². Das Genom beider Organismen ist trotz des hohen Alters sehr robust und unterlag nur wenigen Veränderungen (Anderson et al., 2018). *Armillaria* scheint in seiner genetischen Entwicklung gegenüber äußeren Einflüssen also sehr resistent zu sein.

Sein Überleben sichert der Hallimasch aber auch durch seine hohe morphologische Variabilität, welche er sowohl in freier Natur als auch in Kultur innehat:
Basidiomyceten sind in ihrer vegetativen Phase normalerweise dikaryotisch. Einige *Armillarien* können hier jedoch diploid sein. Die meiotischen Basidiosporen der Fruchtkörper keimen zu haploidem, monokaryotischem Myzel aus (Korhonen und Hintikka, 1974). Kompatible Partner können sich kreuzen und kurzzeitig dikaryotische Zellen bilden. Deren Kerne verschmelzen nach kurzer Zeit zu diploidem Sekundärmyzel, welches monokaryotisch ist (Korhonen, 1978).

Unter Laborbedingungen lässt sich diploides und haploides Myzel züchten. Auf festem Medium bilden die stark pigmentierten, haploiden Stämme Rhizomorphen, diploide Stämme sind meist frei von Pigmenten, somit schneeweiß (Hintikka, 1973) und bilden deutlich weniger Rhizomorphen aus.

Neben den morphologischen und reproduktiven Besonderheiten, besitzen Armillarien ein breites Arsenal an bioaktiven Sekundärstoffen. Zu besonderer Bedeutung gelangten neben den ebenfalls bioaktiven Emestrinen und Cephalosporoliden (Herath et al., 2013) vor allem die Melleolide. Es wird vermutet, dass der Pilz diese hochdiverse Stoffgruppe zur Kommunikation mit anderen Organismen bzw. als Selektionsvorteil zur chemischen Abwehr verwendet, (Peipp und Sonnenbichler, 1992). Die genauen Wirkmechanismen sind jedoch noch unbekannt, genauso, wie der Umgang mit reaktiven Sauerstoff-Spezies (ROS). Die ROS könnten vom Pilz sekretiert werden, um aromatische Polymere wie Lignin in Hölzern zu zersetzen, oder aber gegen Nahrungskonkurrenten eingesetzt werden (Collins et al., 2017).

Versuche, Schäden durch *Armillarien* in Nutzwäldern und Obstplantagen mit Hilfe natürlicher Antagonisten zu begrenzen, scheiterten bisher. Mit *Trichoderma* spec. wie *T. asperellum*, *T. gamsii* oder *T. harzianum* hoffte man, eine biologische Kontrolle gegen die durch *Armillarien* verursachte Stumpf- und Wurzelfäule gefunden zu haben, da diese zu den Ascomyceten zählenden, filamentösen Pilze eine Resistenz gegen *Armillarien* zeigen (Schnabel et al., 2011; Tarus et al., 2003). Der Schädling ist dennoch häufig so potent, dass es seiner Abschwächung bedarf, bevor der biologische Antagonist wirksam werden kann (Ohr und Munnecke, 1974; Ohr et al., 1973).

Vermutlich um sich selbst vor ROS zu schützen, sind viele *Armillarien* zur Biolumineszenz befähigt (Mogil'naya et al., 2015). Hierbei wird zunächst ein Luciferin-Precursor durch NAD(P)H-abhängige Enzyme in Luciferin überführt und dieses katalytisch durch eine Luciferase unter Verwendung von Sauerstoff oxidiert (Purtov et al., 2015). Dabei wird grünes Licht (520 – 530 nm) emittiert. Die Luciferin-Synthese ist in den Fruchtkörpern blockiert. Sie produzieren keine ROS, vor denen sie sich schützen müssten, können somit auch kein Holz zersetzen (Purtov et al., 2017). Die eukaryotische Biolumineszenz in Pilzen auf genetischer Ebene wurde erst vor kurzem eingehend untersucht und beschrieben (Kotlobay et al., 2018).

Die Fruchtkörper (siehe Abbildung 1 A) sind nicht nur unfähig zur Lumineszenz, sie produzieren auch (fast) keine Melleolide. Das macht den Hallimasch zu einem potenziellen Speisepilz für all jene, die nach dem Genuss gründlich gekochter, junger Fruchtkörper keine Unverträglichkeitsreaktionen zeigen. In der traditionellen chinesischen Medizin (TCM) werden vor allem *A. mellea* verschiedenste Heilwirkungen u. a. gegen Lähmung, Schwindel, Bluthochdruck, Kopfschmerzen und Schlaflosigkeit zugeschrieben. Zusammen mit dem parasitischen Wirt *Gastrodia elata* ist *A. mellea* in der TCM auch als „Tianma" mit vergleichbaren Wirkungen bekannt (Chen et al., 2016). Wissenschaftlich erforscht werden zurzeit die antitumoralen Wirkungen der beiden Tianma-Bestandteile (Chang et al., 2016; Chen et al., 2016; Heo et al., 2007).

1.2. Chemische Vielfalt und metabolische Diversität von Naturstoffen

Die Natur hat eine Vielzahl komplexer Verbindungen hervorgebracht, welche noch heute nur mit unverhältnismäßigem Aufwand in Vollsynthesen nachzubilden sind. Dies betrifft vor allem sogenannte Sekundärmetaboliten, welche im Gegensatz zu Primärmetaboliten wie Kohlenhydraten, Lipiden und Aminosäuren nicht lebensnotwendig sind, aber häufig zu einem Selektionsvorteil für Organismen einer Gruppe oder sogar Art führen.
Der Mensch hat gelernt, sich die Wirkungen einiger Sekundärstoffe, wie Erythromycin, Vinblastin oder Paclitaxel (Abbildung 2) pharmazeutisch zu erschließen und diese medizinisch als Wirkstoff zu nutzen.

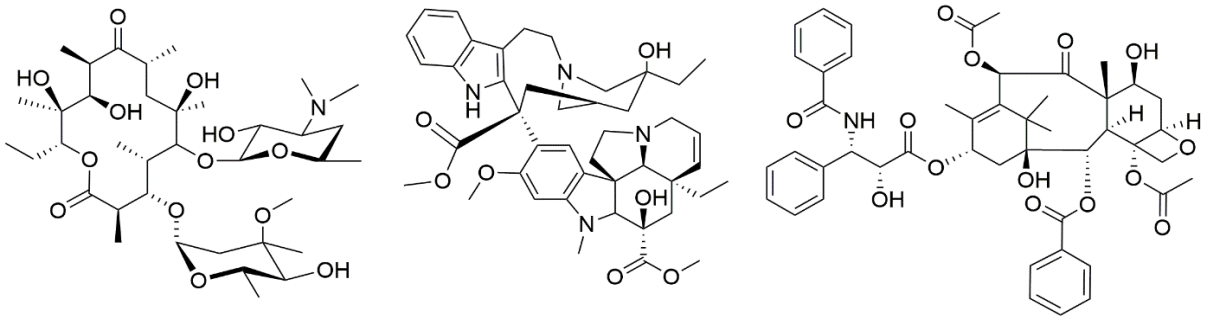

Erythromycin A
Saccharopolyspora erythraea

Vinblastin
Catharanthus roseus

Paclitaxel
Taxus brevifolia

Abbildung 2. Ausgewählte Naturstoffe aus Bakterien und Pflanzen

Das 1949 entdeckte Makrolidantibiotikum Erythromycin wurde erstmals 1981 in einer 50-stufigen Vollsynthese hergestellt. Zeit- und Kostenaufwand der Synthese rechtfertigten keine großtechnischen Gewinnung (Woodward et al., 1981). Noch heute wird das biosynthetisch auf einem Polyketid basierende Antibiotikum biotechnologisch durch den Actinomyceten *Saccharopolyspora erythraea* (ehemals *Streptomyces erythreus*) in großen Fermentern produziert (Hamedi et al., 2005; Martin und Bushell, 1996).

Das Chemotherapeutikum Vinblastin (Abbildung 2) wurde ursprünglich im Madagaskar-Immergrün (*Catharanthus roseus)* entdeckt. Biosynthetisch entsteht das terpenoide Alkaloid durch die Dimerisierung der Vorläufermoleküle Tabersonin und Catharanthin (Caputi et al., 2018), welche ihren Ursprung in Stemmadeninacetat, bestehend aus Tryptamin (Shikimat-Weg) und Secologanin (Terpen) haben (Zhu et al., 2015). Bisher wird Vinblastin ausschließlich aus der Pflanze isoliert (Heijden et al., 2004). Der Verbrauch von 15 t der Pflanze zur Isolation von 28,35 g (Meyers, 2007), spiegelt sich auch im Preis von ca. 2 Mio $ pro kg (Alam und Sharaf-Eldin, 2016). Die erste, 17-stufige Totalsynthese ist auch hier ein wichtiger Schritt für die zukünftige Bedarfssicherung des antitumoralen Wirkstoffes (Kuehne et al., 1991), welcher die Mikrotubuli-Polymerisierung durch kovalentes Binden an Tubulin hemmt (Wilson et al., 1975).

Das 1971 entdeckte Zytostatikum Paclitaxel (Taxol) (Abbildung 2) aus der pazifischen Eibe (*Taxus brevifolia*) hemmt ebenfalls die Mikrotubuli-Polymerisierung und so die Zellteilung (Schiff et al., 1979; Wani et al., 1971). Gewann man zunächst aus 1 kg Rinde nur 138 mg Paclitaxel, wurde mit der halbsynthetischen Herstellung aus der natürlichen Vorstufe Baccatin III eine Produktion von 1 g Taxol aus 1 kg Nadeln möglich (Denis et al., 1988). Mit den Totalsynthesen, welche Mitte der 1990er Jahre erarbeitet wurden, konnte der Bedarf ebenfalls nicht gedeckt werden, da diese zu komplex und unwirtschaftlich sind (Bartsch, 2004; Holton et al., 1994; Nicolaou und Guy, 1994). Bis heute ist die 2002 zugelassene „Plant Cell Fermentation“ (PCF) die ausschließliche Methode zur Deckung des Weltbedarfs. Hier werden Pflanzenzellen in Suspension über 8 Monate kultiviert (Bartsch, 2004). Final lassen sich laut Hersteller (Phyton Biotech, Ahrensburg, Deutschland) bis zu 1000 kg pro 200.000 L Charge herstellen (≙ 5 g/L).

Die Beispiele belegen, wie gut der Mensch Naturstoffe erforscht hat und sich diese zu Nutze macht. Im Laufe der Zeit entdeckte man, dass die Biosynthese von Naturstoffen gegenüber einer Totalsynthese wirtschaftlich sinnvoll ist, da sie Zeit und Geld spart. Doch wie genau entsteht diese Diversität und warum sind viele Naturstoffe so schwer durch den Menschen reproduzierbar? Diese Fragen sollen im folgenden Abschnitt am Beispiel pilzlicher Naturstoffe geklärt werden.

1.3. Naturstoffe aus Pilzen

Während der Großteil der Pflanzen (ca. 80%) mittlerweile als bekannt gilt, wurden nur ca. 5% der geschätzt 1,5 Mio Pilz-Arten identifiziert (Hawksworth, 2001). Das Reich der Pilze verspricht also einen reichen Fundus an neuen Sekundärstoffen. Vor allem pilzliche Sekundärstoffe sind hier von großer Bedeutung für die Pharmazie. Die Sekundärstoffe lassen sich in Abhängigkeit von ihrem Biosyntheseweg grob in drei Gruppen einteilen: Aminosäure-abgeleitete Stoffe, Polyketide und Terpene. Auf die Synthese der Polyketide und Terpene wird aufgrund ihrer Bedeutung für diese Arbeit nachfolgend detaillierter eingegangen.

1.3.1. Naturstoffe aus Aminosäure-abgeleiteten Bausteinen

Zunächst soll nicht unerwähnt bleiben, dass Bakterien und Pilze bei der Synthese von kleineren Peptiden aus Aminosäuren eine Besonderheit aufweisen. Sie besitzen nichtribosomale Peptidsynthetasen (NRPS). Bei NRPS handelt es sich um große Enzymkomplexe aus verschiedenen Domänen. Sie dienen als Matrize und legen somit die Aminosäuresequenz, sowie Modifizierungen am fertigen Peptid fest. Im Vergleich zu ribosomalen Proteinen mit Kettenlängen von teilweise mehr als 10.000 Aminosäuren ist die Länge der NRPS-Produkte im Schnitt auf 2-15 Aminosäurereste begrenzt (Mootz und Marahiel, 1999). NRPSen produzieren Peptide unabhängig von den Ribosomen. Als Substrat für NRPSen, sowie NRPS-ähnliche Enzyme dienen Aminosäuren. Im Gegensatz zur RNA-abhängigen, ribosomalen Peptidsynthese, können NRPS und NRPS-artige neben den 20 proteinogenen L- Aminosäuren weitere Substrate wie D- Amino-, α-Keto-, α-Hydroxy- oder andere nicht proteinogene Aminosäuren miteinander verknüpfen und sogar Fettsäuren als Startereinheiten nutzen (Marahiel, 2016; Marahiel et al., 1997). Dies führt zu einzigartigen pharmazeutischen Leitstrukturen wie den Penicillinen oder Ciclosporinen und zeigt die diversitätsorientierte Strategie der Naturstoffbildung auf.

1.3.2. Polyketide

Die Polyketide sind eine Gruppe oft stark mit Sauerstoff angereicherter Substanzen. Ihre Bildung erfolgt ähnlich der Fettsäuresynthasen an großen Enzymkomplexen, den Polyketid-synthasen (PKS). Man unterscheidet hierbei zwischen nicht-reduzierenden PKS (NR-PKS), den stark (highly)-reduzierenden (HR)-PKS und den teilweise (partially)-reduzierenden (PR)-PKS. Der Aufbau der Polyketide erfolgt aus thioesteraktivierten Carbonsäurebausteinen wie Acetyl-CoA oder Malonyl-CoA. Durch die schrittweise Verbindung von Acyl-CoA-Bausteinen durch eine KS-Domänen-vermittelte Claisen-Kondensation (C-C-Bindung) wird das Produkt verlängert (Staunton und Weissman, 2001).

Eine minimal-PKS besteht aus den drei Domänen Ketoacylsynthase- (KS), Acyltransferase-(AT) und einer Acyl Carrier Protein-Domäne (ACP). Je nach Modul können reduzierende

Domänen wie Dehydratasen (DH), Enoyl-Reduktasen (ER) oder Ketoreduktasen (KR) vorhanden sein (Abbildung 3). Bei NR-PKS fehlen diese reduzierenden Domänen.

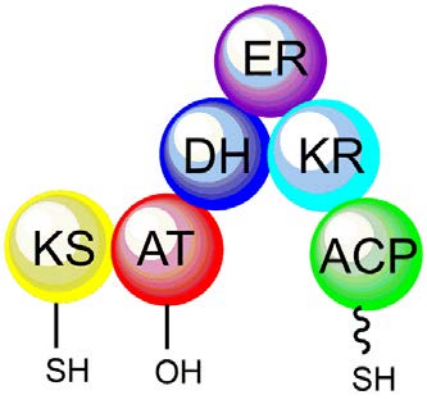

Abbildung 3 Vereinfachte Darstellung eines PKS-Moduls. Das Modul enthält eine Ketosynthase (KS), eine Acyltransferase (AT), ein Acyl Carrier Protein (ACP), an welchem ein Phosphopantetheinylat-Rest (Ppant) gebunden ist, sowie optional eine Dehydratase (DH), eine Enoylreduktase (ER) und eine Ketoreduktase (KR).

Die modifizierenden Domänen (DH, ER, KR) reduzieren β-Ketoeinheiten zu β-Hydroxy-einheiten (KR), dehydrieren diese zu konjugierten Alkenen (DH) und können diese final absättigen (ER). Durch diese partiell reduktiven Veränderungen entsteht im Vergleich zur Fettsäuresynthese eine hohe Diversität an PKS-Produkten (Hertweck, 2009). Bei der Synthese von Fettsäuren erfolgt immer eine komplette Reduktion bei jedem Verlängerungsschritt. Bei PKS erfolgt diese nur graduell und in jedem Schritt unterschiedlich stark. Die Abspaltung der fertigen Produkte erfolgt meist über eine Thioesterasedomäne (TE). Die Länge der PKS-Produkte wird bei pilzlichen NR-PKS durch die Produkttemplate (PT)-Domäne bestimmt, welche über ihre Hot-Dog-Struktur nicht nur die Anzahl der Kondensationszyklen bestimmt, sondern auch die Art der Zyklisierungsreaktion des finalen aromatischen Systems (Crawford et al., 2009).

Pilzliche PKS-Synthasen sind meistens vom Typ I und arbeiten iterativ, d. h. eine KS-Domäne katalysiert mehr als einen Elongationszyklus. Die modifizierenden Domänen können in jeder Runde, in welcher das Produkt verlängert wird, am β-Keto-Kohlenstoff eingreifen und die Moleküldiversität beeinflussen (Hertweck, 2009). Es gibt aber auch nicht-iterative Typ I-Synthasen, welche vor allem in Bakterien vorkommen. Diese synthetisieren beispielsweise Makrolid-Antibiotika wie Erythromycin (Abbildung 2). Typ II PKS findet man ausschließlich in Bakterien. Hier wird ausschließlich Malonyl-CoA zur Kettenverlängerung durch einen Satz iterativ arbeitender Enzymuntereinheiten benutzt (Hertweck et al., 2007). Typ III-Synthasen, hauptsächlich in Pflanzen und teilweise in Bakterien und selten in Pilzen vorkommend, verwenden Acyl-CoA unabhängig von einer ACP-Domäne (Hertweck, 2009). Heute weiß man, dass PKS je nach genetischer Ausstattung ebenfalls in der Lage sind, verschiedenste Carboxyl-Startereinheiten wie Fettsäuren oder Arylsäuren zu verarbeiten und somit die Diversität dieser Stoffklasse zu erhöhen (Ray und Moore, 2016).

Eine der aufgrund des pharmazeutischen Interesses am besten erforschten pilzlichen PKS ist die nicht-reduzierende Lovastatin-Nonaketidsynthase (LNKS, LovA). Lovastatin (Abbildung 4), ist ein Hemmstoff der 3-Hydroxy-3-methylglutaryl-CoA (HMG-CoA)-Reduktase. Es wurde um

1970 in *Aspergillus terreus* entdeckt (Alberts et al., 1980) und 1987 zur Behandlung von Hypercholesterinämie zugelassen. Der weltweite Jahresbedarf von ca. 300 Tonnen (Schäfer, 2010) wird heute immer noch fermentativ erzeugt (Pérez-Sánchez et al., 2017). Stereoselektive Totalsynthesen sind wegen aufwändiger Aufreinigungen und der Verwendung ungewöhnlicher Edukte ineffektiv (Clive et al., 1990; Heathcock et al., 1987; Hirama und Iwashita, 1983). Biosynthetisch handelt es sich bei Lovastatin um das veresterte Produkt zweier Polyketide, der LNKS (C18), LovA und einer Lovastatin-Diketid-(C4)-synthase (LDKS, LovB).
Der Nutzen der Statin-Produktion für den Pilz selbst ist bis heute nicht vollständig aufgeklärt. Vermutlich bieten Statine einen Vorteil gegenüber Konkurrenten (Cabral et al., 2010).

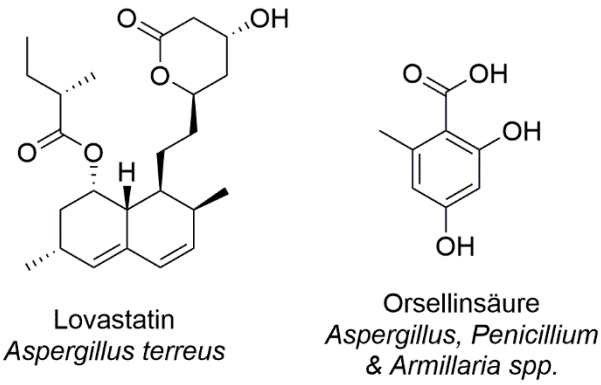

Abbildung 4 Strukturen von Polyketiden. Der HMG-CoA-Inhibitor Lovastatin (auch Mevinolin oder Monacolin-K) und das Tetraketid Orsellinsäure

Ein weit verbreitetes PKS-Produkt ist Orsellinsäure (Abbildung 4). Das Tetraketid kommt in vielen Pilzen wie *Aspergillus*- oder *Penicillium*-Arten vor (Cox, 2007), findet sich aber auch in Flechten (Parrot et al., 2015). Aufgrund seiner Einfachheit gilt Orsellinsäure als ein evolutionär sehr früh entstandenes Tetraketid, dessen Funktion in vielen Organismen noch völlig unbekannt ist (Schroeckh et al., 2009).
In *Armillaria spp.* ist Orsellinsäure ein wichtiger Bestandteil sämtlicher Melleolid-Antibiotika, auf welche in dieser Arbeit noch detaillierter eingegangen werden soll. Die Orsellinsäure wird hier von einer PKS auf verschiedene Sesquiterpenalkohole übertragen (Lackner et al., 2013).

1.3.3. Terpene

Die Terpene bieten mit über 80.000 bekannten Verbindungen die größte Diversität der hier genannten Naturstoffklassen (Christianson, 2017). Die meisten Terpene sind pflanzlicher Herkunft, da sie als Duft-, Signal- oder Abwehrstoffe bisher gründlich erforscht wurden (Balandrin et al., 1985; Gershenzon und Dudareva, 2007). Als ein prominentes Beispiel eines nichtflüchtigen Terpens sei hier das Zytostatikum Paclitaxel (Abbildung 2) genannt.
Wie in Abbildung 5 gezeigt, werden Terpene aus den C_5-Bausteinen Isopentenylpyrophosphat (IPP) und Dimethylallylpyrophosphate (DMAPP) aufgebaut, welche wiederum bei allen

pilzlichen Vertretern aus Acetyl-CoA über den Mevalonat-Biosyntheseweg erzeugt werden (Xiao und Zhong, 2016). Durch eine 1‘-4-Kopf-zu-Schwanz-Kondensation werden ein bis drei IPP-Verlängerungseinheiten durch eine *all-trans*-Isoprenylpyrophosphat-Synthase (IPPS), eine Terpen-Synthase, an DMAPP gebunden. So entstehen diphosphorylierte Isoprene unterschiedlicher Länge. Produkte sind Monoterpene aus Geranyldiphosphat (GPP, C_{10}), Sesquiterpene aus Farnesyldiphosphat (FPP, C_{15}) oder Diterpene aus Geranylgeranyl-diphosphat (GGPP, C_{20}). Längere Ketten werden durch 1‘-1-Kopf-an-Kopf Kondensation zweier FPPs über eine Squalen-Synthase zu Triterpenen (C_{30}) oder zweier GPPs über eine Phytoen-Synthase zu Tetraterpenen (C_{40}) katalysiert (Schmidt-Dannert, 2015).

Die linearen Substrate werden durch unterschiedliche Enzyme umgewandelt. Prenyltransferasen übertragen beispielsweise eine Prenylkette auf bevorzugt aromatische Strukturen, Terpenzyklasen zyklisieren die Ketten zu einer Vielzahl neuer Moleküle (Christianson, 2017). Monooxygenasen, vor allem Cytochrom P450-Enzyme führen Hydroxylgruppen ins Molekül ein.

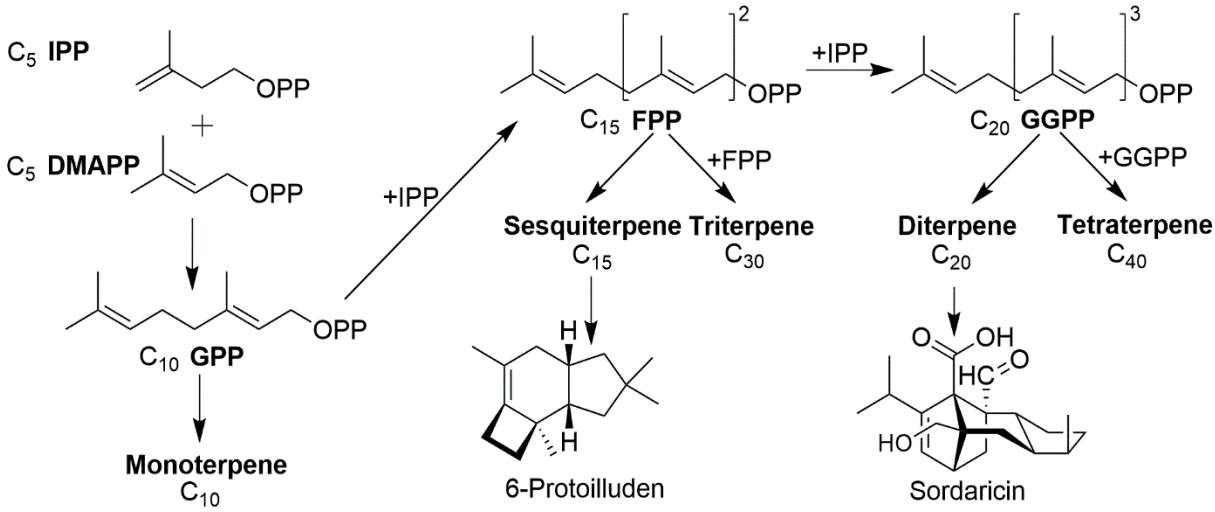

Abbildung 5. Biosynthese des Terpen-Grundgerüstes. Ausgehend von Isopentenyldiphosphat (IPP) und Dimethylallyldiphosphat (DMAPP) wird das Produkt immer um eine weitere IPP-Einheit verlängert. Durch enzymatische Modifikationen entstehen z. B. das Sesquiterpen 6-Protoilluden oder das Diterpen Sordaricin, welches das Aglycon von Sordarin darstellt.

Monoterpene sind in Pilzen nur äußerst selten zu finden, Sesquiterpene, Diterpene und Triterpene hingegen sehr häufig. Beispielhaft sollen hier nur die antifungalen Trichothecene aus *Trichothecium roseum*, phytomodulatorische Gibberelline aus *Gibberella fujikuroi* und das in Pilzen weit verbreitete Ergosterol, ein wichtiger Angriffspunkt für Antimykotika, als Vertreter genannt werden (Hanson, 2008).

Auf das Sesquiterpen 6-Protoilluden und das Diterpen Sordaricin soll hier etwas genauer eingegangen werden, da diese Moleküle in abgewandelter Form im Fokus dieser Arbeit stehen:

Sordaricin ist das Aglycon des Antibiotikums Sordarin. Dieses Diterpen wird unter anderem von dem auf Tierdung wachsenden (coprophilen) Pilz *Sordaria araneosa* gebildet. GGPP wird hierfür durch eine Terpenzyklase zu einem 5-8-5 Trizyklus umgebaut. Nach zahlreichen Modifikationen durch CYP P450 Monooxygenasen wird das Molekül am Octazyklus oxygeniert und der Ring in einem noch unbekannten Mechanismus geöffnet und neu geschlossen. So ergibt sich das komplexe in Abbildung 5 gezeigte überbrückte Ringsystem. Durch eine Glycosyltransferase wird Desoxyaltrose aus GDP-6-deoxy-D-altrose auf das Terpengerüst übertragen und bildet das Sordarin (Kudo et al., 2016).
Sordarin wurde 1969 unter dem Namen SL 2266 von der Schweizer Firma Sandoz patentiert (Odds, 2001) und die antifungale Wirkung erstmals 1971 beschrieben (Hauser und Sigg, 1971). Schnell gab es einen Wettbewerb der Pharmafirmen Merck und Glaxo Wellcome um die Etablierung eines neuen, nebenwirkungsarmen, antifungalen Medikaments am Pharma-Markt (Vicente et al., 2003). Eigentlich auf der Suche nach einem selektiven Inhibitor gegen den Translations-Elongationsfaktor 3 (EF3) (Odds, 2001), welcher nur in Pilzen vorkommt (Sturtevant, 2002), zeigte sich Sordarin als ein sehr spezifischer Inhibitor des eukaryotischen Elongationsfaktors 2 (eEF2) (Domínguez und Martín, 1998; Justice et al., 1998). Sordarin inhibiert dessen GTPase Aktivität, wodurch die Translokation blockiert wird (Domínguez et al., 1999).
Bisher ist Sordarin immer noch nicht als Medikament auf dem Markt. Sordarin und seine Derivate zeigten im Tiermodell gute Wirkungen und Verträglichkeit, jedoch eine zu geringe Plasma-Halbwertszeit (Odds, 2001). Derivate der Substanz werden deshalb weiterhin erforscht, um weitere Antimykotika mit diesem Wirkprinzip zu finden (Herreros et al., 1998; Liang, 2008; Søe et al., 2007; Vicente et al., 2003). In dieser Arbeit dient Sordarin als gut erforschte Referenzsubstanz zur Untersuchung der ribosomalen Translationshemmung, speziell bedingt durch die Inhibierung des eEF2.

Für diese Arbeit ebenfalls von Relevanz ist das Sesquiterpen 6-Protoilluden, dessen gesättigtes Derivat auch als Protoilludan bezeichnet wird. Das Molekül wird über eine Protoilluden-Synthase aus FPP zyklisiert. Protoilluden stellt i. d. R. nur ein Zwischenprodukt dar, aus welchem enzymatisch Sekundärmetabolite wie Illudine, Formannosine oder Marasmane abgeleitet werden (Abraham, 2001; Schmidt-Dannert, 2015).
Protoilluden-Alkohole wie Illudol wurden zuerst in *Fomitopsis insularis* entdeckt (Hanson, 2008). Ebenso wie Illudine (Illudin M & S) oder Marasmane (Marasmansäure) haben sie antibakterielle Eigenschaften, um den Produzenten vor Bakterien zu schützen (Arnone et al., 1989). Die Totalsynthesen dieser recht kleinen Protoilluden-Moleküle zeigen, wie effektiv natürliche Enzyme neue, komplexe Verbindungen schaffen, wofür Menschen aufwändige Synthesen entwickeln müssen (Hovey et al., 2017; Oppolzer und Nakao, 1986). Deshalb lohnt sich der Aufwand, die Biosynthese und Struktur-Aktivitätsbeziehungen (SAR) zu ergründen.

Protoilludenalkohole sind ein Hauptbestandteil der Melleolid-Antibiotika. Änderungen am Protoilludan-Grundgerüst durch *Armillaria*-eigene Enzyme, bieten eine Vielzahl an Möglichkeiten, das Molekül durch Hydroxylgruppen oder Doppelbindungen zu modifizieren.

1.3.4. Hybride Naturstoffe

Wie eingangs angedeutet gibt es in der Natur nicht nur eindeutig klassifizierbare Sekundärstoffe, welche ausschließlich aus Produkten der vorangestellten drei Naturstoffgruppen bestehen. Durch eine Kombination der verschiedenen Substanzklassen kommt es zur Bildung von „Hybriden“. Naturstoffe, welche aus Bausteinen derselben biosynthetischen Herkunft zusammengesetzt sind, wie z. B. Lovastatin aus zwei unterschiedlichen Polyketiden, werden hier nicht als Hybride bezeichnet.

Hybride Naturstoffe können durch eine Kondensation von Produkten z. B. aus einer PKS und einer NRPS, wie bei den Echinocandinen aus *A. nidulans* bestehen. Diese Stoffe bilden die neueste Gruppe derzeit bekannter Antimykotika. Sie hemmen durch die Blockade der β-(1,3)-D-Glucan-Synthase den pilzlichen Zellwandaufbau (Sucher et al., 2009). Bei der Echinocandin-Biosynthese wird die von einer PKS erzeugte Myristinsäure als Startermolekül auf die T-Domäne einer NRPS mit 6 Modulen geladen (Cacho et al., 2012). Durch schrittweise Verlängerung einer sich bildenden Peptidkette entsteht final ein Hexapeptid mit einer stark reduzierten Polyketid-Seitenkette (Hüttel et al., 2016). Durch die Verwendung verschiedener langkettiger Säuren als Starter, sowie den Einbau unterschiedlicher Aminosäuren ergibt sich auch unter den Echinocandinen eine hohe Diversität (Hüttel, 2017).

Doch keine der bisher genannten Sekundärstoffgruppen bietet eine ähnlich hohe Diversität wie die Melleolide – PKS/Terpen Hybride aus *Armillaria spp*., die im nachfolgenden Kapitel genauer beleuchtet werden sollen.

1.4. Melleolid-Antibiotika - Naturstoffe aus *Armillaria mellea*

Die Einzelbausteine Protoilluden (Sesquiterpen) und Orsellinsäure (Polyketid) sind weit verbreitete Metaboliten verschiedener Organismen. Die Kombination der Bausteine in Vertretern der Gattung *Armillaria* gilt bisher als einzigartig (Misiek und Hoffmeister, 2012). Heute sind mehr als 70 verschiedene Metabolite bekannt. Dies spricht für eine diversitäts-orientierte Biosynthese. Die PKS ArmB bildet hierbei das Polyketid Orsellinsäure (Lackner et al., 2012). Des Weiteren ist ArmB in der Lage, die Veresterung der Orsellinsäure mit einem Protoilludenalkolhol zu katalysieren. ArmB funktioniert daher nicht nur als Polyketid-Synthase sondern auch als intermolekulare Transferase (Lackner et al., 2013). Eine ähnliche Reaktion wurde bisher auch für die Orsellinsäuresynthase OrsA aus *A. nidulans* beobachtet. Das Enzym bildet hier neben Orsellinsäure auch Lecanorsäure, welches ein transesterifiziertes Orsellinsäuredimer darstellt (Gressler et al., 2015).

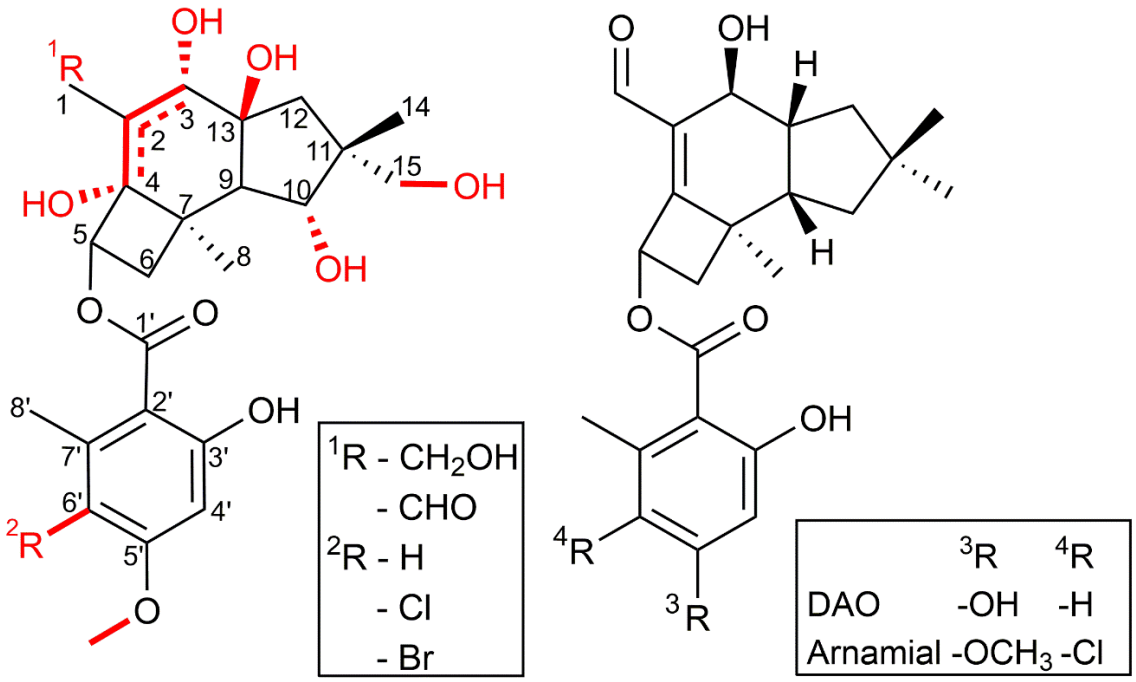

Abbildung 6. Variationsmöglichkeiten am Melleolid-Grundgerüst. Veränderungen wie die Lage einer möglichen Doppelbindung, potenzielle Hydroxylierungsstellen am Protoilludan oder eine Methylierungsstelle, sowie eine Position zur Halogenierung an der Orsellinsäure, sind links in Rot dargestellt. Rechts sind zwei für diese Arbeit wichtige Vertreter, nämlich Dehydroarmillylorsellinat (DAO) und Arnamial dargestellt.

Die Protoilludenalkohole werden durch eine Protoilludensynthase gebildet (Engels et al., 2011). ArmB verestert die Orsellinsäure mit dem Alkohol eines Protoilludenderivates. Hier entsteht die hohe Diversität: Die Charakterisierung der Substrat-Derivate für ArmB scheint für die Veresterung keine wesentliche Rolle zu spielen. Protoilludene mit unterschiedlichsten Substitutionsmustern werden mit dem Polyketid verestert. Sechs verschiedene Kohlenstoffe (C1, C3, C4, C10, C13, C15) können hierbei in allen möglichen Kombinationen hydroxyliert sein. Ebenso ergeben sich je nach Substitutionsmuster bis zu sechs Stereozentren. Am Kohlenstoff C1 kann anstelle eines Alkohols auch ein Aldehyd vorliegen. Des Weiteren unterscheidet sich der Terpenkörper regioselektiv anhand der Lage und dem Vorhandensein einer Doppelbindung: Diese kann entweder komplett fehlen oder zwischen den Kohlenstoffen C2 und C4 ($\Delta^{2,4}$) bzw. zwischen C2 und C3 ($\Delta^{2,3}$) liegen.

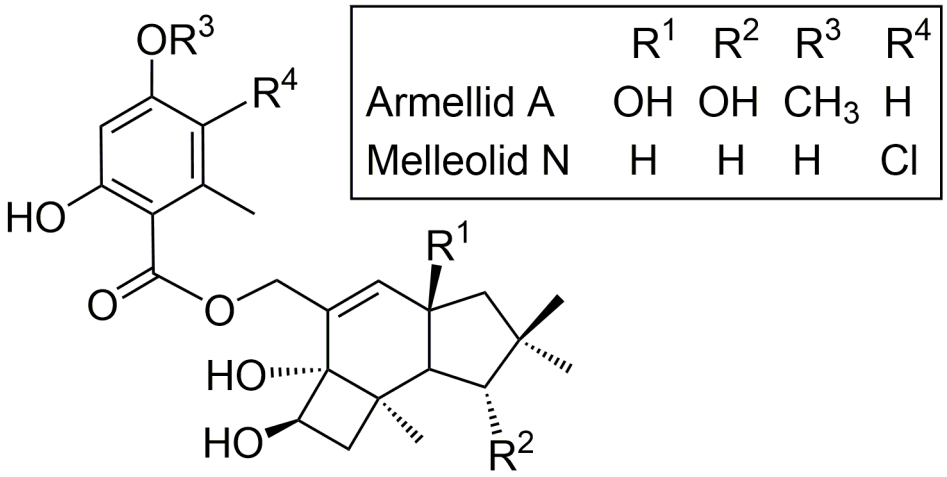

Abbildung 7. Melleolid N und Armellid A, Esterbindung der Orsellinsäure an C1 des Protoilludans

Die PKS ArmB verbindet die beiden Bausteine bevorzugt, aber nicht völlig selektiv über die Hydroxygruppe am C5 des Protoilludans, denn es wurden auch Veresterungen über den Alkohol an C1 z. B. bei Armellid A (Arnone et al., 1988) oder Melleolid N gefunden (Chen et al., 2011). Nach der Verbindung der beiden Bausteine ist eine Halogenierung am Kohlenstoff C6´ der Orsellinsäure möglich. Hier wurden bisher neben Chlorierungen auch eine artifizielle Bromierung *in vitro* beobachtet (Wick et al., 2016). Außerdem wird vermutet, dass die C5´-Hydroxylgruppe nachträglich von einer Methyltransferase methyliert wird.

Die kombinatorische Ausstattung einer großen Anzahl von Molekülen mit verschiedenen strukturellen Merkmalen entlang eines einzelnen Stoffwechselweges gilt als hoch effizient und unterstützt die sogenannte „Screening-Hypothese“ (Bohnert et al., 2014a). Diese Hypothese besagt, dass eine höhere Wahrscheinlichkeit für Bioaktivität dann erreicht wird, wenn eine Spezies möglichst viele strukturähnliche Produkte bildet (Firn und Jones, 2003). So wird die Wahrscheinlichkeit erhöht, ein zelluläres Ziel bei Konkurrenten zu treffen, um sich selbst einen Vorteil zu schaffen (Firn und Jones, 2009).

Die Diversität der Melleolide ist für den Pharmazeuten hierbei Segen und Fluch zugleich. Problematisch bei der Fülle an sich stark ähnelnden Metaboliten ist die Isolierung und Aufreinigung einzelner Substanzen. Sehr vorteilhaft ist jedoch, dass sich die SAR der Melleolide allein anhand isolierter Derivate aufklären lassen. Synthetische Derivatisierungen sind aufgrund der vielen bereits bekannten und isolierten Melleolide nicht notwendig.

Bisher wurden verschiedene SAR beobachtet: Melleolide mit einem Aldehyd am C1 und einer $\Delta^{2,4}$-Doppelbindung haben eine antifungale Wirkung. Die antifungale Wirkung geht verloren, wenn sich die Doppelbindung in $\Delta^{2,3}$-Position befindet oder gänzlich fehlt (Bohnert et al., 2014a). Vorarbeiten zeigten für die antifungale Wirkung der Melleolide keine ursächliche Erklärung. Es wurde aber herausgefunden, dass Melleolide die Transkription von *A. nidulans* beeinflussen.

Der Hauptteil dieser Arbeit beschäftigte sich mit der Identifikation des zellulären Wirkziels am

Modellorganismus *A. nidulans*. Speziell wurden hier $\Delta^{2,4}$-ungesättigte Melleolid-Derivate wie Dehydroarmillylorsellinat (DAO) und Arnamial untersucht (Abbildung 6).

In weiteren Untersuchungen zeigten sich viele Melleolide als zytotoxisch gegen humane Krebszelllinien (Chang et al., 2016; Chen et al., 2015; Li et al., 2016; Misiek et al., 2009). Interessanterweise ist die Lage der Doppelbindung für die zytotoxische Wirkung kaum relevant. Entscheidend ist vielmehr die Anzahl an Hydroxylierungen (Bohnert et al., 2011; Bohnert et al., 2014b).
In Vorarbeiten zeigte sich, dass der Zelltod humaner Zellen durch Melleolide besonders schnell herbeigeführt wird. Im Gegensatz zu gängigen Vergleichssubstanzen für Zellviabilitätsassays wie Staurosporin oder Pretubulysin, deren Wirkung nach mehreren Stunden einsetzt, zeigten einige Melleolide schon nach 15 Minuten erste zytotoxische Effekte mit apoptotischen und nekrotischen Merkmalen (Bohnert et al., 2014b). Beobachtet wurde auch eine starke Abnahme der ribosomalen Translation, welche ebenfalls nicht den Grund für einen so raschen Zelltod darstellen kann (Bohnert et al., 2011).
Da die Doppelbindungsposition für die zytotoxische Wirkung nicht entscheidend ist, wird bisher von zwei verschiedenen Wirkmechanismen ausgegangen. Ein Teil dieser Arbeit beschäftigt sich deshalb mit dem Wirkmechanismus der Melleolid-Antibiotika an menschlichen Zellen.

1.5. Klassifizierung bekannter Antibiotika

Antibiotika sind dem Ursprung des Wortes nach (von griechich ἀντί- anti- „gegen“ und βίος bios- „Leben“) Stoffe, welche das Wachstum anderer Organismen behindern, oder diese abtöten. Im heutigen Sprachgebrauch meint man mit Antibiotika aber vor allem niedermolekulare Stoffe, ursprünglich meist aus Bakterien oder Pilzen, welche ihre Wirkung gegen andere Mikroorganismen, vor allem Bakterien ausüben (Mutschler, 2013). Wirkstoffe, welche sich gezielt gegen menschliche Zellen, im pharmazeutischen Sinne vor allem gegen schnell proliferierendes Gewebe wie Krebszellen richten, bezeichnet man als Zytostatika oder Chemotherapeutika. Wirkstoffe mit einem wachstumshemmenden oder zerstörenden Einfluss auf Pilzzellen kennt man als Antimykotika. Nachfolgend werden Melleolid-Antibiotika mit Zytostatika und Antimykotika verglichen.

1.5.1. Einteilung der Zytostatika

Zytostatika lassen sich grob in vier große Gruppen einteilen:
Zunächst gibt es **Quervernetzende Substanzen**, welche die Basen der DNA (meist Purinbasen) vernetzen. Die einzelnen DNA-Stränge werden kovalent miteinander verbunden. Die codierte Information kann nicht mehr abgelesen werden (Mutschler, 2013). Zu dieser Gruppe zählen zahlreiche Wirkstoffe der N-Lost-Verbindungen, der Alkylsulfonate, der Nitroharnstoff-Derivate, der Platinsalze, oder der Triazene.

Eine weitere Zytostatika-Gruppe stellen die **Antimetaboliten** dar. Diese hemmen die DNA oder RNA-Synthese durch Unterdrückung der *de novo* Synthese von Nukleotiden oder durch den Einbau falscher Nukleotide (Peters, 2014). Gängige Wirkstoffe sind Dihydrofolatreduktase-Hemmer wie Methotrexat, Pyrimidinanaloga oder Purinanaloga.
Außerdem großen Absatz finden **Mitosehemmstoffe** wie Vincaalkaloide, oder Taxole, welche durch eine Hemmung der Polymerisierung von Tubulinen den Auf-/Abbau des Spindelapparates und somit einen Kernprozess der Zellteilung behindern.
Auch Antibiotika wie Mitomycine, Anthrazykline, Actinomycine oder Bleomycin finden Verwendung als Zytostatika. Diese Stoffe sind **DNA-Interkalatoren**. Die Substanzen führen durch eine Einlagerung in die DNA Doppelhelix zu Strangbrüchen, zur Hemmung von Topoisomerasen oder von RNA/DNA Polymerasen (Mutschler, 2013)
Neben den genannten Haupt-Wirkmechanismen sind noch **hormonelle Therapeutika** zu nennen, welche meist antagonistisch bei Hormon-abhängigen Tumoren eingesetzt werden (Riemsma et al., 2010).
Seit einigen Jahren auf dem Vormarsch sind die sogenannten Biological Response Modifiers, welche über einen Eingriff in die Signaltransduktion die Zellproliferation beeinflussen (Liu et al., 2016). Auch die individualisierte Tumortherapie zum Beispiel über eine gentechnische Veränderung von T-Zellen des Patienten bietet eine innovative Alternative zu den „klassischen“ Zytostatika-Gruppen (Androulla und Lefkothea, 2018), soll hier aber nicht näher thematisiert werden.

1.5.2. Einteilung der Antimykotika

Die meisten Antimykotika interagieren mit der Bildung der pilzlichen Zellwand bzw. –membran. **Azole** wirken durch eine Hemmung der pilzlichen Lanosterol-14α-Demethylase (CYP51A) fungistatisch bis fungizid. Dadurch kommt es zum einen zur Akkumulation toxischer Vorläufermoleküle der Zellmembran, als auch zur Störung des Membranaufbaus (Zonios und Bennett, 2008). Als neuer Wirkmechanismus wird auch eine Überproduktion von Zellwand-Kohlenhydrat-Patches postuliert, welche durch Penetration der Plasmamembran zum Tod eines Pilzes führen (Geissel et al., 2018). **Allylamine** hemmen ebenfalls die Ergosterol-Biosynthese, speziell die Squalenepoxidase, und somit den Aufbau der Zellmembran (Petranyi et al., 1984). **Polyene** integrieren sich in die Ergosterol-haltige Zellmembran, führen zur Bildung durchlässiger Poren und somit zum Zelltod (Hamilton-Miller, 1974; Holz, 1974). **Echinocandine** stören durch eine Hemmung der β-1,3-D-Glucan Synthase den Aufbau der Zellwand und führen über eine osmotische Instabilität zur Zelllyse (Denning, 1997; Georgopapadakou, 2001).
Ein weiterer Angriffspunkt ist die Ausbildung von Mikrotubuli. Ähnlich der Wirkung des Vinblastins wird durch eine Interaktion mit **Griseofulvin** die pilzliche Mitose gehemmt (Rathinasamy et al., 2010).

Außerdem sind Hemmstoffe der Nucleinsäuresynthese (DNA/RNA) bekannt. Beispielsweise hemmt **Flucytosin** die pilzliche Thymidylat Synthase und somit die DNA Synthese. Als Prodrug wird es in 5-Fluorodeoxyuridin umgewandelt in die RNA eingebaut, was zusätzlich eine Hemmung der Proteinbiosynthese bewirkt (Vermes et al., 2000).

1.6. Forschungsbedarf

Bisher war unklar, welche Funktion die Melleolide für ihren Wirt einnehmen. Zwar war schon sehr früh bekannt, dass Melleolide antibiotisch wirksam sind (Oduro et al., 1976), über die Nutzung dieser bioaktiven Sekundärstoffe als Selektionsvorteil gegenüber Konkurrenten wurde erst später spekuliert (Misiek und Hoffmeister, 2012). Bohnert et al. entdeckten neben cytotoxischen Effekten auf humane Zelllinien erstmals konkretere Wirkziele an Pilzen, nämlich die pilzliche Transkription (Bohnert et al., 2014a; Bohnert et al., 2014b), jedoch fehlte es auch hier an Nachweisen für molekulare Angriffspunkte für die jeweils entdeckten Effekte. In dieser Arbeit sollen erstmals konkrete Wirkmechanismen ausgewählter Melleolide hinsichtlich einer cytotoxischen und antifungalen Wirkung aufgedeckt werden.

2. Zielsetzung der Arbeit

Das Substitutionsmuster v.a. des Terpens und die Lage der darin befindlichen Doppelbindung ($\Delta^{2,3}$, $\Delta^{2,4}$) tragen maßgeblich zur Diversität der antibiotischen Wirkung gegen verschiedenste Organismen bei. Daraus ergab sich die Fragestellungen und Zielsetzung dieser Arbeit:

1. Welches ist das molekulare Ziel, über das die antimykotische Wirkung der Melleolide erfolgt?

2. Ist es möglich, am Beispiel von DAO durch eine chemische Synthese eine Sonde zu erzeugen, um dieses Wirkziel aus einem pilzlichen Modellorganismus (*A. nidulans)* und aus menschlichen Zellen zu isolieren und zu identifizieren?

3. Welche Mechanismen führen in humanen Zelllinien zur raschen Zytotoxizität? Worin bestehen die Unterschiede zu antifungalen Wirkzielen?

3. Publikationen

3.1. Publikation 1 – Melleolides impact fungal translation *via* elongation factor 2

Maximilian Dörfer, Daniel Heine, Stefanie König, Sagar Gore, Oliver Werz, Christian Hertweck, Markus Gressler, Dirk Hoffmeister

Organic & Biomolecular Chemistry, 2019, Volume 17, 4906-4916.

Zusammenfassung

In dieser Arbeit ist es gelungen, mit DAO, einem Naturstoff aus der Stoffgruppe der Melleolide aus der Gattung *Armillaria,* eine Zielstruktur von $\Delta^{2,4}$-ungesättigten Melleoliden in *Aspergillus nidulans* zu identifizieren. In einer chemischen Synthese wurde DAO an Biotin gekoppelt, um eine Streptavidin-basierte, affinitätschromatographische Proteinextraktion am Modell *A. nidulans* durchzuführen. Die MALDI-TOF-basierte Peptidanalyse der angereicherten Proteine identifizierte den eukaryotischen Elongationsfaktor eEF2 als Wirkziel von DAO, was über Western Blot bestätigt werden konnte. Die Inhibition der Proteinproduktion und der damit einhergehenden antifungalen Wirkung von $\Delta^{2,4}$-ungesättigten Melleoliden konnte *in vivo* mittels transgener mCherry-Stämme nachgewiesen werden. Über *in silico* Protein-Modellierung wurden putative Bindestellen identifiziert und diese mit DAO-sensitiven bzw. resistenten Hefen verglichen.

Eigenanteil 50%:

Maximilian Dörfer: Kultivierung von *A. mellea*, Isolation und Analyse der Naturstoffe, Synthese von Sonden für Pull-Down Assays, Target Fishing, Western Blotting, *in vivo*-Translationsassay in *A. nidulans*, Wachstums-experimente mit Hefen, Verfassen des Manuskripts

Jena, den

_____

Prof. Dr. Dirk Hoffmeister

Organic & Biomolecular Chemistry

PAPER

View Article Online
View Journal | View Issue

Cite this: *Org. Biomol. Chem.*, 2019, **17**, 4906

Melleolides impact fungal translation *via* elongation factor 2†

Maximilian Dörfer,[a] Daniel Heine,[b] Stefanie König,[c] Sagar Gore,[d] Oliver Werz,[c] Christian Hertweck,[b] Markus Gressler*[a] and Dirk Hoffmeister*[a]

Received 8th March 2019,
Accepted 24th April 2019

DOI: 10.1039/c9ob00562e

rsc.li/obc

Melleolides from the honey mushroom *Armillaria mellea* represent a structurally diverse group of polyketide-sesquiterpene hybrids. Among various bioactivites, melleolides show antifungal effects against *Aspergillus* and other fungi. This bioactivity depends on a $\Delta^{2,4}$-double bond present in dihydroarmillylorsellinate (DAO) or arnamial, for example. Yet, the mode of action of $\Delta^{2,4}$-unsaturated, antifungal melleolides has been unknown. Here, we report on the molecular target of DAO in the fungus *Aspergillus nidulans*. Using a combination of synthetic chemistry to create a DAO-labelled probe, protein pulldown assays, MALDI-TOF-based peptide analysis and western blotting, we identify the eukaryotic translation elongation factor 2 (eEF2) as a binding partner of DAO. We confirm the inhibition of protein biosynthesis *in vivo* with an engineered *A. nidulans* strain producing the red fluorescent protein mCherry. Our work suggests a binding site dissimilar from that of the protein biosynthesis inhibitor sordarin, and highlights translational elongation as a valid antifungal drug target.

Introduction

The fungal genus *Armillaria* (honey mushrooms) includes notorious and globally distributed tree pathogens that cause severe butt and root rot, thus impacting timber production, fruit and crop trees, and ornamentals.[1] A physiological hallmark of these fungi is the production of numerous hybrid polyketide-sesquiterpene antibiotics, referred to as the melleolides.[2] From a chemical perspective, they are intriguing for two reasons. Firstly, the tricyclic protoilludene-type sesquiterpenoid secondary alcohol that is esterified to an orsellinic acid (or derivatives thereof) makes them structurally unique among natural products, even though protoilludenes and orsellinic acid – as separate entities – are common fungal compounds.[3,4] Secondly, with more than 70 known structural congeners, the melleolides form one of the largest classes of fungal natural products. From a pharmaceutical perspective it is remarkable that numerous melleolides exert potent antifungal effects against *Aspergilli* and various other fungi.[5] Yet, the bioactivity of these compounds reaches further and also includes phytotoxicity and toxicity on human monocytes and cancer cells.[2,6–8] Human 5-lipoxygenase, *i.e.*, the key enzyme in the biosynthesis of pro-inflammatory leukotrienes, was identified as molecular target of dihydroarmillylorsellinate (DAO, **1**) whose α,β-unsaturated aldehyde represents a Michael acceptor that selectively reacts with the 5-lipoxygenase surface cysteine 159.[9] Remarkably, the structural prerequisites for the antifungal and the cytotoxic activities are incongruent. Thus, the melleolides unite completely dissimilar structure–activity-relationships, which adds to the uniqueness of this class of natural products.[10] Previous work identified the protoilludene $\Delta^{2,4}$-carbon–carbon double bond as being critical for antifungal activity. Conversely, those compounds that possess a $\Delta^{2,3}$-double bond are inactive, even though an α,β-unsaturated carbonyl moiety is still present, suggesting that the spatial conformation of the sesquiterpene as consequence of the shifted double bond impacts bioactivity.[10]

While the mode of action on human cells has been established, the cellular target that mediates antifungal activity remained elusive. Here, we show that **1** interferes with protein biosynthesis and interacts with *Aspergillus* eukaryotic translation elongation factor 2 (eEF2). The findings were confirmed by *in vivo* translation inhibition with arnamial (**2**), another melleolide that possesses a $\Delta^{2,4}$-double bond. **1** adds to the

[a]*Department Pharmaceutical Microbiology at the Hans Knöll Institute, Friedrich-Schiller-University, Beutenbergstrasse 11a, 07745 Jena, Germany. E-mail: dirk.hoffmeister@hki-jena.de, markus.gressler@hki-jena.de; Fax: +49-3641-949852; Tel: +49-3641-949851*

[b]*Department Biomolecular Chemistry, Leibniz Institute for Natural Product Research and Infection Biology – Hans Knöll Institute, Beutenbergstrasse 11a, 07745 Jena, Germany*

[c]*Department Pharmaceutical and Medicinal Chemistry, Friedrich-Schiller-University Jena, Philosophenweg 14, 07743 Jena, Germany*

[d]*Department Systems Biology and Bioinformatics, Leibniz Institute for Natural Product Research and Infection Biology – Hans Knöll Institute, Beutenbergstrasse 11a, 07745 Jena, Germany*

†Electronic supplementary information (ESI) available. See DOI: 10.1039/C9OB00562E

very few mushroom metabolites whose modes of action are understood and represents a unique scenario of a natural product that exerts bioactivity *via* dissimilar targets in human *versus* fungal cells, yet acting highly selectively in either case.

Results and discussion

For more profound insight into the antifungal mode of action of the melleolides, we used the model fungus *Aspergillus nidulans* and relied on a combined approach that included (i) design and synthesis of a DAO-coupled affinity matrix, (ii) pulldown assays and western blots to enrich, identify and verify protein targets *in vitro* and subsequently (iii) a recombinant *A. nidulans* strain producing the fluorescent protein mCherry to monitor translational activity of the fungal cells *in vivo*.

$\Delta^{2,4}$-Unsaturated melleolides confer antifungal activity against *Aspergillus nidulans*

The antifungal activity of three unsaturated melleolides, **1**, **2** and melleolide D (**3**) was tested against the filamentous model fungus *A. nidulans* (Fig. 1). Consistent with previous data, we observed antifungal activity for **1** and **2**. Both compounds belong to the $\Delta^{2,4}$-unsaturated aldehyde melleolides, whose double bond is predicted to be critical for antifungal activity.[10] In contrast, **3** harboring a $\Delta^{2,3}$-double bond and a hydroxyl group in place of the aldehyde, was inactive.

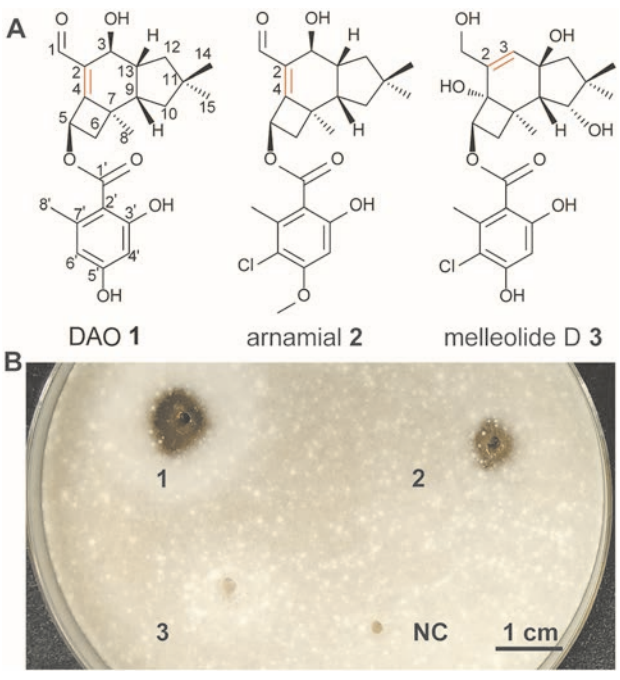

Fig. 1 Growth inhibition of *A. nidulans* by unsaturated melleolides. A. Structures of unsaturated melleolides. B. Solid medium with germinating *A. nidulans* conidia which were exposed to **1**, **2**, and **3** (20 μg per well). Methanol served as negative solvent control (NC).

Synthesis of a DAO-coupled chemical probe

To identify putative fungal target proteins for $\Delta^{2,4}$-unsaturated melleolides by an unbiased affinity-based protein fishing approach, we synthesized DAO probes with covalently bound biotin. In order to leave the terpenoid pharmacophore intact, biotin was coupled *via* an alkynyl linker and cycloaddition to the 5′-hydroxy group of the orsellinic acid. Initial attempts to introduce the alkynyl moiety using propargyl halides under basic conditions (Cs_2CO_3 or K_2CO_3) led to degraded **1**. Similarly, coupling of propiolic acid to the 5′-hydroxy group using benzotriazol-1-yl-oxytripyrrolidinophosphonium hexafluorophosphate (PyBOP) or 4-dimethylaminopyridine (DMAP) in the presence of 1-ethyl-3-(3-dimethylaminopropyl)carbodiimide (EDC) or *N*,*N*′-dicyclohexylcarbodiimide (DCC), supported by Hünig's base, pyridine or trimethylamine, were not effective either. Eventually, 5-hexynoic acid was successfully coupled using EDC and Hünig's base (Scheme 1). Esterification of 5-hexynoic acid with the 5′-hydroxy group was confirmed by ^{13}C-NMR spectroscopy. The signals of C-4′ and C-6′ (δ_C 102.3 ppm (C-4′), δ_C 113.1 ppm (C-6′)) in **1** were shifted downfield in dihydroarmillylorsellinate-5′-*O*-hexynoylester (**4**) due to deshielding of the aromatic ring system (δ_C 108.2 ppm (C-4′), δ_C 116.6 ppm (C-6′)) (ESI, Fig. S1–S5, Table S1†). Besides the characteristic signals for **1**, six additional carbon signals (C-1′–C-6′) were observed (ESI, Fig. S2†), thus indicating correct 5′-*O*-esterification. The unaltered signal of C-1 at δ_C 192.6 ppm confirmed that the highly reactive aldehyde has remained intact and not been reduced to a primary alcohol. The reaction on position 5′ was preferred, leading to **4** (Scheme 1) as the major product (yield: 72%, 2.7 mg), most likely due to an unfavourable steric environment around hydroxy groups on positions 3 and 3′. Ascorbate served as reducing agent in a subsequent copper-catalyzed Huisgen 1,3-cycloaddition with azide-PEG$_3$-biotin, yielding the desired probe **5** (yield: 34%, 1.0 mg) (Scheme 1). A parallel coupling reaction of **3** with 5-hexynoic acid (to create a negative control for subsequent protein pull-down assays) showed poor regioselectivity. Consequently, we synthesized a compound (**6**, yield: 92%, 11.8 mg) in which **1** was replaced by butylparabene (ESI, Scheme S1†). The structures of **5** and **6** were confirmed by HR-MS spectrometry and NMR spectroscopy (ESI, Fig. S6–S10, Table S2†).

DAO binds to *Aspergillus nidulans* eEF2

Compounds **5** (probe) and **6** (control) were bound to streptavidin-coated beads *via* the biotin moiety. These affinity matrices were used for protein fishing experiments that were performed with cell-free total protein extracts from *A. nidulans* as target source. Proteins binding to the affinity matrix were eluted, electrophoretically separated by SDS-polyacrylamide electrophoresis, and visualised by Coomassie staining (Fig. 2). Using **5** as bait, we identified two enriched protein bands at 28 kDa (band 1) and 95 kDa (band 2) that were absent in pulldowns with the negative control **6**. Both bands were cut out and subjected to trypsin digestion and subsequent MALDI-TOF ana-

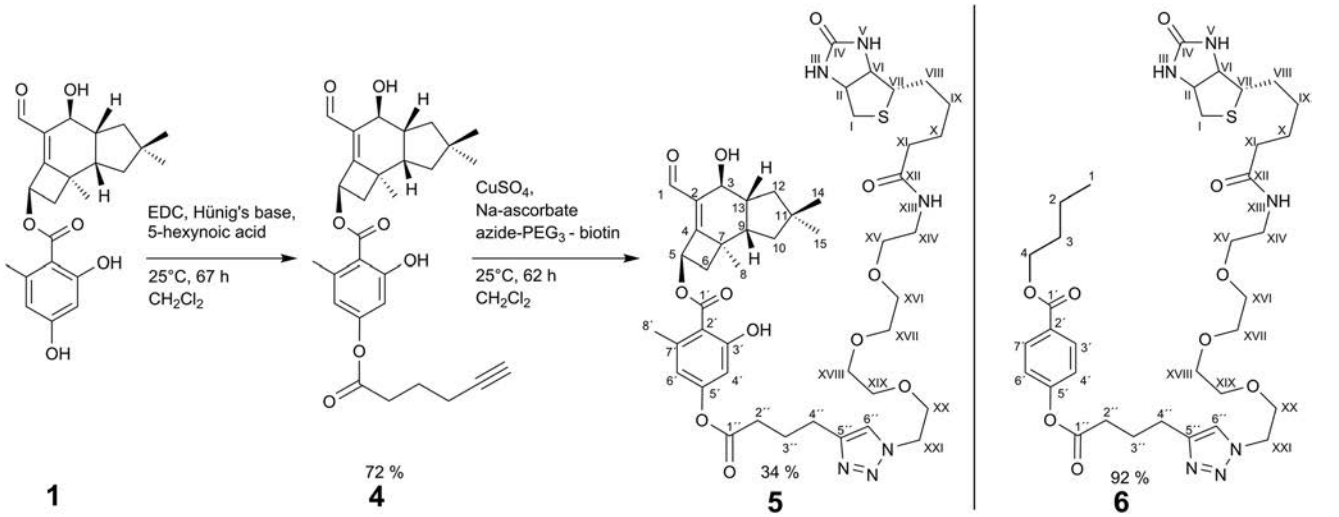

Scheme 1 Chemical synthesis of biotin-labelled DAO probe **5** and control probe **6**. For detailed information on the synthesis of **6**, see also ESI, Scheme S1.†

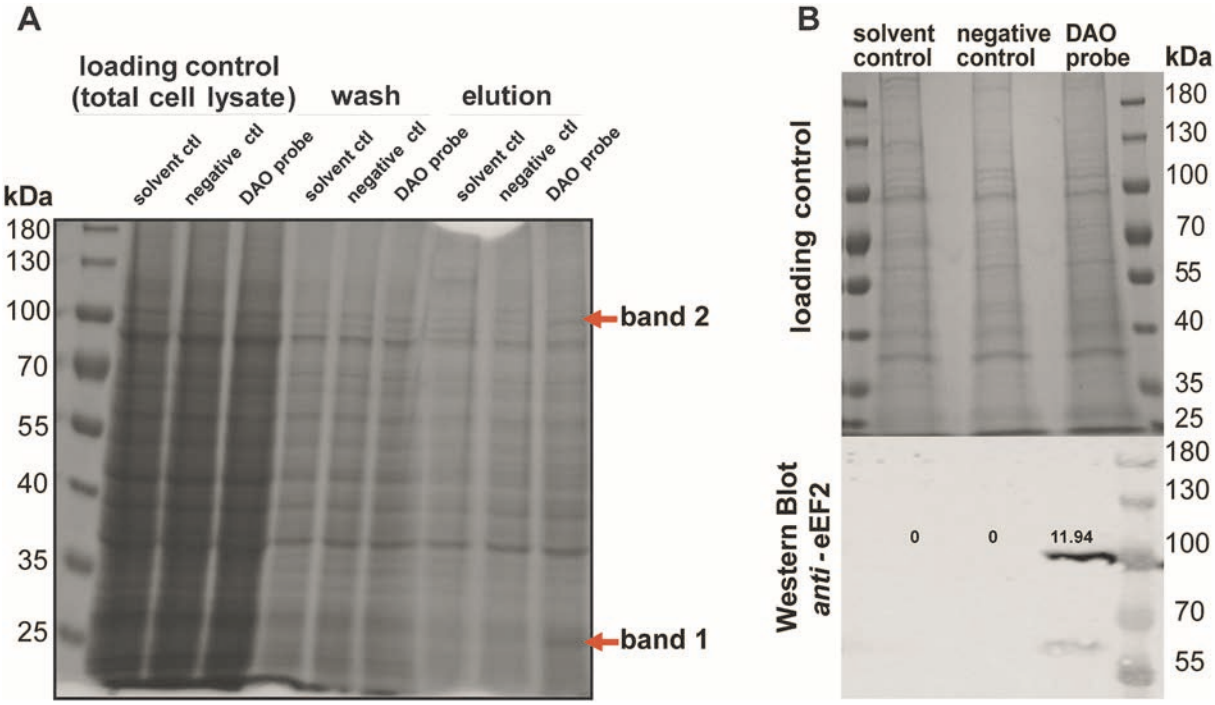

Fig. 2 Identification of eEF2 as molecular target of **1**. (A) SDS-polyacrylamide electrophoresis of fractions of the protein pulldown assay. Streptavidin beads were incubated with DMSO (solvent control), **6** (negative control), or **5** (probe). A total protein lysate of *A. nidulans* was applied (total cell lysate). The beads were washed with buffer (wash) and eluted with Laemmli buffer (elution). Indicated bands were digested with trypsin, and peptides were analysed by MALDI-TOF (ESI, Table S3†). (B) Western blot analyses of protein elution fractions from protein pull-down assays using rabbit anti-human eEF2 IgG. The upper panel shows the loading control (Coomassie stained SDS-PAGE), while the lower panel shows the membrane using IRDye® 800CW goat anti-rabbit IgG as secondary antibody. Indicated values represent relative fluorescence intensities (exposure λ = 778 nm; emission λ = 795 nm).

lyses (ESI, Table S3†). Peptides from band 1 revealed the eukaryotic elongation factor 1α (eEF1α) as a candidate. However, due to only five short peptide fragments (4–6 amino acids), low abundance of the peptides, and a band position (28 kDa) that deviated from the expected size (50.8 kDa), protein identification remained ambiguous. In contrast, band 2 was identified as eEF2 by 19 peptide fragments and a sequence coverage of 29.4% (ESI, Fig. S11†). Therefore, we con-

cluded that **1** interacts with the 93.8 kDa eEF2 in *A. nidulans*. To independently test this hypothesis, we performed a western blot analysis with the pulled-down proteins. Since no antibody against fungal eEF2 was available and since the N-terminal eEF2 epitope of *A. nidulans* is 78% identical to the human eEF2, we used a rabbit anti-human eEF2 IgG to detect fungal eEF2 in the fractions. Western blot analysis clearly confirmed the enrichment of the protein and, thus, the binding of eEF2 to the probe **5** but not to the corresponding negative control. These results indicate that eEF2 directly binds $\Delta^{2,4}$-unsaturated melleolides which may compromise its activity, leading to inhibited translation, and hence, to antifungal activity.

In silico blind docking studies revealed a putative binding pocket

Similar to the melleolides **1** and **2**, the diterpene glycoside sordarin (**7**) targets translational elongation in fungi *via* eEF2,[11] whereas other pharmaceutically relevant antifungals, such as azoles, allylamines, echinocandins, or polyenes, interfere with cell wall or membrane biosynthesis or integrity.[12] Specifically, **7** selectively binds to eEF2 of *Saccharomyces cerevisiae* in a well-defined binding pocket (^{517}CVLTYMSE^{524}) which is located in close vicinity to the GDP/GTP binding site of eEF2.[13] By stabilising the eEF2-80S ribosome complex, **7**-bound eEF2 is kept in a GTPase activation state and prevents the tRNA-mediated translocation reaction.[14] Prior studies showed that the different susceptibility to **7** in various yeast species is due to mutations in this **7** binding pocket.[13,15] However, *in silico* molecular fingerprint similarity values between **1** and **7** indicated structural and chemical differences between both molecules (ESI, Table S4†). Thus, we compared the sensitivity and resistance profile of **1** in various yeast species to those of **7** and found that both profiles differ strongly (Fig. 3A). We observed growth inhibition by **1** for *Candida albicans*, *Candida parapsilosis* and *Candida lusitaniae*, while *Candida glabrata* and *S. cerevisiae* were resistant. In contrast, *S. cerevisiae* and *C. albicans* are susceptible to **7**, while no inhibition by **7** was detected for the other yeast species. Similarly, *A. nidulans* is inhibited by **1**, but not by **7**. From these results and given the different chemistry of the molecules (ESI, Table S4†) we hypothesised that **1** and **7** might target dissimilar sites in eEF2. To corroborate our assumption and to obtain first insight into the potential place of binding, we relied on *in silico* methods: 3D modelling of *S. cerevisiae* and *C. albicans* eEF2 revealed highly conserved amino acid residues in the binding pockets for **7** (Y521 and S523), as shown in Fig. 3B. Differences in the binding pocket for **7** in *A. nidulans* eEF2 (M522 and N524) may alter the binding pocket shape and van der Waals interactions (Fig. 3B) and hence may cause resistance to **7** (Fig. 3A). In contrast, the highly hydrophobic bulky terpenoid moiety of **1** does not fit into the binding pocket of **7**. Blind docking studies with 3D structural model of *A. nidulans* eEF2, built with template crystal structure of *S. cerevisiae* eEF2 revealed possible binding sites for **1** (ESI, Table S5†).[16] However, in some cases, these are buried inside the protein and hence are not accessible to **1**. The most likely binding site depicts a proper orientation of the protoilludene moiety inside eEF2 and is located next to the GTP binding domain of *A. nidulans* eEF2 (Fig. 3C). In addition, binding of **1** can be modelled into eEF2 of the **1** sensitive *C. albicans* and of the **1** resistant yeast *S. cerevisiae*, although their amino acid sequence in the binding region differs from that of *A. nidulans* eEF2 at positions 170, 249, and 261–265. Interestingly, the two **1** resistant organisms *S. cerevisiae* and *C. glabrata*, share an altered amino acid sequence in the binding pocket which may lead to insensitivity to **1** (T170, F249, T262). Specifically, the side-chain amino group of K262 in *C. albicans* eEF2 may interact with the 5′ hydroxy group of **1**, whereas T262 in both resistant strains faces away from the metabolite and seems not to interact (Fig. 3A and C). Similarly, eEF2 from all tested **1** susceptible strains exhibit a Y249 whose hydroxy group may stabilize the ester (C-1′) or the aldehyde (C-1) of **1**. In contrast, in both resistant strains, Y249 is replaced by F249 lacking this important hydroxy group (Fig. 3A). Although other resistance mechanisms cannot be ruled out, the proposed binding pocket is fully consistent with the observed susceptibility profile. For a more comprehensive perspective, a phylogenetical survey of eEF2 – an indispensable component of the fungal translational machinery – revealed a high degree of conservation both in Mucoromycota ("lower fungi") and in Asco- and Basidiomycota ("higher fungi", *e.g.*, mushrooms) (ESI, Fig. S12†). Resistance towards $\Delta^{2,4}$-unsaturated melleolides is not congruent with a particular evolutionary group of fungi and may have evolved independently several times.

Arnamial inhibits the protein biosynthesis in *A. nidulans in vivo*

Unbiased target fishing and blind docking experiments suggested binding of $\Delta^{2,4}$-unsaturated melleolides to *A. nidulans* eEF2. This elongation factor is essential for GTP-dependent translocation of the ribosome during protein biosynthesis but not involved in other cellular processes. Therefore, if eEF2 is compromised due to small molecule binding, we expected selective inhibition of translation while transcription remains intact. To test if the translation, but not transcription, is inhibited *in vivo*, we constructed *A. nidulans* strain tMD03 that expresses a gene encoding the easily detectable red fluorescent protein mCherry under control of the strongly inducible promoter P*alcA* (Fig. 4A).[17] In contrast to other fluorescent proteins, mCherry is highly stable and supports a quick *in situ* read-out that does not require an addition of substrates.[18] Both wild type *A. nidulans* and the strain tMD03 are susceptible to the translational inhibitor hygromycin B (**8**), which is widely used as antifungal agent against *Aspergillus* species (Fig. 4B).[19,20] In contrast to wild type, tMD03 shows a strong fluorescent emission signal at 595 nm in the mycelium (Fig. 4A). As expected from prior studies on the *alcA* promoter,[21] production of mCherry is repressed by D-glucose, yet induced by ethanol, and its production rate can be monitored from cell-free protein extracts. When D-glucose is

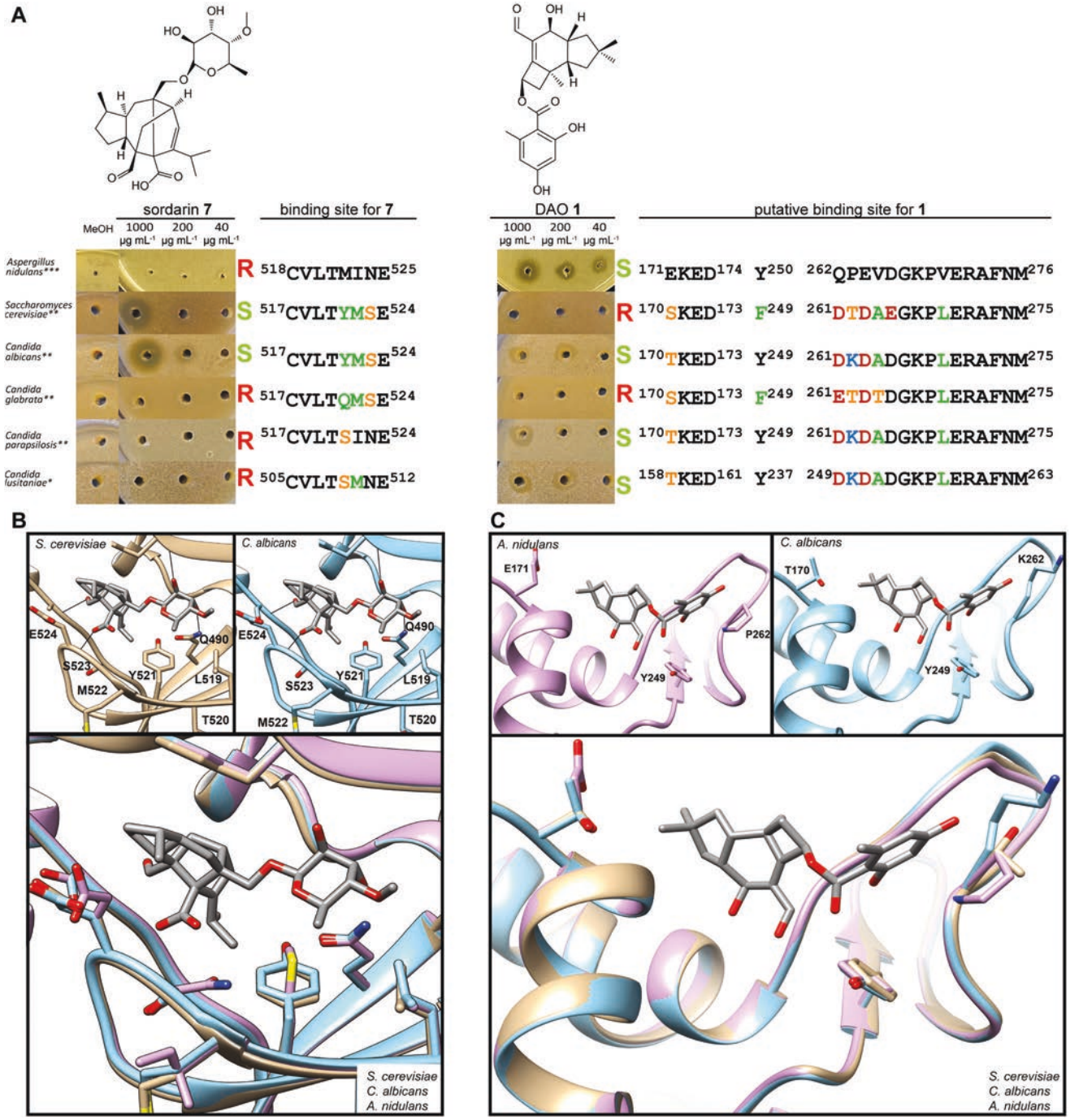

Fig. 3 Predicted binding sites of **7** and **1** in eEF2. (A) Structural formulas and antifungal activities of **7** and **1**. Susceptible and resistant strains are indicated by "S" and "R", respectively. *C. albicans* and *S. cerevisiae* are susceptible to **7**, while *C. glabrata*, *C. parapsilosis* and *C. lusitaniae* are resistant. Note the incongruent resistance pattern against **7** and **1**. Putative binding sites for **7** and **1** are indicated. Amino acid exchanges in comparison to *A. nidulans eEF2* are colour coded: red, acidic; blue, basic; green, hydrophobic; orange, hydrophilic. Initial optical densities (OD_{600}) of 0.02 (*) or 0.1 (**) were used for yeast strains. Plates with *A. nidulans* were initially inoculated with 1×10^6 conidia per mL (***). (B) Close-up views of the **7** binding pocket in eEF2 of *S. cerevisiae* (brown peptide backbone), *C. albicans* (blue), and *A. nidulans* (violet). **7** bound *S. cerevisiae* eEF2 (PDB ID:1N0U) was used to model the 3D structure of *C. albicans* eEF2 and *A. nidulans* eEF2. **7** was subsequently transferred to the binding pocket. Hydrogen bonding interactions are shown in black lines. Important residues of the binding pocket are shown in stick representations. eEF2 from *S. cerevisiae*, *C. albicans*, *A. nidulans* were superimposed onto each other. Residue positions that differ in eEF2 from *A. nidulans* (M522 and N524) in comparison to *S. cerevisiae* or *C. albicans* (both Y521 and S523) are depicted and may lead to **7** resistance. (C) Close-up view of the predicted **1** binding pocket by Achilles blind docking server with 3D structural model of *A. nidulans* eEF2 (violet peptide backbone). *C. albicans* (blue) and *S. cerevisiae* (PDB ID:1N0V, brown) protein structures were superimposed onto *A. nidulans* eEF2 to compare predicted binding pocket residues. Residues that might be crucial for **1** binding and that also differ between *A. nidulans*, *C. albicans*, and *S. cerevisiae* are shown in stick representations. Figures in panels 3B and 3C were generated with UCFSF Chimera.[32]

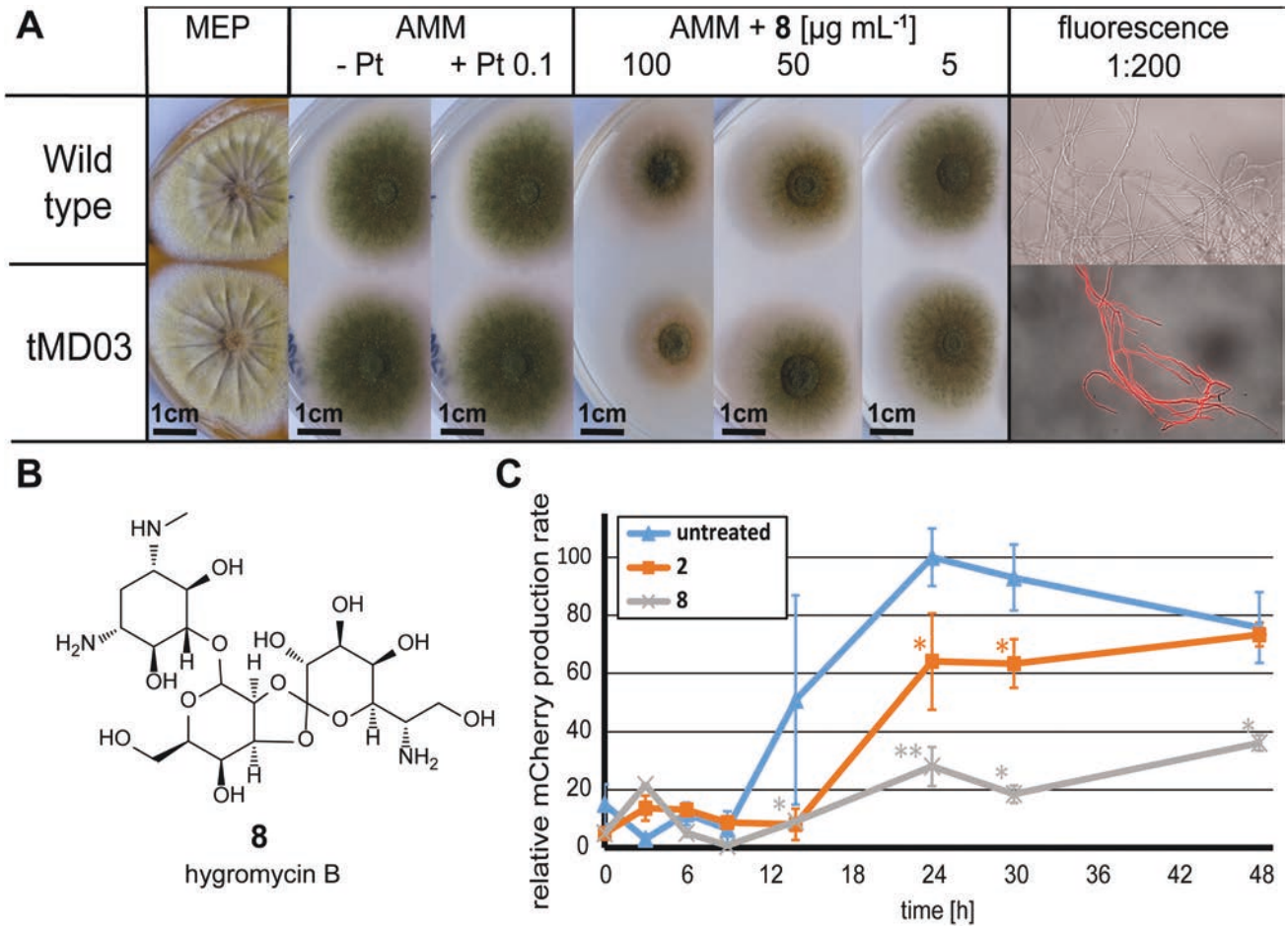

Fig. 4 *In vivo* inhibition of protein biosynthesis in *A. nidulans* FGSC A4_tMD03. (A) Growth comparison between tMD03 and its parental strain FGSC A4. tMD03 is pyrithiamine (Pt) resistant but it is susceptible towards the translational inhibitor hygromycin B (**8**) as the wild type. Note that the mutant produces the red fluorescent protein mCherry after induction with ethanol (right panel). (B) Chemical structure of **8**. (C) Decreased production rates of mCherry by **2** and **8** treatments in *A. nidulans*. tMD03 was pre-cultivated in 100 mM ethanol and 10 mM glucose and subsequently 10 µg mL^{-1} **2** or 10 µg mL^{-1} **8**. *P*-Value significance levels are given with *($p < 0.05$) and **($p < 0.01$).

completely exhausted, the fungus metabolises ethanol as carbon source which then induces transgene expression. Optimum mCherry production was observed in an autoinduction medium with 10 mM D-glucose and 100 mM ethanol (ESI, Fig. S13†). Both **1** and **2** are antifungally active, share an identical pharmacophore and a near-identical overall structure (Fig. 1). However, for this subsequent *in vivo* translation inhibition assay, only **2** was obtained in sufficient quantities from *A. mellea* cultures in order to perform the experiment. After pre-cultivation of the test strain for 16 h, translation was inhibited by adding 10 µg mL^{-1} **2** or 25 µg mL^{-1} **8** (positive control) (Fig. 4C). Untreated mycelium served as internal fluorescence reference. The fluorescent signals of the protein crude extracts were determined over a total cultivation time of 48 h. The treatment with both inhibitors did not alter the expression levels of the *mCherry* gene or the intrinsic *alcA* gene, as determined by qRT-PCR (ESI, Fig. S14†). However, at early stages of treatment, either inhibitor induced the expression of genes encoding ribosomal structural proteins 2-fold, most likely to compensate translational inhibition (ESI, Fig. S14†). In the untreated control, mCherry production began 15 h after inoculation and reached its maximum after 24 h. In contrast, cultures treated with **8** showed a weak, slowly increasing fluorescent signal (20–40% of the control), indicating a strong translational inhibition. This is in agreement with the described mode of action of **8** to inhibit peptide chain elongation by preventing eEF2-dependent translocation on eukaryotic ribosomes.[20] mCherry production in cultures treated with **2** was moderately, but significantly inhibited (40–80%). After 48 h, the fluorescence reached values similar to those of the untreated control. Treatment with 2 µg mL^{-1} of **2** did not inhibit the translation *in vivo* (ESI, Fig. S15†). These results indicate that **2** exerts transient effects, probably as it acts as a fungistatic agent rather than representing a fungicide, such as **8**, under the tested conditions. This is supported by the observation that cultures treated with **1** or **2** recover over time (ESI, Fig. S16†). However, under natural conditions, *A. mellea* produces a complex mixture of melleolides which may increase or prolong antifun-

gal properties.[5] Resistance to fungicidal drugs, such as echinocandins or 5-flucytosine, usually requires multiple cell generations and is a long-term resistance mechanism.[12] In contrast, resistance against fungistatic azoles is mediated by over-production of the target enzyme, the lanosterol 14-α-demethylase Erg11 or by efficient drug efflux mediated by multi-drug transporters.[12] However, in the case of **2**, the expression of target protein eEF2 is not affected (ESI, Fig. S14†). Therefore, the observed recovery after initial inhibition may reflect increasing clearance from *Aspergillus* cells or, alternatively, intracellular modification to inactivate the pharmacophore.

Conclusions

Exploiting an unbiased target fishing approach using a bioactive melleolide as bait, we have identified eEF2 as molecular target for one of the largest families of fungal metabolites produced by the globally distributed fungal genus *Armillaria*. Our work has elucidated the mechanism of the antifungal activity of the melleolides that is conferred by interference with eEF2-mediated translation. A binding site dissimilar from that of the protein biosynthesis inhibitor **7** was identified as most plausible area of interaction, which underscores translational elongation as a valid antifungal drug target. This work at the interface of chemistry and biology should encourage further research on the melleolides for pharmaceutical purposes. As *Armillaria* is a long-lived organism competing with other fungi for nutritional supply in its natural habitat, antifungal melleolides represent an alternative, but effective defence mechanism compared to known antifungals. Therefore, our results also contribute to the chemical ecology of this important pathogen.

Experimental

Materials, and general microbiological procedures

Chemicals, reagents, solvents, and media components were purchased from Carl Roth, Sigma-Aldrich, and VWR. *Armillaria mellea* FR-P75 was cultured in glucose minimal medium (GMM).[10] *A. nidulans* FGSC A4 and tMD03 were maintained on *Aspergillus* minimal medium (AMM) agar plates[22] or on malt extract – peptone (MEP) solid medium (per litre: 30 g malt extract, 3 g soy peptone, 1.8% agar, pH 5.6 with acetic acid). Antifungal agents were **8** at 5, 10, or 100 μg mL^{-1}, or pyrithiamine hydrobromide at 0.1 μg mL^{-1}. Plasmid propagation was carried out in *E. coli* XL1 blue strains cultivated in LB medium supplemented with 50 μg mL^{-1} carbenicillin.

Preparative and analytical chemistry

Metabolite extraction and isolation. 16 L of culture broth from *A. mellea* was extracted as described.[10] The crude extract was initially fractionated *via* solid phase extraction on a SepPak Vac C-18, 35 cc, 10 g column (Waters). A step gradient (40, 60, 80, and 100% methanol) was applied that yielded four fractions which were analyzed by UHPLC-MS (method 1). **1** and **2** were detected in the 80% fraction by MS (*m*/*z* 423 and *m*/*z* 461 $[M + Na]^+$, respectively), which were further separated by preparative HPLC (method 2). Fractions were again analysed by method 1. Final work-up of **1**- and **2**-containing fractions was accomplished by semi-preparative HPLC (method 3). Structures of purified **1** and **2** were confirmed by NMR spectroscopy in comparison to described data.[6]

HPLC and LC-MS methods. Method 1 was carried out on an Agilent 1290 Infinity II chromatograph equipped with a Zorbax Eclipse C18 2.1 × 50 mm column (1.8 μm particle size) and interfaced to a 6130 quadrupole mass spectrometer using electrospray ionization for molecular ionization. The flow was 1 mL min^{-1} using 0.1% formic acid in water (solvent A) and acetonitrile (ACN, solvent B). Initially, 5% B was held for 2 min, then increased to 100% B within 5 min.

Method 2 was run on a preparative Agilent 1260 Infinity HPLC instrument, connected to a Phenomenex Luna C18 column (250 × 21.2 mm, 10 μm particle size), using water (A) and ACN (B). Initially, 50% B was held for 2 min, then increased to 85%, held for 2 min, again increased within 9 min to 100%. The flow rate was 20 mL min^{-1}.

Semi-preparative methods (methods 3 through 7) were performed on an Agilent 1200 instrument using a Zorbax Eclipse column (C18, 9.4 × 250 mm; 10 μm particle size). Method 3 was run with water (A) and ACN (B) at a flow rate of 1.7 mL min^{-1} and with a Zorbax Eclipse Plus column (C18, 9.4 × 250 mm; 5 μm particle size). Methods 4–7 were run with 0.1% trifluoroacetic acid in water (A) and ACN (B) at a flow of 4 mL min^{-1}.

Method 3 included an isocratic run of 85% B for 25 min, followed by an increase to 100% within 2 min. Method 4 was a gradient of initially 10% B for 1 min, linear increase to 40% within 2 min and to 90% in further 15 min, then held for 4 min, and increased to 100% B within 1 min. Method 5 was initially 10% B for 1 min, linear increase to 65% within 2 min and to 90% in further 13 min, then held for 4 min, increased to 100% B within 4 min. Method 6 was initially 10% of B for 1 min, linear increase to 70% within 2 min, further increase to 90% within 13 min and to 100% B in 0.5 min. Method 7 was 5% B for 1 min, linear increase to 20% in 4 min and further to 90% within 5 min, terminal linear increase to 100% in 1 min. High resolution mass spectrometry was performed on a Q Exactive Plus mass spectrometer (Thermo Scientific).

Structure elucidation. One- and two-dimensional NMR spectra of purified compounds were recorded in CD_3OD on Bruker Avance III spectrometers, operating at 500 and 600 MHz (^1H spectra) or at 125 and 150 MHz (^{13}C spectra), respectively. Chemical shifts were referenced to residual CH_3OH (δ_H 3.31 ppm; δ_C 49.1 ppm).

MALDI-TOF-based peptide analysis. Peptide samples embedded in an α-cyano-4-hydroxycinnamic acid (HCCA) matrix for peptides (Bruker) were measured on a Bruker Ultraflextreme instrument using a Smartbeam II Laser and MTP Standard AnchorChip Target (800 μm) in positive reflector-mode (MS and MS-MS).

Chemical synthesis

Synthesis of 5. One equivalent hexynoic acid (7.1 μmol; 0.87 mg) and 1.05 equivalents of **1** (7.5 μmol; 3 mg) were mixed with 1.2 equivalents of *N*-(3-dimethylaminopropyl)-*N*′-ethylcarbodiimide (EDC) (8.5 μmol; 0.46 mg) in water-free dichloromethane (DCM). The solvent was evaporated to dryness and 0.5 equivalents of Hünig's base (3.6 μmol; 0.46 mg) in 300 μL dried DCM were subsequently added. The mixture was stirred at room temperature for 67 h and the final product (**4**) was purified *via* HPLC method 4. One equivalent of **4** (3.2 μmol; 1.59 mg) and 1.2 equivalents of azide-PEG_3-biotin (Jena Bioscience) (3.9 μmol; 1.72 mg) were mixed in a final volume of 400 μL DCM. 5 μL of 0.5 M $CuSO_4$ and 15 μL of 0.5 M sodium ascorbate solution were added every 24 h while stirring. After 62 h, **5** was purified *via* HPLC method 5. The structure of **5** was elucidated by NMR spectroscopy and high resolution mass spectrometry (ESI, Fig. S1–S5, Table S1†).

Synthesis of 6. A reaction mixture with one equivalent of *n*-butyl 4-hydroxybenzoate (51.5 μmol; 10 mg), 1.15 equivalents of 5-hexynoic acid (59.2 μmol; 6.64 mg), 0.7 equivalents of trimethylamine (36.0 μmol; 2.55 mg) and 1.15 equivalents of EDC (59.2 μmol; 11.35 mg) was stirred in a total volume of 500 μL DCM for 72 h at ambient temperature. The reaction product (intermediate **9**, ESI, Scheme S1†) was purified *via* HPLC method 6. For the final click reaction, one equivalent of **9** (17.3 μmol; 5 mg) was added to 1.15 equivalents of azide-PEG_3-biotin (19.9 μmol; 8.87 mg) with 8 μL of a 0.5 M $CuSO_4$ solution and 50 μL of a 0.5 M sodium ascorbate solution in a total volume of 370 μL DCM. After incubation for 36 h at ambient temperature, purification carried out *via* HPLC method 7 resulted in product **6**. The structure of **6** was elucidated by NMR spectroscopy and high resolution mass spectrometry (ESI, Fig. S6–S10, Table S1†). The reaction is shown in Scheme S1 (ESI†).

Cell biology

Production of cell lysate. *A. nidulans* FGSC A4 at a final concentration of 1×10^6 conidia per mL was inoculated in 50 mL of liquid AMM[22] supplemented with 0.1% (m/v) yeast extract. After incubation at 180 rpm and 37 °C for 16 h, the mycelium was filtered and washed with phosphate buffered saline (PBS; 137 mM NaCl, 2.7 mM KCl, 10 mM Na_2HPO_4, 1.8 mM KH_2PO_4, pH 7.4), supplemented with 0.1% D-glucose. The mycelium was frozen in liquid nitrogen, ground to a powder, and resuspended in 10 ml PBS. After centrifugation (1 h, 10 621*g*, 4 °C) and size exclusion filtration (Amicon, 10 kDa cut off, 550*g*, 20 min, 4 °C), the supernatant was used for biotin/streptavidin affinity chromatography (below).

Affinity chromatography. Affinity chromatography was performed according to the protocol of the Pierce Pull-Down Biotinylated Protein:Protein Interaction Kit (Thermo Scientific). In brief, 100 μL of streptavidin beads were washed with Tris-buffered saline (TBS; 25 mM Tris-HCl, 150 mM NaCl, pH 7.0) and pretreated for 30 min either with probe **5**, control **6**, or equivalent amounts of DMSO as negative control. After blocking with biotin-blocking solution (Thermo Scientific), the beads were washed with TBS and then incubated with 200 μL cell lysate (1–10 mg mL^{-1} protein) for 16 h at 4 °C. After a subsequent wash step with TBS, proteins were eluted with 50 μL of SDS loading buffer (50 mM Tris-HCl, 2% SDS, 10% glycerol, 1% β-mercaptoethanol, 12.5 mM EDTA, 0.02% bromophenol blue, pH 6.8). Samples were loaded on a 10% SDS polyacrylamide gel, electrophoresed, and subsequently stained with Coomassie Brilliant Blue.[23] For further protein identification, protein bands were cut out with a scalpel, digested with trypsin as described,[24] and subjected to MALDI-TOF peptide analysis.

Western blot. Proteins separated by SDS polyacrylamide gels were transferred to a nitrocellulose membrane as described.[25,26] The membrane was stained with Ponceau red and washed with water, TBS with 0.1% (v/v) tween 20, and again with water. The membrane was blocked by 5% milk powder in TBS for 1 h. The primary antibody (rabbit anti-human eEF2 antibody; Cell Signaling) was diluted 1 : 1000 in TBS + 5% milk powder and applied to the membrane. After incubation overnight at 4 °C, the membrane was washed three times with 0.1% (v/v) tween 20 in TBS, followed by a final wash with TBS for 5 min. The secondary antibody (IRDye® 800CW goat anti-rabbit IgG, Li-Cor) was diluted 1 : 10 000 with 5% milk powder in TBS and applied to the membrane. After incubation for 30 min, the membrane was washed three times with TBS + 0.1% (v/v) Tween 20 for 5 min and dried at 37 °C prior to detection of the fluorescent signal on an Odyssey CLx Imaging System (excitation 778 nm, emission 795 nm).

Antifungal assays. Antifungal activity tests against yeast strains were performed with *Candida albicans* SC5314, *Saccharomyces cerevisiae* ATCC9763, *Candida glabrata* ATCC2001, *Candida parapsilosis* GA1-wt, and *Candida lusitaniae* 10-09-05-73/5169.[13] Prior to pouring plates, 50 °C warm liquid YPD agar was inoculated with an overnight YPD culture of the respective strain to a final OD_{600} = 0.1 or OD_{600} = 0.02. Holes were punched with a cork borer, and 20 μL of an **1** solution (in methanol) or **7** (aqueous) at a concentration of 1000, 200, or 40 μg mL^{-1} were applied. Pure methanol served as negative control. Plates were incubated for 24 h at 30 °C.

Molecular biology

Construction of *Aspergillus nidulans* tMD03. The *Magnaporthe oryzae* pRP27 promoter in plasmid pMS01 containing the mCherry protein coding sequence under control of the RP27 promoter was replaced by the ethanol inducible *A. nidulans alcA* promoter (P*alcA*) using the Fast Cloning method.[27] P*alcA* was amplified from genomic DNA of *A. nidulans* FGSCA4 using oligonucleotide primers oMG234 und oMG235 (Table 1), the vector backbone was amplified from pMS01 with primers oMG233 and oMG170 using Phusion DNA polymerase according to the supplier's protocol (Thermo Scientific). Both fragments were purified, mixed in an equimolar ratio and used for transformation of. *E. coli* XL1 blue. 10 μg of the resulting plasmid pMD03 (containing the mCherry gene downstream of the *alcA* promoter) were used for

Table 1 Oligonucleotides used in this study. Underlined: Overlapping flanks to the vector backbone

Oligonucleotide	5′–3′-Sequence	Target
oMG234	TTACGCCGGCGCGCCGTAG ATATTTTCGAAGGGATTC	P*alcA* (FGSCA4 gDNA)
oMG235	GCCCTTGCTCACCATTTTGA GGCGAGGTGATAGGATTG	P*alcA* (FGSCA4 gDNA)
oMG170	ATGGTGAGCAAGGGCGAGGAG	pMS01
oMG233	GGCGCGCCGGCGTAATCATGGTC	pMS01
oMG171	TTACTTGTACAGCTCGTCCATGC	*mCherry*
oMD01	CCTGAAGGGCGAGATCAAGC	*mCherry* (qPCR)
oMD02	GTTCCACGATGGTGTAGTCC	*mCherry* (qPCR)
oMD03	CTTTCGCTGAGGACGACTGG	*enoA* (qPCR)
oMD04	CTTGAGAAGGAGAGCGTTGC	*enoA* (qPCR)
oMD05	TACGACCAGATCAAGGATGC	*gpdA* (qPCR)
oMD06	CATCGAAGATGGAAGAGCGG	*gpdA* (qPCR)
oMD09	GTTGAGATGCACCACCAGC	*eef1α* (qPCR)
oMD10	CCTGACCAGGGTGGTTAAGG	*eef1α* (qPCR)
oMD13	GACGAGAAGGACCTTACTGG	*eef2* (qPCR)
oMD14	GTCACGGATACCAGCGAAGG	*eef2* (qPCR)
oMD17	GTGAGCCTCACTCTCTGCC	*40sS2* (qPCR)
oMD18	TGTAGGCATCCTGGACACC	*40sS2* (qPCR)
oMD19	GCTCAACCTCCTTCAACTCG	*60sL4* (qPCR)
oMD20	GAAGAGTTGATAAGGCGGGC	*60sL4* (qPCR)
oMD21	TCAGAGAAGCCCTTCCAGC	*alcA* (qPCR)
oMD22	CGAAGAAGTCCAGAGCCTCG	*alcA* (qPCR)

transformation of *A. nidulans* FGSC A4 wild type according to a published procedure.[28] Transformants were streaked out on AMM[22] plates containing 0.1 μg ml^{-1} pyrithiamine and were then checked by PCR using primers oMG234 and oMG171. Prior to the translational inhibition assay, 40 transformants were screened by fluorescence microscopy (Zeiss Imager M2 AXIO, excitation 550 ± 25 nm, emission 605 ± 70 nm, laserlight irradiation time 2000 ms, brightfield 3 ms) to identify the transformant with strongest fluorescence intensity (tMD03). The wild type served as control.

Quantitative real time-PCR (qRT-PCR). RNA from mycelium of *A. nidulans* tMD03 grown for 0, 14 and 36 h in the presence of translation inhibitors (see below) was isolated using the SV Total RNA Isolation System (Promega). Genomic DNA was digested by Baseline ZERO DNase (Biozyme), and 500 ng RNA was reverse transcribed to cDNA by RevertAid Reverse Transcriptase (Thermo Scientific). To assess transcription efficiency, qPCR experiments were performed with a QuantStudio 3 thermal cycler (Thermo Scientific) using the primer in Table 1. Expression levels were normalized using *enoA* and *gpdA* transcription levels as reference.[29] To determine primer efficiencies, 12 μL of MyTaq™ HS mix (Bioline) were mixed with 1 μL of Biotium EvaGreen® Dye (20× stock solution, 25 μM) for each test reaction. 1 μL of water and 4 μL of a mixture of corresponding oligonucleotide primer pairs (forward/reverse; 10 μM), were added, as well as 2 μL of a 1 : 10 dilution of template cDNA.

Translation inhibition of *A. nidulans*. AMM plates containing 5, 10, or 100 μg mL^{-1} **8** and MEP plates (positive control) were inoculated with 2 × 10^5 conidia and incubated for 72 h at 37 °C.

For translation inhibition in liquid media, 100 mL AMM containing 10 mM D-glucose and 100 mM ethanol were inoculated with *A. nidulans* FGSC A4 (wild type, fluorescent blank control) or tMD03 (1 × 10^6 conidia per mL) and pre-incubated for 16 h at 37 °C and 180 rpm. After adding 50 mM ethanol, translation was inhibited by addition of 25 μg mL^{-1} **8**, or 2 μg mL^{-1} or 10 μg mL^{-1} **2** (solved in methanol). Pure methanol served as negative control. After further cultivation at 37 °C, 180 rpm for 0, 3, 6, 9, 14, 24, 30, and 48 h, mycelium was harvested and lyophilised. 10–20 mg mycelium was suspended in 500 μL of LET buffer (100 mM LiCl, 20 mM EDTA, 10 mM Tris HCl, pH 8.0) and ground with 0.25–0.5 mm glass beads for 4.5 m s^{-1} for 60 s in a cell disruptor. The mycelium was removed by centrifugation at 16 595*g* for 30 min. 150 μL supernatant or dilutions thereof (1 : 2 and 1 : 4) were transferred to black 96-well plates. Fluorescence was detected (excitation at 544 nm; emission at 595 nm) with a BMG FluoStar Galaxy microplate reader (gain 80). Relative fluorescence (RF) was determined as follows:

$$\mathrm{RF} = \frac{\dfrac{\mathrm{fluorescence(tMD03, treated)}}{\mathrm{biomass(tMD03, treated)}} - \dfrac{\mathrm{fluorescence(WT)}}{\mathrm{biomass(WT)}}}{\dfrac{\mathrm{fluorescence(tMD03, control)}}{\mathrm{biomass(tMD03, control)}} - \dfrac{\mathrm{fluorescence(WT)}}{\mathrm{biomass(WT)}}}$$

In silico modelling and blind docking studies

Molecular fingerprint (FP) comparison between 1 and 7. Simplified molecular-input line-entries (SMILE) for **1** (CID 51351608) and **7** (CID 485851) were obtained from the Pubchem database. SMILE strings were encoded into Morgan and 2D pharmacophore FP for structural comparisons.[30] Morgan FP considers circular neighbourhood of atoms while 2D pharmacophore FP combines two-dimensional topological distances of atoms with chemical features. Morgan FPs with feature-based atomic environment definitions were used. After encoding them into FPs Tanimoto and Dice similarities were calculated, which are listed in Table S4 (ESI†). Tanimoto (Jaccard) and Dice are widely used similarity coefficients to compare molecular structures which take into account shared substructures or chemical features.

3D structural modelling of *A. nidulans* and *C. albicans* eEF2. Template based structural modelling of *A. nidulans* and *C. albicans* eEF2 was accomplished using MODELLER (mod9.21).[31] Since eEFs are highly conserved, *S. cerevisiae* eEF2 crystal structures (PDB ID 1N0U & 1N0V) were selected as templates for the modelling purpose. PDB ID:1N0U structure harbours **7** in the binding pocket, hence it was transferred to modelled *C. albicans* eEF2 for binding interaction comparisons. The *A. nidulans* eEF2 3D model obtained using PDB ID:1N0V (**7** unbound structure) was subsequently used as an input for blind docking studies for **1**. Figures of 3D structural models were generated with UCSF Chimera.[32]

Prediction of binding pockets for 1 on *A. nidulans* eEF2 by blind docking. 3D coordinates of model constructed through comparative modelling (PDB ID:1N0V) were used as an input for blind docking servers. The mol2 formatted structure of **1** from Pubchem and *A. nidulans* eEF2 model were submitted to the Achilles blind docking server (http://bio-hpc.ucam.edu/

achilles/).[33] Binding poses for **1** were rank-ordered based upon their predicted free energies of binding. Top seven binding poses with corresponding binding residues showing lowest binding free energies and high number of clustered poses are listed in Table S5 (ESI†).

Statistics. Significance levels in translational inhibition assays were estimated by the Wilcoxon–Mann–Whitney (WMW) test.[34] Significance levels of expression levels obtained from qRT-PCR analyses were calculated using the independent two-sample student's *t*-test.

Conflicts of interest

There are no conflicts of interest to declare.

Acknowledgements

Plasmid pMS01 was kindly provided by M. Samalova (Central European Institute of Technology, Brno, Czech Republic). Yeast strains for antifungal tests were kindly provided by S. Brunke (Leibniz Institute for Natural Product Research and Infection Biology – Hans Knöll Institute (HKI), Jena). The authors are grateful to A. Perner and H. Heinecke for recording mass and NMR spectra, respectively, and to T. Kindel (all HKI Jena) for supporting MALDI-TOF-based peptide analyses. M. D. and M. G. thank N. Stefani and T. Heinekamp (both HKI, Jena) for introduction in fluorescence microscopy. The groups of O. W., C. H., and D. H. are supported by the DFG Collaborative Research Centre SFB1127 (ChemBioSys).

References

1 K. Baumgartner, M. P. Coetzee and D. Hoffmeister, *Mol. Plant Pathol.*, 2011, **12**, 515–534.
2 M. Misiek, J. Williams, K. Schmich, W. Huttel, I. Merfort, C. E. Salomon, C. C. Aldrich and D. Hoffmeister, *J. Nat. Prod.*, 2009, **72**, 1888–1891.
3 I. Schmitt, S. Kautz and H. T. Lumbsch, *Mycol. Res.*, 2008, **112**, 289–296.
4 W. R. Abraham, *Curr. Med. Chem.*, 2001, **8**, 583–606.
5 M. Misiek and D. Hoffmeister, *Mycol. Prog.*, 2012, **11**, 7–15.
6 M. Bohnert, S. Miethbauer, H. M. Dahse, J. Ziemen, M. Nett and D. Hoffmeister, *Bioorg. Med. Chem. Lett.*, 2011, **21**, 2003–2006.
7 M. Bohnert, O. Scherer, K. Wiechmann, S. König, H. M. Dahse, D. Hoffmeister and O. Werz, *Bioorg. Med. Chem.*, 2014, **22**, 3856–3861.
8 H. Kobori, A. Sekiya, T. Suzuki, J. H. Choi, H. Hirai and H. Kawagishi, *J. Nat. Prod.*, 2015, **78**, 163–167.
9 S. König, E. Romp, V. Krauth, M. Ruhl, M. Dörfer, S. Liening, B. Hofmann, A. K. Hafner, D. Steinhilber, M. Karas, U. Garscha, D. Hoffmeister and O. Werz, *Cell Chem. Biol.*, 2019, **26**, 60–70.
10 M. Bohnert, H. W. Nützmann, V. Schroeckh, F. Horn, H. M. Dahse, A. A. Brakhage and D. Hoffmeister, *Phytochemistry*, 2014, **105**, 101–108.
11 L. Capa, A. Mendoza, J. L. Lavandera, F. Gómez de las Heras and J. F. García-Bustos, *Antimicrob. Agents Chemother.*, 1998, **42**, 2694–2699.
12 A. Srinivasan, J. L. Lopez-Ribot and A. K. Ramasubramanian, *Drug Discovery Today: Technol.*, 2014, **11**, 65–71.
13 M. Shastry, J. Nielsen, T. Ku, M. J. Hsu, P. Liberator, J. Anderson, D. Schmatz and M. C. Justice, *Microbiology*, 2001, **147**, 383–390.
14 C. M. Spahn, M. G. Gomez-Lorenzo, R. A. Grassucci, R. Jorgensen, G. R. Andersen, R. Beckmann, P. A. Penczek, J. P. Ballesta and J. Frank, *EMBO J.*, 2004, **23**, 1008–1019.
15 J. M. Dominguez, V. A. Kelly, O. S. Kinsman, M. S. Marriott, F. Gomez de las Heras and J. J. Martin, *Antimicrob. Agents Chemother.*, 1998, **42**, 2274–2278.
16 M. G. Gomez-Lorenzo, C. M. T. Spahn, R. K. Agrawal, R. A. Grassucci, P. Penczek, K. Chakraburtty, J. P. G. Ballesta, J. L. Lavandera, J. F. Garcia-Bustos and J. Frank, *EMBO J.*, 2000, **19**, 2710–2718.
17 Y. M. Chiang, C. E. Oakley, M. Ahuja, R. Entwistle, A. Schultz, S. L. Chang, C. T. Sung, C. C. Wang and B. R. Oakley, *J. Am. Chem. Soc.*, 2013, **135**, 7720–7731.
18 A. P. Siegel, M. A. Baird, M. W. Davidson and R. N. Day, *Int. J. Mol. Sci.*, 2013, **14**, 20340–20358.
19 P. J. Punt and C. A. van den Hondel, *Methods Enzymol.*, 1992, **216**, 447–457.
20 A. González, A. Jiménez, D. Vázquez, J. E. Davies and D. Schindler, *Biochim. Biophys. Acta*, 1978, **521**, 459–469.
21 C. Bailey and H. N. Arst Jr., *Eur. J. Biochem.*, 1975, **51**, 573–577.
22 G. Pontecorvo, J. A. Roper, L. M. Hemmons, K. D. Macdonald and A. W. Bufton, *Adv. Genet.*, 1953, **5**, 141–238.
23 D. H. Kang, Y. S. Gho, M. K. Suh and C. H. Kang, *Bull. Korean Chem. Soc.*, 2002, **23**, 1511–1512.
24 A. Shevchenko, H. Tomas, J. Havlis, J. V. Olsen and M. Mann, *Nat. Protoc.*, 2006, **1**, 2856–2860.
25 O. Salinovich and R. C. Montelaro, *Anal. Biochem.*, 1986, **156**, 341–347.
26 H. Towbin, T. Staehelin and J. Gordon, *Proc. Natl. Acad. Sci. U. S. A.*, 1979, **76**, 4350–4354.
27 C. Li, A. Wen, B. Shen, J. Lu, Y. Huang and Y. Chang, *BMC Biotechnol.*, 2011, **11**, 92.
28 E. Brandenburger, M. Gressler, R. Leonhardt, G. Lackner, A. Habel, C. Hertweck, M. Brock and D. Hoffmeister, *Appl. Environ. Microbiol.*, 2017, **83**, e01478-17.
29 M. Gressler, F. Meyer, D. Heine, P. Hortschansky, C. Hertweck and M. Brock, *eLife*, 2015, **4**.
30 A. Gobbi and D. Poppinger, *Biotechnol. Bioeng.*, 1998, **61**, 47–54.
31 N. Eswar, B. Webb, M. A. Marti-Renom, M. S. Madhusudhan, D. Eramian, M. Y. Shen, U. Pieper and A. Sali, *Curr Protoc Bioinformatics*, 2006, ch. 5, unit-5.6.

32 E. F. Pettersen, T. D. Goddard, C. C. Huang, G. S. Couch, D. M. Greenblatt, E. C. Meng and T. E. Ferrin, *J. Comput. Chem.*, 2004, **25**, 1605–1612.
33 I. Sanchez-Linares, H. Perez-Sanchez, J. M. Cecilia and J. M. Garcia, *BMC Bioinf.*, 2012, **13**(Suppl 14), S13.
34 A. Marx, C. Backes, E. Meese, H. P. Lenhof and A. Keller, *Genomics, Proteomics Bioinf.*, 2016, **14**, 55–61.

Melleolides impact fungal translation via Elongation Factor 2

Maximilian Dörfer,[a] Daniel Heine,[b] Stefanie König,[c] Sagar Gore,[d] Oliver Werz,[c] Christian Hertweck,[b] Markus Gressler,[a] Dirk Hoffmeister[a,*]

a Department Pharmaceutical Microbiology at the Hans Knöll Institute, Friedrich-Schiller-University, Beutenbergstrasse 11a, 07745 Jena, Germany
b Department Biomolecular Chemistry, Leibniz Institute for Natural Product Chemistry and Infection Biology - Hans Knöll Institute, Beutenbergstrasse 11a, 07745 Jena, Germany
c Department Pharmaceutical and Medicinal Chemistry, Friedrich-Schiller-University Jena, Philosophenweg 14, 07743 Jena, Germany
d Department Systems Biology and Bioinformatics, Leibniz Institute for Natural Product Chemistry and Infection Biology - Hans Knöll Institute, Beutenbergstrasse 11a, 07745 Jena, Germany
*Correspondence: Dirk Hoffmeister, Markus Gressler, Department Pharmaceutical Microbiology at the Hans Knöll Institute, Friedrich-Schiller-University, Beutenbergstrasse 11a, 07745 Jena, Germany; Phone: +49-3641-949851; Fax: +49-3641-949852; e-mail: dirk.hoffmeister@hki-jena.de, markus.gressler@hki-jena.de.

Electronic supplementary information

Table of contents

Table S1. NMR data of **5** in CD_3OD. [a]3-OH and 3'-OH not observed; [b] not assigned due to signal overlap.

no.	δ_C, type	δ_H (*J* in Hz)	HMBC
1	192.6, CH	9.86 s	1, 2, 3, 4
2	134.6, qC		
3	73.3, CH[a]	4.31 dd (2.3; 7.3)	2, 4, 9
4	169.5, qC		
5	71.3, CH	6.33 m	2, 4, 6
6	46.3, CH_2	a: 2.15 dd (5.8; 9.4) b: 2.74 dd (6.9; 9.3)	b: 4, 8, (1') a: 5, 6
7	41.1, qC		
8	21.3, CH_3	1.20	4, 6, 7
9	47.6, CH	2.48 m	8, (3), (6), (11)
10	41.9, CH_2	1.53-1.42 m	10, 13, 14, 15
11	40.6, qC		
12	47.4, CH_2	a: 1.24 dd (9.0; 10.3) b: 1.84 m	b: 9, 15 a: 3, 15
13	50.2, CH	2.34-2.38 m	3, 12
14	29.9, CH_3	1.12 s	9, 11, 15
15	27.6, CH_3	1.00 s	9, 11, 14
1'	169.8, qC		
2'	114.9, qC		
3'	161.8, qC[a]		
4'	108.8, CH	6.52 d (2.0)	3', 5', 6'
5'	155.3, qC		
6'	116.7, CH	6.49 d (1.9)	2', 4', 5', 8'
7'	142.4, qC		
8'	22.3, CH_3	2.40 s	6', 7'
1''	172.7, qC		
2"	34.2, CH_2	2.61	1", 3", 4"
3"	25.5, CH_2	2.07	1", 2", 4", 5"
4"	25.6, CH_2	2.81	2", 3", 5", 6"
5"	147.9, qC		
6"	124.4, CH	7.83 s	
I	41.2, CH_2	a) 2.66 m b) 2.88 dd (4.3; 10.6)	II, VII, VI
II	61.6, CH	4.45 m	I, IV, VII
III	NH	6.20	
IV	166.1, qC		
V	NH	6.16	
VI	63.3, CH	4.25 m	I, IV, VII
VII	57.0, CH	3.15 m	IX, X
VIII	26.8, CH_2	1.62 m	VI, IX, X, XI
IX	29.8, CH_2	1.40 m	VII, XI
X	29.5, CH_2	1.67-1.72 m	IX, (VII)
XI	36.7, CH_2	2.18 t (6.0)	
XII	176.1, qC		
XIII	NH	8.45	
XIV	40.3, CH_2	3.31 m	XVI-XIX, XII
XV	70.6, CH_2	3.48 t(4.63)	XIV, XVI-XIX
XVI[b]			
XVII[b]	71.5 – 71.2, 4 x CH_2	3.54-3.59 m	XVI-XIX
XVIII[b]			
XIX[b]			
XX	70.4, CH_2	3.85 m	XXI, XIX
XXI	51.4, CH_2	4.55 m	XX, C6"

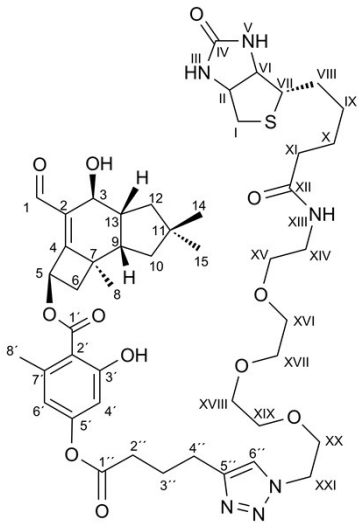

Table S2. NMR data of **6** in CD_3OD. [a]not assigned due to signal overlap.

no.	δ_C, type	δ_H (*J* in Hz)	HMBC
1	14.1, CH_3	0.98 t (7.4)	2, 3
2	19.8, CH_2	1.47 sext (7.5)	3, 4, 1
3	31.3, CH_2	1.74 quin (6.6)	1, 2, 4
4	65.5, CH_2	4.30 t (6.6)	2, 3, 1'
1'	166.3, qC		
2'	128.8, qC		
3'	131.5, CH	8.05 d (8.7)	7', 6', 4', 5', 2'
4'	122.2, CH	7.17 d (8.7)	6', 2', 5', 1', (1'')
5'	154.9, qC		
6'	122.2, CH	7.17 d (8.7)	4', 2', 5', 1', (1'')
7'	131.5, HC	8.05 d (8.7)	3', 6', 4', 5' 2'
8'			
1''	172.0, qC		
2"	34.1, CH_2	2.67 t (7.5)	1", 3", 4"
3"	25.1, CH_2	2.12 m	1", 2", 4", 5"
4"	25.3, CH_2	2.83 t (7.5)	2", 3", 6"
5"	147.3, qC		
6"	122.7, CH	7.55 s	5''
I	41.1, CH_2	a) 2.71 s b) 2.90 dd (5.1; 7.8)	II, VI, VII II
II	60.7, CH	4.47 m	I, VII, IV (VI)
III	NH	6.02	
IV	164.1, qC		
V	NH	6. 2	
VI	62.3, CH	4.30 m	I, VII, IV, (II)
VII	56.0, CH	3.15 dt (4.6; 7.4)	IX, X
VIII	26.1, CH_2	1.64 m	VII, VI, IX, X, XI
IX	28.6, CH_2	1.43 m	VIII, X, XI, VII
X	28.6, CH_2	1.62-1.75 m	
XI	36.3, CH_2	2.18 t (7.5)	X, IX, VIII, XII
XII	173.4, qC		
XIII	NH	6.43 s	XII
XIV	39.8, CH_2	3.38 quar (5.2)	XV, XII
XV	70.4, CH_2	3.51 t (5.2)	XVI-XIX, XIV
XVI[a] **XVII**[a] **XVIII**[a] **XIX**[a]	71.2-70.7, 4 x CH_2	3.55-3.60 m	XVI-XIX
XX	70.1, CH_2	3.86 t (5.2)	XXI, XVI-XIX
XXI	50.8, CH_2	4.51 t (5.2)	XX, C6''

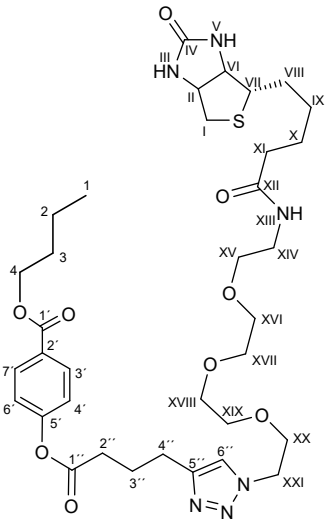

Table S3. MALDI-TOF-based peptide identification of eEF1α and eEF2 in protein fractions after elution from 5-labelled streptavidin beads. The sequence coverage (SC) and the root mean square at 90% (RMS90), which is used to compare distributions without large non-gaussian tails dominating, are indicated.

band no.	identified protein	pI	MW [kDa]	Meta Score	Peptides	SC [%]	RMS90 [ppm]
1	TPA: elongation factor 1-alpha (eEF 1α) [*Aspergillus nidulans* FGSC A4]	9.9	50.5	55.0	5	15.0	5.87
2	EF2_NEUCR Elongation factor 2 (eEF 2) [*Aspergillus nidulans* FGSC A4]	6.2	93.8	199.0	19	29.4	10.38

Table S4. **Molecular fingerprint (FP) similarity analysis of 1 and 7 by encoding them into Morgan and 2D Pharmacophore FPs.** Tanimoto similarity values higher than 0.5 could be used as cut-off for similarity when Morgan FPs are used. Dice coefficients may have a higher cut-off depending on the FPs used to encode the given molecules.

Similarity metric	2D Pharmacophore	Morgan
Tanimoto	0.147	0.164
Dice	0.257	0.283

Table S5. Predicted binding pockets for 1 in *A. nidulans* eEF2 model by the Achilles blind docking server. Ranks for the first seven binding pockets are given along with their predicted free energies of binding (BE). 5 Å residues around the predicted binding coordinates for **1** in *A. nidulans* eEF2 are listed. Residue numbering is shown in accordance with *A. nidulans* eEF2 (*An*), *C. albicans* eEF2 (*Ca*) and *S. cerevisiae* eEF2 (*Sc*). Amino acid residues differences are highlighted in bold.

#	BE	organ.	5 Å residues from predicted DAO binding location
1	-8.3	*An*	466K 484FS 515SDPC 534**A**G 537LH 541IC 545D 550H 731F 795PQ**SV**
		Ca	K FS SDPC **T**G LH IC D H F PQ**LI**
		Sc	K FS SDPC **T**G LH IC D H F PQ**MV**
2	-7.5	*An*	171**E**KED 250**Y** 262**QPE** 267GKP**V**ER 275NM
		Ca	**T**KED **Y** **DKD** GKP**L**ER NM
		Sc	**S**KED **F** **DTD** GKP**L**ER NM
3	-7.5	*An*	418N 484FSVS 565R 600**K** 603E**E** 638GPD 643G**A**N 672T 681**PM**RS 799FDHW
		Ca	N FSVS R **L** E**N** GPD G**P**N T **NC**RS FDHW
		Sc	N FSVS R **L** E**N** GPD G**P**N T **EM**RS FDHW
4	-7.1	*An*	42**R** 79**AKFA** 86D 224RQF 228**VK** 305E 327KFLP 333ADA 336LE
		Ca	**K** **ASMT** D RQF **NK** E KFLP ADA LE
		Sc	**R** **SEMS** D RQF **TR** E KFLP ADA LE
5	-7.0	*An*	492**R** 536E 559**D**PVV 564Y 727E 752R 776NE 779F 805**L** 816K 819**Q**I 823**E**
		Ca	**V** E **P**PVV Y E R NE F **M** K **A**I **E**
		Sc	**V** E **P**PVV Y E R NE F **L** K **E**I **A**
6	-7.0	*An*	165LLE 169Q**VE**K 280D 283**YK** 286F**Q** 290**T**N
		Ca	LLE Q**TT**K D **FR** F**A** **M**N
		Sc	LLE Q**VS**K D **FR** F**T** **M**N
7	-7.0	*An*	226F 229**KF** 232KKF 251F 253P 276MFI 280DP 284**K** 303K**I**E
		Ca	F **KY** KKF F P MFI DP **R** K**L**E
		Sc	F **RY** KKF F P MFI DP **R** K**L**E

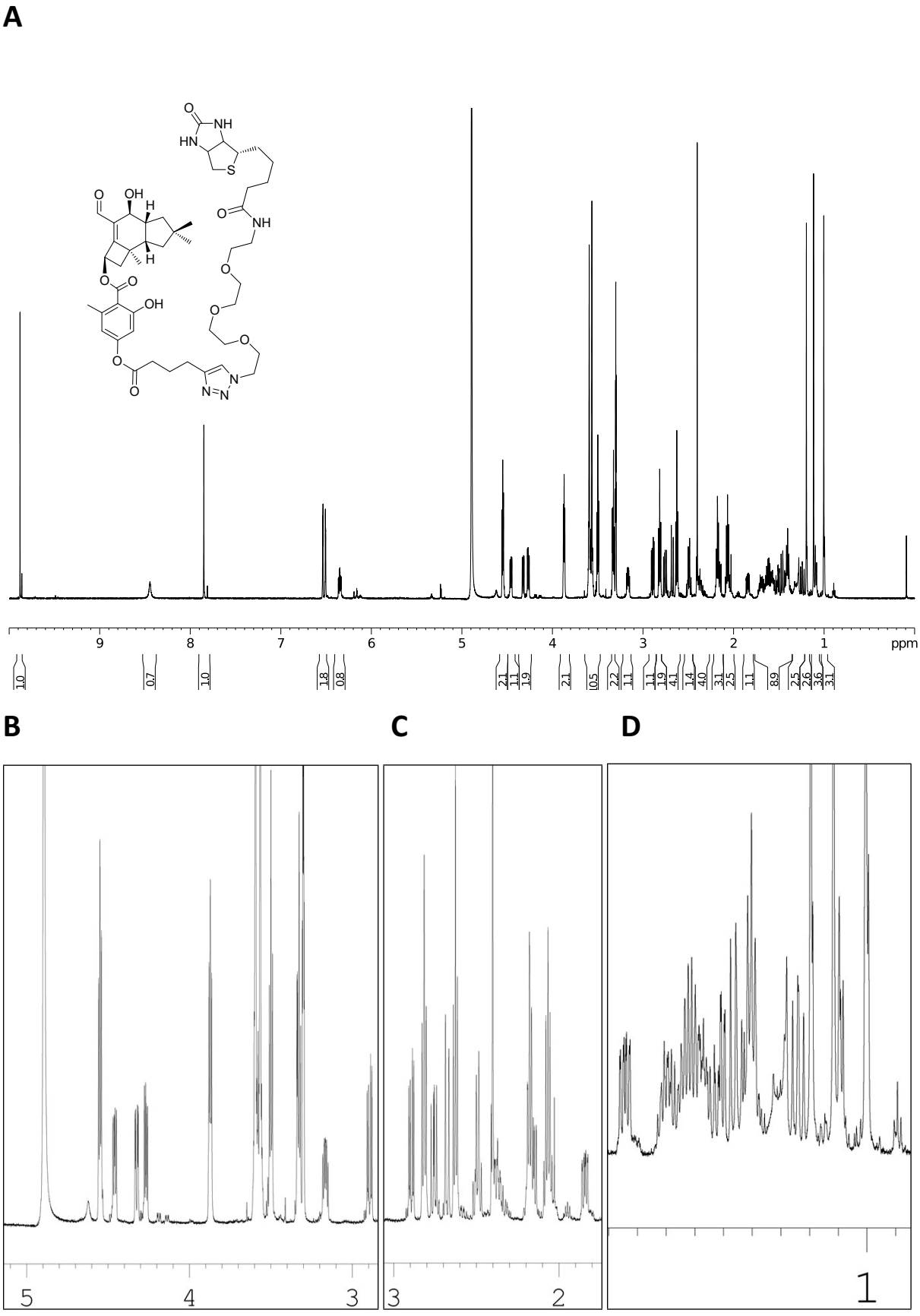

Figure S1. ^{1}H NMR spectra of **5** in CD_3OD. **A.** Full range ^{1}H NMR spectrum of **5** in CD_3OD. **B-D.** Close-up view of portions (5.0-3.0 ppm, 3.0-2.0 ppm, and 1.8-1.0 ppm) of the ^{1}H NMR spectrum of **5**.

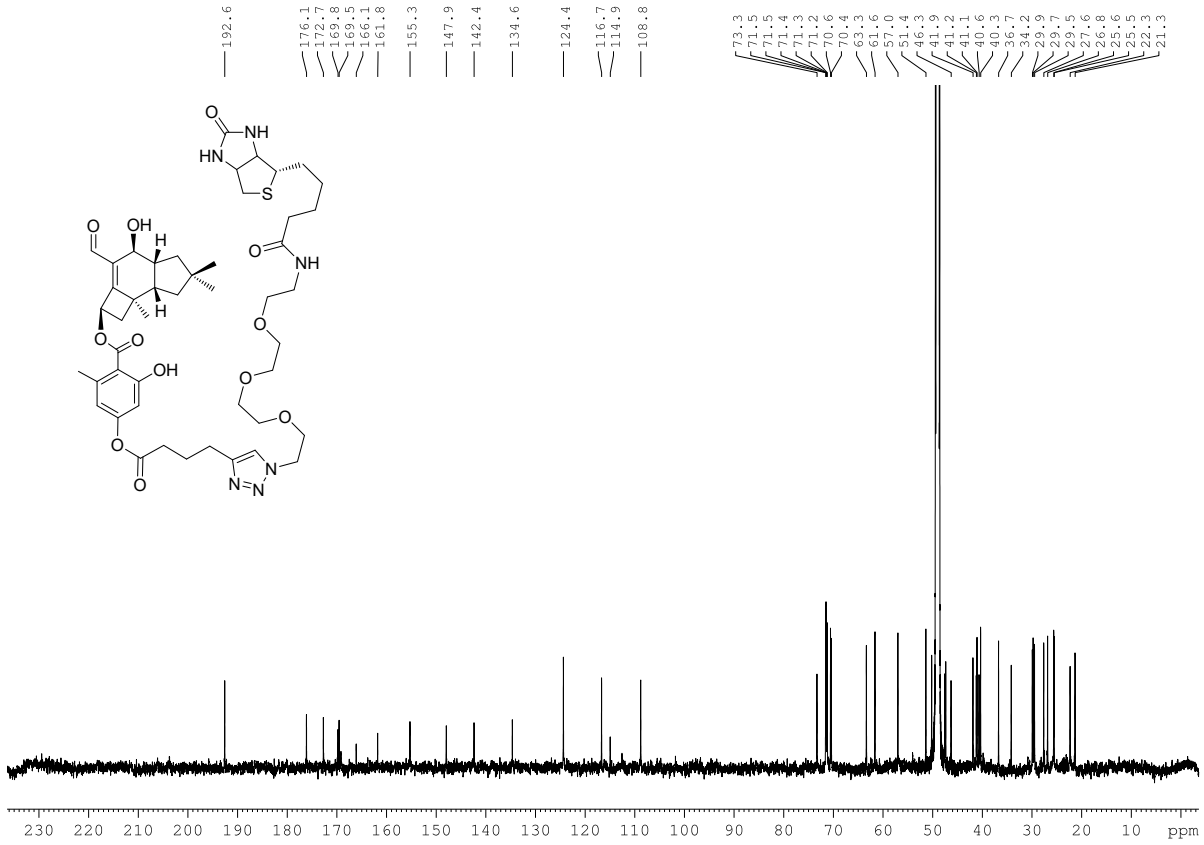

Figure S2. ^{1}H-decoupled ^{13}C NMR spectra of **5** in CD_3OD.

A

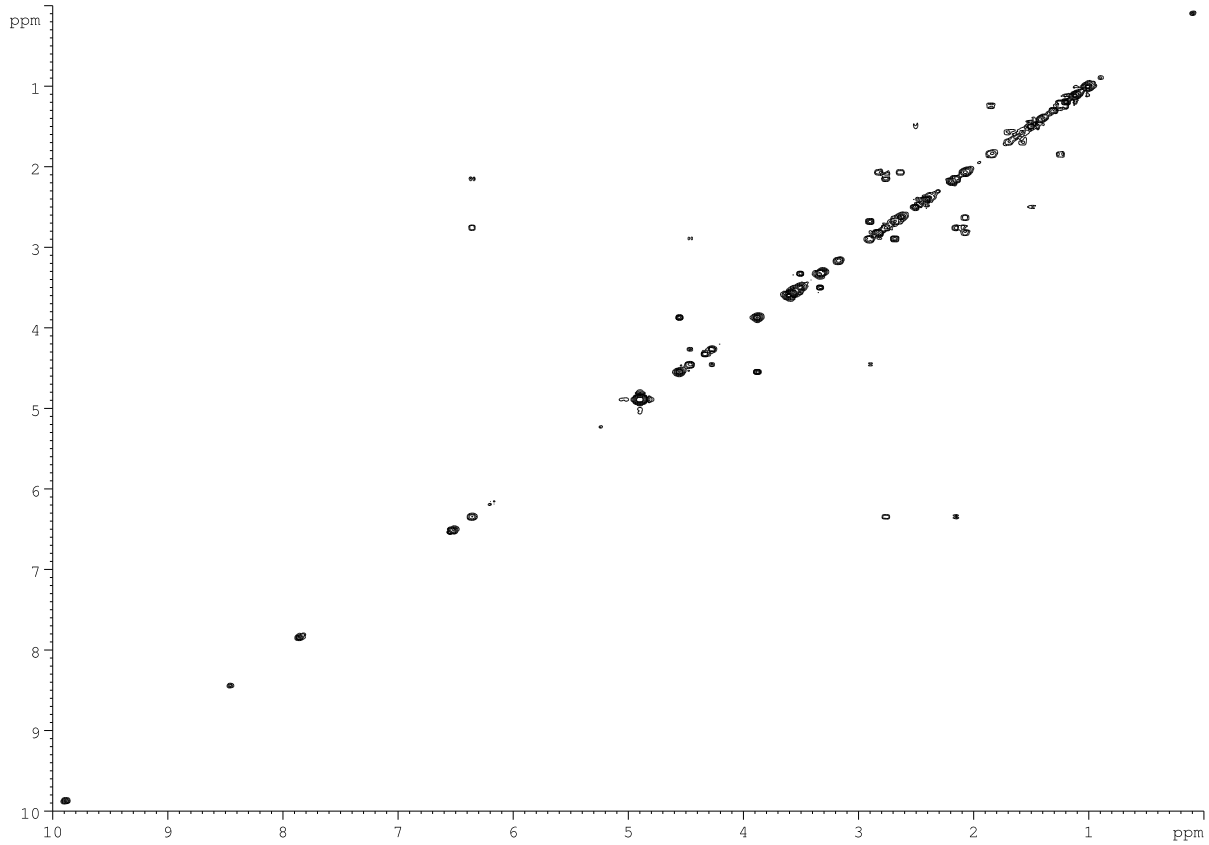

B

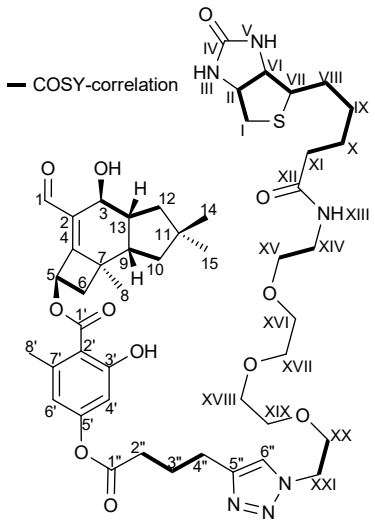

Figure S3. $^{1}H,^{1}H$ COSY spectrum of **5** in CD_3OD. **A.** Full range $^{1}H,^{1}H$ COSY spectrum of **5**. **B.** COSY key correlations.

A

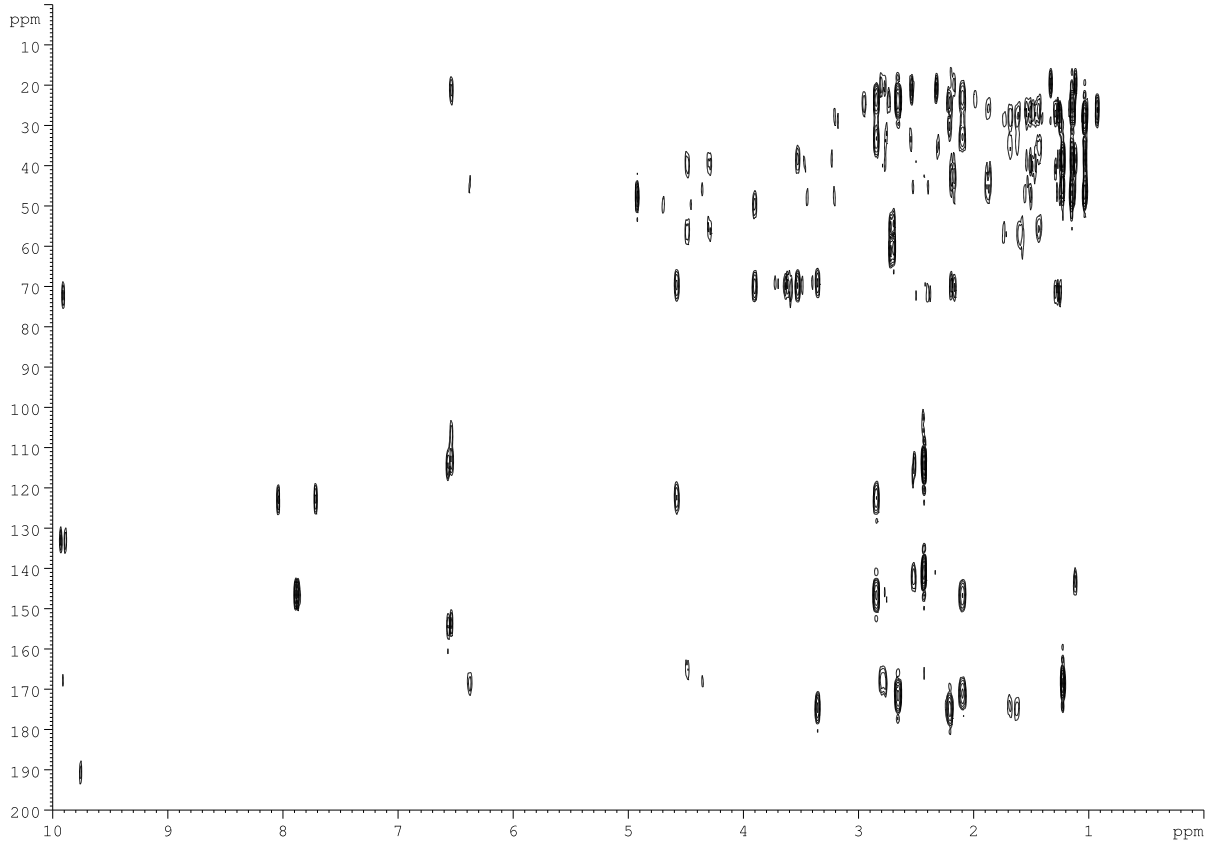

B

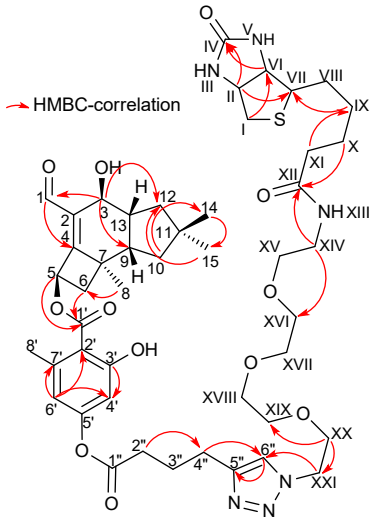

Figure S4. $^{1}H,^{13}C$ HMBC spectrum of **5** in CD_3OD. **A.** Full range $^{1}H,^{13}C$ HMBC spectrum of **5**. **B.** HMBC key correlations.

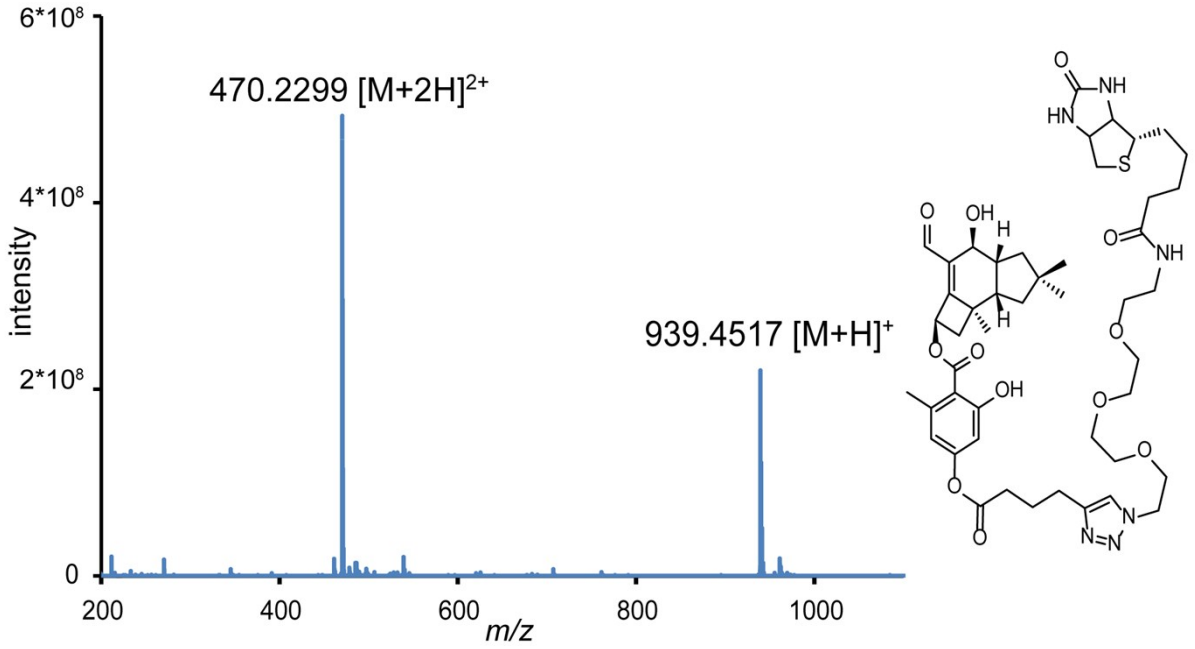

Figure S5. ESI-MS spectrum of **5**.

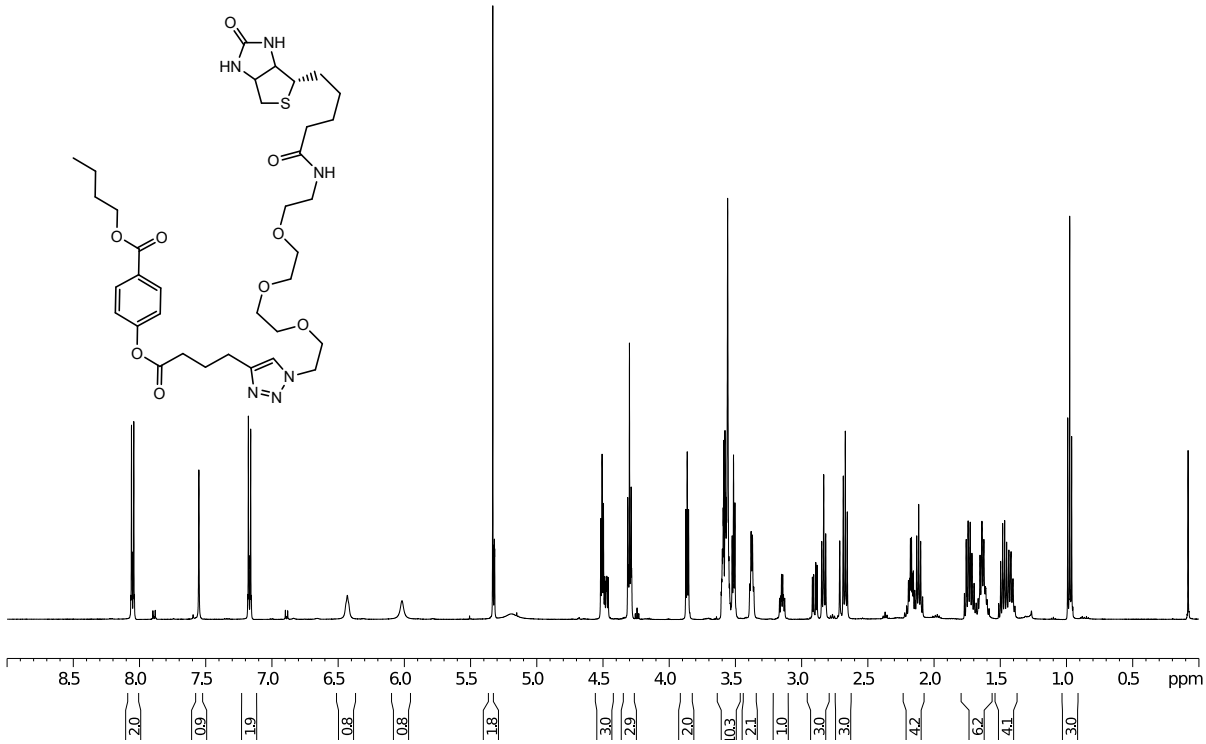

Figure S6. ^{1}H NMR spectrum of **6** in CD_3OD.

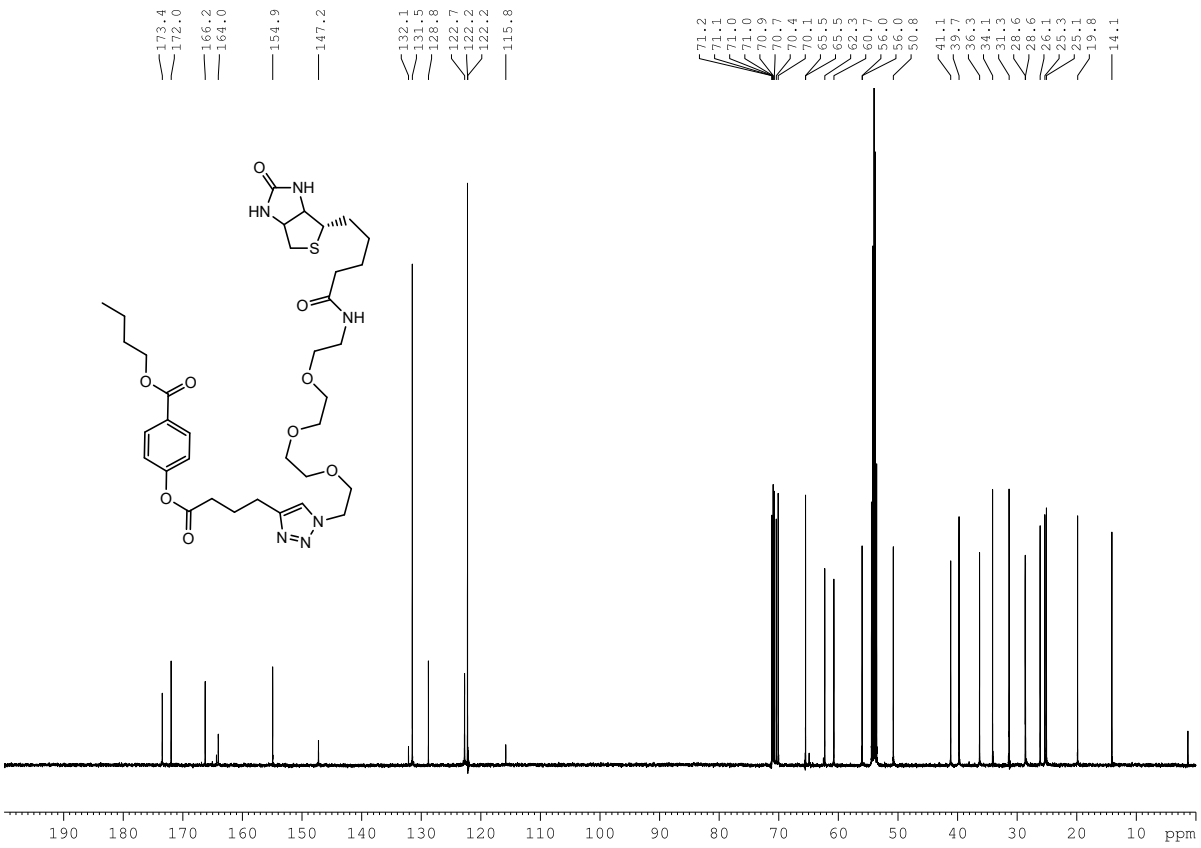

Figure S7. ^{1}H-decoupled ^{13}C NMR spectrum of **6** in CD_3OD.

A

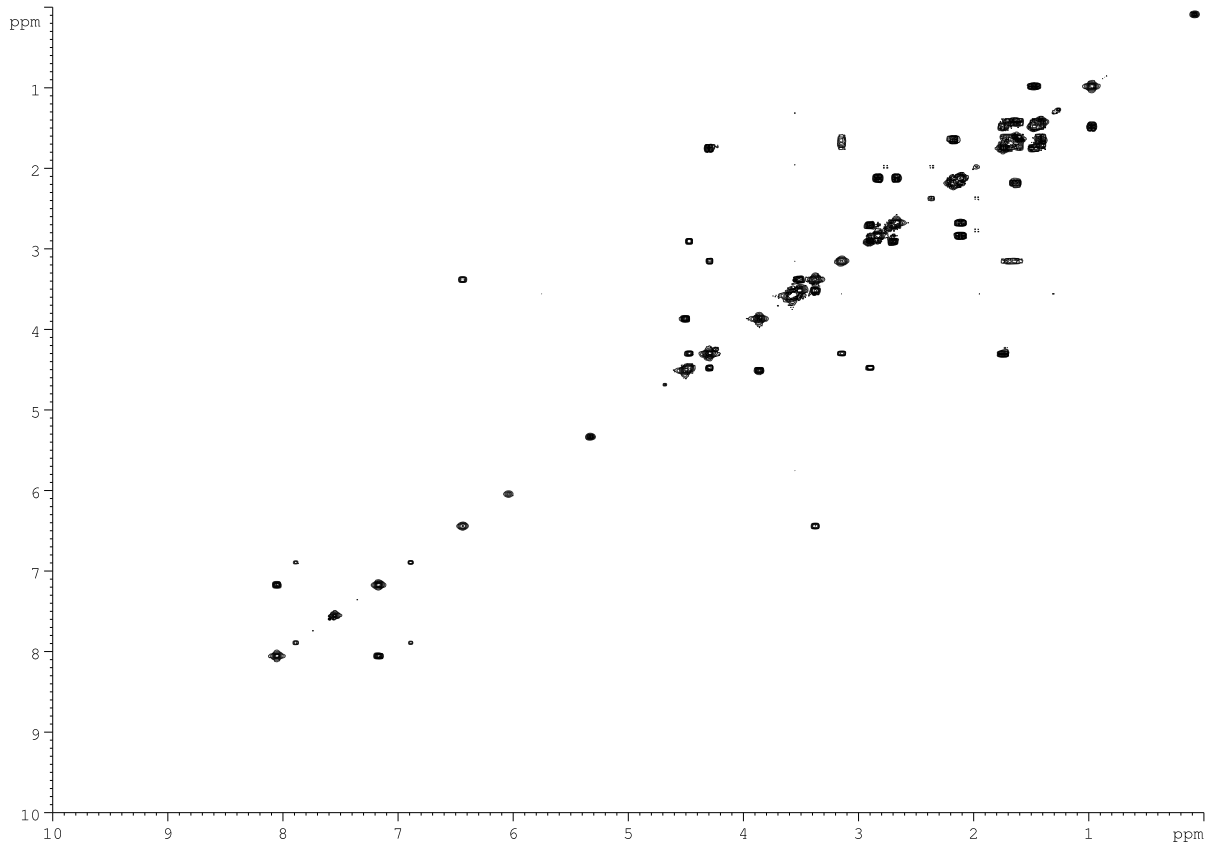

B

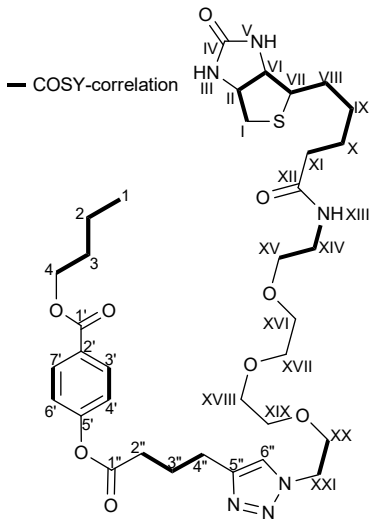

Figure S8. ^{1}H, ^{1}H COSY spectrum of **6** in CD_3OD. **A.** Full range ^{1}H, ^{1}H COSY spectrum of **6**. **B.** COSY key couplings in **6**.

A

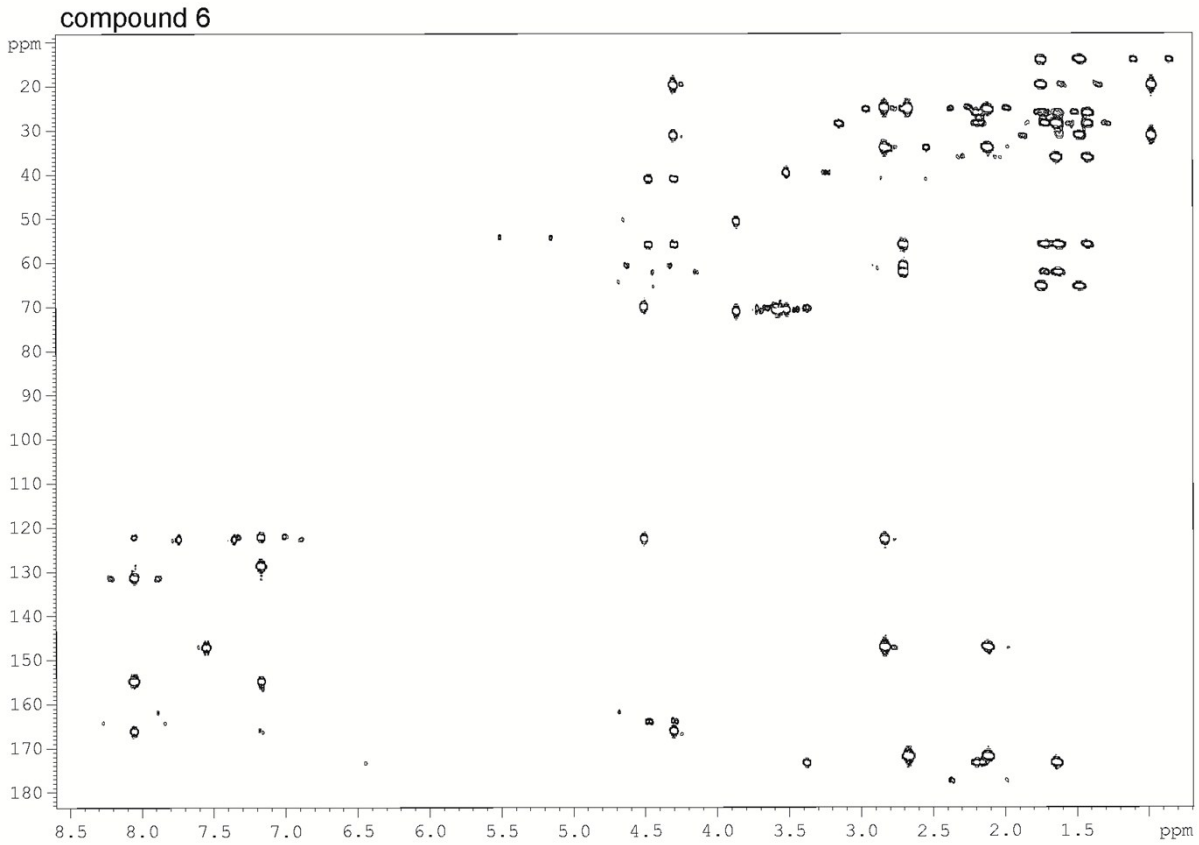

B

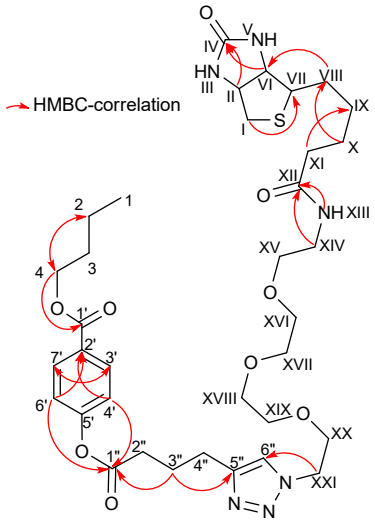

Figure S9. $^{1}H,^{13}C$ HMBC spectrum of **6** in CD_3OD. **A.** Full range $^{1}H,^{13}C$ HMBC spectrum. **B.** HMBC key correlations.

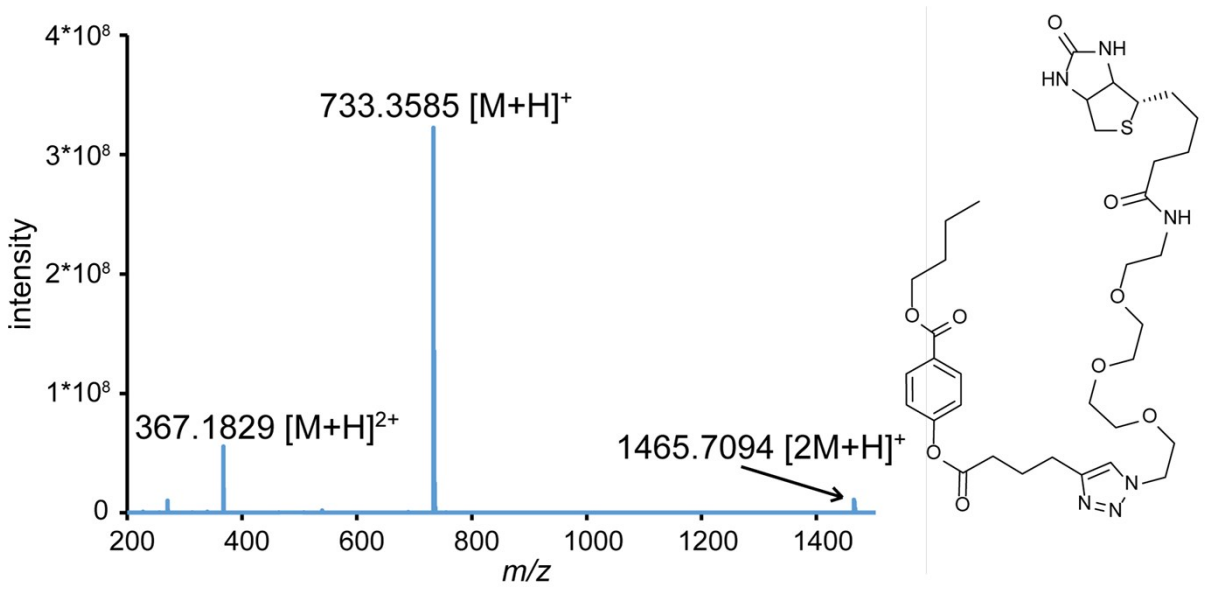

Figure S10. ESI-MS data of **6.**

Figure S11. MALDI-TOF-based peptide fingerprinting. Identified peptides from *A. nidulans* eEF2 in protein pull-down fraction with **5**-labelled streptavidin beads. Identified peptides from trypsin treated samples were aligned to *A. nidulans* eEF2 (highlighted in red). Grey bars indicate the reliance of the identified peptides: The darker the bar the lower is the difference between the measured *m/z* and the calculated *m/z*.

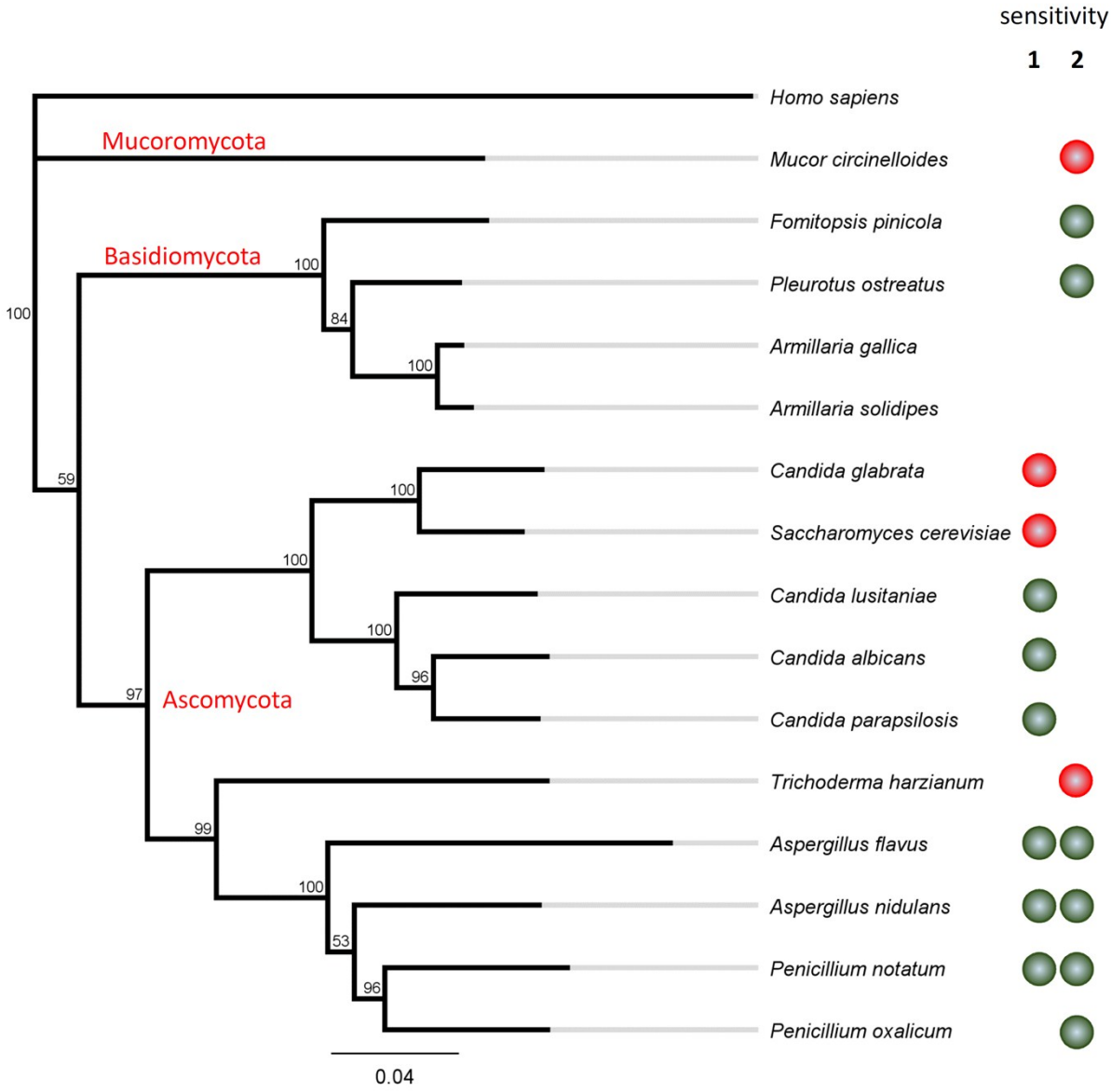

Figure S12. Phylogenetic analysis of fungal eEF2 with documented resistance or sensitivity towards 1 (DAO) and 2 (arnamial). Multiple amino acid sequence alignments were performed using the MUSCLE Alignment tool implemented in the Geneious 10.2.3 software carried out in default mode with a maximum of 1,000 iterations and 1,000 trees to be build. Phylogenetic analyses were performed with Geneious Tree Builder software using the Jukes-Cantor genetic distance model and the neighbour-joining method. The amino acid sequence of the human eEF2 was used as outgroup to root the tree. The bootstrap method was used as a resampling technique to estimate statistics on 1,000 replicates. Bootstrap values (consensus support in %) are given next to the branches in the consensus tree. Red and green spheres indicate resistance and sensitivity, respectively, towards **1** and **2** as reported by Misiek *et al.*[1], Bohnert *et al.*[2], and by this work (Figure 3 A).

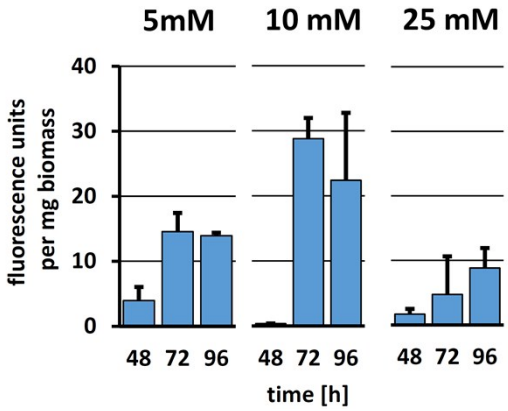

Figure S13. Optimization of cultivation conditions. *A. nidulans* tMD03 was cultivated for 48, 72, and 96 h in AMM containing 100 mM ethanol and 5, 10, or 25 mM D-glucose. Fluorescence units of cell-free total protein extracts were determined and normalised against the fungal biomass.

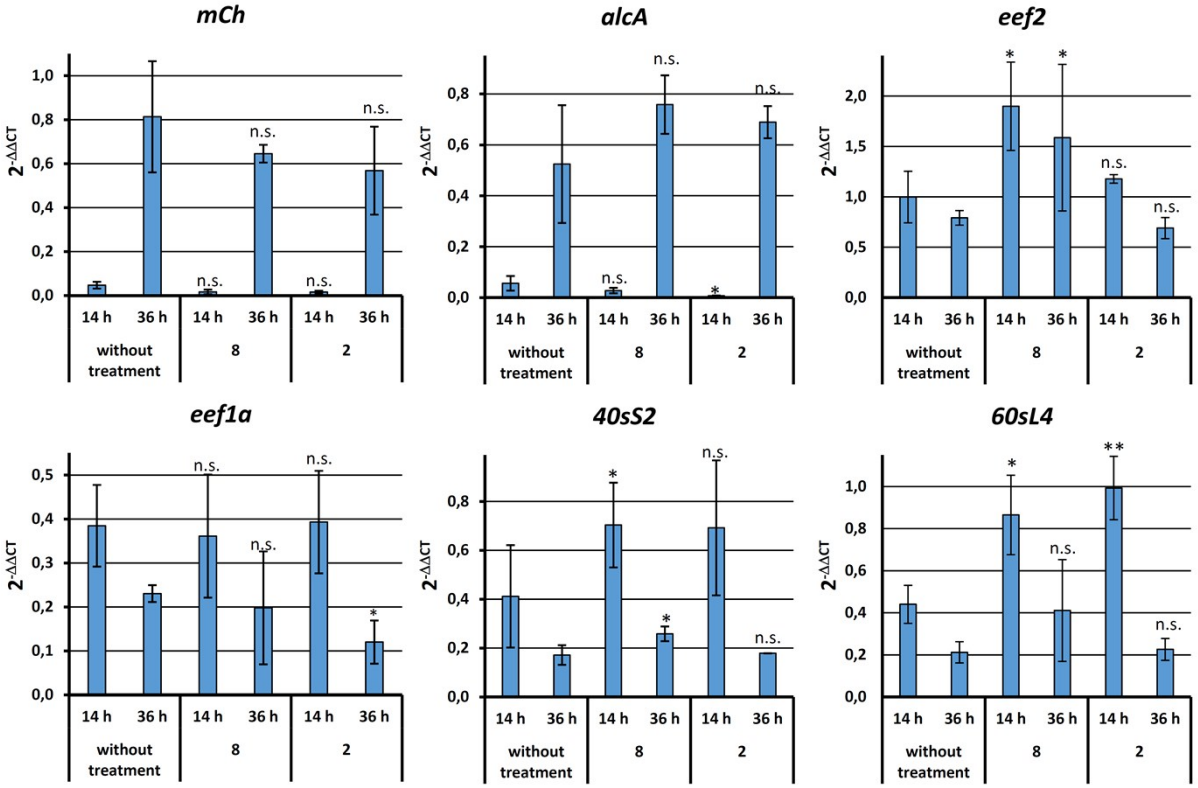

Figure S14. Gene expression analyses by qRT-PCR. *A. nidulans* tMD03 was pre-cultivated for 16 h in presence of 10 mM D-glucose and 100 mM ethanol. Compounds **8** (72 µM) or **2** (22 µM) were added, and cultures were grown for additional 14 or 36 h prior to expression analysis. Untreated cultures served as control. qRT-PCR targeted the genes for mCherry (*mCh*), alcohol dehydrogenase (*alcA*), eEF2 (*eef2*), eEF1α (*eef1α*), and proteins for the small (*40sS2*) and large (*60sL4*) ribosomal subunits. Expression levels were normalised against two housekeeping genes, i.e., enolase (*enoA*) and glycerinaldehyde-3-phosphate dehydrogenase (*gpdA*). Significance of gene expression levels were calculated against the respective untreated control by pairwise student´s t-test (n.s., $p > 0.05$; *, $p < 0.05$; **, $p < 0.01$).

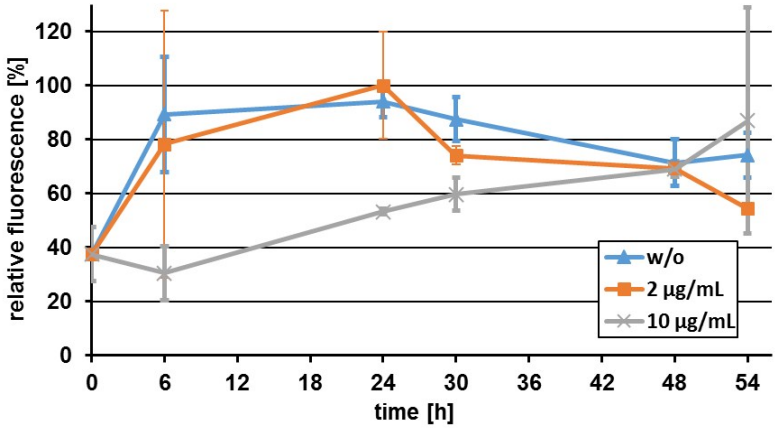

Figure S15. *In vivo* inhibition of protein biosynthesis in *A. nidulans* tMD03. The fungus was treated with **2** at 2 and 10 µg mL^{-1}. The untreated control served as internal fluorescence reference standard. The experiment was carried out as described in Figure 4.

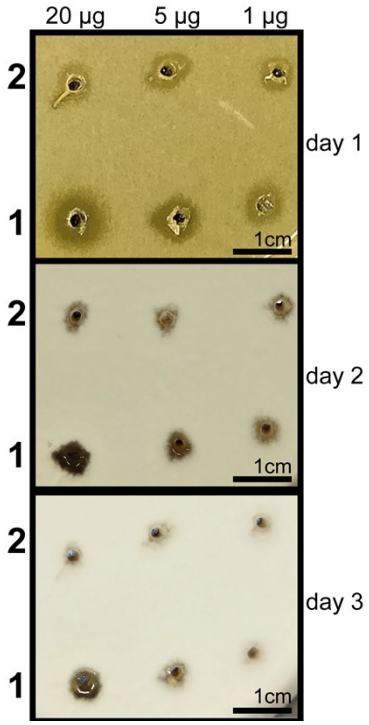

Figure S16. Recovery of *A. nidulans* in presence of 1 and 2. AMM plates were inoculated with *A. nidulans* FGSC A4 at a concentration of 1 x 10^6 conidia mL^{-1}, and 20, 5 or 1 µg of **1** and **2** were supplied. Plates were incubated for 1, 2, or 3 days at 30 °C. The size of inhibition zones is time-dependently reduced, indicating a fungistatic activity of **1** and **2**.

Scheme S1. Synthesis route for compound **6**.

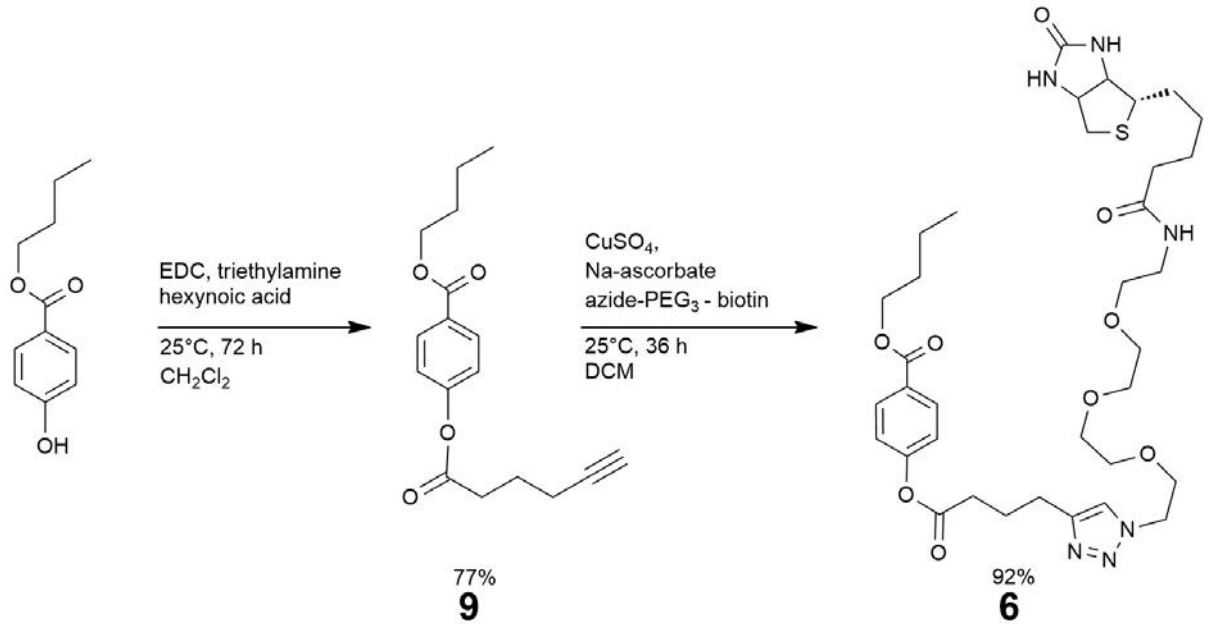

References

1. Misiek, M.; Hoffmeister, D. *Mycol. Prog.* **2012,** *11*, 7.
2. Bohnert, M.; Nützmann, H. W.; Schroeckh, V.; Horn, F.; Dahse, H. M.; Brakhage, A. A.; Hoffmeister, D. *Phytochemistry* **2014,** *105*, 101.

3.2. Publikation 2 – Melleolides from Honey Mushroom Inhibit 5-Lipoxygenase via Cys 159

Stefanie König, Erik Romp, Verena Krauth, Michael Ruhl, **Maximilian Dörfer**, Stefanie Liening, Bettina Hofmann, Ann-Kathrin Hafner, Dieter Steinhilber, Michael Karas, Ulrike Garscha, Dirk Hoffmeister, Oliver Werz

Cell Chemical Biology, 2019, Volume 26, 1-11.

Zusammenfassung

Die humane 5-Lipoxigenase (5-LO) wurde in einem Screening als molekulares Wirkziel von Melleoliden aus *Armillaria mellea* identifiziert. Melleolide wie DAO hemmen die 5-LO und damit eine Entzündungsreaktion aufgrund einer inhibierten Leukotrienbildung. DAO stellt aufgrund des α- β-ungesättigten Aldehyds in Verbindung mit einem Alkohol einen starken Michael Akzeptor dar. Dieser bindet oberflächlich exponierte Cysteine am Eingang des aktiven Zentrums des Entzündungsmediators 5-LO. Die Cysteine 159, 300, 416 und 418 wurden in 5-LO gegen Serine ausgetauscht. Durch die verhinderte Bildung des 5-LO/FLAP-Komplexes konnte eine direkte Wechselwirkung, basierend auf einer kovalenten Bindung, zwischen DAO und dem Cystein 159 nachgewiesen werden. Cys159 scheint also eine wichtige Funktion in der Bildung des 5-LO/FLAP Komplexes an der Membran des Zellkerns und somit für die Leukotrienbiosynthese zu besitzen.

Eigenanteil 10%:

Maximilian Dörfer: Kultivierung von *A. mellea*, Extraktion, Isolierung und Strukturaufklärung von DAO & Derivaten

Jena, den

_____

Prof. Dr. Dirk Hoffmeister

Article

Cell Chemical Biology

Melleolides from Honey Mushroom Inhibit 5-Lipoxygenase via Cys159

Graphical Abstract

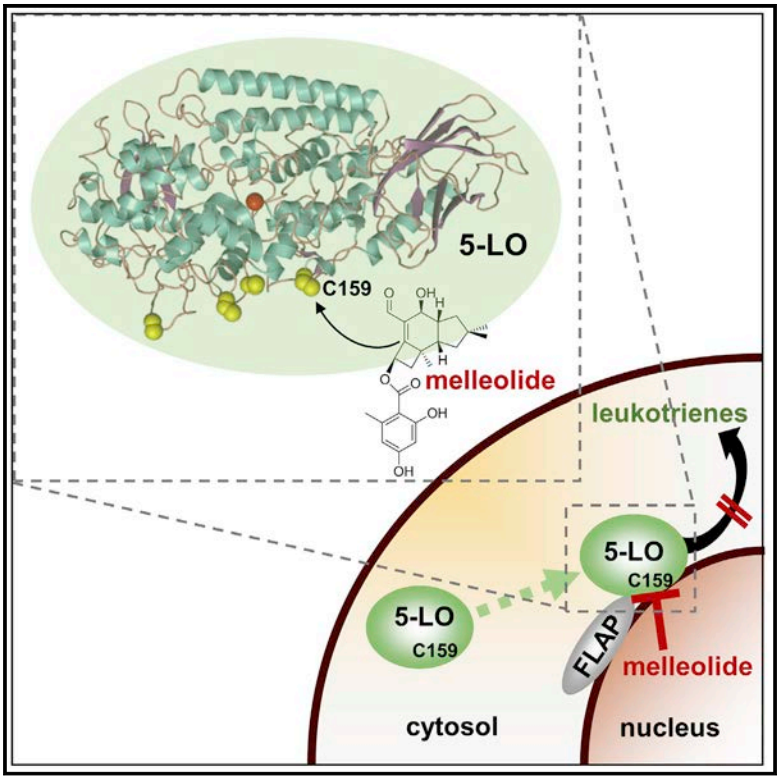

Highlights

- Human 5-lipoxygenase (5-LO) was identified as a molecular target of melleolides
- Melleolides inhibit 5-LO via two or more of the cysteines 159, 300, 416, and 418
- Melleolides prevent interaction of 5-LO with its helper protein via Cys159 in 5-LO
- Cys159 in 5-LO determines interaction with its helper protein and 5-LO activity

Authors

Stefanie König, Erik Romp, Verena Krauth, ..., Ulrike Garscha, Dirk Hoffmeister, Oliver Werz

Correspondence

oliver.werz@uni-jena.de

In Brief

König et al. revealed human 5-lipoxygenase as a functional target of melleolides from honey mushroom, where cysteines at the substrate entrance of 5-lipoxygenase mediate enzyme inhibition. Exploiting melleolides as a tool they identified Cys159 as a determinant for interaction of 5-lipoxygenase with its helper protein.

König et al., 2019, Cell Chemical Biology *26*, 1–11
January 17, 2019
https://doi.org/10.1016/j.chembiol.2018.10.010

CellPress

Please cite this article in press as: König et al., Melleolides from Honey Mushroom Inhibit 5-Lipoxygenase via Cys159, Cell Chemical Biology (2018), https://doi.org/10.1016/j.chembiol.2018.10.010

Cell Chemical Biology
Article

Melleolides from Honey Mushroom Inhibit 5-Lipoxygenase via Cys159

Stefanie König,[1] Erik Romp,[1] Verena Krauth,[1] Michael Rühl,[2] Maximilian Dörfer,[3] Stefanie Liening,[1] Bettina Hofmann,[2] Ann-Kathrin Häfner,[2] Dieter Steinhilber,[2] Michael Karas,[2] Ulrike Garscha,[1] Dirk Hoffmeister,[3] and Oliver Werz[1,4,*]
[1]Department of Pharmaceutical/Medicinal Chemistry, Institute of Pharmacy, Friedrich-Schiller-University Jena, 07743 Jena, Germany
[2]Institute of Pharmaceutical Chemistry, Goethe University Frankfurt, 60438 Frankfurt, Germany
[3]Department of Pharmaceutical Microbiology at the Hans Knöll Institute, Friedrich-Schiller-University Jena, 07745 Jena, Germany
[4]Lead Contact
*Correspondence: oliver.werz@uni-jena.de
https://doi.org/10.1016/j.chembiol.2018.10.010

SUMMARY

5-Lipoxygenase (5-LO) initiates the biosynthesis of pro-inflammatory leukotrienes from arachidonic acid, which requires the nuclear membrane-bound 5-LO-activating protein (FLAP) for substrate transfer. Here, we identified human 5-LO as a molecular target of melleolides from honey mushroom (*Armillaria mellea*). Melleolides inhibit 5-LO via an α,β-unsaturated aldehyde serving as Michael acceptor for surface cysteines at the substrate entrance that are revealed as molecular determinants for 5-LO activity. Experiments with 5-LO mutants, where select cysteines had been replaced by serine, indicated that the investigated melleolides suppress 5-LO product formation via two distinct modes of action: (1) by direct interference with 5-LO activity involving two or more of the cysteines 159, 300, 416, and 418, and (2) by preventing 5-LO/FLAP assemblies involving selectively Cys159 in 5-LO. Interestingly, replacement of Cys159 by serine prevented 5-LO/FLAP assemblies as well, implying Cys159 as determinant for 5-LO/FLAP complex formation at the nuclear membrane required for leukotriene biosynthesis.

INTRODUCTION

Natural products are discovered at a rapid rate, and bioactivities are extensively screened for in routine assays. However, the knowledge on the modes of action and molecular targets of these bioactive compounds is severely lagging behind. In the arena of mushroom toxins, the mode of action is understood only for very few compounds, among them the amanitins, psilocybin, muscarine, coprine, and ibotenic acid. The melleolides (Figure 1A) are natural products of the basidiomycete *Armillaria mellea* (honey mushroom), a globally distributed mushroom that also represents an important plant pathogen (Baumgartner et al., 2011). Bioactivities include antimicrobial and antifungal effects, as well as cytotoxicity against human monocytes and cancer cells (Bohnert et al., 2011, 2014b; Misiek et al., 2009; Momose et al., 2000). Intriguingly, these activities follow dissimilar structure-activity relationships (SARs) (Bohnert et al., 2014a). With more than 60 published members, melleolides rank among the largest and most diverse classes of fungal natural products. Structurally, they are composed of an orsellinic acid moiety esterified to a protoilludene-type sesquiterpene secondary alcohol. Many melleolides feature an α,β-unsaturated aldehyde moiety that may act as Michael acceptor, but molecular targets of the melleolides are thus far unknown. We previously showed that Michael acceptor-containing drugs such as thymoquinone (TQ) (Maucher et al., 2017) or nitro fatty acids (Awwad et al., 2014) are direct covalent inhibitors of human 5-lipoxygenase (5-LO) by targeting Cys416 and Cys418.

5-LO is the key enzyme in the biosynthesis of pro-inflammatory leukotrienes (LTs) from arachidonic acid (AA) that play important roles in disorders such as asthma, rheumatoid arthritis, allergic rhinitis, neurodegenerative and cardiovascular diseases, and cancer (Radmark et al., 2015). LT biosynthesis is mainly restricted to leukocytes where the cytosolic phospholipase A_2 ($cPLA_2$) and 5-LO translocate to the nuclear envelope upon cell activation. $cPLA_2$ releases AA from membrane phospholipids (Leslie, 2015), and AA is then transferred by the nuclear membrane-bound 5-LO-activating protein (FLAP) to 5-LO, which assembles a complex with FLAP. 5-LO oxygenates AA to yield the intermediate 5(S)-hydroperoxyeicosatetraenoic acid (5-HPETE) and then dehydrates 5-HPETE to LTA_4, again aided by FLAP (Radmark et al., 2015). LTA_4 can be enzymatically converted to the chemoattractant LTB_4 or to cysteinyl-LTs (LTC_4, D_4, or E_4) that contract smooth muscles in the airways and microcirculation (Haeggstrom and Funk, 2011). FLAP binds AA and is essential for 5-LO activity in intact cells, seemingly by accomplishing appropriate substrate access for 5-LO (Evans et al., 2008). The 5-LO/FLAP complex assembly at the nuclear membrane requires AA, and FLAP inhibitors prevent 5-LO/FLAP interactions and 5-LO product formation in an AA-competitive fashion (Bair et al., 2012; Gerstmeier et al., 2014, 2016b). Recently, we showed that the cysteines 159, 300, 416, and 418, located on the 5-LO protein surface close to the AA entry site, are important for co-localization with FLAP (Hafner et al., 2015).

The poor knowledge on the pharmacology behind mushroom toxins, and the fact that honey mushrooms are considered edible and collected in many regions prompted us to investigate the mode of action of the melleolides. To explore their molecular

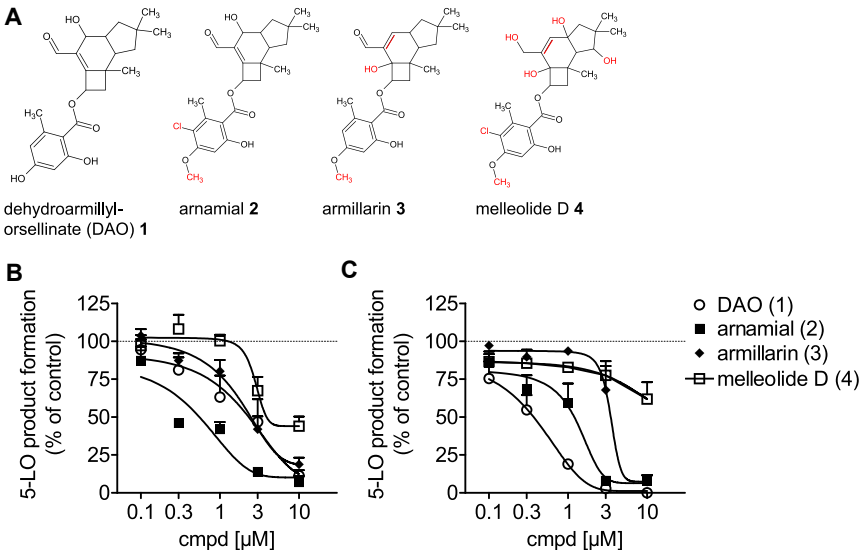

Figure 1. Melleolides Inhibit 5-LO Activity in Cell-Free and Cell-Based Systems

(A) Chemical structures of melleolides **1**–**4**.

(B) Effect of **1**–**4** on 5-LO product formation in a cell-free assay. Purified human recombinant 5-LO (0.5 μg/mL) was pre-incubated with compounds or vehicle (0.1% DMSO) at 4°C for 10 min. Samples were pre-warmed for 30 s at 37°C and incubated with 2 mM $CaCl_2$ and 20 μM AA for another 10 min. The reaction was terminated and 5-LO products were then analyzed by reverse-phase high-performance liquid chromatography (RP-HPLC).

(C) Effect of **1**–**4** on 5-LO product formation in a cell-based system. Neutrophils (5 × 10^6/mL) were pre-incubated with compounds or 0.1% DMSO (vehicle) for 10 min at 37°C prior to stimulation with 2.5 μM A23187 for 10 min at 37°C, and 5-LO product formation was determined. Data are expressed as percentage of vehicle control (100%), means ± SEM, n = 3.

targets in mammalian cells, we investigated four structurally different representatives (Figure 1A) for interference with human 5-LO. We identified 5-LO as a molecular target for those melleolides that possess an α,β-unsaturated aldehyde with thiol-reactive Michael acceptor functionality. These melleolides mediate their 5-LO-inhibitory effects via surface cysteines of 5-LO. Our data suggest that melleolides interact with Cys159 at the entrance of the catalytic center of 5-LO, which prevents the complex assembly with FLAP and thus abrogates 5-LO activity. We conclude that Cys159 of 5-LO is critical for the assembly of the 5-LO/FLAP complex, whereas cysteines 300, 416, and 418 do not contribute.

RESULTS

Melleolides Inhibit 5-LO Activity in Cell-Free and Cell-Based Systems

We investigated the effects of four structurally related melleolides isolated from *Armillaria mellea* (Figure 1A) on the activity of 5-LO in a cell-based model using Ca^{2+}-ionophore A23187-stimulated human neutrophils, and in a cell-free assay using purified human recombinant 5-LO as enzyme source. The investigated compounds included dehydroarmillylorsellinate (DAO) (**1**), arnamial (**2**), armillarin (**3**), and melleolide D (**4**). Concentration-response experiments with these melleolides in the cell-free assay revealed **2** as most potent derivative with a half maximal inhibitory concentration (IC_{50}) of 0.3 ± 0.02 μM, followed by **3** (IC_{50} = 2.5 ± 0.4 μM) and **1** (IC_{50} = 2.8 ± 0.9 μM, Figure 1B). Compound **4** was much less efficient (IC_{50} > 10 μM). Of interest, in neutrophils, **1** was the most efficient derivative against 5-LO (IC_{50} = 0.3 ± 0.1 μM, Figure 1C), with 10-fold higher potency versus cell-free assay conditions. Melleolides **2** (IC_{50} = 1.0 ± 0.2 μM) and **3** (IC_{50} = 5.2 ± 1.4 μM) showed comparable efficiency as in the cell-free test system. Again, **4** caused only moderate inhibition of 5-LO activity in neutrophils (IC_{50} > 10 μM). Cell viability analysis (trypan blue and light microscopy) exclude detrimental effects of **1**–**4** during the 10 min pre-incubation period of neutrophils (data not shown).

DAO (1) Potently Inhibits 5-LO Activity in Intact Neutrophils and Monocytes

To explore 5-LO inhibition by melleolides, we focused on **1**, which was the most potent derivative in neutrophils. First, we analyzed the effect of **1** against 5-LO in neutrophil homogenates, another cell-free test system for assessment of 5-LO activity (Werz and Steinhilber, 2005). Compared with its high potency in neutrophils, **1** was less active against 5-LO in corresponding homogenates (IC_{50} = 1.1 ± 0.2 μM), similar as for isolated 5-LO (Figure 2A). In contrast, the 5-LO inhibitor zileuton was equally effective for isolated 5-LO and cellular 5-LO activity (IC_{50} ~ 0.8 μM, Figure 2B). This suggested that **1** may interact with other enzyme(s) or factors involved in cellular 5-LO product formation such as $cPLA_2$ or FLAP. Analysis of AA release using [^{3}H]AA-labeled neutrophils indicated weak suppression of AA liberation by **1** (at 1 μM), which was much less pronounced as compared with RSC-3388, a specific $cPLA_2$ inhibitor (Table S1). We next supplemented neutrophils with exogenous AA (20 μM), to overcome potential deficiencies in endogenous AA supply due to potential $cPLA_2$ or FLAP inhibition (Werz and Steinhilber, 2005). The strong potency of **1** in absence of exogenous AA (i.e., IC_{50} = 0.3 μM) was about 7-fold decreased upon AA supplementation (IC_{50} = 2.1 μM, Figure 2C), suggesting that **1** may interfere with AA-related action(s). We also tested whether **1** may interfere with signaling processes important for 5-LO activation, such as its activation by mitogen-activated protein kinases (MAPKs) (Radmark et al., 2015). However, up to 10 μM, **1** failed to suppress the phosphorylation of p38 MAPK and extracellular signal-regulated kinase-1/2, and thus of $cPLA_2$ in neutrophils (Figure S1). Moreover, **1** did not cause strong inhibition of other enzymes in LT or eicosanoid biosynthesis such as LTC_4 synthase, cyclooxygenase-1/2, or microsomal prostaglandin E2 synthase-1 (Table S1), indicating a certain selectivity against 5-LO.

Besides neutrophils, also monocytes have high capacities to biosynthesize 5-LO products (Surette et al., 1993). Melleolide **1** inhibited 5-LO activity also in human monocytes stimulated with A23187, with comparable efficiency (IC_{50} = 0.8 μM), as in neutrophils (Figure 2D). A more detailed analysis showed that **1**

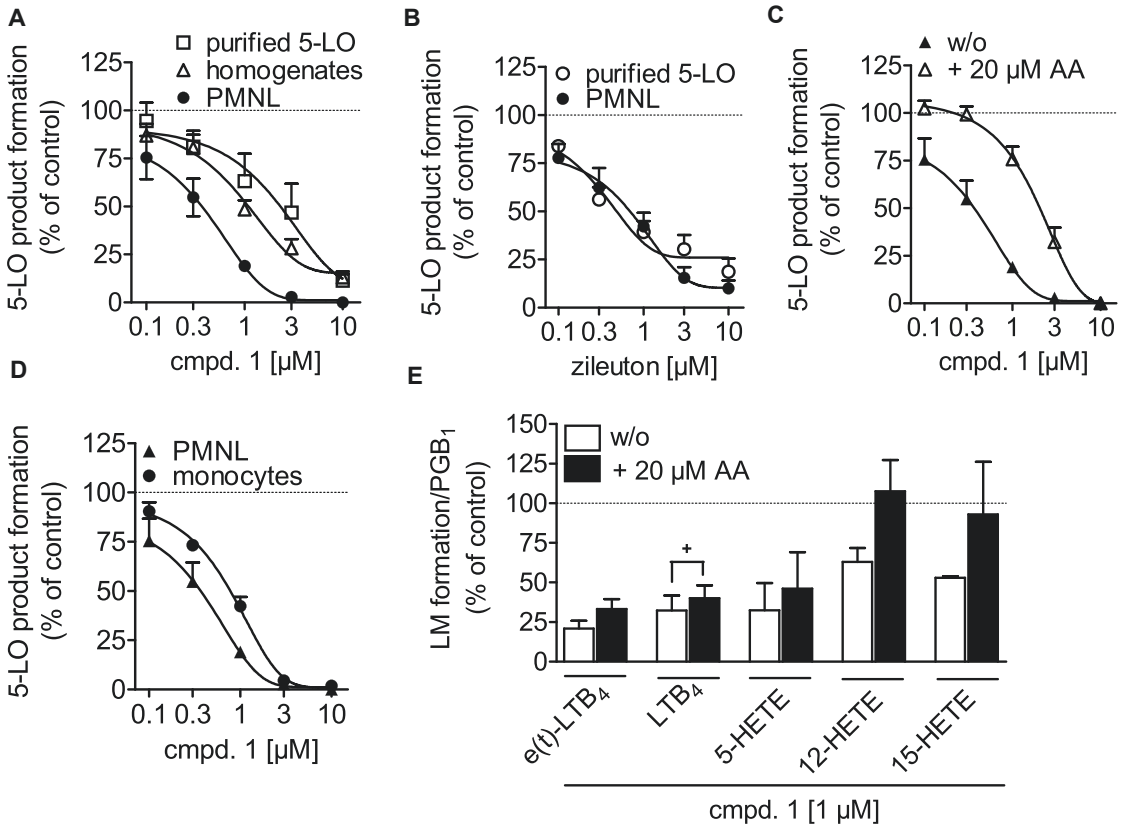

Figure 2. DAO (1) Potently Inhibits 5-LO Activity in Intact Neutrophils and Monocytes

(A) Purified human recombinant 5-LO, intact human neutrophils (5 × 10^6/mL), or neutrophil homogenates (corresponding to 5 × 10^6 cells/mL) were incubated with **1** or vehicle (0.1% DMSO) for 10 min at 37°C (neutrophils) or 4°C (5-LO, homogenates) prior to addition of 2.5 μM A23187 (neutrophils) or 2 mM $CaCl_2$ and 20 μM AA (5-LO, homogenates).

(B) Neutrophils or purified human recombinant 5-LO were pre-incubated for 10 min with zileuton or vehicle (0.1% DMSO) prior to addition of 2.5 μM A23187 (neutrophils) or 2 mM $CaCl_2$ and 20 μM AA (5-LO).

(C) Neutrophils were pre-incubated for 10 min with **1** or vehicle (0.1% DMSO) prior to addition of 2.5 μM A23187 with or without 20 μM AA.

(D) Effect of **1** on 5-LO product formation in neutrophils and monocytes. Cells (5 × 10^6/mL) were pre-treated with **1** or vehicle (0.1% DMSO) for 10 min. 5-LO product formation was started by 2.5 μM A23187.

(E) Effect of **1** (1 μM) on eicosanoid biosynthesis in intact monocytes stimulated with 2.5 μM A23187 in the presence or absence of 20 μM AA. All incubations (A–E) were performed for 10 min at 37°C, and then 5-LO product formation was determined by RP-HPLC and eicosanoids in (E) were analyzed by ultra-performance liquid chromatography-MS/MS. Data are expressed as percentage of uninhibited control (100%), means ± SEM, n = 3, +$p < 0.05$ versus vehicle control, paired t test.

See also Figure S1 and Table S1.

(at 1 μM) decreased all lipid mediators formed by 5-LO (i.e., tr-LTB_4 isomers, LTB_4, and 5-hydroxyeicosatetraenoic acid [HETE]) to a similar degree, which again was less pronounced when exogenous AA was supplemented (Figure 2E). Formation of 12- and 15-HETE was less affected by **1**, and, in the presence of exogenous AA (20 μM), **1** lost its inhibitory potency to suppress the biosynthesis of these lipid mediators.

Characterization of 5-LO Inhibition by Melleolides and Interaction with Cysteine

We characterized 5-LO inhibition by **1** in more detail. Washout experiments with isolated 5-LO revealed that **1** acts in a partially irreversible manner (Figure 3A), since the suppressive effect of **1** against 5-LO was hardly reversed upon 10-fold dilution. 5-LO activity studies with increasing AA concentrations (3–60 μM) in the cell-free assay revealed that the inhibitory potency of **1** is markedly improved at higher AA concentrations (IC_{50} = 7 μM at 3 μM AA versus IC_{50} = 0.3 μM at 60 μM AA, Figure 3B, left panel), even though the absolute activities of 5-LO strongly differ at the various AA concentrations (Figure 3B, right panel). Note that in intact neutrophils, exogenous supplementation of 20 μM AA gave the opposite effect and decreased the potency of **1** to inhibit 5-LO product formation, suggesting that the molecular mechanisms for suppression of 5-LO activity differ between intact cells and cell-free assays.

Compounds featuring a Michael acceptor, such as TQ or nitro fatty acids, were shown to act as direct covalent enzyme inhibitors that target the catalytically relevant Cys416 and Cys418 in 5-LO (Awwad et al., 2014; Maucher et al., 2017). It appeared reasonable that the α,β-unsaturated aldehyde in **1**, **2**, and **3** may function as Michael acceptors and react with these cysteines. Incubation of melleolides with glutathione (GSH) for

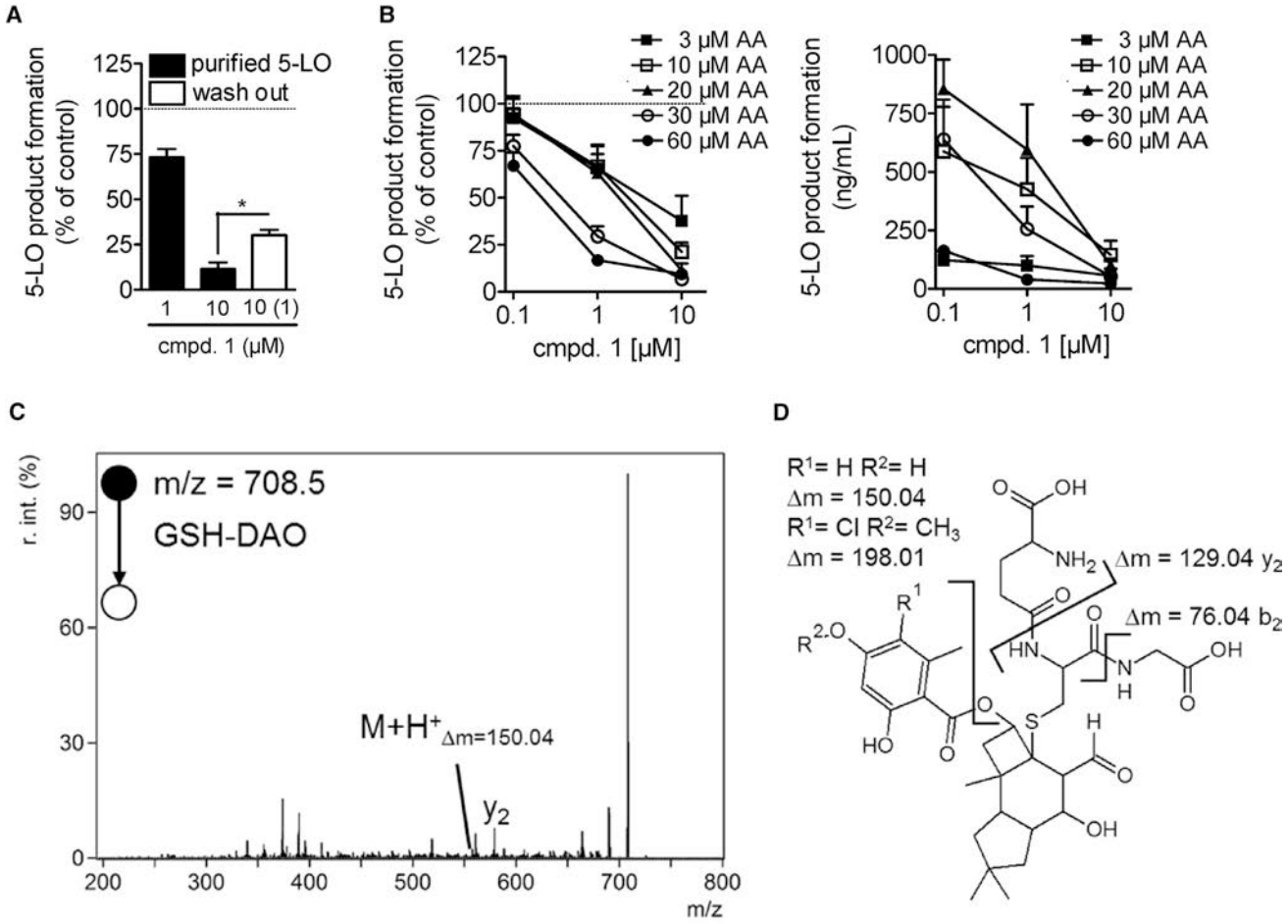

E

		Amino acid/Peptide terminus				
		Cys	His	Lys	Ser	N-Term
cmpd.	1	X**	X**	X**	-	X*
	2	X**	X**	X**	-	X*

Figure 3. Characterization of 5-LO Inhibition by Melleolides and Interaction with Cysteine

(A) Reversibility of 5-LO inhibition by **1**. Purified 5-LO (0.5 μg/mL) was pre-incubated with **1** (1 or 10 μM) or vehicle (0.1% DMSO) at 4°C for 10 min, pre-warmed at 37°C for 30 s, and 2 mM $CaCl_2$ and 20 μM AA were added. "Wash out" samples had been diluted 10-fold with assay buffer prior to addition of 2 mM $CaCl_2$ and 20 μM AA. After 10 min at 37°C, 5-LO products were analyzed by RP-HPLC. Data are expressed as percentage of control (100%), means ± SEM, n = 3, *$p < 0.05$ versus control, paired t test.

(B) Effect of various AA concentrations on 5-LO inhibition by **1**. Purified 5-LO (0.5 μg/mL) was pre-incubated with **1** or vehicle (0.1% DMSO) at 4°C for 10 min. Samples were pre-warmed at 37°C for 30 s, and 2 mM $CaCl_2$ and the indicated concentrations of AA were added and then incubated for 10 min at 37°C. Data are expressed as percentage of control (100%, left panel) or as ng/mL 5-LO products formed (right panel) and are given as means ± SEM, n = 3.

(C) MS^2 spectrum of **1** (DAO)-modified glutathione.

(D) Schematic fragmentation reactions with expected mass shifts.

(E) Results of specificity analysis with standard peptides. X, modification observed; –, no modification observed. *Indicates the detection of imine-formation in mass spectrum (side reaction), **Indicates the modification of peptide confirmed in MS^2 and/or MS^3.

See also Figures S2 and S3.

60 min at 37°C and subsequent analysis of the reaction mixture by tandem mass spectrometry (MS/MS) showed that **1** (Figures 3C and 3D) and **2** (Figure S2) reacted with the thiol group of GSH. The spectra revealed the expected signals for the resulting GSH-melleolide adducts (708.5 Da for **1**, Figure 3C, and 756.7 Da for **2**, Figure S2).

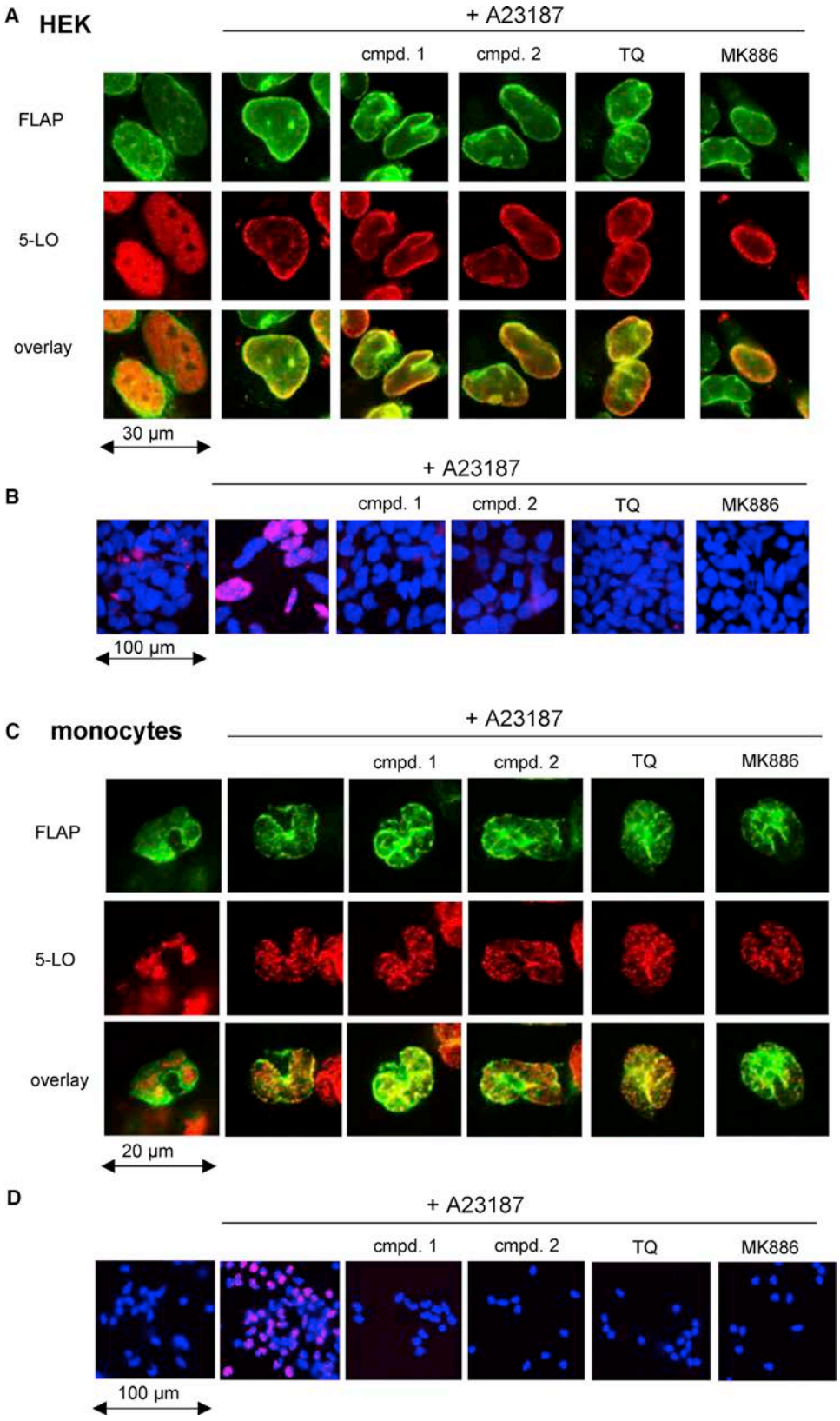

(legend on next page)

We next performed an amino acid residue specificity analysis (Figure 3E) to study binding of the melleolides to cysteine, histidine, serine, or lysine residues. These residues react in a Michael-like reaction but can also yield a semi-thioacetal or a semi-aminal. High-resolution MS spectra display the predicted masses of the reaction products that show the modification of cysteine, histidine, and lysine by **1** and **2**. MS/MS spectra displayed one main peak, which indicated the loss of chloroorsellinic acid or orsellenic acid, depending on the used melleolide. MS^3-spectra then showed the expected peptide fragment ion spectra and pointed out the binding side of the reactive sesquiterpene (Figure S3). The reaction of the melleolides with 5-LO displayed the mass of the modified peptide of **2** containing Cys159. MS/MS spectra yielded poor fragment ion abundance, so the exact modification site could not be confirmed.

Modulation of 5-LO Translocation and 5-LO/FLAP Interaction by Melleolides

5-LO translocation to the nuclear envelope and interaction with FLAP is a determinant for cellular 5-LO product formation (Gerstmeier et al., 2016a; Mandal et al., 2008). The superior potency of **1** against 5-LO activity in intact cells versus isolated enzyme led us to investigate if melleolides could block 5-LO translocation and/or interaction with FLAP. A convenient model based on HEK293 cells, stably transfected with 5-LO and FLAP, as well as human primary monocytes, were used. Immunofluorescence (IF) microscopy was performed to visualize the localization of the target proteins in the cell (Gerstmeier et al., 2014, 2016a). In agreement with previous data, 5-LO in resting HEK cells or human monocytes was mainly nucleosolic but co-localized with FLAP at the nuclear envelope upon A23187 stimulation (Figures 4A and 4C). However, neither **1** or **2** nor the Michael acceptor TQ or the FLAP inhibitor MK886 blocked A23187-induced 5-LO translocation (Figures 4A and 4C). Of interest, **1** and **2** (3 μM, each) as well as TQ (10 μM) impeded A23187-induced 5-LO/FLAP complex assembly in HEK cells (Figure 4B) and in monocytes (Figure 4D) that was monitored by *in situ* proximity ligation assay (PLA). The FLAP inhibitor MK886 (0.3 μM, used as control) blocked 5-LO/FLAP complex formation (Figures 4B and 4D), while the 5-LO inhibitor zileuton failed in this respect (not shown), as reported previously (Gerstmeier et al., 2016b). Taken together, the melleolides **1** and **2** as well as TQ impede the assembly of the LT-biosynthetic 5-LO/FLAP complex at the nuclear membrane, yet without blocking 5-LO translocation. This effect may be causative for superior inhibition of 5-LO product formation in intact cells.

Mutation of 5-LO Cysteines Affects Product Formation and Susceptibility for Melleolides

Previous studies suggested a role of the four surface cysteines 159, 300, 416, and 418 in 5-LO for cellular product formation (Hafner et al., 2015). Michael acceptors can act at either at Cys416 or Cys418 causing inhibition of 5-LO (Maucher et al., 2017). Thus, we studied if melleolides require these critical cysteines (Figure 5A) for inhibition of 5-LO. HEK cells were co-transfected with FLAP and with wild-type 5-LO (5-LO_WT) or with 5-LO mutants in which all four cysteines (5-LO_4C) or single cysteines had been replaced by serine. The mutated 5-LO proteins were expressed in HEK cells to a similar (5-LO_4C) or somewhat minor degree (5-LO_C159S, 5-LO_C300S, 5-LO_C416S, and 5-LO_C418S) versus 5-LO_WT (Figure 5B). Along these lines, the enzymatic capacities of corresponding HEK cell homogenates containing these 5-LO mutants were about 2- to 4-fold lower versus 5-LO_WT (Table 1). In HEK cell homogenates, **1** (Figure 5C, Table 1) and **2** (Figure S4) blocked 5-LO_WT activity, whereas 5-LO_4C was not affected at all. As for 5-LO_WT, the enzymatic activities of the mutants 5-LO_C159S, 5-LO_C300S, 5-LO_C416S, or 5-LO_C418S were also inhibited by **1** (Figure 5C, Table 1) and **2** (Figure S4). In contrast, zileuton inhibited 5-LO_WT and all mutated 5-LOs about equally well (Figure 5D).

Next, we analyzed cellular 5-LO product formation in intact HEK cells. Since previous data showed that 5-LO/FLAP-expressing HEK cells require exogenous AA for significant 5-LO product formation (Gerstmeier et al., 2014, 2016a), the cells were stimulated with A23187 plus 3 μM AA. In contrast to 5-LO activity in homogenates, all mutated 5-LOs formed much less amounts of products versus 5-LO_WT in intact cells (approximately 5- to 10-fold lower), in particular 5-LO_C159S (Table 1). Of interest, while product formation of 5-LO_WT was efficiently inhibited by **1** (10 μM), in HEK cells expressing 5-LO_4C but also 5-LO_C159S, melleolide **1** (or **2**, Figure S4) failed to markedly inhibit 5-LO product formation (Figure 5E, Table 1). Note that in cells expressing either 5-LO_C300S, 5-LO_C416S, or 5-LO_C418S, treatment with **1** (or **2**, Figure S4) caused efficient and concentration-dependent inhibition of 5-LO product formation comparable with cells expressing 5-LO_WT (Figure 5E). In contrast, zileuton consistently inhibited 5-LO activity in HEK cells regardless of the 5-LO mutations (Figure 5F). Hence, **1** and **2** may inhibit 5-LO product formation in intact cells via Cys159.

Role of Cysteines in 5-LO for Translocation and 5-LO/FLAP Interaction

In agreement with previous data (Hafner et al., 2015), the strikingly reduced capacities of the cysteine-mutated 5-LOs in intact HEK cells versus the moderately decreased activity of the 5-LO mutants in homogenates implied that cysteine mutations could affect 5-LO translocation and/or interaction with FLAP. Analysis of 5-LO translocation and co-localization with FLAP by IF microscopy revealed no impact of the cysteine mutations. That is, the subcellular localization of 5-LO_WT and all 5-LO mutants in resting HEK cells was comparable, and, upon A23187

Figure 4. Modulation of 5-LO Translocation and 5-LO/FLAP Interaction by Melleolides

Stably transfected HEK293 cells expressing 5-LO and FLAP (A and B) or human monocytes (C and D) were pre-incubated with compounds or vehicle (0.1% DMSO) for 10 min at 37°C, and subsequently incubated with 2.5 μM A23187 for 10 min. Images show single staining for FLAP (green), 5-LO (red), and overlay of 5-LO and FLAP (bottom lane). Results are representative for 100 individual cells of three independent experiments. (B and D) Proximity ligation assay (PLA) for assessing cellular *in situ* 5-LO/FLAP complex assembly. Stably transfected HEK293 cells expressing 5-LO and FLAP (B) or human monocytes (D) were pre-incubated with compounds or vehicle (0.1% DMSO) for 10 min at 37°C, and subsequently incubated with 2.5 μM A23187 for 10 min. DAPI (blue) was used to stain the nucleus and PLA signals (magenta dots) visualize 5-LO/FLAP interactions. Results are representative for 100 individual cells analyzed in three independent experiments.

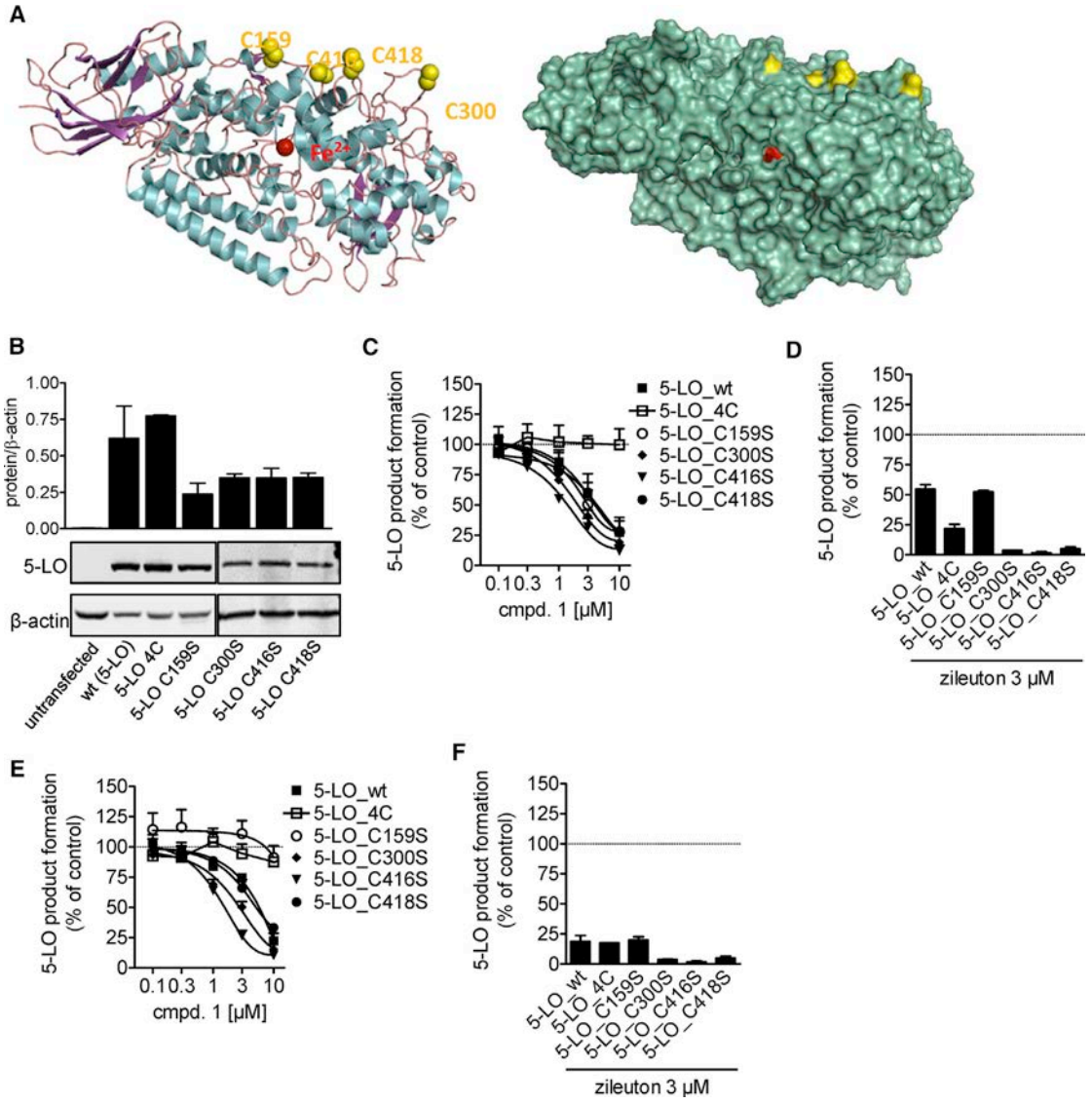

Figure 5. Mutation of 5-LO Cysteines Affects Product Formation and the Susceptibility for Melleolides

(A) Computational model of human 5-LO highlighting cysteine residues 159, 300, 416, and 418. The active site iron is highlighted in red.

(B) Western blot analysis of 5-LO protein expression in stably transfected HEK293 cells expressing FLAP and various 5-LO proteins (5-LO_WT and the mutants 5-LO_4C, 5-LO_C159S, 5-LO_C300S, 5-LO_C416S, and 5-LO_C418S). Results are representative for three independent experiments. Densitometric protein analysis: correlation of 5-LO density to β-actin density, means ± SEM, n = 3.

(C and D) Inhibition of 5-LO product formation in homogenates of HEK cells expressing FLAP and 5-LO (WT or mutants) by **1** at the indicated concentrations (C) and by 3 μM zileuton (D). HEK cells were sonicated on ice and pre-incubated with compounds or vehicle (0.1% DMSO) at 4°C for 10 min. Samples were pre-warmed for 30 s at 37°C and incubated with 2 mM $CaCl_2$ and 20 μM AA for another 10 min.

(E and F) Inhibition of 5-LO product formation in intact HEK cells expressing FLAP and 5-LO (WT or mutants) by **1** at the indicated concentrations (E) and by 3 μM zileuton (F). HEK cells (1 × 10^6/mL) were pre-incubated with **1**, zileuton, or vehicle (0.1% DMSO) for 10 min at 37°C and then stimulated with 2.5 μM A23187 and 3 μM AA for 10 min. Data are expressed as percentage of vehicle control (100%), means ± SEM, n = 4.

See also Figure S4.

stimulation, they all translocated to FLAP at the nuclear envelope (Figure 6A). Of interest, Cys159 seems to be instrumental for the 5-LO/FLAP interaction which was visualized by *in situ* PLA (Figure 6B). Thus, in HEK cells expressing 5-LO_WT, 5-LO_C300S, 5-LO_C416S, or 5-LO_C418S, stimulation with A23187 led to 5-LO/FLAP complex assembly. However, in HEK cells expressing 5-LO_4C or 5-LO_C159S, challenge with A23187 failed in this respect, implying a critical role of Cys159 in 5-LO/FLAP interaction.

DISCUSSION

Here, we identified human 5-LO as a molecular target of melleolides from honey mushroom. Exploiting **1** and **2** as the most

Table 1. Formation of 5-LO Products of Wild-Type and Mutated 5-LOs in HEK Cells and Corresponding Homogenates; Effects of Compound 1

	5-LO Product Formation			
	HEK Homogenates (ng/10^6 Cells)		Intact HEK Cells (ng/10^6 Cells)	
Enzyme	w/o	+ Compound **1** (% Inhibition)	w/o	+ Compound **1** (% Inhibition)
5-LO_WT	919.4 ± 40.0	243.0 ± 80.0 (72.6%)	346.8 ± 97.2	101.9 ± 23.3 (77.7%)
5-LO_4C	484.3 ± 58.8	477.7 ± 74.0 (0.4%)	48.1 ± 7.1	42.1 ± 6.3 (12.4%)
5-LO_C159S	456.9 ± 177.5	76.5 ± 11.9 (72.6%)	31.2 ± 12.4	24.6 ± 6.5 (9.8%)
5-LO_C300S	374.5 ± 29.7	71.6 ± 12.2 (81.0%)	71.5 ± 8.9	11.8 ± 4.5 (87.6%)
5-LO_C416S	223.1 ± 18.3	28.3 ± 12.0 (88.1%)	48.9 ± 9.5	5.0 ± 0.8 (89.6%)
5-LO_C418S	465.3 ± 22.8	124.9 ± 5.2 (73.2%)	66.6 ± 23.1	23.0 ± 9.5 (66.7%)

For analysis of 5-LO product formation in intact cells, HEK cells (1 × 10^6/mL) stably expressing FLAP and 5-LO enzymes (wild-type or mutants) were pre-incubated with 10 μM of **1** or vehicle (0.1% DMSO), and then stimulated with 2.5 μM A23187 and 3 μM AA for 10 min at 37°C. For analysis of 5-LO product formation in homogenates, the HEK cells (1 × 10^6/mL) were sonicated, the resulting homogenates were pre-incubated with 10 μM of **1** or vehicle (0.1% DMSO) and then incubated with 20 μM AA for 10 min at 37°C. Data are expressed as ng 5-LO products formed per 10^6 cells; means ± SEM, n = 4. w/o, without.

potent melleolide representatives revealed Cys159 in 5-LO as a crucial moiety for functional interaction of 5-LO with FLAP in LT biosynthesis. Our data suggest that melleolides suppress 5-LO product formation by two distinct modes of action: (1) by direct interference with the 5-LO enzyme activity involving two or more of the cysteines 159, 300, 416, and 418, and (2) by a more efficient mechanism that selectively involves Cys159 and prevents cellular 5-LO/FLAP complex assembly without affecting 5-LO translocation. Thus, our results shed light on the catalytic and regulatory role of cysteines at the substrate entrance of the 5-LO active site for the cellular capacity to biosynthesize LTs.

Melleolides were shown to exhibit antimicrobial activity and cytotoxic properties for cancer cells and primary human monocytes (Bohnert et al., 2011, 2014b), but interference with LT biosynthesis is thus far unexplored. With 5-LO, we identified a molecular target for these bioactive natural products. The efficient 5-LO-inhibitory melleolides possess a reactive aldehyde group at position 1 and a $\Delta^{2,4}$ (i.e., **1** and **2**) or $\Delta^{2,3}$ (i.e., **3**) double bond in the sesquiterpene moiety. Our SAR analysis indicates that the Michael acceptor functionality impacts 5-LO inhibitory activity, but also minor structural arrangements in the sesquiterpene moiety (α,β double bond at $\Delta^{2,4}$ versus $\Delta^{2,3}$ position, and the 4-OH moiety) and in the orsellinic acid residue (5′-OH methylation, 6′-chlorine). Strong potencies of 5-LO inhibitors often correlate with high lipophilicity (Werz, 2002), which may explain the superior effect of **2** with 5′-methoxy and 6′-chlorine residues over **1** in the cell-free assay.

Unexpectedly, the SARs for 5-LO inhibition by melleolides in intact neutrophils differ and reveal **1** as the most potent compound with a 10-fold lower IC_{50} value compared with interference with 5-LO in cell-free assays. Such superior potency in intact cells was not observed for the 5-LO inhibitor zileuton (this study and others [Carter et al., 1991]) and implies that additional factors that govern cellular 5-LO activity might be affected by melleolides. In fact, cellular regulation of 5-LO is complex, and several points of attack are conceivable that eventually cause or potentiate suppression of 5-LO product formation including interference with (1) AA release, (2) AA transfer via FLAP, (3) 5-LO translocation, and (4) upstream 5-LO signaling pathways such as MAPK and Ca^{2+}, and other 5-LO-activating processes (Radmark et al., 2015; Werz and Steinhilber, 2005). Our data show that melleolides, in addition to directly inhibiting 5-LO activity, prevent the 5-LO/FLAP complex assembly and, thus, could interfere with the AA transfer from FLAP to 5-LO. This may explain why excess of AA (20 μM) in intact cells diminishes the 5-LO-inhibitory potency of melleolides, although inhibition of 5-LO activity in cell-free assays is favored by high AA concentrations.

Most direct 5-LO inhibitors comprise lipophilic redox-active and/or iron-chelating compounds as well as AA mimetics that reversibly block AA conversion at the active or allosteric sites of 5-LO (Werz, 2002; Werz and Steinhilber, 2005). Based on the chemical structures of melleolides, fatty acid-like features are not readily apparent, and iron-chelating or redox properties have not been reported. Of interest, structurally different compounds containing SH-reactive groups such as the Michael acceptors TQ (Maucher et al., 2017), nitro fatty acids (Awwad et al., 2014), unsubstituted aminophenols (Kretschmer et al., 2017), or the maleimide-featured inhibitor U73122 (Feisst et al., 2005; Hornig et al., 2012) were shown to form covalent adducts with the surface cysteines 159, 416, and/or 418 and thereby potently and irreversibly inhibit 5-LO activity. The 5-LO structure exposes nine cysteine residues on the surface (Gilbert et al., 2011). We previously identified four cysteines (cysteines 159, 300, 416, and 418) located on the 5-LO surface in the region around the substrate entrance of the catalytic center that mediate dimerization of 5-LO (Hafner et al., 2011) and are important for the co-localization of 5-LO with FLAP at the nuclear membrane (Hafner et al., 2015). In our present study, melleolides failed to inhibit the activity of the 5-LO_4C mutant in cell-free and cell-based assays, suggesting that one or more of these cysteines are necessary to confer the 5-LO suppressive effect. In contrast, zileuton, which chelates the active site iron in 5-LO (Carter et al., 1991), suppressed the activity of this mutant, as expected. Note that 5-LO single mutants, with only one of the cysteines 159, 300, 416, or 418 being replaced by serine, were still effectively inhibited by melleolides in cell-free assays, implying that at least two of these cysteines are involved. This contrasts the suppressive effect of melleolides on 5-LO activity in intact

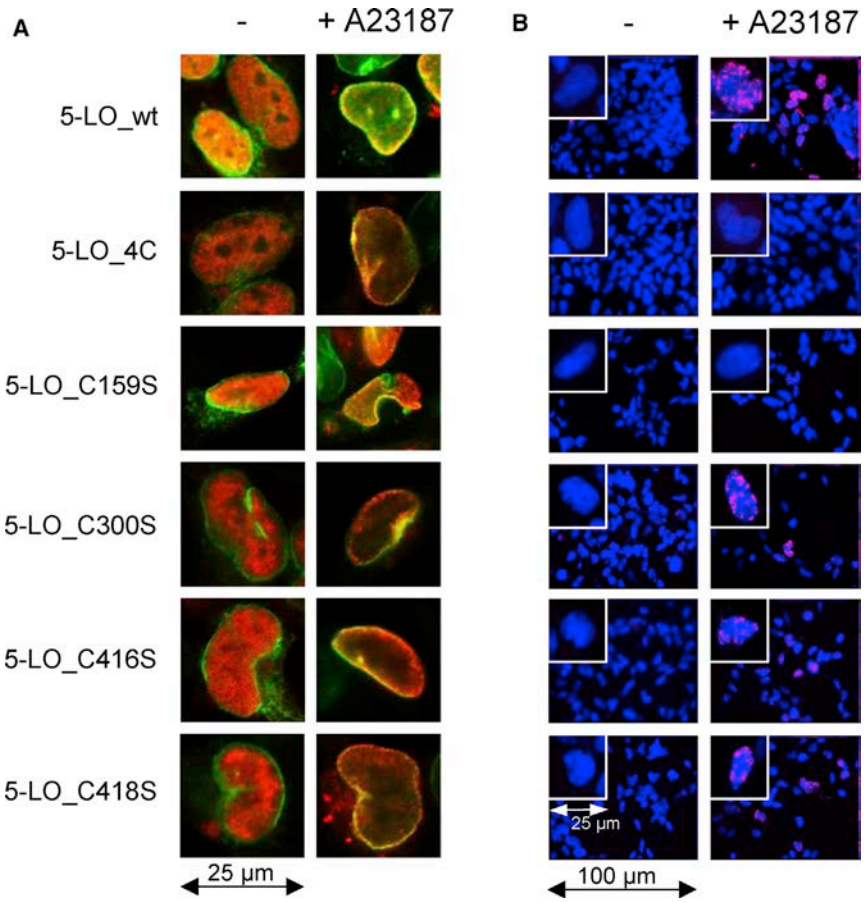

Figure 6. Role of Cysteines in 5-LO for Translocation and 5-LO/FLAP Interaction

(A) Immunofluorescence microscopy analysis of 5-LO translocation and co-localization with FLAP. Images show overlay of 5-LO (red) and FLAP (green).

(B) PLA for analysis of cellular *in situ* 5-LO/FLAP complex assembly. DAPI (blue) was used to stain the nucleus and *in situ* PLA signals (magenta dots) visualize 5-LO/FLAP complexes. Scale bars, 25 µm (insets) and 100 µm (overview). For both (A) and (B), stably transfected HEK cells expressing FLAP and 5-LO (WT or mutants) were incubated with 2.5 µM A23187 or vehicle (0.1% DMSO) for 10 min at 37°C. Results are representative for 100 individual cells of three independent experiments.

cells, where Cys159 emerged as a crucial residue required to mediate inhibition of 5-LO product formation. Thus, our results suggest that melleolides act via Cys159 to prevent the 5-LO/FLAP complex assembly while cysteines 300, 416, and 418 do not contribute.

FLAP, a nuclear membrane protein without any known enzymatic activity, is essential for 5-LO product formation in intact cells (Miller et al., 1990) by enabling AA substrate transfer to 5-LO for conversion to LTA_4 (Ferguson et al., 2007). Accordingly, FLAP inhibitors efficiently inhibit cellular LT biosynthesis by preventing 5-LO/FLAP assemblies (Garscha et al., 2016; Gerstmeier et al., 2016b) but they fail to inhibit 5-LO activity in cell-free assays where FLAP is dispensable for 5-LO to convert AA (Evans et al., 2008). Along these lines, mutation of cysteines 159, 300, 416, or 418, which were postulated to be important for 5-LO/FLAP co-localization (Hafner et al., 2015), hardly affected 5-LO activity in cell-free homogenates, but strikingly in intact cells. Moreover, 5-LO_C159S or 5-LO_4C failed to form complex assemblies with FLAP, in contrast to 5-LOs possessing Cys159. Interestingly, **1** and **2** (but not zileuton) required Cys159 to inhibit 5-LO product formation in intact cells. However, when this cysteine was replaced by serine, these mutants were not susceptible to the tested melleolides. Therefore, Cys159 is of major importance for 5-LO to interact with FLAP and as such mediates suppression of cellular 5-LO product formation by melleolides.

5-LO translocation to the nuclear envelope is mediated by elevated intracellular Ca^{2+} that binds to the C2-like domain of 5-LO (Kulkarni et al., 2002), and is essential for product biosynthesis (Gerstmeier et al., 2016b; Mandal et al., 2008; Radmark et al., 2015). The prenylated acylphloroglucinol hyperforin binds to the 5-LO C2-like domain and blocks 5-LO translocation and activity (Feisst et al., 2009), while FLAP inhibitors primarily prevent 5-LO/FLAP interaction without definite blockade of 5-LO movement (Garscha et al., 2016; Gerstmeier et al., 2016b). In analogy to MK886, **1** and **2** as well as TQ failed to block 5-LO translocation but they clearly inhibited the 5-LO/FLAP interaction.

Taken together, we identified human 5-LO as a molecular target of melleolides from the honey mushroom. We propose that melleolides containing an α,β-unsaturated aldehyde function as Michael acceptors that interfere with critical surface cysteines of 5-LO. While two or more of these cysteines mediate the direct inhibitory effects of melleolides on the enzymatic level, Cys159 confers suppression of cellular 5-LO product formation by melleolides via preventing the 5-LO/FLAP complex assembly. Finally, our data highlight the importance of Cys159 for 5-LO to interact with FLAP, a prerequisite for the biosynthesis of LTs in the cellular context.

SIGNIFICANCE

Only for very few mushroom toxins is the pharmacological mode of action understood and the molecular targets known. Melleolides are a family of sesquiterpene aryl esters of the globally distributed plant pathogenic and edible honey mushroom (*Armillaria mellea*). This family of natural products comprises >60 published members and represents one of the largest family of fungal small bioactive molecules. We discovered human 5-lipoxygenase (5-LO), the key enzyme in leukotriene biosynthesis, as a molecular target for those melleolides that possess an α,β-unsaturated aldehyde with thiol-reactive Michael acceptor functionality. Since leukotrienes are potent bioactive mediators with pivotal functions in inflammation and in the immune

response, their formation needs to be tightly controlled, for example, by temporal assembly of the biosynthetic protein complex of 5-LO with its helper protein FLAP. We provide evidence that melleolides mediate 5-LO inhibition via critical surface cysteines of the enzyme by two distinct modes of action: (1) by direct interference with the 5-LO catalytic activity involving two or more of the cysteines 159, 300, 416, and 418, and (2) by a more efficient cellular mechanism involving selectively Cys159, which prevents assembly of the 5-LO/FLAP complex in leukotriene biosynthesis. In conclusion, identification of 5-LO as a target for melleolides represents a basis for further investigations that will help evaluate the bioactions of this mushroom and its ingredients in view of the use for culinary purposes. By exploiting these melleolides as chemical tools we shed light on the catalytic and regulatory role of cysteines of 5-LO at the substrate entrance of the active site for the cellular capacity to generate bioactive mediators. Therefore, our study also unravels Cys159 in 5-LO as a crucial residue for accomplishing the functional interaction of 5-LO with FLAP in leukotriene biosynthesis, which offers a potential site for novel small-molecule inhibitors to intervene with 5-LO-related disorders.

STAR★METHODS

Detailed methods are provided in the online version of this paper and include the following:

- KEY RESOURCES TABLE
- CONTACT FOR REAGENT AND RESOURCE SHARING
- EXPERIMENTAL MODEL AND SUBJECT DETAILS
  - Human Cells
- METHODS DETAILS
  - Expression and Purification of Human Recombinant 5-LO
  - Determination of 5-LO Product Formation in Intact Cells and Homogenates
  - Determination of Release of [^{3}H]-Labeled Arachidonic Acid
  - LTC_4 Synthase Activity Assay
  - Determination of Isolated COX-1 and -2 Activity
  - Determination of PGE_2 Synthase Activity in a Cell-Free Assay
  - SDS PAGE and Western Blot
  - GSH Incubation
  - Standard Peptide Incubation
  - MALDI-MS Measurement and Data Analysis
  - Analysis of Subcellular Localization of 5-LO by Immunofluorescence Microscopy
  - In Situ Analysis of 5-LO/FLAP Interaction by Proximity Ligation Assay
- QUANTIFICATION AND STATISTICAL ANALYSIS

SUPPLEMENTAL INFORMATION

Supplemental Information includes four figures and one table and can be found with this article online at https://doi.org/10.1016/j.chembiol.2018.10.010.

ACKNOWLEDGMENTS

We thank Sven George for expert technical assistance and Dr. Michael Hörnig for mutation of 5-LO plasmids. The study was supported by Else Kröner-Fresenius-Stiftung (Else Kröner-Graduiertenkolleg), LOEWE TMP and Fraunhofer-Projektgruppe für Translationale Medizin und Pharmakologie (TMP), Deutsche Forschungsgemeinschaft (DFG; SFB 1039). Work in the groups of O.W. and D.H. is supported by the Collaborative Research Center ChemBioSys (SFB1127) of the DFG and by the DFG-funded excellence graduate school Jena School for Microbial Communication (JSMC).

AUTHOR CONTRIBUTIONS

S.K., B.H., D.S., M.K., U.G., D.H., and O.W. designed the research, gave advice, and planed the study. S.K., E.R., V.K., M.R., S.L., A.-K.H., M.D., and U.G., performed the experiments and analyzed the data. S.K. and O.W. wrote the manuscript.

DECLARATION OF INTERESTS

The authors declare no competing interests.

Received: May 28, 2018
Revised: July 25, 2018
Accepted: October 5, 2018
Published: November 8, 2018

REFERENCES

Albert, D., Zundorf, I., Dingermann, T., Muller, W.E., Steinhilber, D., and Werz, O. (2002). Hyperforin is a dual inhibitor of cyclooxygenase-1 and 5-lipoxygenase. Biochem. Pharmacol. *64*, 1767–1775.

Awwad, K., Steinbrink, S.D., Fromel, T., Lill, N., Isaak, J., Hafner, A.K., Roos, J., Hofmann, B., Heide, H., Geisslinger, G., et al. (2014). Electrophilic fatty acid species inhibit 5-lipoxygenase and attenuate sepsis-induced pulmonary inflammation. Antioxid. Redox Signal. *20*, 2667–2680.

Bair, A.M., Turman, M.V., Vaine, C.A., Panettieri, R.A., Jr., and Soberman, R.J. (2012). The nuclear membrane leukotriene synthetic complex is a signal integrator and transducer. Mol. Biol. Cell *23*, 4456–4464.

Baumgartner, K., Coetzee, M.P., and Hoffmeister, D. (2011). Secrets of the subterranean pathosystem of Armillaria. Mol. Plant Pathol. *12*, 515–534.

Bohnert, M., Miethbauer, S., Dahse, H.M., Ziemen, J., Nett, M., and Hoffmeister, D. (2011). In vitro cytotoxicity of melleolide antibiotics: structural and mechanistic aspects. Bioorg. Med. Chem. Lett. *21*, 2003–2006.

Bohnert, M., Nutzmann, H.W., Schroeckh, V., Horn, F., Dahse, H.M., Brakhage, A.A., and Hoffmeister, D. (2014a). Cytotoxic and antifungal activities of melleolide antibiotics follow dissimilar structure-activity relationships. Phytochemistry *105*, 101–108.

Bohnert, M., Scherer, O., Wiechmann, K., Konig, S., Dahse, H.M., Hoffmeister, D., and Werz, O. (2014b). Melleolides induce rapid cell death in human primary monocytes and cancer cells. Bioorg. Med. Chem. *22*, 3856–3861.

Carter, G.W., Young, P.R., Albert, D.H., Bouska, J., Dyer, R., Bell, R.L., Summers, J.B., and Brooks, D.W. (1991). 5-Lipoxygenase inhibitory activity of zileuton. J. Pharmacol. Exp. Ther. *256*, 929–937.

Evans, J.F., Ferguson, A.D., Mosley, R.T., and Hutchinson, J.H. (2008). What's all the FLAP about?: 5-lipoxygenase-activating protein inhibitors for inflammatory diseases. Trends Pharmacol. Sci. *29*, 72–78.

Feisst, C., Albert, D., Steinhilber, D., and Werz, O. (2005). The aminosteroid phospholipase C antagonist U-73122 (1-[6-[[17-beta-3-methoxyestra-1,3,5(10)-trien-17-yl]amino]hexyl]-1H-pyrrole-2,5- dione) potently inhibits human 5-lipoxygenase in vivo and in vitro. Mol. Pharmacol. *67*, 1751–1757.

Feisst, C., Pergola, C., Rakonjac, M., Rossi, A., Koeberle, A., Dodt, G., Hoffmann, M., Hoernig, C., Fischer, L., Steinhilber, D., et al. (2009). Hyperforin is a novel type of 5-lipoxygenase inhibitor with high efficacy in vivo. Cell Mol. Life Sci. *66*, 2759–2771.

Ferguson, A.D., McKeever, B.M., Xu, S., Wisniewski, D., Miller, D.K., Yamin, T.T., Spencer, R.H., Chu, L., Ujjainwalla, F., Cunningham, B.R., et al. (2007). Crystal structure of inhibitor-bound human 5-lipoxygenase-activating protein. Science *317*, 510–512.

Fischer, L., Poeckel, D., Buerkert, E., Steinhilber, D., and Werz, O. (2005). Inhibitors of actin polymerisation stimulate arachidonic acid release and 5-lipoxygenase activation by upregulation of Ca2+ mobilisation in polymorphonuclear leukocytes involving Src family kinases. Biochim. Biophys. Acta *1736*, 109–119.

Fischer, L., Szellas, D., Radmark, O., Steinhilber, D., and Werz, O. (2003). Phosphorylation- and stimulus-dependent inhibition of cellular 5-lipoxygenase activity by nonredox-type inhibitors. FASEB J. *17*, 949–951.

Garscha, U., Voelker, S., Pace, S., Gerstmeier, J., Emini, B., Liening, S., Rossi, A., Weinigel, C., Rummler, S., Schubert, U.S., et al. (2016). BRP-187: a potent inhibitor of leukotriene biosynthesis that acts through impeding the dynamic 5-lipoxygenase/5-lipoxygenase-activating protein (FLAP) complex assembly. Biochem. Pharmacol. *119*, 17–26.

Gerstmeier, J., Newcomer, M.E., Dennhardt, S., Romp, E., Fischer, J., Werz, O., and Garscha, U. (2016a). 5-Lipoxygenase-activating protein rescues activity of 5-lipoxygenase mutations that delay nuclear membrane association and disrupt product formation. FASEB J. *30*, 1892–1900.

Gerstmeier, J., Weinigel, C., Barz, D., Werz, O., and Garscha, U. (2014). An experimental cell-based model for studying the cell biology and molecular pharmacology of 5-lipoxygenase-activating protein in leukotriene biosynthesis. Biochim. Biophys. Acta *1840*, 2961–2969.

Gerstmeier, J., Weinigel, C., Rummler, S., Radmark, O., Werz, O., and Garscha, U. (2016b). Time-resolved in situ assembly of the leukotriene-synthetic 5-lipoxygenase/5-lipoxygenase-activating protein complex in blood leukocytes. FASEB J. *30*, 276–285.

Gilbert, N.C., Bartlett, S.G., Waight, M.T., Neau, D.B., Boeglin, W.E., Brash, A.R., and Newcomer, M.E. (2011). The structure of human 5-lipoxygenase. Science *331*, 217–219.

Haeggstrom, J.Z., and Funk, C.D. (2011). Lipoxygenase and leukotriene pathways: biochemistry, biology, and roles in disease. Chem. Rev. *111*, 5866–5898.

Hafner, A.K., Cernescu, M., Hofmann, B., Ermisch, M., Hornig, M., Metzner, J., Schneider, G., Brutschy, B., and Steinhilber, D. (2011). Dimerization of human 5-lipoxygenase. Biol. Chem. *392*, 1097–1111.

Hafner, A.K., Gerstmeier, J., Hornig, M., George, S., Ball, A.K., Schroder, M., Garscha, U., Werz, O., and Steinhilber, D. (2015). Characterization of the interaction of human 5-lipoxygenase with its activating protein FLAP. Biochim. Biophys. Acta *1851*, 1465–1472.

Hornig, M., Markoutsa, S., Hafner, A.K., George, S., Wisniewska, J.M., Rodl, C.B., Hofmann, B., Maier, T., Karas, M., Werz, O., et al. (2012). Inhibition of 5-lipoxygenase by U73122 is due to covalent binding to cysteine 416. Biochim. Biophys. Acta *1821*, 279–286.

Koeberle, A., Northoff, H., and Werz, O. (2009). Curcumin blocks prostaglandin E2 biosynthesis through direct inhibition of the microsomal prostaglandin E2 synthase-1. Mol. Cancer Ther. *8*, 2348–2355.

Koeberle, A., Siemoneit, U., Buhring, U., Northoff, H., Laufer, S., Albrecht, W., and Werz, O. (2008). Licofelone suppresses prostaglandin E2 formation by interference with the inducible microsomal prostaglandin E2 synthase-1. J. Pharmacol. Exp. Ther. *326*, 975–982.

Kretschmer, S.B., Woltersdorf, S., Vogt, D., Lillich, F.F., Ruhl, M., Karas, M., Maucher, I.V., Roos, J., Hafner, A.K., Kaiser, A., et al. (2017). Characterization of the molecular mechanism of 5-lipoxygenase inhibition by 2-aminothiazoles. Biochem. Pharmacol. *123*, 52–62.

Kulkarni, S., Das, S., Funk, C.D., Murray, D., and Cho, W. (2002). Molecular basis of the specific subcellular localization of the C2-like domain of 5-lipoxygenase. J. Biol. Chem. *277*, 13167–13174.

Leslie, C.C. (2015). Cytosolic phospholipase A(2): physiological function and role in disease. J. Lipid Res. *56*, 1386–1402.

Liening, S., Scriba, G.K., Rummler, S., Weinigel, C., Kleinschmidt, T.K., Haeggstrom, J.Z., Werz, O., and Garscha, U. (2016). Development of smart cell-free and cell-based assay systems for investigation of leukotriene C4 synthase activity and evaluation of inhibitors. Biochim. Biophys. Acta *1861*, 1605–1613.

Mandal, A.K., Jones, P.B., Bair, A.M., Christmas, P., Miller, D., Yamin, T.T., Wisniewski, D., Menke, J., Evans, J.F., Hyman, B.T., et al. (2008). The nuclear membrane organization of leukotriene synthesis. Proc. Natl. Acad. Sci. U S A *105*, 20434–20439.

Maucher, I.V., Ruhl, M., Kretschmer, S.B., Hofmann, B., Kuhn, B., Fettel, J., Vogel, A., Flugel, K.T., Manolikakes, G., Hellmuth, N., et al. (2017). Michael acceptor containing drugs are a novel class of 5-lipoxygenase inhibitor targeting the surface cysteines C416 and C418. Biochem. Pharmacol. *125*, 55–74.

Miller, D.K., Gillard, J.W., Vickers, P.J., Sadowski, S., Leveille, C., Mancini, J.A., Charleson, P., Dixon, R.A., Ford-Hutchinson, A.W., Fortin, R., et al. (1990). Identification and isolation of a membrane protein necessary for leukotriene production. Nature *343*, 278–281.

Misiek, M., Williams, J., Schmich, K., Huttel, W., Merfort, I., Salomon, C.E., Aldrich, C.C., and Hoffmeister, D. (2009). Structure and cytotoxicity of arnamial and related fungal sesquiterpene aryl esters. J. Nat. Prod. *72*, 1888–1891.

Momose, I., Sekizawa, R., Hosokawa, N., Iinuma, H., Matsui, S., Nakamura, H., Naganawa, H., Hamada, M., and Takeuchi, T. (2000). Melleolides K, L and M, new melleolides from *Armillariella mellea*. J. Antibiot. (Tokyo) *53*, 137–143.

Pace, S., Rossi, A., Krauth, V., Dehm, F., Troisi, F., Bilancia, R., Weinigel, C., Rummler, S., Werz, O., and Sautebin, L. (2017). Sex differences in prostaglandin biosynthesis in neutrophils during acute inflammation. Sci. Rep. *7*, 3759.

Pergola, C., Gerstmeier, J., Monch, B., Caliskan, B., Luderer, S., Weinigel, C., Barz, D., Maczewsky, J., Pace, S., Rossi, A., et al. (2014). The novel benzimidazole derivative BRP-7 inhibits leukotriene biosynthesis in vitro and in vivo by targeting 5-lipoxygenase-activating protein (FLAP). Br. J. Pharmacol. *171*, 3051–3064.

Radmark, O., Werz, O., Steinhilber, D., and Samuelsson, B. (2015). 5-Lipoxygenase, a key enzyme for leukotriene biosynthesis in health and disease. Biochim. Biophys. Acta *1851*, 331–339.

Scherer, O., Steinmetz, H., Kaether, C., Weinigel, C., Barz, D., Kleinert, H., Menche, D., Muller, R., Pergola, C., and Werz, O. (2014). Targeting V-ATPase in primary human monocytes by archazolid potently represses the classical secretion of cytokines due to accumulation at the endoplasmic reticulum. Biochem. Pharmacol. *91*, 490–500.

Soderberg, O., Gullberg, M., Jarvius, M., Ridderstrale, K., Leuchowius, K.J., Jarvius, J., Wester, K., Hydbring, P., Bahram, F., Larsson, L.G., et al. (2006). Direct observation of individual endogenous protein complexes in situ by proximity ligation. Nat. Methods *3*, 995–1000.

Steinhilber, D., Herrmann, T., and Roth, H.J. (1989). Separation of lipoxins and leukotrienes from human granulocytes by high-performance liquid chromatography with a Radial-Pak cartridge after extraction with an octadecyl reversed-phase column. J. Chromatogr. *493*, 361–366.

Surette, M.E., Palmantier, R., Gosselin, J., and Borgeat, P. (1993). Lipopolysaccharides prime whole human blood and isolated neutrophils for the increased synthesis of 5-lipoxygenase products by enhancing arachidonic acid availability: involvement of the CD14 antigen. J. Exp. Med. *178*, 1347–1355.

Werz, O. (2002). 5-Lipoxygenase: cellular biology and molecular pharmacology. Curr. Drug Targets Inflamm. Allergy *1*, 23–44.

Werz, O., and Steinhilber, D. (2005). Development of 5-lipoxygenase inhibitors – lessons from cellular enzyme regulation. Biochem. Pharmacol. *70*, 327–333.

STAR★METHODS

KEY RESOURCES TABLE

REAGENT or RESOURCE	SOURCE	IDENTIFIER
Antibodies		
p-ERK1/2 (Thr202/Tyr204)	Cell Signaling Technology	9106S; RRID: AB_331768
ERK1/2	Cell Signaling Technology	9102S; RRID: AB_330744
p-cPLA$_2$ (Ser505)	Cell Signaling Technology	2831S; RRID: AB_2164445
p-p38 (Thr180/Tyr182)	Cell Signaling Technology	9211S; RRID: AB_331641
β-actin	Cell Signaling Technology	3700S; RRID: AB_2242334
GAPDH	Santa Cruz	Sc-47724; RRID: AB_627678
IRDye 800CW Goat anti-Mouse IgG (H+L)	LI-COR	[P/N 925-32210]; RRID: AB_2687825
IRDye 680LT Goat anti-Rabbit IgG (H+L)	LI-COR	[P/N 925-68020]; RRID: AB_2687826
FLAP	Abcam	ab85227; RRID: AB_10673941
Alexa Fluor 488 goat anti-rabbit IgG (H+L)	Invitrogen	A11034; RRID: AB_2576217
Alexa Fluor 555 goat anti-mouse IgG (H+L)	Invitrogen	A21424; RRID: AB_141780
Chemicals, Peptides, and Recombinant Proteins		
DMSO	VWR	1029500500
bovine serum albumin	AppliChem	A1391.0500
penicillin/streptomycin	GE Healthcare Life Sciences	A2213
RPMI-1640	GE Healthcare Life Sciences	R8758-6
fetal calf serum	Sigma	F7524
Histopaque®-1077	Sigma	10771-500ML
Thymoquinone	Sigma	03416-100MG
Celecoxib	Sigma	PZ0008
N-Formyl-Met-Leu-Phe (fMLP)	Sigma	F3506-10MG
Duolink® insitu PLA probe anti-mouse minus	Sigma	DUO92004-100RXN
Duolink® insitu PLA probe anti-rabbit plus	Sigma	DUO92002-100RXN
Duolink® insitu detection reagents far red	Sigma	DUO92013
Duolink® insitu PLA wash buffers fluorescence	Sigma	DUO82049-4L
Rotiszint® eco plus	Carl Roth	0016.4
ovine COX-1	Cayman Chemicals	60100
human recombinant COX-2	Cayman Chemicals	60122
LTA$_4$ methyl ester	Cayman Chemicals	20010.25 μg
LTC$_4$ methyl ester d$_5$	Cayman Chemicals	9001287-50
MK886	Cayman Chemicals	10133-5
arachidonic acid	Cayman Chemicals	90010
Zileuton	Sequoia Research Products	SRP01100z
Critical Commercial Assays		
DC protein assay kit	Biorad	5000111
Experimental Models: Cell Lines		
HEK293	ATCC	CRL-153
HEK293_5-LO	Hafner et al., 2015	N/A
HEK293_5-LO_C159S	Hornig et al., 2012	N/A
HEK293_5-LO_C300S	Hornig et al., 2012	N/A
HEK293_5-LO_C416S	Hornig et al., 2012	N/A
HEK293_5-LO_C418S	Hornig et al., 2012	N/A
HEK293_5-LO_C159S_C300S_C416S_C418S	Hafner et al., 2015	N/A
A549	ATCC	CCL-185

(*Continued on next page*)

Continued

REAGENT or RESOURCE	SOURCE	IDENTIFIER
Experimental Models: Organisms/Strains		
Escherichia coli BL21 (DE3)	New England Biolabs	C2525I
Software and Algorithms		
GraphPad InStat 3	GraphPad Software Inc	https://www.graphpad.com/scientific-software/instat/
Odyssey 3.0 software	LI-COR	https://www.licor.com/bio/products/software/image_studio/index.html
Xcalibur Qual Browser Software 2.0.7	Thermo Fisher Scientific	http://www.thermofisher.com/order/catalog/product/OPTON-30487
mMass version 5.5.0	open source mass spectometry	http://www.mmass.org/download/
AxioVision Se64 Rel. 4.9	Carl Zeiss	https://www.zeiss.de/mikroskopie/downloads/axiovision-downloads.html

CONTACT FOR REAGENT AND RESOURCE SHARING

Further information and requests for resources and reagents should be directed to and will be fulfilled by the Lead Contact, Oliver Werz (oliver.werz@uni-jena.de)

EXPERIMENTAL MODEL AND SUBJECT DETAILS

Human Cells

Neutrophils and monocytes were isolated from peripheral human blood of adult healthy male and female volunteers (18-65 years) as described (Pace et al., 2017; Scherer et al., 2014) and with consent obtained from the Institute of Transfusion Medicine, University Hospital Jena. Individual blood samples provided and used for leukocyte isolation were blinded and thus, the exact age and the sex of the donor was unknown. The protocols for experiments with human neutrophils and monocytes were approved by the ethical commission of the Friedrich-Schiller-University Jena (approval no. 4025-02/14). All methods were performed in accordance with the relevant guidelines and regulations. Leukocyte concentrates were prepared by centrifugation (4000×g, 20 min, 20°C) and erythrocytes were removed by dextran sedimentation, followed by centrifugation on lymphocyte separation medium (Histopaque®-1077, Sigma-Aldrich) to obtain peripheral blood mononuclear cells (PBMC) and neutrophils. Resulting neutrophils were finally resuspended in PBS pH 7.4 containing 1 mg/mL glucose and 1 mM $CaCl_2$ (PGC buffer). PBMC were seeded in RPMI 1640 (Sigma-Aldrich) containing 10% (v/v) heat inactivated fetal calf serum (FCS), 100 U/mL penicillin, and 100 μg/mL streptomycin in cell culture flasks (Greiner Bio-one, Frickenhausen, Germany) for 1.5 h at 37°C and 5% CO_2. Adherent monocytes were washed twice with PBS and were resuspended in PGC buffer. HEK (human embryonic kidney, female fetus)293 cells stably transfected with FLAP and 5-LO or 5-LO mutants (Hornig et al., 2012; Hafner et al., 2015) were cultured in monolayers in DMEM High Glucose (4.5 g/L) medium supplemented with heat-inactivated FCS (10%, v/v), 100 U/mL penicillin, and 100 μg/mL streptomycin at 37°C in a 5% CO_2 incubator.

METHODS DETAILS

Expression and Purification of Human Recombinant 5-LO

Escherichia coli (BL21) cells were transformed with plasmid pT3-5-LO, and human recombinant 5-LO protein was expressed overnight at 30°C as previously described (Fischer et al., 2003). Cells were lysed in 50 mM triethanolamine/HCl pH 8.0, 5 mM EDTA, 1 mM phenylmethanesulphonyl fluoride (PMSF), soybean trypsin inhibitor (STI, 60 μg/mL), and lysozyme (1 mg/mL), homogenized by sonication (3 × 20 s), and centrifuged at 40,000×g for 20 min at 4°C. For purification of 5-LO, ATP affinity chromatography was used and the 40,000×g supernatant (S40) was applied to an ATP agarose column (Sigma-Aldrich). Aliquots of semi-purified 5-LO were diluted with ice-cold PBS containing 1 mM EDTA. Samples were pre-incubated with the test compounds or vehicle (0.1% DMSO). After 10 min at 4°C, samples were stimulated with 2 mM $CaCl_2$ plus the indicated concentrations of AA to start 5-LO product formation. The reaction was stopped after 10 min by addition of one volume of ice-cold methanol, and the formed metabolites were analyzed by RP-HPLC as described (Pergola et al., 2014; Steinhilber et al., 1989). 5-LO products include the all-trans isomers of LTB_4 as well as 5-HPETE and its corresponding alcohol 5-HETE.

Determination of 5-LO Product Formation in Intact Cells and Homogenates

For activity assays with intact cells, 5 × 10^6 freshly isolated neutrophils or monocytes, or 1 × 10^6 HEK293 cells stably producing the indicated recombinant proteins, were resuspended in 1 mL PGC buffer. After pre-incubation with compounds **1-4** (10 min, 37°C), 5-LO product formation was started by addition of 2.5 μM A23187 with or without 20 μM AA (neutrophils, monocytes) or 3 μM AA (HEK cells). After 10 min at 37°C, the reaction was stopped with 1 mL of ice-cold methanol. Formed 5-LO metabolites were extracted

and analyzed by RP-HPLC using a C18 RP Radial PAK column (Waters, Eschborn, Germany) (Pergola et al., 2014; Steinhilber et al., 1989) or optionally by UPLC-MS/MS as described (Pace et al., 2017).

To determine 5-LO product formation in homogenates, neutrophils (5×10^6) or HEK293 cells (1×10^6) were resuspended in 1 mL PBS containing 1 mM EDTA. Cells were lysed on ice by sonication (3×20 s) and resulting cell homogenates were pre-incubated with compounds or vehicle (0.1% DMSO) for 10 min on ice. 5-LO product formation was started by addition of 2 mM $CaCl_2$ and 20 μM AA (neutrophils) or 10 μM AA (HEK cells). After 10 min at 37°C, reaction was stopped by 1 mL ice-cold methanol. 5-LO product formation was analyzed as described above for intact cells.

Determination of Release of [^{3}H]-Labeled Arachidonic Acid

Release of [^{3}H]-labeled AA from human neutrophils was analyzed as described (Fischer et al., 2005). In brief, freshly isolated neutrophils were immediately resuspended at 10^7 cells/mL RPMI 1640 medium containing 5 nM [^{3}H]AA (corresponding to 0.5 μCi/mL, specific activity 200 Ci/mmol) and incubated for 120 min at 37°C in 5% CO_2 atmosphere. Cells were then washed twice with PBS containing 1 mg/mL glucose and 2 mg/mL fatty acid-free bovine albumin, to remove unincorporated [^{3}H]AA. Labelled neutrophils (2×10^7) were resuspended in 1 mL PGC containing 2 mg/mL fatty acid-free bovine albumin and pre-incubated with 0.1% DMSO or test compounds (15 min, 37°C) and then stimulated with 2.5 μM A23187 for 10 min. The samples were then placed on ice, centrifuged and aliquots (300 μL) of the supernatants were assayed for radioactivity by scintillation counting (Micro Beta Trilux, Perkin Elmer, Waltham, MA, USA).

LTC_4 Synthase Activity Assay

Preparation of HEK293 cells stably expressing LTC_4 synthase and generation of microsomes were performed as described (Liening et al., 2016). Microsomes were pre-incubated with compounds or vehicle (0.1% DMSO) for 10 min at 4°C prior stimulation with 1 μM LTA_4 methyl ester (Cayman, Ann Harbor, MI) for 10 min. The reaction was stopped by 1 vol ice-cold methanol and acidified PBS, and the internal standard LTC_4 methyl ester-d_5 was added prior to solid phase extraction. LTC_4 methyl ester formation was analyzed by UPLC-MS/MS as described previously (Liening et al., 2016).

Determination of Isolated COX-1 and -2 Activity

Purified COX-1 (ovine, 50 units) or COX-2 (human recombinant, 20 units) were pre-incubated with compounds or vehicle (0.1% DMSO) for 5 min at 4°C in 1 mL reaction buffer containing 100 mM Tris buffer pH 8, 5 mM GSH, 5 μM hemoglobin, and 100 μM EDTA prior 1 min at 37°C to prewarm samples. COX product formation was started by adding AA (COX-1: 5 μM, COX-2: 2 μM) which resulted in generation of 12-HHT (12(*S*)-hydroxy-5-*cis*-8,10-*trans*-heptadecatrienoic acid) non-enzymatically formed from COX-derived PGH_2. 12-HHT was measured by RP-HPLC as previously reported (Albert et al., 2002).

Determination of PGE_2 Synthase Activity in a Cell-Free Assay

Preparation of A549 cells, induction of mPGES-1 by IL-1β, generation of microsomes, and analysis of mPGES-1 activity was performed exactly as described previously (Koeberle et al., 2008, 2009).

SDS PAGE and Western Blot

Neutrophils (1×10^7/100 μL ice-cold PGC buffer) were pre-incubated for 10 min at 37°C with test compounds at 37°C, stimulated with 1 μM *N*-formyl-methionyl-leucyl-phenylalanine (fMLP) for 1.5 min at 37°C. The reaction was stopped by addition of 100 μL ice-cold 2 × SDS loading buffer (20 mM Tris-HCl pH 8, 2 mM EDTA, 5% (m/v) SDS, 10% (v/v) β-mercaptoethanol, 10 μg/mL leupeptin, 60 μg/mL STI, 1 mM PMSF, 40 μL glycerol and 0.1% bromophenol blue (1:1, v/v). Samples were boiled for 5 min at 96°C, sonicated (3×10 sec, 4°C) and proteins were separated and analyzed by SDS–PAGE and Western Blotting.

To control stable expression of transfected enzymes, HEK cells (1×10^6/100 μL) were washed and lysed with Triton X-100 lysis buffer (20 mM Tris-HCl pH 7.4, 150 mM NaCl, 2 mM EDTA, 1% (v/v) Triton X-100, 0.5% (v/v) NP-40, 10 μg/mL leupeptin, 60 μg/mL STI, 1 mM PMSF) for 15 min on ice with occasional vortexing. Lysates were centrifuged (21,000×g, 10 min, 4°C) and the supernatant was mixed with 4 × Laemmli buffer (50 mM Tris-HCl pH 6.8, 12.5 mM EDTA, 2% (m/v) SDS, 10% (v/v) glycerol, 1% (v/v) β-mercaptoethanol, 0.02% (m/v) bromophenol blue) and samples were boiled for 5 min at 96°C.

Correct protein loading on the gels and transfer of proteins to nitrocellulose membrane (Amersham PROTRAN® supported 0.45 NC, GE Healthcare, Freiburg, Germany) were confirmed by Ponceau staining. Antibodies recognizing phosphorylated ERK1/2 (Thr202/Tyr204), ERK1/2, p-cPLA$_2$ (Ser505), p-p38 (Thr180/Tyr182) or β-actin were from Cell Signaling Technology (Boston, MA) and used at 1:1000 dilution. The antibody against GAPDH (1:1000) was purchased from Santa Cruz (Dallas, TX) and the rabbit FLAP (1:1000) antibody was obtained from Abcam (Cambridge, UK). The rabbit 5-LO antiserum (1551, AK7, 1:8 dilution) was kindly provided by Dr. Olof Rådmark, Karolinska Institutet, Stockholm, Sweden. Infrared-labeled secondary antibody IRDye 800CW goat anti-mouse was from LI-COR Biosciences (Lincoln, NE). For detection, the Odyssey Infrared Imaging System (LI-COR Bioscience, Lincoln, NE) and for analysis the Odyssey application software (version 3.0.25) were used.

GSH Incubation

Glutathione (GSH) adduct formation tests were carried out directly on the MALDI-target in a total volume of 2 μL. 1 μL of 2 mM GSH in PBS pH 7.4 and 1 μL of 20 μM compound or vehicle in PBS pH 7.4 were mixed on the target to obtain a final concentration of 1 mM

GSH and 10 μM compound. The reaction mixture was kept humid for 30 min at 37°C using a SunDigest digestion chamber (SunChrom, Friedrichsdorf, Germany). The reaction was stopped after 30 min of incubation with 1 μL CHCA-solution (3 mg/mL CHCA (α-cyano-4-hydroxy-cinnamic acid) in 70/30/0.1 acetonitrile/water/trifluoroacetic acid (TFA)). After matrix crystallization, we used chilled 5%-formic acid to remove salt contaminations from the matrix crystals and recrystallized the sample with acetonitrile/water (80/20, v/v) mixture containing 0.1% TFA to obtain a homogeneous crystallization.

Standard Peptide Incubation

Binding assays using the standard peptides AAAACAAAAR, AAAAHAAAAR, AAAAKAAAAR, AAAASAAAAR (JPT Peptide technology, Berlin, Germany) were also directly carried out on the MALDI-target. Peptides were diluted in PBS pH 7.4 to a concentration of 20 μM and mixed separately with each compound at a concentration of 20 μM in a total volume of 2 μL to obtain a final concentration of 10 μM peptide and 10 μM compound. Incubation was performed using the SunDigest system for 1 h at 37°C. The reaction was stopped using the same matrix solution as described above. Washing and recrystallization of the formed spots were performed as previously described (Kretschmer et al., 2017).

MALDI-MS Measurement and Data Analysis

MALDI-MS measurements were carried out using a MALDI-Duo ion source coupled to an Orbitrap LTQ XL mass spectrometer (Thermo Fisher Scientific, Bremen, Germany). MS measurements were carried out on an Orbitrap mass analyzer. For GSH adducts, the mass was recorded from m/z 200.00 to 800.00 and for standard peptide assay, the mass range was between m/z 800.00 and 2000.00. 50 subspectra were accumulated for data analysis. Mass resolution was set to 30,000 (FWHM at m/z: 400), laser energy was adjusted to optimize MS spectra quality. MS/MS spectra of reaction products and peptides were recorded using the ion trap mass analyzer. 100 subspectra were accumulated for data analysis. Normalized collision energy was set to 50. Isolation of the particular reaction product was performed using an isolation width of 1 Da. MS spectra were analyzed using the Qual Browser software version 2.0.7 (Thermo Fisher Scientific). This software was also used to compare the theoretical masses. Theoretical masses of peptides, reaction products, and MS/MS ion masses were calculated using mMass version 5.5.0.

Analysis of Subcellular Localization of 5-LO by Immunofluorescence Microscopy

For analysis of 5-LO and FLAP subcellular localization in monocytes, PBMC were seeded in RPMI medium containing 2 mM L-glutamine, 100 U/ml penicillin, and 100 μg/ml streptomycin onto glass coverslips in a 12-well plate and cultured for 1.5 h. The 5-LO/FLAP subcellular localization was also analyzed using HEK293 cells stably transfected with 5-LO enzymes and FLAP. Cells (0.45×10^6/mL) were seeded on poly-D-lysine-coated coverslips and cultured at 37°C, 5% CO_2 until 60% confluence. Cells were washed with PGC buffer and preincubated with test compounds or vehicle (0.1% DMSO) 10 min at 37°C in PGC buffer prior to activation. Cells were then stimulated for 10 min with 2.5 μM A23187 and stopped by fixation with 4% paraformaldehyde solution. Ice-cold acetone (5 min, 4°C) was used for permeabilization prior to blocking with non-immune goat serum. Samples were incubated with mouse monoclonal anti-5-LO antibody (1:300; made in-house, Goethe University Frankfurt, Germany) (Gerstmeier et al., 2014; Pergola et al., 2014) and rabbit polyclonal anti-FLAP antibody (1:500; Abcam, Cambridge, UK) at 4°C overnight. 5-LO and FLAP were stained with the fluorophore-labeled secondary antibodies; Alexa Fluor 488 goat anti-rabbit (1:1000) and Alexa Fluor 555 goat anti-mouse (1:1000, Invitrogen, Darmstadt, Germany). Nuclear DNA was stained with DAPI (Invitrogen). Samples were analyzed with a Zeiss Axiovert 200 M microscope, and a Plan Neofluar ×100/1.30 Oil (DIC III) objective (Zeiss, Jena, Germany). A Zeiss AxioCam MR camera was used for image acquisition.

In Situ Analysis of 5-LO/FLAP Interaction by Proximity Ligation Assay

To analyze the *in situ* interaction of 5-LO with FLAP in monocytes and HEK293 cells, an *in situ* proximity ligation assay (PLA) was performed, according to the manufacturers' protocol (Soderberg et al., 2006) and as described (Gerstmeier et al., 2016b). Samples were treated, fixed and incubated with primary antibody as described for IF microscopy above. Cells were then incubated with species specific secondary antibodies conjugated with oligonucleotides (PLA probe anti-mouse MINUS and anti-rabbit PLUS) for 1 h at 37°C. By addition of two other circleforming DNA oligonucleotides and a ligase (30 min at 37°C) the antibody-bound oligonucleotides form a DNA circle when the target proteins are less than 40 nm distant from each other. The newly generated DNA circle was amplified by rolling circle amplification and visualized by hybridization with fluorescently labeled oligonucleotides. Nuclear DNA was stained with DAPI. The PLA interaction signal appears as a fluorescent spot and was analyzed using the above described microscope and equipment.

QUANTIFICATION AND STATISTICAL ANALYSIS

Results are presented as means ± standard error of the mean (SEM) of *n* independent observations, where *n* represents the number of performed experiments at different days or with different donors. Statistical analysis of the data was performed by one-way ANOVA using GraphPad InStat (Graphpad Software Inc., San Diego, CA) followed by a Bonferroni post-hoc test for multiple or student t-test for single comparisons, respectively. P-values < 0.05 were considered as significant.

Cell Chemical Biology, Volume *26*

Supplemental Information

Melleolides from Honey Mushroom

Inhibit 5-Lipoxygenase via Cys159

Stefanie König, Erik Romp, Verena Krauth, Michael Rühl, Maximilian Dörfer, Stefanie Liening, Bettina Hofmann, Ann-Kathrin Häfner, Dieter Steinhilber, Michael Karas, Ulrike Garscha, Dirk Hoffmeister, and Oliver Werz

Supporting Information

Melleolides from honey mushroom inhibit 5-lipoxygenase via Cys159

Stefanie König, Erik Romp, Verena Krauth, Michael Rühl, Maximilian Dörfer, Stefanie Liening, Bettina Hofmann, Ann-Kathrin Häfner, Dieter Steinhilber, Michael Karas, Ulrike Garscha, Dirk Hoffmeister, and Oliver Werz

Content:

Supplemental Table 1

assay / enzyme	**cmpd. 1** (% remaining activity)	**control inhibitor** (% remaining activity)
[^{3}H]AA release (neutrophils)	75.2 ± 3.1	48.8 ± 2.6 (RSC-3388, 10 μM)
LTC_4 synthase	83.7 ± 14.5	3.5 ± 0.7 (MK886, 10 μM)
COX-1	89.7 ± 5.7	26.2 ± 7.2 (indomethacin, 10 μM)
COX-2	114.3 ± 8.2	59.1 ± 0.8 (celecoxib, 5 μM) 25.4 ± 1.7 (indomethacin, 10 μM)
mPGES-1	79.8 ± 2.9	18.1 ± 3.2 (MK886, 10 μM)

Table S1. **Effects of 1 on various enzymes involved in eicosanoid biosynthesis, related to Figure 2.** Melleolide **1** (1 μM) or control inhibitors (as indicated) were added to the respective enzymes or isolated neutrophils 10 min prior starting the reaction. Data are expressed as percentage of control (vehicle, 100%), mean ± SEM, n = 3.

Supplemental Figure 1

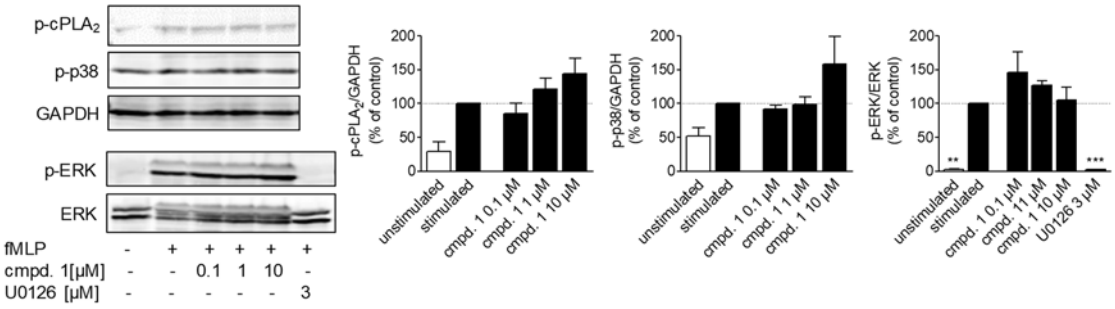

Fig. S1. Effects of 1 on the phosphorylation of p38 MAPK, ERK-1/2 and cPLA$_2$ in neutrophils, related to Figure 2. Neutrophils were pre-incubated with **1**, reference inhibitor U0126 (3 µM), or vehicle (0.1% DMSO) for 10 min at 37 °C prior stimulation with 1 µM *N*-formyl-methionyl-leucyl-phenylalanine (fMLP) for 1.5 min. The amounts of phospho-ERK-1/2 and ERK1/-2 (for normalization), phospho-p38 MAPK, phospho-cPLA$_2$ and GAPDH (for normalization) were analyzed by Western blot. Data, obtained by densitometry (bar charts, mean + S.E.M.; $n = 3$), are expressed as percentage of fMLP-stimulated control.

Supplemental Figure 2

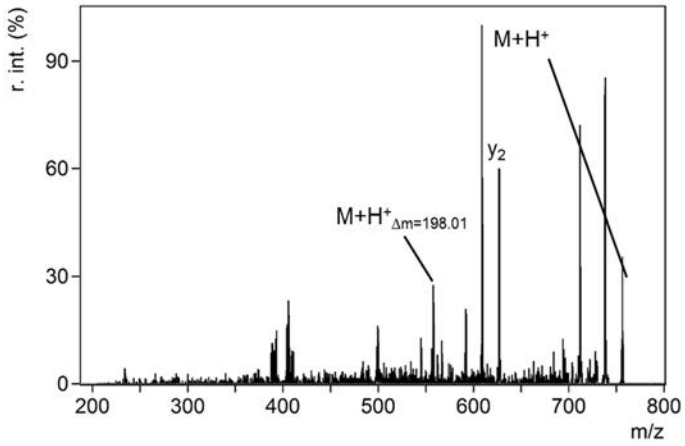

Fig. S2. MS²-spectra of modified cmpd. 2-modified GSH indicate covalent binding of cmpd. 2 to GSH, related to Figure 3.

Supplemental Figure 3

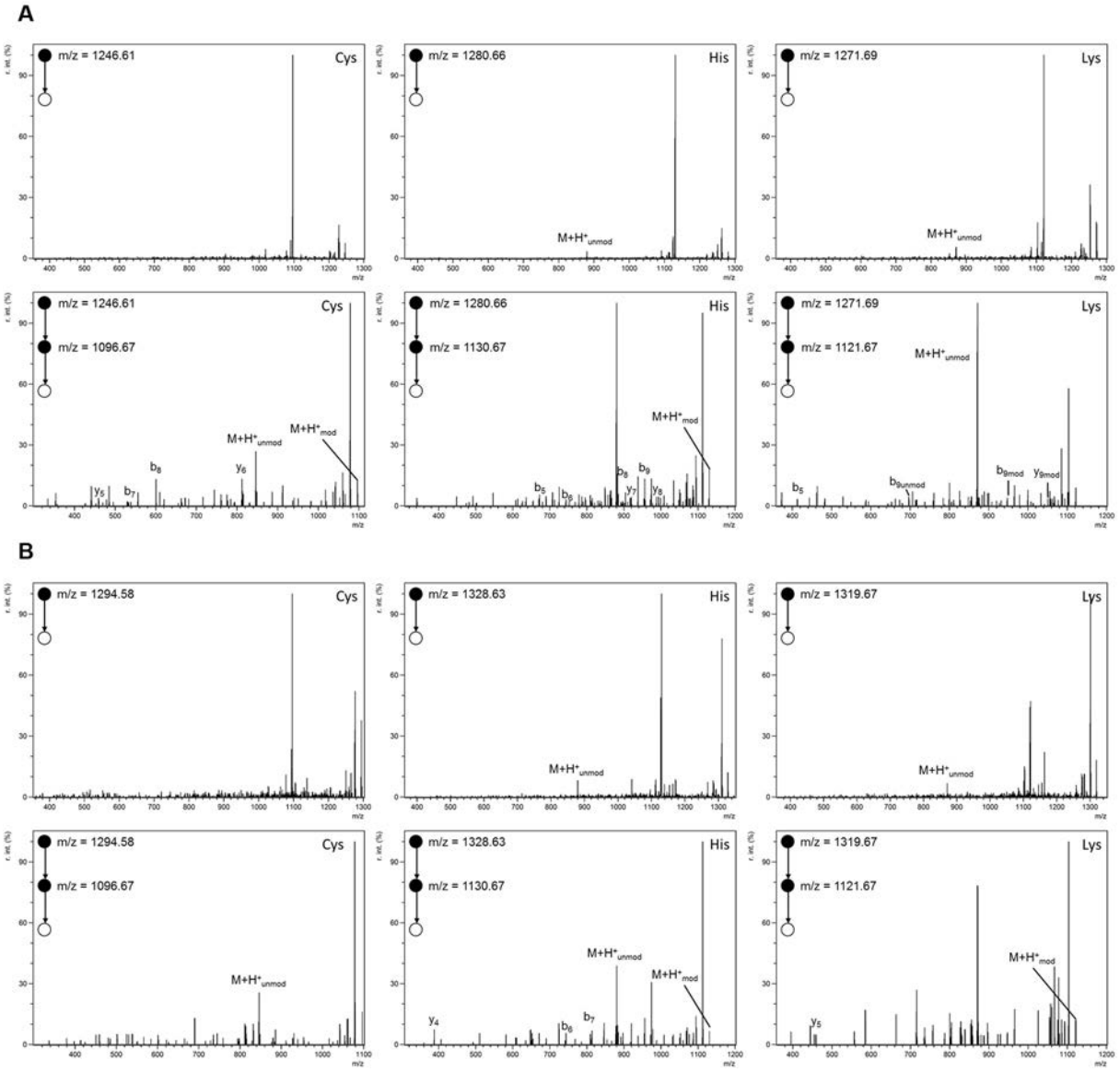

Fig. S3. MS²-spectra covalent binding of cmpd. 1 and cmpd. 2 to synthetic peptides, related to Figure 3. (A) Modification of standard peptides by compd. **1**. Upper panel shows MS² spectra of modified AAAACAAAAR (left row), AAAAHAAAAR (middle row) and AAAAKAAAAR (right row). Lower panel shows MS³ spectra of the main fragments m/z = 1096.67, 1130.67 and 1121.67. (B) Modification of standard peptides by cmpd. **2**. Upper panel shows MS² spectra of modified AAAACAAAAR (left row), AAAAHAAAAR (middle row) and AAAAKAAAAR (right row). Lower panel shows MS³ spectra of the main fragments m/z = 1096.67, 1130.67 and 1121.67.

Supplemental Figure 4

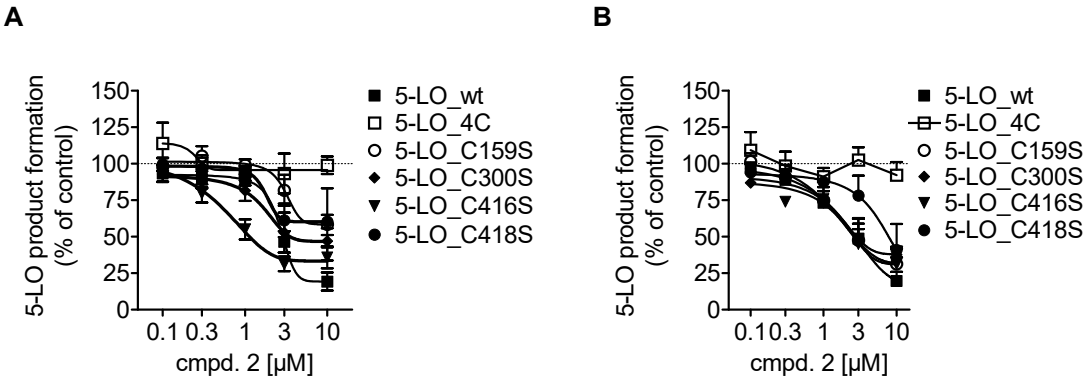

Fig. S4. Inhibition of 5-LO by cmpd. 2, related to Figure 5. (A) Intact HEK cells. (B) HEK homogenates. HEK cells (10^6/ml) expressing 5-LO_FLAP, 4C_FLAP, C159S_FLAP, C300S_FLAP, C416S_FLAP or C418S_FLAP mutant were pretreated with compd. **2** or 0.1% DMSO (vehicle) for 10 min at 37 °C. Cells were stimulated with 2.5 µM A23187 and 3 µM AA for 10 min at 37 °C. Data are expressed as percentage of control (100%), mean ± SEM, n = 4, * $p<0.05$, ** $p< 0.01$, *** $p< 0.001$ versus vehicle control.

3.3. Publikation 3 – Diversity and bioactivity of *Armillaria* sesquiterpene aryl ester natural product

Maximilian Dörfer, Markus Gressler, Dirk Hoffmeister

Mycological Progress, 2019, Volume 18, 1027-1037.

Zusammenfassung

Die Melleolide aus Basidiomyceten der Gattung *Armillaria* sind niedermolekulare Naturstoffe. Biosynthetisch aus einem trizyklischen Sesquiterpen-Protoilludenalkohol verestert mit einem Tetraketid (Orsellinsäure und Derivate) bestehend, stellen die Melleolide mit mehr als 70 bekannten Verbindungen ein Lehrbuchbeispiel für diversitätsorientierte Biosynthese dar. Dieser Übersichtsartikel fasst die strukturelle Vielfalt der Melleolide zusammen und beschreibt, soweit bekannt, die enzymatische Grundlage zur Biosynthese der Verbindungen. Des Weiteren wurden aktuelle Kenntnisse über die antimikrobielle, phytotoxische und cytotoxische Aktivität der Melleolide mit Fokus auf deren molekulare Zielstrukturen sowie deren unterschiedliche Beziehungen zwischen Struktur und Aktivität und letztlich deren Wirkmechanismen herausgearbeitet.

Eigenanteil 40%:

Maximilian Dörfer: Literaturrecherche, Gestaltung von Abbildungen, Verfassen des Manuskripts

Jena, den

_____

Prof. Dr. Dirk Hoffmeister

Mycological Progress (2019) 18:1027–1037
https://doi.org/10.1007/s11557-019-01508-z

DGfM

ORIGINAL ARTICLE

Diversity and bioactivity of *Armillaria* sesquiterpene aryl ester natural products

Maximilian Dörfer[1] · Markus Gressler[1] · Dirk Hoffmeister[1]

Received: 11 June 2019 / Accepted: 25 July 2019

Abstract
Species of the basidiomycete genus *Armillaria* produce bioactive small molecule natural products, referred to as melleolides. With more than 70 described members, this class of natural products is a prime example for diversity-oriented biosynthesis. Chemically, they represent hybrid molecules, composed of a tricyclic, chiral sesquiterpene protoilludene alcohol, esterified with the tetraketide orsellinic acid or its derivatives. In this review article, we summarize the melleolide's structural diversity and present—to the extent elucidated—the enzymatic basis how their backbone structures are biosynthesized and modified. We also highlight the current knowledge on their antimicrobial, phytotoxic, and cytotoxic bioactivities, along with a view on the molecular targets of the melleolides, their unparalleled structure-activity relationships, and their modes of action.

Keywords *Armillaria mellea* · Biosynthesis · Natural product · Melleolide · Orsellinic acid · Protoilludene · Sesquiterpene

Introduction

Probably the most intriguing phenomenon of fungal biology is organismal and morphological diversity. On the molecular and chemical level, this biological diversity is mirrored by the plethora of small yet structurally complex, highly functionalized, and often chiral bioactive natural products that fungi produce. This secondary metabolism has evolved, often in a species- or genus-specific way, towards structural diversity, while the primary metabolism is rather uniform to secure fundamental cellular functions. In the field of basidiomycete secondary metabolism, excellent reviews summarize various aspects of this metabolic wealth (Gill and Steglich 1987; Gill 2003; Zjawiony 2004; Zhou and Liu 2010; Jiang et al. 2011; Sandargo et al. 2019). The so-called screening hypothesis provides the theoretical framework to explain chemical diversity in an evolutionary context. Strong bioactivity is a rare property of a molecule. Consequently, those organisms that have evolved the capacity to produce a maximum number of metabolites at a minimal cost are more likely to produce one or various compounds that confer useful properties on the producer and, hence, the respective biosynthesis is favored by selection (Firn and Jones 2003; Firn and Jones 2009).

This contribution focuses on the melleolides, a unique class of basidiomycete metabolites. They are produced by species of the genus *Armillaria* (Physalacriaceae, Agaricales) in the traditional wide sense (Fig. 1). This genus underwent changes, as the non-annulate species were segregated to represent the closely related genus *Desarmillaria* (*D. ectypa*, *D. tabescens*; Koch et al. 2017). Also, the circumscription of species changed, based on morphological, biological, and phylogenetic species concepts. For example, what was traditionally considered *Armillaria mellea* in North America was confirmed to include ten *Armillaria* species (Brazee et al. 2012). These fungi are best known as notorious hardwood or conifer pathogens as they cause butt and root rot in both managed and unmanaged forests (Baumgartner et al. 2011). Beyond the economic burden for forestry, *Armillaria* species also damage agriculturally important crops, such as peach or coffee trees, and grapes. Yet, as white-rot fungi, *Armillaria* species help disintegrate lignocellulose and thus serve a positive ecological role as they maintain the carbon

This article is part of the "Topic collection on Basidiomycote Mycology in honor of Franz Oberwinkler who passed away in March 2018."

Responsible editor: Marc Stadler

✉ Dirk Hoffmeister
dirk.hoffmeister@hki-jena.de

[1] Department Pharmaceutical Microbiology at the Hans-Knöll-Institute, Friedrich-Schiller-Universität, Winzerlaer Strasse 2, 07745 Jena, Germany

Fig. 1 Carpophores of *Armillaria mellea* in a Central European deciduous forest (photograph taken in September 2018)

flux. Here, we present an overview of the diversity of the melleolides, i.e., the natural products that define the genus *Armillaria* with regard to secondary metabolism. As probably the most diverse family of basidiomycete small molecules, they represent a textbook example of diversity-oriented biosynthesis. Chemical structures are shown in Figs. 2, 3, 4, and 5. We also highlight—to the extent known—the enzymes that create this diversity. An introduction to the bioactivities and pharmacological modes of action concludes this article.

Structural diversity of the melleolides

From antibacterially active chloroform extracts of *A. mellea* cultures, Oduro et al. (1976) identified four compounds and partially characterized one of them by spectroscopic methods. Notably, they discovered a signature UV/vis spectrum and observed nuclear magnetic resonance (NMR) signals that are compatible with those later found for the melleolides. Subsequently, Donnelly et al. (1982, 1984; Donnelly and Coveney 1987) succeeded in isolation and structural elucidation of armillyl orsellinate (Fig. 4b; for references and chemical properties of all melleolides, please refer to Table 1) as the first member of the melleolides. The same authors also showed that armillyl orsellinate inhibited *Bacillus subtilis* and *Staphylococcus aureus*. Ever since *Armillaria* natural products have been studied intensively, and even though only produced by one fungal genus, the melleolides have emerged as one of the largest classes of fungal natural products with as yet 71 described and characterized naturally occurring structural congeners, including one unnatural, yet biocatalytically synthesized compound, 6′-bromomelleolide F (Wick et al. 2016, Fig. 5f). Melleolides represent molecular hybrids as two structural elements of dissimilar biosynthetic origin are merged into one final scaffold: the first element is the C_{15} tricyclic protoilludene framework. It originates from geranyldiphosphate, the universal precursor to the sesquiterpenes. In some melleolides (e.g., 15-hydroxy-5′-

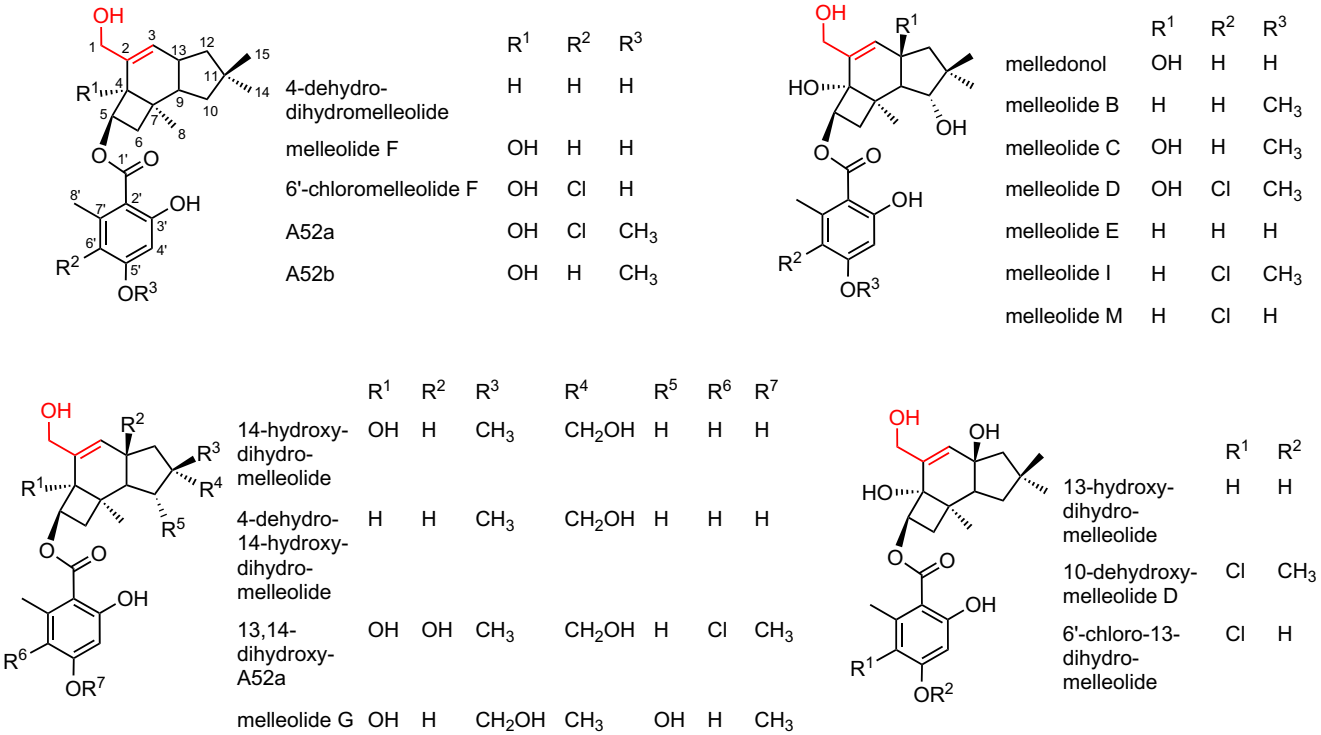

Fig. 2 Chemical structures of melleolides featuring primary alcohol at C-1 and a $\Delta^{2,3}$ skeleton. The numbering of carbon atoms does not follow IUPAC rules but reflects numbering in all previous literature. The structural element typical for the respective sub-category is highlighted in red. Exact molecular weights and literature references for all compounds in Figs. 2 through 5 are given in Table 1

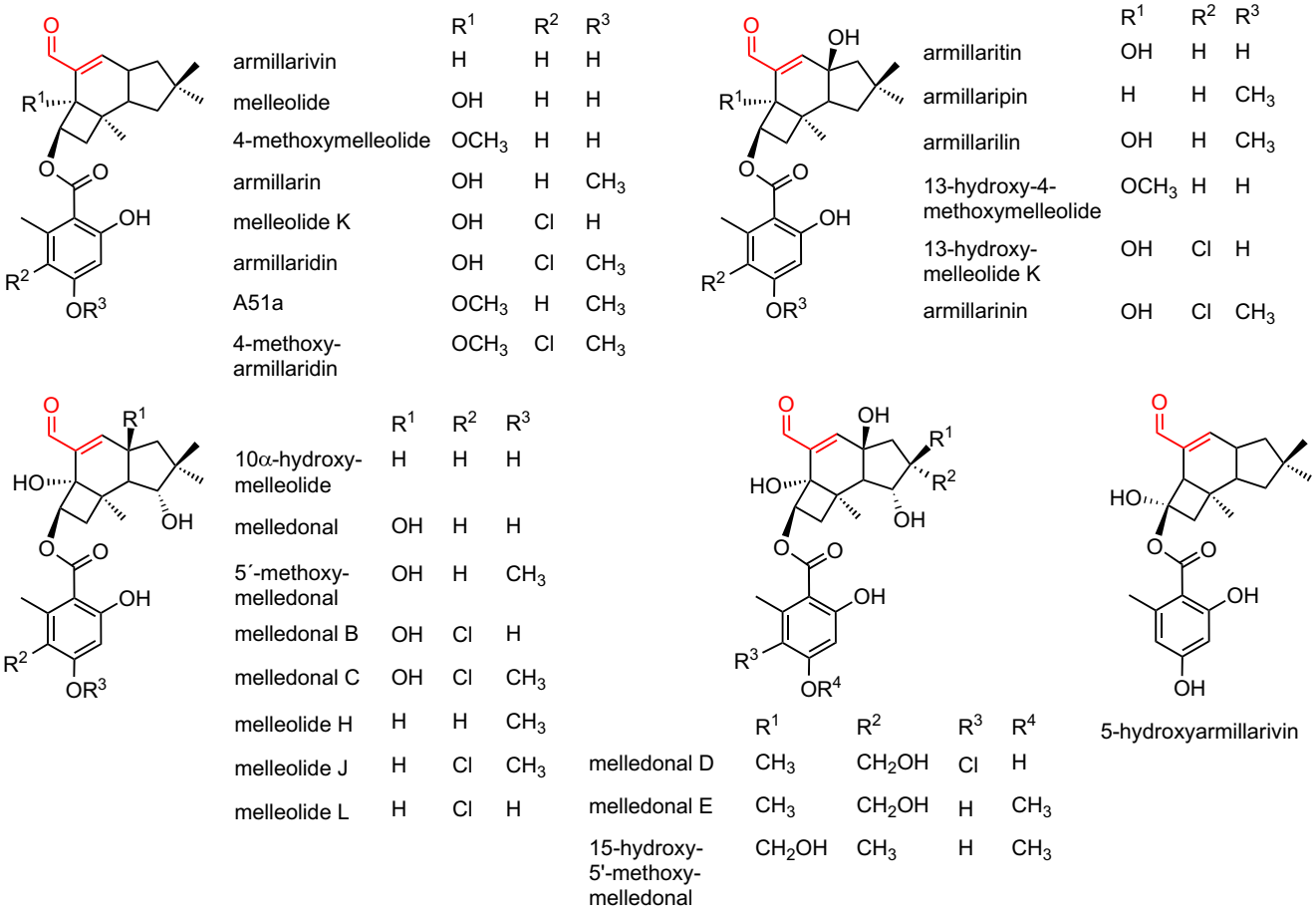

Fig. 3 Chemical structures of melleolides with an aldehyde at C-1 and a $\Delta^{2,3}$ skeleton

methoxymelledonal, Fig. 3) this tricyclic sesquiterpene core features as many as six consecutive stereocenters. The second moiety is orsellinic acid, i.e., a planar phenolic acid derivative of polyketidic origin. *Armillaria* uniquely combines these two moieties by esterification. Intriguingly, the individual structural elements are common natural product classes: orsellinic acid or its derivatives are known from lichen and countless bacterial and fungal sources (Yamazaki et al. 1965; Shen 2003; Schroeckh et al. 2009; Braesel et al. 2017). Likewise, protoilludene derivatives have been isolated from numerous basidiomycetes, among them the tsugicolines A–E from *Laurilia tsugicola* and the prototypical Δ^{6}-protoilludene and Δ^{7}-protoilludene-6-ol, which were first discovered in *Fomitopsis insularis* (Abraham 2001). The terms (proto)illudene or illudol root in the species name *Omphalotus illudens* (= *Clitocybe illudens*), after which these compounds were named (McMorris et al. 1967).

The first layer of structural diversity among the melleolides results from esterification of these two moieties. In the vast

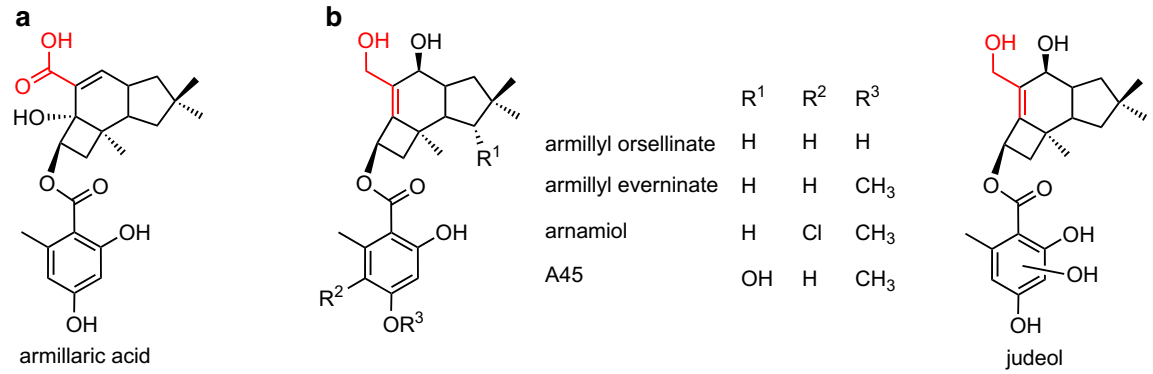

Fig. 4 Chemical structures of melleolides. **a** Armillaric acid that carries a carboxylic acid at C-1. **b** Melleolides with primary alcohol at C-1 and a $\Delta^{2,4}$ terpene moiety

majority of cases, ester formation involves the secondary alcohol at the 5-OH of the protoilludene. Seven melleolides show esterification via the 1-OH group. However, the true structural diversity stems from a near-permutational organization of how the scaffold is modified (Figs. 2, 3, 4, and 5). Modifications that occur invariably are terpene hydroxylations at C-1 to introduce primary alcohol, at C-5 for secondary alcohol, and mutually exclusive hydroxylation at C-3 or C-4 with nearly all melleolides. Other modifications may or may not be introduced and include:

i) Stereoselective hydroxylations at C-10, C-13, e.g., in melledonol (Donnelly et al. 1985b), and at C-14 or C-15, e.g., in melledonal D and melleolide G, respectively (Arnone et al. 1988c)
ii) Oxidation of the primary alcohol at C-1 to an aldehyde or carboxy group, e.g., found for melleolide (Midland et al. 1982), or armillaric acid (Obuchi et al. 1990)
iii) Regioselective orsellinic acid chlorination at C-6′, e.g., armillaridin (Yang et al. 1984) or melleolide D (Arnone et al. 1986)
iv) Methylether formation at O-5′ of the aromatic moiety, e.g., with armillaridin (Yang et al. 1984), or melleolide D (Arnone et al. 1986) to convert orsellinic acid into everninic acid and/or at the oxygen atom O-4 (if present) in the terpene, e.g., with 4-methoxymelleolide (Donnelly et al. 1985a)
v) A double bond shift to isomerize the $\Delta^{2,4}$ to a $\Delta^{2,3}$ skeleton, e.g., in melleolide (Midland et al. 1982). In the two-dimensional structural representation, this isomerization appears a minor modification but has major consequences for the three-dimensional spatial configuration (Fig. 6) which also impacts bioactivity.
vi) Reductive removal of the terpene double bond, e.g., found for armillane (Donnelly and Hutchinson 1990)
vii) Introduction of a second, conjugated double bond, probably by water elimination, to create a cyclohexadiene ring system, e.g., the one of armillaricin (Yang et al. 1989a).

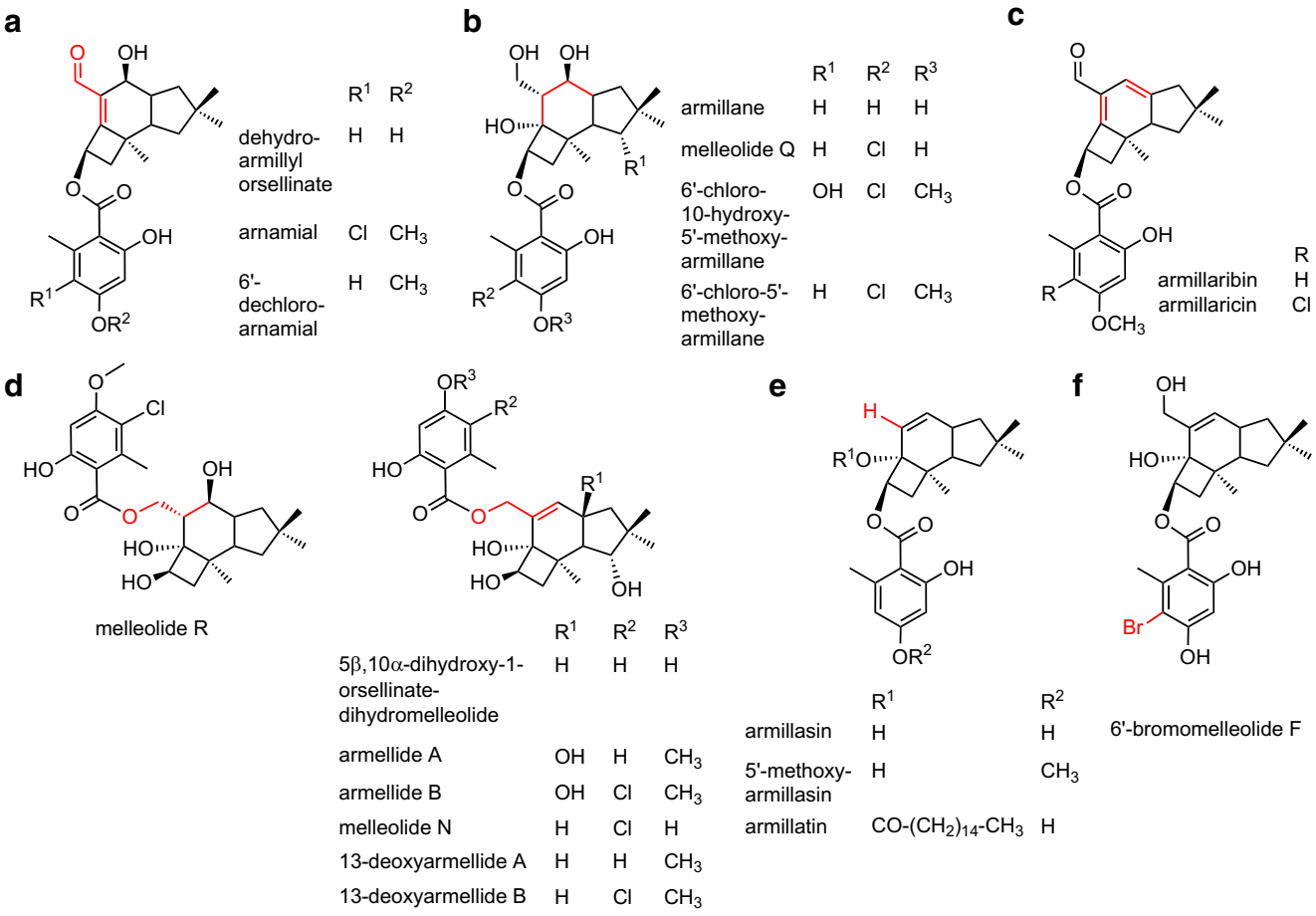

Fig. 5 Chemical structures of melleolides. **a** Representatives featuring an aldehyde at C-1 and a $\Delta^{2,4}$ skeleton. **b** Armillane and congeners whose tricyclic terpene ring system does not possess a double bond. **c** Melleolides whose tricyclic terpene ring systems possess two double bonds ($\Delta^{2,4}$, $\Delta^{3,13}$). **d** Melleolides whose ester bond involves C-1. **e** Melleolides lacking C-1. **f** Structure of the non-natural 6′-bromomelleolide F which was produced biocatalytically

Table 1 Overview on published melleolides. Compounds are grouped according to Figs. 2, 3, 4, and 5

Fig.	Compound	Exact mass (*m/z*)	Sum formula	Species of the first isolation	Reference
2	4-Dehydro-dihydromelleolide	388.2249	$C_{23}H_{32}O_5$	*Desarmillaria tabescens*	Donnelly et al. (1997)
	Melleolide F	402.2042	$C_{23}H_{30}O_6$	*Armillaria mellea*	Arnone et al. (1988c)[a]
	4-Dehydro-14-hydroxy-dihydromelleolide	402.2042	$C_{23}H_{30}O_6$	*D. tabescens*	Donnelly et al. (1997)
	A52b	416.2199	$C_{24}H_{32}O_6$	*A. cepistipes*	Sonnenbichler et al. (1997)
	Melleolide E	418.1992	$C_{23}H_{30}O_7$	*A. mellea*	Arnone et al. (1988c)[b]
	14-Hydroxy-dihydromelleolide	418.1992	$C_{23}H_{30}O_7$	*D. tabescens*	Donnelly et al. (1997)
	13-Hydroxydihydro-melleolide	418.1992	$C_{23}H_{30}O_7$	*A. mellea*	Donnelly et al. (1990)
	Melleolide B	432.2148	$C_{24}H_{32}O_7$	*A. mellea*	Arnone et al. (1986)
	Melledonol	434.1941	$C_{23}H_{30}O_8$	*A. mellea*	Donnelly et al. (1985b)
	6′-Chloromelleolide F	436.1652	$C_{23}H_{29}ClO_6$	*A. mellea*	Bohnert et al. (2014)
	Melleolide C	448.2097	$C_{24}H_{32}O_8$	*A. mellea*	Arnone et al. (1986)
	Melleolide G	448.2097	$C_{24}H_{32}O_8$	*A. mellea*	Arnone et al. (1988c)
	A52a	450.1809	$C_{24}H_{31}ClO_6$	*A. cepistipes*	Sonnenbichler et al. (1997)
	Melleolide M	452.1602	$C_{23}H_{29}ClO_7$	*A. mellea*	Momose et al. (2000)
	6′-Chloro-13-hydroxy-dihydromelleolide	452.1602	$C_{23}H_{29}ClO_7$	*A. mellea*	Bohnert et al. (2011)
	10-Dehydroxymelleolide D	466.1758	$C_{24}H_{31}ClO_7$	*Armillaria sp.*	Kobori et al. (2015)
	Melleolide I	466.1758	$C_{24}H_{31}ClO_7$	*A. novae-zelandiae*	Arnone et al. (1988a)
	Melleolide D	482.1707	$C_{24}H_{31}ClO_8$	*A. mellea*	Arnone et al. (1986)
	13,14-Dihydroxy-A52a	482.1707	$C_{24}H_{31}ClO_8$	*A. mellea*	Bohnert et al. (2011)
3	Armillarivin	384.1937	$C_{23}H_{28}O_5$	*A. mellea*	Yang et al. (1991a)
	5-Hydroxyarmillarivin	400.1886	$C_{23}H_{28}O_6$	*A. mellea*	Li et al. (2016)
	Melleolide = melleolide A	400.1886	$C_{23}H_{28}O_6$	*A. mellea*	Midland et al. (1982)
	4-Methyoxymelleolide	414.2042	$C_{24}H_{30}O_6$	*A. mellea*	Donnelly et al. (1985a)
	Armillarin	414.2042	$C_{24}H_{30}O_6$	*A. mellea*	Yang et al. (1984)
	Armillaripin	414.2042	$C_{24}H_{30}O_6$	*A. mellea*	Yang et al. (1990a)
	A51a	416.2199	$C_{24}H_{32}O_6$	*A. ostoyae*	Peipp and Sonnenbichler (1992)
	Armillaritin	416.1835	$C_{23}H_{28}O_7$	*A. mellea*	Yang et al. (1991a)
	10α-Hydroxymelleolide	416.1835	$C_{23}H_{28}O_7$	*A. mellea*	Donnelly et al. (1990)
	Armillarilin	430.1991	$C_{24}H_{30}O_7$	*A. mellea*	Yang et al. (1990b)
	13-Hydroxy-4-methoxy- melleolide	430.1991	$C_{24}H_{30}O_7$	*D. tabescens*	Donnelly et al. (1997)
	Melleolide H	430.1991	$C_{24}H_{30}O_7$	*A. mellea*	Arnone et al. (1988c)[c]
	Melledonal = melledonal A	432.1784	$C_{23}H_{28}O_8$	*A. mellea*	Donnelly et al. (1985b)
	Melleolide K	434.1496	$C_{23}H_{27}ClO_6$	*A. mellea*	Momose et al. (2000)
	5′-Methyoxymelledonal	446.1940	$C_{24}H_{30}O_8$	*A. mellea*	Donnelly et al. (1987)
	Armillaridin	448.1653	$C_{24}H_{29}ClO_6$	*A. mellea*	Yang et al. (1984)
	Melledonal E	448.1733	$C_{23}H_{28}O_9$	*A. elegans*	Arnone et al. (1988c)
	13-Hydroxymelleolide K	450.1445	$C_{23}H_{27}ClO_7$	*Armillaria sp.*	Kobori et al. (2015)
	6′-Chloro-10α-hydroxy melleolide = melleolide L	450.1445	$C_{23}H_{27}ClO_7$	*A. mellea; A. novae-zelandiae*	Momose et al. (2000); Cremin et al. (2000)
	15-Hydroxy-5′-methoxymelledonal	462.1890	$C_{24}H_{30}O_9$	*A. mellea*	Donnelly et al. (1987)
	4-Methoxyarmillaridin	463.1887	$C_{25}H_{32}ClO_6$	*A. mellea*	Donnelly and Hutchinson (1990)
	Armillarinin	464.1601	$C_{24}H_{29}ClO_7$	*A. mellea*	Yang et al. (1989a)
	Melleolide J	464.1601	$C_{24}H_{29}ClO_7$	*A. mellea*	Arnone et al. (1988c)[d]
	Melledonal B	466.1394	$C_{23}H_{27}ClO_8$	*A. mellea*	Arnone et al. (1988b)

Table 1 (continued)

Fig.	Compound	Exact mass (*m/z*)	Sum formula	Species of the first isolation	Reference
	Melledonal C	480.1550	$C_{24}H_{29}ClO_8$	*A. mellea*	Arnone et al. (1988b)
	Melledonal D	496.1500	$C_{24}H_{29}ClO_9$	*A. elegans*	Arnone et al. (1988c)
4A	Armillaric acid	416.1835	$C_{23}H_{28}O_7$	*A. mellea*	Obuchi et al. (1990)
4B	Armillyl orsellinate	402.2042	$C_{23}H_{30}O_6$	*A. mellea*	Donnelly et al. (1982)
	Armillyl everninate	416.2199	$C_{24}H_{32}O_6$	*A. mellea*	Donnelly et al. (1986)
	Judeol[e]	418.1992	$C_{23}H_{30}O_7$	*A. mellea*	Donnelly et al. (1985a)
	A45	432.2148	$C_{24}H_{32}O_7$	*A. ostoyae*	Peipp and Sonnenbichler (1992)
	Arnamiol	450.1809	$C_{24}H_{31}ClO_6$	*A. mellea*	Donnelly et al. (1986)
5A	Dehydroarmillyl orsellinate	400.1886	$C_{23}H_{28}O_6$	*A. mellea*	Bohnert et al. (2011)[f]
	6′-Dechloroarnamial	414.2042	$C_{24}H_{30}O_6$	*A. mellea*	Bohnert et al. (2014a)
	Arnamial	448.1653	$C_{24}H_{29}ClO_6$	*A. mellea*	Misiek et al. (2009)
5B	Armillane	420.2148	$C_{23}H_{32}O_7$	*A. mellea*	Donnelly and Hutchinson (1990)[g]
	Melleolide Q	454.1758	$C_{23}H_{31}ClO_7$	*A. mellea*	Chen et al. (2015)
	6′-Chloro-5′-methoxy-armillane	468.1912	$C_{24}H_{33}ClO_7$	*A. mellea*	Bohnert et al. (2011)
	6′-Chloro-10-hydroxy-5′-methoxyarmillane	484.1864	$C_{24}H_{33}ClO_8$	*A. mellea*	Bohnert et al. (2014a)
5C	Armillaribin	396.1937	$C_{24}H_{28}O_5$	*A. mellea*	Yang and Cong (1988)
	Armillaricin	430.1547	$C_{24}H_{27}ClO_5$	*A. mellea*	Yang et al. (1989a)
5D	5β-10α-Dihydroxy-1-orsellinate-dihydromelleolide	418.1992	$C_{23}H_{30}O_7$	*D. tabescens*	Donnelly et al. (1997)
	13-Deoxyarmellide A	432.2148	$C_{24}H_{32}O_7$	*A. mellea*	Bohnert et al. (2014a)
	Armellide A	448.2097	$C_{24}H_{32}O_8$	*A. novae-zelandiae*	Arnone et al. (1988a)
	Melleolide N	452.1602	$C_{23}H_{29}ClO_7$	*A. mellea*	Chen et al. (2015)
	13-Deoxyarmellide B	466.1758	$C_{24}H_{31}ClO_7$	*A. mellea*	Bohnert et al. (2014a)
	Melleolide R	468.1912	$C_{24}H_{33}ClO_7$	*A. mellea*	Chen et al. (2015)
	Armellide B	482.1707	$C_{24}H_{31}ClO_8$	*A. novae-zelandiae*	Arnone et al. (1988a)
5E	Armillasin	372.1937	$C_{22}H_{28}O_5$	*A. mellea*	Yang et al. (1991b)
	5′-Methoxyarmillasin[h]	386.2093	$C_{23}H_{30}O_5$	*A. mellea*	Li et al. (2016)
	Armillatin	610.4233	$C_{38}H_{58}O_6$	*A. mellea*	Yang et al. (1991b)
5F	6′-Bromomelleolide F	480.1148	$C_{23}H_{29}BrO_6$	biosynthetic in vitro reaction	Wick et al. (2016)

[a] Also described as dihydromelleolide by Cremin et al. (1995) and as 4-dehydrodihydromelleolide by Donnelly et al. (1997)

[b] Also described as 10α-hydroxydihydromelleolide by Donnelly et al. (1997)

[c] Also described as armillarigin by Yang et al. (1989b) and as 10α-hydroxyarmillarin by Donnelly et al. (1990)

[d] Also described as armillarikin by Yang et al. (1989b)

[e] Structure not fully solved: positions of phenolic hydroxyl groups not assigned

[f] Described by Donnelly et al. (1982) as a synthetic oxidation product of armillyl orsellinate

[g] Also described as armillarizin by Yang et al. (1993)

[h] In Li et al. (2016), stereocenters are shown inversed, compared with armillasin

Further, in rare or singular cases, the following modifications were observed:

viii) Additional hydroxylation of the aromatic ring whose exact position has not been described (judeol, Donnelly et al. 1985a)

ix) A second hydroxylation of C-5 in the case of 5-hydroxyarmillarivin (Li et al. 2016)

x) Palmityl ester formation via O-4 (armillatin, Yang et al. 1991b)

xi) Armillasin, 5′-methoxyarmillasin, and armillatin lack the carbon atom 1 of the protoilludene core (Yang et al. 1991b; Li et al. 2016).

The term melleolides is used as an umbrella term to summarize all *Armillaria* sesquiterpene aryl esters. However, the

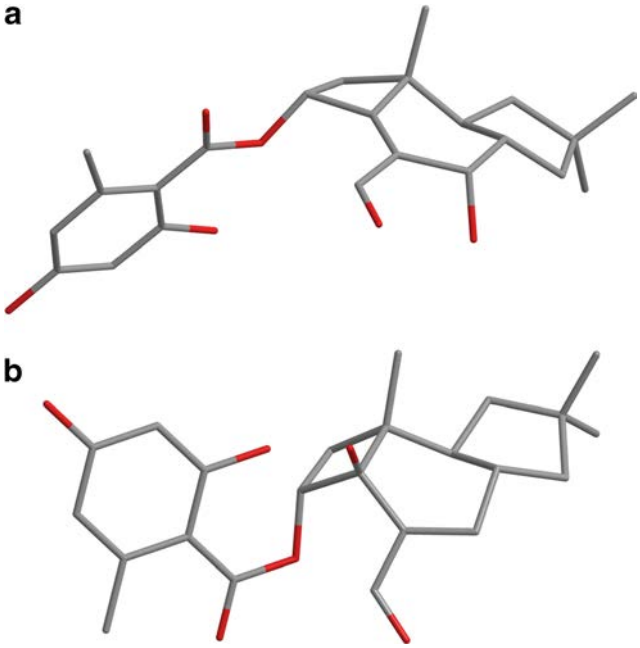

Fig. 6 Three-dimensional representation of dehydroarmillyl orsellinate ($\Delta^{2,4}$ skeleton, panel **a**) and of melleolide ($\Delta^{2,3}$ terpene skeleton, panel **b**)

presence/absence of a double bond and its position is reflected in the nomenclature as well. In the strict sense, the term melleolide, introduced by Midland et al. (1982) for a single compound, refers to compounds whose backbones feature a $\Delta^{2,3}$scaffold whereas terpenes with a $\Delta^{2,4}$double bond are referred to as armillyl orsellinates (Donnelly et al. 1982) and those with a fully saturated terpene as armillanes (Donnelly and Hutchinson 1990). However, a consequent nomenclature does not exist. In this article, the structures of all described melleolides are presented primarily by presence/absence and position of the terpene double bond, using the degree of oxidation of C-1 (alcohol, aldehyde, acid) as a secondary additional criterion (Figs. 2, 3, 4, and 5, Table 1). Likewise, the numbering of carbon atoms in our review does not follow IUPAC nomenclature but is shown according to essentially all previous literature on *Armillaria* terpenes.

Melleolide biosynthesis

Usually, melleolides are present in the mycelium as a complex mixture, although not all *Armillaria* species have been tested yet for melleolide biosynthesis. All ten North American species are confirmed producers (Misiek and Hoffmeister 2012), as well as European and Asian isolates of *A. mellea* (Donnelly et al. 1984; Yang et al. 1984, 1989a; Momose et al. 2000; Chen et al. 2015), *A. gallica* (Engels et al. 2011), *A. cepistipes*, *A. ostoyae*, European and North American isolates of *A. tabescens* (= *Desarmillaria tabescens*, Cremin et al. 1995; Donnelly et al. 1997), and a New Zealand strain of *A. novae-zelandiae* (Cremin et al. 2000). Virtually all melleolides have been isolated from artificially cultivated mycelium, while carpophores contain only very low metabolite titers (Wang et al. 1996). Research into the molecular basis of the biosynthesis of melleolides began with [1,2-^{13}C]acetate incorporation experiments to prove the polyketide origin of the orsellinic acid moiety via 2D INADEQUATE nuclear magnetic resonance (NMR) spectroscopy (Misiek et al. 2009). The results demonstrated that *A. mellea* uses intact acetate units for biosynthesis, which in turn suggested a non-reducing polyketide synthase catalyzing orsellinic acid biosynthesis. Analogously to illudol, whose sesquiterpenoid origin has been established (McMorris et al. 1967), 6-protoilludene was likely to represent a terpene as well. A major achievement was the identification of Pro1, the protoilludene synthase of *A. gallica*, a 40 kDa enzyme whose sequence includes the canonical and characteristic terpene cyclase motifs DExxD and NDxxSxxxE. Heterologous reconstitution of its enzymatic activity in vitro was proven by cyclization of farnesyldiphosphate, i.e., the universal precursor of all sesquiterpenes, into the exclusive product 6-protoilludene (Engels et al. 2011). This result demonstrated that $\Delta^{2,4}$-configured melleolides biosynthetically precede the $\Delta^{2,3}$ configuration. The second major melleolide biosynthesis enzyme discovered was the polyketide synthase (PKS) ArmB which was among the first characterized PKSs of basidiomycete origin. The enzyme was heterologously produced in *E. coli*, and orsellinic acid synthase activity was shown in vitro. ArmB is a non-reducing, seven-domain iterative type I PKS and has 2209 aa and a molecular mass of 237 kDa. Importantly, ArmB was shown to provide a second biosynthetic function, as its terminal thioesterase domain catalyzes transesterification to connect the carboxylic acid functionality of orsellinic acid with the protoilludene via its C-5 hydroxyl to generate the actual melleolide backbone (Lackner et al. 2013). This reaction was shown in vitro, using orsellinic acid that was made in situ by ArmB and 1,4,5,10,13-pentahydroxy-$\Delta^{2,3}$-protoilludene. In its presence, this reaction yielded a product that was identical to melledonol (Fig. 2).

So-called tailoring enzymes decorate a natural product backbone structure, which leads to an incredible diversity of related compounds in the case of the melleolide family. Nearly 30 melleolides are known to show regioselective monochlorination at C-6′ of the aromatic moiety. Five flavin-dependent halogenases (ArmH1–ArmH5) that are phylogenetically distantly related (ArmH1–H3 versus ArmH4 versus ArmH5) were heterologously produced in *E. coli*. The enzymes showed the typical length of flavin-dependent natural product halogenases (504–533 aa and 55.3–58.1 kDa). All of these enzymes feature the fingerprint double tryptophan signature motif GW(A/V)W(F/L)I. In the three-dimensional halogenase structure, this motif is located inside a tunnel through which hypochloric acid, i.e., the chlorinating agent, is routed from the flavin toward the halogen acceptor

substrate. All five *Armillaria* halogenases were active and converted melleolide F into its 6′-chloro analogue (Wick et al. 2016). This remarkable result indicates that melleolide halogenation is secured five-fold, which is an unprecedented degree of biosynthetic redundancy. ArmH4 was used to biocatalytically produce the non-natural 6′-bromomelleolide F (Fig. 5f). Genomic sequencing of *A. mellea* (Collins et al. 2013) revealed a biosynthetic locus in which a total of 16 melleolide biosynthesis genes are clustered, some of them with hypothetical character or encoding proteins of unknown function for melleolide biosynthesis (Fig. 7). While *ArmB* and *Pro1* are located within this gene cluster, they surprisingly do not encode any of the halogenases. Curiously, ArmH1 and ArmH2 are encoded in the vicinity of a quinone synthetase–like gene (*ArmA*) which, however, does not serve any apparent role in melleolide biosynthesis (Misiek et al. 2011). Further, genes for five P_{450}-dependent monooxygenases were found in *A. mellea*, which are incompatible with the total number of eight positions at which oxygen atoms must or may be introduced. This may imply that other hydroxylases, encoded outside the melleolide gene cluster, contribute to the biosynthesis, or that some of the monooxygenases target two positions. Based on elegant experimental design and using transgenic yeast, one P_{450} monooxygenase of *A. gallica* (Cyp-Arm3) was functionally characterized and identified as protoilludene 8α-hydroxylase (Engels 2013).

The melleolides have also attracted the interest of organic chemists. A synthetic route for armillaridin has been developed in which the protoilludene moiety is synthesized in a complex route and esterified to 6-chloroeveninic acid as a penultimate step to yield armillaridin (Fig. 3) after a final deprotection step (Hovey et al. 2017).

Melleolide bioactivities and mode of action

Research into the bioactivity of *Armillaria* metabolites began about 70 years ago, when Oppermann (1951) observed inhibitory effects on other microorganisms. Since then, numerous publications reported growth-inhibiting or microbicidal activities of *Armillaria* extracts and for individual melleolides. Their structural diversity allowed for insights into the relevance of particular structural elements for biological activity. A systematic survey for biological activities of melleolides has not been carried out yet. This is due to various reasons. Firstly, an immense number of different bacterial and fungal species and strains has been used to assay for melleolide bioactivites; some species were not even identified. Secondly, except Bohnert et al. (2014a, b) and Li et al. (2016), prior work did not include complete sets of structurally highly similar melleolides, which would have allowed to systematically observe structure-activity relationships. Thirdly, the assay design varies massively between individual reports. Hence, a direct comparison of these data is complicated. Here, we do not consider data generated with non-identified test strains and activity data of *Armillaria* crude extracts. However, two distinct and non-congruent structure-activity relationships were found for their cytotoxic and antifungal effects, respectively (Bohnert et al. 2014a).

Activity against bacteria At least 29 melleolides have been isolated and tested for antibacterial activity. With the exception of melleolides B–D and their derivatives, which are reported to be active on *Escherichia coli* (Arnone et al. 1986; Sonnenbichler et al. 1997), melleolides are exceptionally active against Gram-positive strains including coccoid (*Micrococcus, Streptococcus, Staphylococcus*), rod-shaped (*Bacillus, Corynebacterium*), or filamentous bacteria (actinomycetes), but not against Gram-negative ones (*Pseudomonas, Escherichia, Proteus, Salmonella, Serratia, Shigella, Xanthomonas*) (Donnelly et al. 1982; Arnone et al. 1988b). Only five of eleven melleolides with a C-3 hydroxylation inhibit bacterial growth, while 18 out of 26 C-4-hydroxylated congeners are active, indicating that the position of this hydroxyl group and/or the double bond position impact antibacterial activity. All ten tested melleolides featuring a C-13 hydroxylation (melleolide B derivatives) inhibit Gram-positive bacteria. Additional methylation at 5′-OH on the orsellinic backbone is associated with the expansion of the activity spectrum to Gram-negative bacteria. In addition, 12 out of 14 melleolides with C-10-hydroxylation inhibit Gram-negative strains. In summary, the most active compounds (melledonal A–C, melleolides B and C, and metabolites A28a and A49a) all meet these criteria and feature at least a 4,10,13-trihydroxylated terpene scaffold (Arnone et al. 1986, 1988b; Sonnenbichler et al. 1997; Cremin et al. 2000).

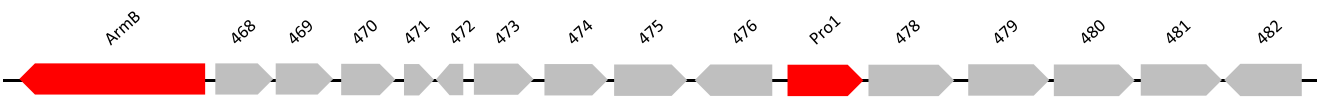

Fig. 7 Schematic representation of the genetic locus for melleolide biosynthesis in *Armillaria mellea*. Arrows represent genes in the transcriptional direction. For clarity, introns are not shown. Some genes are hypothetical. Genes encode the following verified or putative enzymes: ArmB, orsellinic acid synthase (Lackner et al. 2013); 468, NAD(P)-binding dehydrogenase; 469, short-chain dehydrogenase/reductase; 470, NAD-dependent epimerase/dehydratase; 471 and 472, hypothetical protein; 473, O-methyltransferase; 474, aryl-alcohol dehydrogenase; 475, NAD(P)-binding dehydrogenase; 476, cytochrome P_{450} monooxygenase; Pro1, protoilludene synthase (Engels et al. 2011); 478, short-chain dehydrogenase/reductase; 479–482, cytochrome P_{450} monooxygenase

However, the mode of action of antibacterial activity has not been investigated yet but may involve the α,β-unsaturated carbonyl as a Michael acceptor.

Fungi In contrast to antibacterial activity, the position of the protoilludene double bond is critical for the inhibition of fungi. $\Delta^{2,4}$-unsaturated melleolides are highly active against filamentous ascomycetes and basidiomycetes, but not against zygomycetes (Peipp and Sonnenbichler 1992; Momose et al. 2000; Misiek and Hoffmeister 2012; Dörfer et al. 2019), whereas $\Delta^{2,3}$-unsaturated melleolides are not active against filamentous ascomycetes (Misiek and Hoffmeister 2012; Bohnert et al. 2014a). The latter melleolides, but not their reduced 1-OH analogs, are growth inhibitors for basidiomycetes such as *Heterobasidion annosum* and *Gloeophyllum abietinum* (Peipp and Sonnenbichler 1992). Esterification of the sesquiterpene backbone via 1-OH (rather than 5-OH) reduces activity (Bohnert et al. 2014a). Neither methylation on 5′-OH nor chlorination on C-6′ on the orsellinate residue alters antifungal activity (Sonnenbichler et al. 1997; Cremin et al. 2000; Momose et al. 2000). The mode of action on antifungal activity has recently been elucidated: dehydroarmillyl orsellinate (DAO) and arnamial (Fig. 5a) inhibit fungal translation by binding to the fungal elongation factor 2 (eEF2) in *Aspergillus* and probably *Candida* strains (Dörfer et al. 2019). However, dermatophytes (*Trichoderma*) and some yeasts (*Saccharomyces*) are resistant to DAO, most likely conferred by mutations in the putative DAO binding site of eEF2 (Dörfer et al. 2019).

Plants With regard to saturation, state of oxidation, or the degree of hydroxylation of the terpenoid moiety, no clear structure-action-relationship emerges for the phytotoxic activity, suggesting that the mode of action differs from those against microorganisms (Peipp and Sonnenbichler 1992; Kobori et al. 2015). In contrast, alterations at the orsellinic acid moiety significantly impact phytotoxicity: a methyl ester on the 5′-OH increases phytotoxicity against *Picea abies* calli and lettuce seedlings (Peipp and Sonnenbichler 1992; Kobori et al. 2015).

Mammalian cells Pharmacologically, the most relevant feature of melleolides is their ability to induce apoptosis in adherent or human cancer cell lines. There is a clear correlation that aldehyde melleolides such as DAO and armillaridin are more potent (MIC 1.7–15.4 μM) than their reduced counterparts (13-hydroxy-dihydromelleolide and melleolide B) (MIC > 100 μM). Unlike with the antifungal activity, here, the double bond position does not impact cytotoxicity. This has been demonstrated for the pairs of armillarin versus 6′-dechloroarnamial and armillaridin versus arnamial, which each differ only in the $\Delta^{2,3}$- versus $\Delta^{2,4}$-unsaturation. All compounds are equally cytotoxic, e.g., against K-562 human leukemia cells with GI_{50} values between 2.3 and 9.9 μM (Bohnert et al. 2014a). DAO and arnamial were subjected to an in-depth investigation of their mode of action (Bohnert et al. 2014b): in monocytes and HeLa cells, DAO caused a rapid onset on cell death within 5 h mainly due to rapid cell lysis after forming organelle-free membrane blebs within the first 15–60 min of contact. Necrosis and apoptotic pathways were induced, and reduced viability of mitochondria was evident. This is in agreement with mechanistic studies on the toxicity of melleolide, a $\Delta^{2,3}$-unsaturated aldehyde metabolite, which causes apoptosis, condensation of chromatin, and fragmentation of the cell's nucleus (Li et al. 2016). Melleolide-treated HepG2 cells are arrested at the G2/M phase by reducing the activity of Ki67, a nuclear cell proliferation marker. Recent studies on human leukocytes showed that DAO and arnamial inhibit 5-lipoxygenase (5-LO) at 1 μM, i.e., the key enzyme in the biosynthesis of pro-inflammatory leukotrienes from arachidonic acid (König et al. 2019). The melleolide aldehyde at C-1 serves as a selective Michael acceptor to covalently bind to Cys-159 of 5-LO. This reduces its enzymatic activity and, consequently, decreased all lipid mediators formed by 5-LO (König et al. 2019). This offers the potential of melleolides as low molecular weight inhibitors of 5-LO-related disorders such as asthma, rheumatoid arthritis, allergic rhinitis, or neurodegenerative and cardiovascular diseases.

Concluding remarks

Numerous questions around the melleolides, their biosynthesis, and their activities and mode of actions are yet to be answered. In the area of biosynthesis, the as yet unresolved sequential and combinatorial hydroxylation and the underlying enzymes deserve attention. From the pharmacological perspective, further work is warranted to explore the intriguing phenomenon of rapid eukaryotic cell death upon exposure to melleolides. Perhaps the most complex problem remaining to be solved is the ecological reason that drove on the evolution of this unparalleled biosynthesis. Future work needs to show why *Armillaria* relied on a permutationally varied backbone structure to elaborate a breathtakingly diverse repertoire of bioactive natural products.

Funding information Studies on melleolide biosynthesis and mode of action in D.H.'s laboratory were supported by the Excellence Graduate School JSMC (Jena School for Microbial Communication) and by the Collaborative Research Center ChemBioSys (Deutsche Forschungsgemeinschaft, grant SFB1127).

Compliance with ethical standards

Conflict of interest The authors declare that they have no conflict of interest.

References

Abraham WR (2001) Bioactive *sesquiterpenes* produced by fungi: are they useful for humans as well? Curr Med Chem 8:583–606

Arnone A, Cardillo R, Nasini G (1986) Structures of melleolides B-D, three antibacterial sesquiterpenoids from *Armillaria mellea*. Phytochemistry 25:471–474

Arnone A, Cardillo R, Nasini G (1988a) Isolation and structure elucidation of melleolides I and J and armellides A and B, novel sesquiterpenoid aryl esters from *Armillaria novae-zelandiae*. Gazz Chim Ital 118:523–527

Arnone A, Cardillo R, Nasini G (1988b) Secondary mould metabolites part 19: structure elucidation and absolute configuration of melledonals B and C, novel antibacterial sesquiterpenoids from *Armillaria mellea*. X-ray molecular structure of Melledonal C. J Chem Soc Perkin Trans 1 I:503–510

Arnone A, Nasini G, Di Modugno V, Cardillo R (1988c) Isolation and structure elucidation of melledonals D and E and melleolides E-H, novel sesquiterpenoid aryl esters from *Clitocybe elegans* and *Armillaria mellea*. Gazz Chim Ital 118:517–521

Baumgartner K, Coetzee MP, Hoffmeister D (2011) Secrets of the subterranean pathosystem of *Armillaria*. Mol Plant Pathol 12:515–534

Bohnert M, Miethbauer S, Dahse HM, Ziemen J, Nett M, Hoffmeister D (2011) *In vitro* cytotoxicity of melleolide antibiotics: structural and mechanistic aspects. Bioorg Med Chem Lett 21:2003–2006

Bohnert M, Nützmann HW, Schroeckh V, Horn F, Dahse HM, Brakhage AA, Hoffmeister D (2014a) Cytotoxic and antifungal activities of melleolide antibiotics follow dissimilar structure–activity relationships. Phytochemistry 105:101–108

Bohnert M, Scherer O, Wiechmann K, König S, Dahse HM, Hoffmeister D, Werz O (2014b) Melleolides induce rapid cell death in human primary monocytes and cancer cells. Bioorg Med Chem 22:3856–3861

Braesel J, Fricke J, Schwenk D, Hoffmeister D (2017) Biochemical and genetic basis of orsellinic acid biosynthesis and prenylation in a stereaceous basidiomycete. Fungal Genet Biol 98:12–19

Brazee NJ, Ortiz-Santana B, Banik MT, Lindner DL (2012) *Armillaria altimontana*, a new species from the western interior of North America. Mycologia 104:1200–1205

Chen CC, Kuo YH, Cheng JJ, Sung PJ, Ni CL, Chen CC, Shen CC (2015) Three new sesquiterpene aryl esters from the mycelium of *Armillaria mellea*. Molecules 20:9994–10003

Collins C, Keane TM, Turner DJ, O'Keeffe G, Fitzpatrick DA, Doyle S (2013) Genomic and proteomic dissection of the ubiquitous plant pathogen, *Armillaria mellea*: toward a new infection model system. J Proteome Res 12:2552–2570

Cremin P, Donnelly DMX, Wolfender JL, Hostettmann K (1995) Liquid chromatography–thermospray mass spectrometric analysis of sesquiterpenes of *Armillaria* (Eumycota: Basidiomycotina) species. J Chromatogr A 710:273–285

Cremin P, Guiry PJ, Wolfender JL, Hostettmann K, Donnelly DMX (2000) A liquid chromatography–thermospray ionisation–mass spectrometry guided isolation of a new sesquiterpene aryl ester from *Armillaria novae-zelandiae*. J Chem Soc Perkin Trans 1:2325–2329

Donnelly DMX, Sanada S, O'Reilly J, Polonsky J, Prangé T, Pascard CJ (1982) Isolation and structure (X-ray analysis) of the orsellinate of armillol, a new antibacterial metabolite from *Armillaria mellea*. J Chem Soc Chem Comm 135–137

Donnelly DMX, Polonsky J, Prangé T, Snatzke, G, Wagner U (1984) The absolute configuration of the orsellinate of armillol; application of the coupled oscillator theory. J Chem Soc Chem Comm 222–223

Donnelly DMX, Abe F, Coveney D, Fukuda N, O'Reilly J, Polonsky J, Prangé T (1985a) Antibacterial sesquiterpene aryl esters from *Armillaria mellea*. J Nat Prod 48:10–16

Donnelly DMX, Coveney DJ, Polonsky J (1985b) Melledonal and melledonol, sesquiterpene esters from *Armillaria mellea*. Tetrahedron Lett 26:5343–5344

Donnelly DMX, Coveney DJ, Fukuda N, Polonsky J (1986) New sesquiterpene aryl esters from *Armillaria mellea*. J Nat Prod 49:111–116

Donnelly DMX, Coveney DJ (1987) Antibacterial sesquiterpene aryl esters from *Armillaria mellea*. In: Hostettmann K, Lea PJ (eds) Biologically active natural products. Clarendon Press, Oxford, pp 19–32

Donnelly DMX, Quigley PF, Coveney DJ, Polonsky J (1987) Two new sesquiterpene esters from *Armillaria mellea*. Phytochemistry 26:3075–3077

Donnelly DMX, Hutchinson RM (1990) Armillane, a saturated sesquiterpene ester from *Armillaria mellea*. Phytochemistry 29:179–182

Donnelly DMX, Hutchinson RM, Coveney DJ, Yonemitsu M (1990) Sesquiterpene aryl esters from *Armillaria mellea*. Phytochemistry 29:2569–2572

Donnelly DMX, Konishi T, Dunne O, Cremin P (1997) Sesquiterpene aryl esters from *Armillaria tabescens*. Phytochemistry 44:1473–1478

Dörfer M, Heine D, König S, Gore S, Werz O, Hertweck C, Gressler M, Hoffmeister D (2019) Melleolides impact fungal translation via Elongation Factor 2. Org Biomol Chem 17:4906–4916

Engels B, Heinig U, Grothe T, Stadler M, Jennewein S (2011) Cloning and characterization of an *Armillaria gallica* cDNA encoding protoilludene synthase, which catalyzes the first committed step in the synthesis of antimicrobial melleolides. J Biol Chem 286:6871–6878

Engels B (2013) Untersuchungen zur Biosynthese sesquiterpenoider Naturstoffe, der Melleolide. In *Armillaria gallica*. Dissertation, RWTH Aachen

Firn RD, Jones GC (2003) Natural products – a simple model to explain chemical diversity. Nat Prod Rep 20:382–391

Firn RD, Jones GC (2009) A Darwinian view of metabolism: molecular properties determine fitness. J Exp Bot 60:719–726

Gill M, Steglich W (1987) Pigments of fungi (Macromycetes). Prog Chem Org Nat Prod 51:1–317

Gill M (2003) Pigments of fungi (Macromycetes). Nat Prod Rep 20:615–639

Hovey MT, Cohen DT, Walden DM, Cheong PH, Scheidt KA (2017) A carbene catalysis strategy for the synthesis of protoilludane natural products. Angew Chem Int Ed 56:9864–9867

Jiang MY, Feng T, Liu JK (2011) *N*-containing compounds of macromycetes. Nat Prod Rep 28:783–808

Kobori H, Sekiya A, Suzuki T, Choi JH, Hirai H, Kawagishi H (2015) Bioactive sesquiterpene aryl esters from the culture broth of *Armillaria* sp. J Nat Prod 78:163–167

Koch RA, Wilson AW, Séné O, Henkel TW, Aime MC (2017) Resolved phylogeny and biogeography of the root pathogen *Armillaria* and its gasteroid relative, Guyanagaster. BMC Evol Biol 17:33

König S, Romp E, Krauth V, Rühl M, Dörfer M, Liening S, Hofmann B, Häfner AK, Steinhilber D, Karas M, Garscha U, Hoffmeister D, Werz O (2019) Melleolides from honey mushroom inhibit 5-lipoxygenase via Cys159. Cell Chem Biol 26:60–70

Lackner G, Bohnert M, Wick J, Hoffmeister D (2013) Assembly of melleolide antibiotics involves a polyketide synthase with cross-coupling activity. Chem Biol 20:1101–1106

Li Z, Wang Y, Jiang B, Li W, Zheng L, Yang X, Bao Y, Sun L, Huang Y, Li Y (2016) Structure, cytotoxic activity and mechanism of protoilludane sesquiterpene aryl esters from the mycelium of *Armillaria mellea*. J Ethnopharmacol 184:119–127

McMorris TC, Nair MSR, Anchel M (1967) The structure of illudol, a sesquiterpenoid triol from *Clitocybe illudens*. J Am Chem Soc 89:4562–4563

Midland SL, Izac RR, Wing RM, Zaki AL, Munnecke DE, Sims JJ (1982) Melleolide, a new antibiotic from *Armillaria mellea*. Tetrahedron Lett 23:2515–2518

Misiek M, Williams J, Schmich K, Hüttel W, Merfort I, Salomon CE, Aldrich CC, Hoffmeister D (2009) Structure and cytotoxicity of arnamial and related fungal sesquiterpene aryl esters. J Nat Prod 72:1888–1891

Misiek M, Braesel J, Hoffmeister D (2011) Characterization of the ArmA adenylation domain implies a more diverse secondary metabolism in the genus *Armillaria*. Fungal Biol 115:775–781

Misiek M, Hoffmeister D (2012) Sesquiterpene aryl ester natural products in North American *Armillaria* species. Mycol Prog 11:7–15

Momose I, Sekizawa R, Hosokawa N, Iinuma H, Matsui S, Nakamura H, Naganawa H, Hamada M, Takeuchi T (2000) Melleolides K, L and M, new melleolides from *Armillariella mellea*. J Antibiot 53:137–143

Obuchi T, Kondoh H, Watanabe N, Tamai M, Omura S, Yang JS, Liang XT (1990) Armillaric acid, a new antibiotic produced by *Armillaria mellea*. Planta Med 56:198–201

Oduro KA, Munnecke DE, Sims JJ, Keen NT (1976) Isolation of antibiotics produced in culture by *Armillaria mellea*. Trans Br Mycol Soc 66:195–199

Oppermann A (1951) Das antibiotische Verhalten einiger holzzersetzender Basidiomyceten zueinander und zu Bakterien. Arch Mikrobiol 16:364–409

Peipp H, Sonnenbichler J (1992) Secondary fungal metabolites and their biological activities, II. Occurrence of antibiotic compounds in cultures of *Armillaria ostoyae* growing in the presence of an antagonistic fungus or host plant cells. Biol Chem Hoppe Seyler 373:675–683

Sandargo B, Chepkirui C, Cheng T, Chaverra-Munoz L, Thongbai B, Stadler M, Hüttel S (2019) Biological and chemical diversity go hand in hand: Basidiomycota as source of new pharmaceuticals and agrochemicals. Biotechnol Adv. https://doi.org/10.1016/j.biotechadv.2019.01.011

Schroeckh V, Scherlach K, Nützmann HW, Shelest E, Schmidt-Heck W, Schümann J, Martin K, Hertweck C, Brakhage AA (2009) Intimate bacterial-fungal interaction triggers biosynthesis of archetypal polyketides in *Aspergillus nidulans*. Proc Natl Acad Sci U S A 106:14558–14563

Shen B (2003) Polyketide biosynthesis beyond the type I, II and III polyketide synthase paradigms. Curr Opin Chem Biol 7:285–295

Sonnenbichler J, Guillaumin JJ, Peipp H, Schwarz D (1997) Secondary metabolites from dual cultures of genetically different *Armillaria* isolates. Eur J Forest Path 27:241–249

Wang C, Guo S, Chen X, Ca W, Xu J, Xiao P (1996) Studies on the contents of armillarin and melleolide at different stages of development of *Armillaria mellea*. Zhongguo Zhong Yao Za Zhi 21:274–276

Wick J, Heine D, Lackner G, Misiek M, Tauber J, Jagusch H, Hertweck C, Hoffmeister D (2016) A fivefold parallelized biosynthetic process secures chlorination of *Armillaria mellea* (honey mushroom) toxins. Appl Environ Microbiol 82:1196–1204

Yamazaki M, Matsuo M, Shibata S (1965) Biosynthesis of lichen depsides, lecanoric acid and atranorin. Chem Pharm Bull 13:1015–1017

Yang JS, Chen Y, Feng X, Yu D, Liang X (1984) Chemical constituents of *Armillaria mellea* mycelium I. Isolation and characterization of armillarin and armillaridin. Planta Med 50:288–290

Yang JS, Cong PZ (1988) Mass spectrometric studies on the sesquiterpenol aromatic esters from mycelium of *Armillaria mellea*. Acta Chim Sin 46:1093–1100

Yang JS, Chen YW, Zeng XZ, Yu DQ, He CH, Zheng QT, Yang J, Liang XT (1989a) Isolation and structure elucidation of armillaricin. Planta Med 55:564–565

Yang JS, Su YL, Wang YL, Feng XZ, Yu DQ, Cong PZ, Tamai M, Obuchi T, Kondoh H, Liang XT (1989b) Isolation and structures of two new sesquiterpenoid aromatic esters: armillarigin and armillarikin. Planta Med 55:479–481

Yang JS, Su YL, Wang YL, Feng XZ, Yu DQ, Liang XT, He CH, Zheng QT, Yang JJ, Yang J (1990a) Chemical constituents of *Armillaria mellea* mycelium VI. Isolation and structure of armillaripin. Acta Pharm Sin 25:353–356

Yang JS, Su YL, Wang YL, Feng XZ, Yu DQ, Liang XT (1990b) Studies on the chemical constituents of *Armillaria mellea* mycelium V. Isolation and characterization of armillarin and armillarinin. Acta Pharm Sin 24:24–28

Yang JS, Su YL, Wang YL, Feng XZ, Yu DQ, Liang XT (1991a) Chemical constituents of *Armillaria mellea* mycelium VII. Isolation and characterization of chemical constituents of the acetone extract. Acta Pharm Sin 26:117–122

Yang JS, Su YL, Wang YL, Feng XZ, Yu DQ, Liang XT (1991b) Two novel protoilludane norsesquiterpenoid esters, armillasin and armillatin from *Armillaria mellea*. Planta Med 57:478–480

Yang JS, Su YL, Yu DQ, Liang XT (1993) Carbon-13 nuclear magnetic resonance spectra of some protoilludane sesquiterpenoid aromatic esters from *Armillaria mellea*. J Chin Pharm Sci 2:11–17

Zhou ZY, Liu JK (2010) Pigments of fungi (macromycetes). Nat Prod Rep 27:1531–1570

Zjawiony JK (2004) Biologically active compounds from Aphyllophorales (polypore) fungi. J Nat Prod 67:300–310

4. Unveröffentlichte Ergebnisse

4.1. Rapid cell death induction by the honey mushroom mycotoxin dehydroarmillyl-orsellinate through covalent reaction with membrane phosphatidylethanolamines

Stefanie König, Konstantin Löser, Helmut Pein, Konstantin Neukirch, Anna Czapka, Stephanie Hoeppener, **Maximilian Dörfer**, Dirk Hoffmeister, Andreas Koeberle, Oliver Werz

Manuskript in Erstellung, geplante Publikation: erstes Quartal 2020 in Cell Chemical Biology

Zusammenfassung

Das Melleolid DAO aus *Armillaria mellea* induziert in humanen Krebszellen und primären humanen Monozyten einen raschen Zelltod innerhalb von 15 Minuten. Durch die kovalente Bindung von DAO an Phosphatidylethanolamin (PE) in der Zellmembran kommt es zu einem drastischen Verlust der Plasmamembranpermeabilität und somit der zellulären Viabilität in Verbindung mit einer PARP-Spaltung.

Das α-β ungesättigte Aldehyd des DAO-Moleküls fungiert als Michael-Akzeptor und reagiert über eine 1,4-Addition kovalent mit reinem Ethanolamin (EA) und mit PE, jedoch nicht mit anderen Phospholipiden, welche Serin- oder Cholin-Kopfgruppen besitzen. Die DAO-PE Produktbildung geht zeitlich mit der Membranschädigung einher. Die exogene Zugabe von EA verhindert einen DAO-induzierten Zelltod. Fraktionierungsuntersuchungen zeigten, dass die DAO-PE-Produktakkumulation mit einer Abnahme des PE in der Membran einhergeht.

Eigenanteil 10%

Maximilian Dörfer: Isolation von DAO aus *A. mellea*

Jena, den

_____

Prof. Dr. Dirk Hoffmeister

Rapid cell death induction by the honey mushroom mycotoxin dehydroarmillylorsellinate through covalent reaction with membrane phosphatidylethanolamines

Stefanie König[1*], Konstantin Löser[1*], Helmut Pein[1*], Konstantin Neukirch[1], Anna Czapka[1], Stephanie Hoeppener[2,3], Maximilian Dörfer[4], Dirk Hoffmeister[4], Andreas Koeberle[1], and Oliver Werz[1,3§]

[1] Department of Pharmaceutical/Medicinal Chemistry, Institute of Pharmacy, Friedrich Schiller University Jena, Philosophenweg 14, D-07743 Jena, Germany.

[2] Laboratory of Organic and Macromolecular Chemistry (IOMC), Friedrich Schiller University Jena, Humboldtstr. 10, D-07743 Jena, Germany

[3]Jena Center of Soft Matter (JCSM), Friedrich Schiller University Jena, Philosophenweg 7, D-07743 Jena, Germany

[4] Department of Pharmaceutical Microbiology at the Hans Knoell Institute, Friedrich Schiller University Jena, Winzerlaer Straße 2, D-07745 Jena, Germany

[*] contributed equally

[§] **corresponding author**: Prof. Dr. Oliver Werz, Chair of Pharmaceutical/ Medicinal Chemistry, Institute of Pharmacy, Friedrich Schiller University Jena, Philosophenweg 14, D-07743 Jena, Germany; Phone: +49-03641-949801; Fax: +49-03641-949802;

e-mail: oliver.werz@uni-jena.de.

Abbreviations

ATP – adenosine triphosphate, DAO - dehydroarmillylorsellinate, EA – ethanolamine, ER – endoplasmic reticulum, LDH – lactate dehydrogenase, PL – phospholipid, PE – phosphatidylethanolamine, ROS – reactive oxygen species, Stsp – staurosporine.

Summary

Melleolides form a group of fungal mycotoxins of the basidiomycete genius *Armillaria mellea* that induce rapid cell death in various mammalian cells with yet unknown mode of action. Here, we show that the melleolide dehydroarmillylorsellinate (DAO) covalently binds to phosphatidylethanolamine (PE) contained in cell membranes, accompanied by rapid loss of plasma membrane integrity and cellular viability. DAO caused a remarkable rapid onset of cell death of human cancer cells and primary human monocytes (i.e. within 15 min), which was temporally accompanied by PARP cleavage and loss of membrane integrity. DAO possesses a reactive α,β-unsaturated aldehyde group as Michael acceptor and covalently reacted via 1,4-addition with ethanolamine (EA) and with PE but not with other phospholipids containing serine or choline head groups. DAO-PE adduct formation coincided with membrane damage, and excess of exogenous EA prevented DAO-induced cell death. Moreover, DAO caused leakage of artificial PE-composed liposomes in a cell-free system. Subcellular fractionation studies indicate that DAO-PE adducts accumulate in cellular membranes along with decreased PE contents. Conclusively, DAO causes cell death by membrane damage seemingly due to covalent modification of PE with detrimental consequences for cell integrity and viability.

Introduction

The honey mushroom *Armillaria mellea* produces antimicrobial and cytotoxic natural products belonging to the large group of melleolides with more than 60 elucidated members [1-5]. These secondary metabolites combine sesquiterpene arylesters with orsellinic acid residues and exhibit mainly secondary alcohols. Up to now only a few targets and mode of actions are investigated for these mushroom toxins [6, 7]. Several melleolides show antitumor and cytotoxic effects in various human cells [1, 3, 8-10]. For example, armillarikin induces ROS-mediated and caspase-dependent apoptosis by downregulation of the mitochondrial transmembrane potential in leukemia cells [9, 11], and armillaridin induces autophagy-associated apoptosis in human leukemia cells and negatively influences the mitochondrial transmembrane potential [8, 12, 13]. Furthermore, decreased DNA synthesis was observed in different human cancer cell lines for some melleolides [1].

Cell death can be classified in three major subgroups – apoptosis, autophagic cell death and necrosis [14-16]. Typical characteristics for apoptosis are caspase activation, mitochondrial outer membrane permeabilization, cell rounding, nuclear condensation, and cell fragmentation to apoptotic bodies [17]. Autophagy is also a programmed physiological process in organism required to recycle macromolecules, cytoplasmic material, and cell organelles [18] but also for ATP production [19] via a lysosomal degradation pathway. In contrast, necrosis is an uncontrolled process and is constituted by signaling- and damage-induced lesions like mitochondrial dysfunction, ATP depletion, increased reactive oxygen species (ROS) formation or early plasma membrane ruptures [20, 21].

Membrane phospholipids (PL) constitute of a phosphate-bound head group (sn-3 position) and a glycerol residue connected with two ester-linked fatty acid chains (sn-1/sn-2 position). PL are classified by the functional head group, encompassing PE, phosphatidylcholine (PC), phosphatidylserine (PS), phosphatidylinositol (PI), phosphatidylglycerol (PG), phosphatidic

acid (PA), sphingomyelins (SP), and cardiolipins (CL). Typical cellular membranes consists of 45-55% PC, 15-25% PE, 10-15% PI, and 5-10% PS, where PE and PS are mainly found in the inner membrane leaflet [22]. During the early stage of apoptosis, PE and PS are exposed to the outer leaflet of the plasma membrane [23]. PE is participating in a wide range of cellular processes like the formation of hexagonal phases within the membrane because of its cone shape [24], protein arrangement inside the membrane [25], enhancing membrane fusion [24, 26], oxidative phosphorylation [27], mitochondrial stability [28] and autophagy [29, 30] and plays a substantial role in lipid synthesis as precursor of other lipids [31].

Here we show that the melleolide dehydroarmillylorsellinate (DAO, **Fig. 1A**) interferes with PE in cellular membranes by covalent binding to the EA head group. DAO possesses an α,β-unsaturated aldehyde that functions as Michael acceptor to react with nucleophilic residues such as thiol moieties of cysteine residue in 5-lipoxygenase (5-LO) [7]. Previous data showed that in contrast to other cytotoxic cell death-inducing agents, DAO causes remarkably rapid cell death with equal effectiveness in primary human monocytes and various cancer cell lines [3]. Our data suggest that covalent binding of DAO to membranous PE is the cause for the rapid perturbation of membrane integrity and consequent induction of cell death with characteristics of apoptosis and necrosis.

Results

DAO causes rapid cell death in human cells with unique characteristics

As reported before [3], the effectiveness of DAO and of the pan kinase inhibitor staurosporine (Stsp) for induction of cell death (assessed by MTT assay) in HeLa cells and primary monocytes was strikingly different. Thus, while Stsp-induced cell death is mainly mediated by apoptosis [32], DAO might confer its cytotoxicity primarily via necrotic features [3]. Moreover, DAO was about equipotent in monocytes and HeLa cells (EC_{50} = 1.6 and 2.3 μM, respectively), while Stsp was much more (40-fold) effective in HeLa cells (EC_{50} = 0.01 μM) as compared to monocytes (EC_{50} = 0.4 μM). The onset in cell death induction by DAO was remarkably rapid. Thus, exposure to DAO for only 15 min caused significant loss of viability of monocytes which was hardly different from 1 hr or 24 hrs treatment (**Fig. 1B**). In contrast, for Stsp, exposure for more than 5 hrs was needed to cause cytotoxicity in monocytes (not shown, see [3]). Release of lactate dehydrogenase (LDH) from cells to the external space reflects the loss of plasma membrane integrity. In agreement with the loss of cell viability assessed by MTT assay, LDH release from monocytes and HeLa cells was rapidly induced by DAO with almost maximal effects after about 30 min of exposure (**Fig. 1C**).

We next studied the effects of DAO and Stsp on cell morphology using light microscopy and transmission electron microscopy (TEM). DAO (even at low concentrations such as 0.1 μM) caused morphological signs of cells death within 3 hrs, reflected by wrinkling and shriveling of the plasma membrane (PM, **Fig. 1D**), which is actually a typical feature of necrosis. In contrast, Stsp caused classical signs of apoptosis in HeLa cells such as cellular fragmentation and formation of apoptotic bodies, along with shrinkage of the cells (**Fig. 1D**). Analysis by TEM revealed typical morphological features of monocytes with bean-shaped nucleus as well as intact organelles and plasma membrane (**Fig. 1E**). Upon Stsp-treatment (3 hrs), the nucleus lost its bean shape and rendered to a round structure with seemingly intact nuclear membrane and

also intact mitochondria. In contrast, 3 hrs treatment of monocytes with DAO caused defects of the nuclear membrane and in particular, mitochondria appeared to be lost (**Fig. 1E**). Together, DAO induces a remarkable rapid onset of cell death of primary cells and cancer cells accompanied by apparent membrane damages, which are characteristics that differ from those of classical apoptotic cell death inducers like Stsp.

Contribution of apoptotic pathways in mediating cell death by DAO

In order to explore the contribution of apoptotic pathways in mediating cell death by DAO, we analyzed hallmarks of apoptosis and stress signaling on a molecular level in monocytes. In fact, the rapid cell death induction by DAO (5 µM) within 15 min coincided with cleavage of PARP to a 89 kDa fragment as marker for apoptosis in monocytes; in contrast Stsp failed to induce PARP cleavage during short term treatment (within 1 hr, **Fig. 2A**) but instead required at least 5 hrs (**Supplemental Fig. 1**). The intrinsic pathway of apoptosis is initialized by a loss of mitochondrial membrane potential ($\Delta\Psi_m$) and the release of cytochrome c from mitochondria [33]. We found that in contrast to vehicle-treated monocytes exposure to 10 µM DAO for 3 hrs caused substantial release of cytochrome c into the cytosol, while in parallel the cytochrome c levels in organelles was minute (**Fig. 2B**). Also Stsp (3 µM) induced cytochrome c release from mitochondria within 3 hrs, albeit much less pronounced as compared to DAO.

Protein kinase signaling critically regulates the initiation of apoptosis, where the survival kinase Akt counteracts apoptosis [34] while p38 MAPK rather promotes it [35]. Exposure of monocytes to DAO (5 µM) and Stsp (3 µM) suppressed phosphorylation and thus activation of Akt. In contrast, both compounds elevated phosphorylation/activation of p38 MAPK (**Fig. 2C**). Again, the effects of DAO were more rapidly apparent (15 min) as compared to Stsp (30-60 min, **Fig. 2C**). The activation of p38 MAPK was independent on endoplasmic reticulum (ER)

stress and on the activation of the unfolded protein response (UPR), reflected by the failure of DAO to induce the UPR genes immunoglobulin heavy chain-binding protein (BiP), C/EBP [CCAAT/enhancer-binding protein]-homologous protein (CHOP), and activating transcription factor 4 (ATF4), at the protein level assessed by Western blot (**Fig. 2D**). Finally, we employed the pan-caspase inhibitor QVD to block apoptotic signaling. QVD (10 μM) inhibited DAO-induced PARP cleavage in monocytes (**Fig. 2E**). In contrast, QVD failed to reverse cell death induction by DAO after 3 and 48 hrs, but also loss of cell viability in response to Stsp was not completely reversed by QVD (**Fig. 2F**), in line with the reported necroptosis induction in monocytic U937 cells [36]. Conclusively, DAO-induced cell death is accompanied by apoptotic features which are seemingly not operative but rather necrotic pathways are responsible.

DAO interacts with the ethanolamine residue of phosphatidylethanolamine

The α,β-unsaturated aldehyde of DAO functions as Michael acceptor to react with nucleophilic residues such as thiol moieties of cysteine residue in 5-lipoxygenase [7]. It appeared reasonable that the rapid induction of cell death by DAO and the associated detrimental membrane alterations could be due to reaction of the α,β-unsaturated aldehyde of DAO with amine moieties of ethanolamine (EA) or serine (Ser) head group of membrane PE and PS thereby perturbing membrane integrity. We incubated different types of phospholipids (i.e., PE, PC, PS) with DAO followed by cleavage of the PL between the phosphate and the EA, Ser or choline moiety, respectively, using exogenously added phospholipase (PL)D and UPLC-MS/MS analysis of potentially formed adducts of DAO with the head group moieties. As shown in **Fig. 3A**, two major signals at 442.4 and 485.3 m/z appeared upon incubation of DAO with PE and subsequent PLD cleavage which may represent adducts of DAO with one or two EA molecules. These DAO-EA adducts are reaction products, where (i) the primary amine of one EA molecule forms an α,β-unsaturated Schiff base with the aldehyde group of DAO (resulting in 442.4 m/z)

and/or (ii) the primary amine moieties of two EA molecules react in 1,4-addition to yield imine structures (485.3 m/z) (**Fig. 3A**). Note that only a weak signal was detectable for DAO itself (399.4 m/z), suggesting that DAO efficiently reacted with PE to form the two adducts. In contrast, when DAO was incubated in parallel with PS or PC, the signal for DAO remained pronounced, whereas peaks with 442.4 or 485.3 m/z were not detectable (**Fig. 3B**), suggesting that DAO does not react with PS or PC.

We then studied if DAO-PE adducts might be formed also from intact monocytes and HeLa cells upon exposure to DAO for 3 hrs, by analysis of DAO-EA after treatment of cell lysates with exogenous PLD. Incubation of these cells with DAO caused concentration-dependent increases in DAO-EA adducts, starting at 0.1 μM DAO (**Fig. 3C**). The cellular amount of PE was maintained/decreased (**Fig. XY**). Next, we explored if DAO-PE interactions temporally correlate with detrimental effects on membrane integrity and thus with cell death induction. Treatment of monocytes or HeLa cells with 5 μM DAO resulted in rapid formation of DAO-PE adducts already after 15 min, reaching a plateau after about 1 hr to 3 hrs (**Fig. 3D**), which resembles the kinetics for the loss of membrane integrity (**Fig. 1C**) and decrease in cell viability (**Fig. 1B**). Note that for both the loss of membrane integrity and DAE-PE adduct formation, DAO displays more pronounced effects in monocytes versus HeLa cells (**Fig. 3D** and **Fig. 1C**). Taken together, DAO-EA adduct formation proceeds in parallel to membrane damage, suggesting that the interaction of DAO with PE in the plasma membrane might be eventually causative for cell death induction. In fact, incubation of DAO (10 μM) or Stsp (3 μM) with 50 mM EA for 2 hrs prior to addition to monocytes or HeLa cells abrogated the cytotoxic effect of DAO but not of Stsp (**Fig. 3E**), assessed by MTT assay. Note that preincubation of DAO with choline failed in this respect and L-serine could only marginally restore cell viability (**Fig. 3F**). Again, Stsp-induced loss of monocyte viability was not affected by preceeding reaction with EA, serine or choline (**Fig. 3F)**. Together, DAO binds to EA in PL and exogenous EA prevents

DAO-induced cell death suggesting that DAO acts by covalent modification of PE in cellular membranes.

Subcellular locales of DAO-PE interactions and consequences for PE contents

In order to explore the interaction between DAO and PE in the cellular context and to locate the subcellular PE binding sites of DAO, we performed subcellular fractionation of HeLa cells to obtain fractions enriched in nuclei, mitochondria, cytosol, and membranes. HeLa cells were preincubated with or without DAO for 15 or 180 min and cells were subjected to hypotonic lysis by passing them through a 25 G needle and subsequent differential centrifugation. Western blot for respective markers proteins confirmed correct cell fractionation and enrichment of related organelles (**Supplemental Fig. 2**). In cells treated with vehicle for 15 min, the cellular PE content was about equally distributed between fractions where nuclei, mitochondria, or membranes are enriched, while no PE was detectable in the cytosol (**Fig. 4A**). DAO did not significantly alter the subcellular distribution of PE (**Fig. 4A**). After 180 min, nuclear PE increased at the expense of membranous PE, and about 5% of the total PE was cytosolic. DAO further promoted this redistribution and increased nuclear PE at the expense of membranous PE (**Fig. 4A**). Importantly, when we analyzed the subcellular fractions for DAO-PE adducts (measured as DAO-EA after treatment of the fractions with PLD to cleave PE), we found that most of the DAO-PE (44% after 15 min and 62% after 180 min) was formed in the membrane fraction, with about equal or somewhat elevated contents in the mitochondrial as compared to the nuclear fraction (**Fig. 4B**).

Next, we analyzed whether DAO affects specific PE species in the subcellular fractions of HeLa cells after 3 hrs incubation using a targeted phospholipidomics approach (UPLC-MS/MS). In general, PE(18:0/18:1) and PE(18:1/18:1) were the most abundant species in the nuclear, mitochondrial and membrane fraction (**Fig. 4C**). However, the contents of PE species were not

markedly affected by DAO in comparison to the vehicle, the amounts of PE(18:0/18:1) and PE(18:1/18:1) were slightly increased in the nuclear fraction upon exposure to DAO after 3 hrs (**Fig. 4C**). Interestingly, after 15 min, PE(18:0/18:1) was the most common PE species in the membrane fraction closely followed by PE(18:1/18:1) (**Fig. 4D**) and after 3 hrs, these two PE species behaved exactly the other way (**Fig. 4C**). If we compared PE levels after 15 min DAO exposure with PE levels after 3 hrs DAO treatment in correlation to the total PE amount, a potent reduction of PE levels in the membrane fraction, especially PE(18:0/18:1) and PE(18:1/18:1) was obvious. Similar effects were observed also for less abundant PE species, such as PE(18:0/20:4), PE(16:0/18:1) or PE(16:1/18:1) (**Fig. 4F**). Together, DAO covalently reacts with the major PE species, preferably with those in membranes, which as a consequence leads to a subcellular rearrangement of single PE species within cell organelles.

In order to confirm that DAO reacts with PE in membranes and thus abrogates membrane integrity, we studied if DAO could cause leakage of artificial PE-composed liposomes in a cell-free system [37]. DAO caused release of the fluorescent dye 8-hydroxypyrene-1,3,6-trisulfonic acid trisodium salt (HPTS) from liposomes composed PE but not of PC indicating that it induces liposome leakage (**Fig. 4G** and **Supplemental Fig. 3**). Moreover, incubation of monocytes with DAO induced rapid (within 15 min) acidification of vesicles, starting at 1 μM DAO being comparable to the effect of the protonophore carbonyl cyanide m-chlorophenyl hydrazine (CCCP), as demonstrated by fluorescence microscopy using Lysotracker® as pH-sensitive dye for lysosomal staining (**Fig. 4H**).

Discussion

Melleolides belong to one of the largest globally distributed mycotoxin group of mushrooms. Only for a few of these mycotoxins the modes of action and targets are explored like for muscarine, coprine, psilocybin, and ibotenic acid. Since the last century, researchers have followed up with the bioactions of secondary metabolites of the basidiomycete species *Armillaria mellea* in plants and human cells [38-41]. Here, we reveal a mode of action underlying the cytotoxic properties of the melleolide DAO in human cells. We showed before [3] that DAO induces remarkably rapid cell death in human cancer cell lines and in primary immune cells, but the mode of action remained obscure. Here, we provide evidence that DAO covalently binds to PE in cellular membranes. Our data suggest, that DAO covalently reacts with the EA head group of PE thereby perturbing plasma membrane structure and integrity, eventually leading to rapid cell death.

Besides DAO, several other melleolides display cytotoxic properties [1, 2, 4, 8, 9], but the rapid onset of cell death by DAO is unique. Interestingly, in contrast to other well-known cell death-inducing agents such as Stsp or pretubulysin that are more effective in cancer cells versus normal untransformed cells, DAO is equally potent in primary monocytes and cancer cell lines, and loss of cell viability due to DAO is apparent within few minutes as compared to Stsp that needed at least 5 hrs to cause cell death [3]. As described before, DAO displayed apoptotic as well as necrotic features of cell death measured by flow cytometry with an Annexin V/7-amino-actinomycin staining, and marked apoptosis induction was only obvious after 5 hrs [3]. Here, we find that DAO causes cleavage of the classical apoptosis marker PARP in human monocytes to a 89 kDa fragment within 15 min. Furthermore, the increase of phosphorylation of the stress-regulated p38 MAPK and the simultaneous decrease of the phosphorylation of the survival factor Akt due to DAO may contribute to cell death induction. Cells treated with Stsp demonstrated classical apoptotic characteristics like apoptotic bodies and fragmentation of

nuclei [15, 17], DAO-treated cells were crumpled and shrunk along with membrane rupture, particular of mitochondrial membranes. These properties are typical characteristics of necrosis [20, 21] suggesting that both apoptotic and necrotic features of DAO-induced cell death.

Recently, the plant toxin ophiobolin A from the *Bipolaris* genus [42] was shown to react with PE and/or EA [43], accompanied by strong cytotoxic properties in various cancer cells [44-46]. Of interest also ophiobolin A possesses an α,β-unsaturated aldehyde moiety that covalently reacts with the EA moiety in one PE molecule yielding the formation of a pyrrole [43], while DAO forms first an imine (as for ophiobolin A) with PE but then couples via 1,4 addition to a second PE molecule. Our data suggest that via covalent binding to the amine moiety of EA residues DAO interacts with the head group of PE without forming adducts with PC, and seemingly also not with PS, although serine possesses a primary amine function like EA. In fact, substantial excess of exogenously added L-serine partially reverted the cytotoxic effects of DAO (Fig. 3G), while choline failed in this respect.

We suggest that DAO-PE adduct formation causes perturbances of cellular membranes resulting in loss of membrane integrity. Thus, formation of DAO-EA adducts from cells treated with DAO temporally correlated to LDH release as marker for impaired plasma membrane integrity, processes that occurred within 15 min upon cell exposure to DAO, and DAO caused disappearance of mitochondria as visualized by TEM. PE is a cone-shaped lipid and responsible for the formation of hexagonal membrane phases [24]. If DAO covalently binds to the EA moiety in PE, the arranged membrane structure might become perturbed and prone to ruptures with consequent LDH release. In fact, the cytotoxic effects of DAO were abrogated by supplementation of exogenous EA and serine, but not of choline, that may capture the reactive aldehyde moiety of DAO, and DAO cause leakage of liposomes composed of PE but not of liposomes made from PC. Therefore, we hypothesize that the interaction of DAO with membranous PE is the major cause for the rapid cell death induction.

In normal untransformed cells, PE is arranged in the inner leaflet of the plasma membrane and the mitochondrial membrane [22] but during cell death PE and also PS are translocated to the outer plasma membrane [23]. Upon treatment of HeLa cells with DAO, adducts with PE were most abundant in the membrane fraction, supporting the hypothesis that DAO acts on membranous PE. Moreover, treatment of HeLa cells with DAO caused primarily a rearrangement of various PE species (particularly PE (18:0/18:1) and PE (18:1/18:1)) in the plasma membrane fraction leading to the presumption that DAO might affect various metabolic processes.

PE is necessary for autophagosomal membranes and autophagy which is essential to gain ATP by recycling cytoplasmic compounds [19]. During apoptosis, cells increase the autophagic response to support cell functions and to eliminate toxic molecules. These effects were intensified by reduced caspase-8 levels [47, 48]. Cells become hyperactive and lysosomal resorption of DAO is enhanced. Simultaneously, DAO interacts with PE in the inner leaflet of lysosomes followed by a lysosomal membrane rupture and as consequence the pH declines, as shown in monocytes by using the pH-sensitive dye Lysotracker®, eventually inducing necrosis. Taken together, DAO causes apoptosis and necrosis by manipulating several cellular mechanisms initialized by perturbing membrane integrity.

In conclusion, we identified membrane PE as molecular target for the melleolide DAO that via the α,β-unsaturated aldehyde moiety covalently reacts with the EA headgroup of PE. These DAO-PE interactions translate into perturbation of cellular membrane structure with consequent loss of integrity which eventually causes the remarkably rapid onset of cell death in various cell types.

Materials and Methods

Materials

DAO was isolated as described before [3]. Antibodies against Lamin B1, Lamp1, and syntaxin 6, abcam (Cambridge, United Kingdom); DPX, abcr GmbH (Karlsruhe, Deutschland); bovine serum albumin (BSA), EDTA, and Tris, AppliChem (Darmstadt, Germany); DOPC, and DOPE, Avanti Polar Lipids (Alabaster, AL); L-glutamine, BioChem GmbH (Karlsruhe, Germany); AA, Cayman Chemical (Biomol, Hamburg, Germany); Antibodies against cleaved PARP (Asp214), phospho-p38 MAPK (Thr180/Tyr182), phospho-Akt (Ser473), ATF-4, CHOP, BiP, calnexin, COX IV, and β-actin were from Cell Signaling Technology (Boston, MA); phosphoplipase D from *Streptomyces chromofuscus*, ENZO life sciences (Lörrach, Germany); cytochrome c, Epitomics Inc. (Burlingame, CA); acetonitrile, Dulbecco's modified Eagle's high glucose medium with glutamine, penicillin/streptomycin-solution, sepharose and trypsin-EDTA, GE Healthcare Life Science (Freiburg, Germany); goat anti-rabbit IgG Alexa Fluor 488 antibody, and goat anti-mouse IgG Alexa Fluor 555 antibody, Invitrogen (Darmstadt, Germany); DMSO, Merck (Darmstadt, Germany); ATP, Roche (Mannheim, Germany); SDS, Roth GmbH (Karlsruhe, Germany); GAPDH, and β-tubulin, Santa Cruz Biotechnology (Heidelberg, Germany); Dulbecco´s Buffer Substance (PBS), staurosporine, and HPLC solvents, VWR (Darmstadt, Germany); dextrane, fetal calf serum (FCS), 3-(4,5-dimethylthiazol-2-yl)-2,5-diphenyltetrazolium bromide (MTT), RPMI 1640 Medium, phenylmethanesulfonyl fluoride, soybean trypsin inhibitor, lysozyme, leupeptin, HPTS, ethanolamine, choline, L-serine, triton X-100, chicken egg PE, chicken egg PC, QVD, LysoTracker® as well as other chemicals were from Sigma-Aldrich (Taufkirchen, Germany).

Cells

Monocytes were isolated from peripheral human blood of adult (18-65 years) healthy volunteers with written informed consent, obtained from the Institute of Transfusion Medicine, University Hospital Jena, as described [49]. The experimental protocol was approved by the ethical

committee of the University Hospital Jena. All methods were performed in accordance with the relevant guidelines and regulations. Leukocyte concentrates were prepared by centrifugation (4000×g, 20 min, 20 °C) and erythrocytes were removed by dextran sedimentation followed by centrifugation on lymphocyte separation medium (Histopaque®-1077, Sigma, Taufkirchen, Germany) to obtain peripheral mononuclear blood cells (PBMCs). PBMCs were seeded in RPMI 1640 (Sigma Aldrich, Taufkirchen, Germany) containing 10% (v/v) heat inactivated fetal calf serum (FCS), 100 U/mL penicillin, and 100 µg/mL streptomycin in cell culture flasks (Greiner Bio-one, Frickenhausen, Germany) for 1.5 h at 37 °C and 5% CO_2. Adherent monocytes were washed twice with PBS and were resuspended in PBS containing 1 mg/ml glucose. HeLa cells were cultured in monolayers in DMEM High Glucose (4.5 g/L) medium supplemented with heat-inactivated fetal calf serum (FCS, 10%, v v), 100 U/mL penicillin, and 100 µg/mL streptomycin at 37 °C in a 5% CO_2 incubator.

Analysis of cell viability by MTT assay

Monocytes (2 × 10^6/mL in RPMI 1640 containing 5% heat inactivated FCS, 100 U/mL penicillin and 100 µg/mL streptomycin) or 0.1 × 10^6/mL HeLa cells in DMEM High Glucose supplemented with 5% FCS, 100 U/mL penicillin and 100 µg/mL streptomycin were seeded in a 96-well plate. Monocytes were allowed to adhere for 1.5 h at 37 °C, 5% CO_2. Cell were incubated at 37 °C and 5% CO_2 with vehicle (0.5% DMSO) or compounds (i.e. DAO or Stsp) for indicated time points. In some experiments, EA, choline, L-serine or QVD were added 15 min prior to DAO or Stsp. After the times indicated, cells were incubated with thiazolyl blue tetrazolium bromide (MTT, 5 mg/mL PBS) until blue staining of the vehicle-containing control cells. Formazan formation was stopped by 100 µL SDS lysis buffer (10%, w/v in 20 mM HCl) and the well plate was shake overnight. Finally, absorbance was measured at 570 nm with a Multiskan™ microplate spectrophotometer (Thermo Scientific, Ulm, Germany). The pan protein kinase inhibitor staurosporine (1 µM) was used as cytotoxic control inhibitor.

LDH release assay

For analysis of extracellular LDH as marker for loss of plasma membrane integrity, we used the CytoTox96® Non-Radioactive Cytotoxicity assay kit (Promega, Madison, WI, USA). Freshly prepared monocytes (0.5×10^6/mL RPMI 1640 containing 5% heat inactivated FCS, 100 U/mL penicillin and 100 µg/mL streptomycin) or 0.1×10^6/mL HeLa cells in DMEM High Glucose supplemented with 5% FCS, 100 U/mL penicillin and 100 µg/mL streptomycin were seeded in a 96-well plate. Monocytes were allowed to adhere for 1.5 h at 37 °C, 5% CO_2 prior treatment with vehicle (0.5% DMSO), triton X-100 (lysis control) or 5 µM DAO for indicated time points. After incubation, the manufactures instructions were followed and the LDH release was measured by recording the absorbance at 490 nm with a Multiskan™ microplate spectrophotometer (Thermo Scientific, Ulm, Germany).

Microscopic morphology analysis

HeLa cells (0.25×10^6/mL DMEM High Glucose supplemented with 5% FCS, 100 U/mL penicillin and 100 µg/mL streptomycin) were incubated for 3 hrs with vehicle (0.1% DMSO, v/v), DAO or Stsp. Then, cells were placed on ice, washed with PBS, and analyzed by light microscopy using an AxioCam MR3 camera (Zeiss, Jena, Germany). Images were acquired, cut, linearly adjusted in the overall brightness and contrast, and exported to TIF by the AxioVision 4.8 software. The microscope incubator (Axio Observer Z1 inverted microscope, LCI Plan-Neofluar 63x/1.3 Imm Corr DIC M27 objective, Carl Zeiss, Jena, Germany) was kept at 37 °C and 5% CO_2.

Lysotracker® analysis

For acidification analysis of monocytes by fluorescence microscopy, freshly isolated monocytes (2.5×10^5/mL RPMI 1640 containing 5% heat inactivated FCS, 100 U/mL penicillin and 100 µg/mL streptomycin) were seated in Glass Bottom Microwell Dishes (MatTek Corporation, MA). After 1.5 hr adhesion time at 37 °C and 5% CO_2, cells were treated for 1 hr

with vehicle (0.1% (v/v) DMSO), 10 µM CCCP or 0.1 µM, 1 µM, 10 µM DAO at 37 °C and 5% CO_2 followed by washing with pre-warmed PBS. Cells were resuspended in PBS containing 1 mM $CaCl_2$, 1 mM $MgCl_2$ and 0.1% glucose. For the staining, 50 nM LysoTracker® Red-DND-99 (Sigma, Taufkirchen, Germany) was added to the cells and after 5 min, red fluorescence of the accumulated probe in acidic cell organelles was imaged using an Axio Observer Z1 microscope (Carl Zeiss, Jena, Germany).

For analysis by a fluorescence microplate reader (NOVOstar®, BMG Labtechnologies, Offenburg, Germany), freshly isolated monocytes (1.5×10^6/mL RPMI 1640 containing 5% heat inactivated FCS, 100 U/mL penicillin and 100 µg/mL streptomycin) were seated into a black 96-well plate with glass bottom. Monocytes were allowed to adhere for 1.5 hr at 37 °C, 5% CO_2 prior treatment with vehicle (0.1% (v/v) DMSO), 10 µM CCCP as control, and DAO as indicated concentrations for 1 hr. After washing and resuspension in PBS (0.1% glucose, 1 mM $CaCl_2$, 1 mM $MgCl_2$), cells were stained with 50 nM LysoTracker® and 0.5% (v/v) Hoechst for 5 min at 37 °C, 5% CO_2. After washing, fluorescence was excited at 577 nm (LysoTracker®) and 350 nm (Hoechst staining) and the emission was recorded at 590 nm (LysoTracker®) and 480 nm (Hoechst staining). Acidification was calculated from ratio of fluorescence intensities of LysoTracker® in relation to the fluorescence of Hoechst staining.

TEM

Monocytes, resuspended in RPMI 1640 containing 5% heat-inactivated FCS, 5 ml L-glutamine, 100 U/mL penicillin and 100 µg/mL streptomycin, were incubated with DAO, Stsp or vehicle for 3 hrs at 37 °C and 5% CO_2. Cells were washed in PBS pH 7.4, centrifuged (800×g, 5 min, 20 °C) and resuspended in 2.5% glutaraldehyde (v/v, in water) for fixation. After 20 min at RT, cells were washed by centrifugation (5000 rpm, 5 min, 4 °C) and resuspended in PBS. For the embedding process, cells were washed 3 times with PBS pH 7.4 for 5 min. After each washing step, the sample was centrifuged at 2000 rpm for 2 min. Post-fixation was performed by osmium tetroxide (1% OsO_4 in PBS pH 7.4) for 1 hr. Samples were washed again with PBS pH 7.4 and the monocytes were gradually dehydrated by a series of increasing

ethanol:water mixtures (50%, 70%, 90% and 100% ethanol, 10 min for each step and centrifugation at 2000 rpm for 2 min). Resin infiltration was performed in 2 steps (Embed812: EtOH 2:1 with 18 µL per mL resin DMP-30 (for 1 hr at RT), Science Services). Samples were centrifuged at 2000 rpm for 8 min. The second infiltration step was performed in undiluted Embed812 resin (overnight at RT). After an additional centrifugation step the resin was exchanged and infiltrated for 2 hrs. Samples were subsequently transferred to BEEM capsules (Plano), centrifuged once (2000 rpm, 8 min) and cured at 60° C for 24 hrs. The embedded samples were sectioned in 80 to 100 nm thick slices utilizing an ultramicrotome (PowerTome PC, RMC Products) equipped with a diamond knife (Diatome). The slices were placed on a carbon coated TEM grid (Quantifoil) and imaged with a 200 kV FEI Tecnai G²20 (FEI Company).

Detection of DAO-PE adducts *in vitro*

For analysis of DAO-PE adduct formation, 5.2 µL solution of DAO (5 mM) and 2 µL transphosphorylated chicken egg PE (13 mM, Sigma Aldrich, Taufkirchen, Germany) were added to 44.8 µL reaction buffer containing 1 M triethylammonium acetate, $CHCl_3$ and MeOH (1:1:3, v/v/v). Vehicle and chicken egg PC (13 mM, instead of PE) were used as controls. After 3 hrs incubation at 37 °C, samples were diluted with MeOH to 500 µL, internal standard was added and 50 µL were dried under a nitrogen stream. The pellet was resuspended with 25 µL MeOH and diluted to 250 µL with PBS, following incubation with 275 U phospholipase D from *Streptomyces chromofuscus* (ENZO life sciences, Lörrach, Germany) for 16 hrs at 37 °C. DAO adducts were extracted with 1 mL $CHCl_3$/MeOH (2:1, v/v). The lower organic phase was dried by a nitrogen stream and the pellet was resuspended with 1 mL MeOH before measuring by UPLC-MS/MS.

Isolation of cellular DAO-PE adducts

Monocytes (5×10^6 cells/mL) in RPMI 1640 containing 5% FCS, 100 U/mL penicillin and 100 µg/mL streptomycin or HeLa cells (0.25×10^6 cells/mL) in DMEM High Glucose supplemented with 5% FCS, 100 U/mL penicillin and 100 µg/mL streptomycin were incubated with vehicle

(0.1% DMSO, v/v) or DAO for the indicated time points at 37 °C and 5% CO_2. Cells were placed on ice and washed twice with ice-cold PBS. The cell pellet was resuspended with ice-cold 200 µL $CHCl_3$/MeOH (2:1, v/v) supplemented with 50 mM pentyl-pyridoxamine. The cell suspension was allowed to homogenize for 20 min at RT followed by addition of internal standard and extraction with 40 µL 0.9% NaCl solution. The suspension was vortexed for 30 sec and centrifuged (4000 rpm, 5 min, 4 °C). The lower phase was dried under a stream of nitrogen and the pellet was resuspended with 50 µL MeOH by sonication. An aliquot of the solution (50 µL) was diluted with 200 µL PBS and sonicated for 2 min in an ultrasonic bath, followed by incubation of extracted phospholipids with 875 U phospholipase D from *S. chromofuscus* for 16 hrs at 37 °C. The solution was extracted with 1 mL ice-cold $CHCl_3$/MeOH mixture (2:1, v/v). The lower organic phase was dried, and the pellet was resuspended with 0.5 mL $CHCl_3$/MeOH mixture (2:1, v/v) followed by addition of 125 µL 0.9% NaCl solution and another extraction. The dried lower phase was resuspended with 100 µL MeOH and DAO-EA adducts were measured by UPLC-MS/MS.

Reversed phase liquid chromatography and mass spectrometry

Chromatography was carried out on an Acquity UPLC BEH C8 column (1.7 µm, 1 × 100 mm) using an Acquity^{TM} Ultra Performance liquid chromatography system from Waters (Milford, MA, USA). DAO, PL's, and DAO-PE conjugates were separated at 0.75 ml/min and 45°C using a gradient of 30% mobile phase A (acetonitrile/water, 10/90, 10 mM ammoniumacetate)/70% mobile phase B (acetonitrile/water, 95/5, 10 mM ammonium acetate) to 20% mobile phase A/80% mobile phase B within 5 min and to 100% mobile phase B within 2 min followed by isocratic elution for another 2 min. The chromatography system, controlled by Acquity UPLC Software 1.40 (Waters), was coupled to a QTRAP 5500 Mass Spectrometer (Sciex, Darmstadt, Germany) equipped with an electrospray ionization source.

For identification of DAO, the precursor-to-product ion transitions in multiple reaction monitoring were m/z 399.2 → 104.9 (collision energy: -50 eV; collision cell exit potential: -13

V), and 399.2 → 148.9 (collision energy: -24 eV; collision cell exit potential: -16 V). Quantification of DAO was based on the transition 399.2 → 148.9 using an external calibration curve, quantification of phospholipids and PL-conjugates was based on the internal standard DMPC (collision energy: -38 eV; collision cell exit potential: -12 V). Analytes with varying collision energies (CE) and collision cell exit potentials are listed below in table 1. The ion spray voltage was set to -4000 V, the heated capillary temperature to 650°C, the curtain gas pressure to 30 psi, the declustering potential to -50 V, collisionally activated dissociation (CAD) to medium, nebulizer gas (GS1) to 50, heater gas (GS2) to 60, and the entrance potential -10 V. Analyst software 1.6 (Sciex, Darmstadt, Germany) was used for the processing of analytical data.

analyt	precursor-to-product ion transition (m/z)	Collision energy (CE)	Collision cell exit potential (CXP)
DAO 1xEA T1	442.4 → 149.0	-20 → 50	-17 → 64
DAO 1xEA T2	442.4 → 105.0	-56 → 36	-7 → 2
DAO 2xEA T1	484.8 → 149.0	-41 → 46	-52
DAO 2xEA T2	484.4 → 105.0	-66 → 44	-52 → 90
DAO-PE(16:0/18:1)	1098.7 → 948.5	-52 → 35	-42 → 7
DAO-PE(16:0/18:11)	1098.7 → 281.2	-76 → 80	-42 → 7
DAO-PE(18:1/18:1)	1126.8 → 976.6	-49 → 20	-12
DAO-PE(18:0/20:4)	1148.7 → 998.5	-49 → 51	-12
DAO-PE(18:0/20:41)	1148.7 → 283.4	-79 → 33	- 12
d8-AA	311.3 → 267.1	-16	-18
d4-LTB4	339.3 → 197.2	-22	-13
d4-PGE2	355.3 → 193.2	-38	-18

Liposomal leakage assay

Solutions containing either 5 µmol dioleoyl-PC (DOPC) or 2.5 µmol dioleoyl-PE (DOPE) plus 2.5 µmol DOPC (Avanti Polar Lipids, Inc.) were prepared in $CHCl_3$. The solvent was removed using a nitrogen stream and subsequent evaporation under vacuum. Lipid films were rehydrated by vortexing in a water bath (30 °C) with 1 mL of a solution of 35 mM 8-hydroxypyrene-1,3,6-trisulfonic acid trisodium salt (HPTS, fluorophore) and 50 mM 1,1'-[1,4-phenylenebis(methylene)]-bis pyridinium dibromide (DPX, colissional quencher) in 20 mM HEPES, 150 mM NaCl, and 1 mM EDTA forming essentially heterogenous multilamellar vesicles (MLV). Then, large unilamellar vesicles (LUV) were formed by six freeze-thaw cycles. Liposome suspensions were extruded 20 times through 100 nm polycarbonate filters (LiposoFast-Basic, Avestin Inc.) to generate LUVs with HPTS/DPX encapsulated [50]. LUVs were separated from free HPTS/DPX by size exclusion chromatography using a Sepharose column and 20 mM HEPES, 150 mM NaCl, 1 mM EDTA as buffer.

A 100 µL sample of HPTS/DPX-containing liposomes diluted (1:20) in 20 mM HEPES, 150 mM NaCl, 1 mM EDTA was dispensed in 96-well-plates. Then, 10 µM DAO was added and the fluorescence of HPTS was monitored each 14 s on a NOVOstar (BMG LABTECH GmbH) using excitation at 450 nm and emission at 520 nm over 15 min and at RT. A negative control using DMSO was used as the 0% leakage reference, and 0.2% Triton X-100 was used as positive control yielding 100% leakage. For each time point, the fluorescence data were normalized to these two reference samples.

Cytochrome c release

Cells were seeded in RPMI 1640 containing 5% FCS, 100 U/mL penicillin and 100 µg/mL streptomycin (4×10^6/ml) and incubated with the test compounds or vehicle (DMSO). After 3 hrs, cells were washed once in PBS and 10^7 cells were resuspended in 200 µl PBS. For permeabilization of the plasma membrane, 20.3 µM digitonin was added and immediately

vortexed (10 sec), incubated for another 30 seconds at room temperature and centrifuged at 20,000g at 4°C for 1 min. The supernatant (cytosolic fraction) and pellet (non-cytosolic fraction) were transferred to a new tube, respectively, and mixed 1:1 (vol/vol) with 5% trichloroacetic acid. Precipitation of cytosolic proteins was performed at 4°C overnight. Proteins were pelleted by centrifugation at 20,000g at 4°C for 30 min and resuspended in 25 µl PBS. Aliquots of 5 µl were used for determination of protein concentration using Roti-Nanoquant (Roth, Karlsruhe, Germany). Equal amounts of protein were mixed 1:1 (vol/vol) with 2 × SDS/PAGE sample loading buffer and analyzed for cytochrome c by SDS-PAGE and Western Blot using an anti-cytochrome c-antibody (Epitomics Inc., Burlingam, CA).

Subcellular fractionation

HeLa cells (0.25×10^6 cells/mL, in DMEM High Glucose supplemented with 5% FCS, 100 U/mL penicillin and 100 µg/mL streptomycin) were pre-incubated with vehicle (0.1% DMSO, v/v) or DAO (5 µM) for the indicated time points at 37 °C and 5% CO_2. Cells were placed on ice and the cell pellet was washed with 500 µL PBS followed by 5 min centrifugation (4600 rpm) at 4 °C. The cell pellet was resuspended with hypotonic lysis buffer pH 7.4 (10 mM HEPES, 2 mM $MgCl_2$, 0.1 mM EDTA, 0.1 mM EGTA, 10 mM KCl, 1 mM DTT) and cells were passed through a 25 G needle (sterican 0.5 × 40 mm, Gr 17/42, B. Braun Melsungen AG) 10 times using a 10 mL syringe. The cell suspension was kept on ice for 20 min before adding kinase inhibitor cocktail. To get nuclei, the cell suspension was centrifuged for 10 min at 550 g and 4 °C. Supernatant was used for continuing subcellular fractionation and pellet was again washed with hypotonic lysis buffer, centrifuged (550 g, 10 min, 4 °C) and frozen at -20 °C. The supernatant was centrifuged at 10,000 g and 4 °C for 10 min. The resulting mitochondrial pellet was again washed as described for the nuclear pellet and subsequently frozen at -20 °C. The supernatant was used to obtain the cytosolic and microsomal fraction by ultracentrifugation at 100,000 g and 4 °C for 1 h. The cytosolic fraction corresponds to the supernatant and was

evaporated until dryness with Eppendorf® concentrator at 30 °C. The pellet corresponds to the microsomal fraction and was frozen at -20 °C.

For preparation of Western Blot samples, pellets were resuspended in 100 µL Western Blot lysis buffer and homogenized by sonification on ice. On the other hand, pellets were used for mass spectroscopy analysis. Lipids were extracted as described before by Bligh and Dyer method [51] and cellular DAO-PE adducts were analyzed as specified above.

SDS PAGE and Western Blot

Subcellular fractions (see above) or isolated monocytes were resuspended in 100 µL ice-cold 2 × SDS loading buffer (20 mM Tris-HCl pH 8, 2 mM EDTA, 5% (m/v) SDS, 10% (v/v) β-mercaptoethanol, 10 µg/mL leupeptin, 60 µg/mL soybean trypsin (STI), 1 mM PMSF, 40 µL glycerol and 0.1% bromophenol blue (1:1, v/v). Samples were heated for 5 min at 96 °C and proteins were separated by SDS-PAGE on a 10% acrylamide gel. Correct protein loading on the gels and transfer of proteins to the nitrocellulose membrane (Amersham PROTRAN® supported 0.45 NC, GE Healthcare, Freiburg; Germany) was confirmed by Ponceau staining. Antibody recognizing cleaved PARP (Asp214), phospho-p38 MAPK (Thr180/Tyr182), phosho-Akt (Ser473), ATF-4, CHOP, BiP, calnexin, syntaxin 6, COX IV and β-actin were from Cell Signaling Technology (Boston, MA) and used at 1:1000 dilution. Antibodies against GAPDH and β-tubulin were purchased from SantaCruz (Dallas, TX) and also used at 1:1000 dilution. Antibodies against Lamin B1 (1:200), syntaxin 6 (1:1000) and Lamp1 (1:1000) were purchased from abcam (Cambridge, United Kingdom). Infrared labeled secondary antibody IRDye 800CW goat anti-mouse was from LI-COR Biosciences (Lincoln, NE). For detection, the Odyssey Infrared Imaging System (LI-COR Bioscience, Lincoln, NE) and for analysis the Odyssey application software (version 3.0.25) were used.

Statistics

Results are presented as means ± standard error of the mean (SEM) of *n* independent observations, where *n* represents the number of performed experiments at different days or with different donors. Statistical analysis of the data was performed by one-way ANOVA using GraphPad InStat (Graphpad Software Inc., San Diego, CA) followed by a Bonferroni post-hoc test for multiple or student t-test for single comparisons, respectively. P-values < 0.05 were considered as significant.

Acknowledgments

This work was supported by the Collaborative Research Centers ChemBioSys (SFB1127) and Polytarget (SFB1278) of the Deutsche Forschungsgemeinschaft (DFG) and by the DFG-funded excellence graduate school Jena School for Microbial Communication (JSMC).

Declaration of Interests

The authors declare no competing interests.

Legends for the figures

Figure 1: DAO causes rapid cell death in human cells with unique characteristics.

(A) Chemical structure of DAO. (B) Monocytes were incubated with DAO at indicated concentrations for 15 min, 60 min, and 24 hrs. Cell viability was analyzed by MTT assay. Means ± SEM, n =3. (C) Monocytes or HeLa cells were incubated with DAO (5 µM) for the indicated time points. Plasma membrane integrity was analyzed by LDH assay. Means ± SEM, n =3. *p < 0.05, **p < 0.01, ***p < 0.001 vs vehicle control; ANOVA plus Bonferroni post hoc test. (D) Morphological analysis of HeLa cells by light microscopy. Cells were treated with the compounds at indicated concentrations for 3 hrs and were then analyzed by light microscopy. Pictures shown are representatives out of three independent experiments. (E) TEM analysis of monocytes. Freshly isolated human monocytes were pretreated with 10 µM DAO, 3 µM Stsp or vehicle (0.1% DMSO) for 3 hrs. Cells were prepared for TEM analysis which was performed as described in the Method section. Arrows indicate the presence of mitochondria.

Figure 2: Contribution of apoptotic pathways in mediating cell death by DAO.

(A) Monocytes were treated with DAO (5 μM) or staurosporine (Stsp, 3 μM) for the indicated time points. Then, PARP cleavage to an 89 kDa fragment was assessed by Western Blotting (left panel) and densitometric analysis (right panel) was performed in correlation to GAPDH. Means ± SEM, n = 3. (B) Cytochrome C release from human monocytes. Intact monocytes were pretreated with 10 μM DAO, 3 μM Stsp or vehicle (0.1% DMSO) for 3 hrs. Then, cells were fractionated by mild detergent lysis and the cytosolic and the non-cytosolic fractions were analyzed by Western blot for cytochrome (Cyt) c. β-Actin and calnexin were used as marker proteins for respective fractions. (C) Monocytes were incubated with 5 μM DAO, 3 μM Stsp or vehicle. Total cell lysates were prepared after the indicated times and analyzed for phospho-p38 MAPK and phospho-Akt by Western blot (left panel). Densitometric analysis (right panel) was performed in correlation to β-actin. Means ± SEM, n = 3. (D) Protein expression of BiP, ATF-4 and CHOP in monocytes. Cells were incubated with DAO (5 μM) or vehicle (0.1% DMSO) for the indicated time points and then analyzed by Western blot (left panel). Densitometric analysis (right panel) was performed in correlation to β-actin. Means ± SEM, n = 3. (E) Monocytes were pre-incubated with the pan-caspase inhibitor QVD (10 μM) 30 min prior incubation with 5 μM DAO, 3 μM Stsp or vehicle for 3 hrs. Protein levels were analyzed by Western Blot (lower panel) and densitometric analysis (upper panel) were performed in correlation to GAPDH. (F) Monocytes were pre-incubated with the pan-caspase inhibitor QVD (10 μM) 30 min prior incubation with 10 μM DAO, 3 μM Stsp or vehicle for 3 hrs (left panel) or 48 hrs (right panel). Then, cell viability was assessed by MTT assay. Means ± SEM, n = 3. *$p < 0.05$, **$p < 0.01$, ***$p < 0.001$ vs vehicle control; ANOVA plus Bonferroni post hoc test.

Figure S1: Effect of staurosporine on PARP cleavage after 5 hrs incubation.

Monocytes were treated with DAO (5 μM) or staurosporine (Stsp, 3 μM) for 5 hrs. Then, PARP cleavage to a 89 kDa fragment was assessed by Western Blotting (left panel) and densitometric analysis (right panel) was performed in correlation to GAPDH. Means ± SEM, n = 3. $p < 0.05$, **$p < 0.01$, ***$p < 0.001$ vs vehicle control; students t-test.

Figure 3: DAO interacts with the ethanolamine (EA) residue of phosphatidylethanolamine.

(A, B) DAO (0.5 mM) was incubated with chicken egg PE (13 mM in $CHCl_3$), chicken PC (13 mM in $CHCl_3$) and bovine brain PS in reaction buffer for 3 hrs at 37 °C. Then, phospholipids were cleaved by exogenously added phospholipase D for 16 hrs at 37 °C (insert panel A). DAO-EA, -choline or –serine adducts were analyzed by UPLC-MS/MS. (C) Monocytes and HeLa cells were incubated with DAO at the indicated concentrations for 3 hrs. DAO-PE adducts were extracted with $CHCl_3$/MeOH (3:1) and cleaved by phospholipase D treatment for analysis of DAO-EA adducts by UPLC-MS/MS. Means ± SEM, n = 3. (D) Monocytes and HeLa cells were incubated with 5 μM DAO for the indicated periods. DAO-PE adducts were extracted and analyzed by UPLC-MS/MS. Means ± SEM, n = 3. (E) DAO (5 μM), Stsp (1 μM) or vehicle (0.1% DMSO) were incubated with 50 mM EA for 2 hrs at 37 °C and subsequently extracted using MeOH/$CHCl_3$ (1:2, vol:vol) as described in the Method section. Extracts containing EA-adducts or unreacted DAO or Stsp were resolved in ethanol (vehicle) and added to monocytes (left panel) or HeLa cells (right panel) for 3 hrs, and cell viability was assessed by MTT assay.

(F) DAO (10 µM), Stsp (3 µM) or vehicle (0.1% DMSO) were incubated with EA, choline (Chol) or L-serine (L-Ser) (50 mM, each) for 2 hrs at 37 °C and subsequently extracted as described above. Extracts containing adducts or unreacted agents (in ethanol as vehicle) were added to monocytes for 3 hrs (left panel) or 48 hrs (right panel), and cell viability was assessed by MTT assay. Data are means ± S.E, n = 3. *p < 0.05, **p < 0.01, ***p < 0.001, ****p < 0.0001 vs vehicle control; ANOVA plus Bonferroni post hoc test.

Figure S2: Markers subcellular fractionation.

HeLa cells were incubated with DAO (5 µM) or vehicle (0.1% DMSO) 15 min. Subcellular fractions were generated by hypotonic cell lysis and differential centrifugation. Respective fractions were analyzed by Western blot for specific fraction proteins. Western blots are representative for three independent experiments.

Figure 4: Subcellular locales of DAO-PE interactions and consequences for PE contents and membrane stability.

HeLa cells were incubated with DAO (5 µM) or vehicle (0.1% DMSO) for the indicated time points. Subcellular fractions were generated by hypotonic cell lysis and differential centrifugation. (A) Subcellular distribution of PE in HeLa cells after 15 min (left panel) and 3 hrs (right panel). (B) Subcellular distribution of DAO-PE adducts. The DAO-PE adducts formed within 15 min (left panel) or after 3 hrs (right panel) were extracted with $CHCl_3$/MeOH (3:1), cleaved by phospholipase D from PE, and then analyzed with UPLC-MS/MS. (C, D, E) HeLa cells were pre-incubated with 5 µM DAO for 3 hrs (C) or 15 min only (D). PE species were extracted by the Bligh and Dyer method and were analyzed by UPLC-MS/MS. (E) Correlation of PE species obtained after 15 min and after 3 hrs to total PE. (F) Correlation of PE species obtained after 15 min and after 3 hrs to vehicle control, shown as heat map. Data are given as mean + S.E, n = 3. *p < 0.05, **p < 0.01, ***p < 0.001 vs vehicle control; ANOVA plus Bonferroni post hoc test. (G) Liposomal leakage test. Liposomes (LUVs) composed of DOPC or DOPC/DOPE (1:1) containing HPTS/DPX were incubated with DAO (10 µM) and the fluorescence was measured. Liposomal leakage is expressed as % of the positive control incubated with Triton X-100 (=100%). (H) Monocytes were incubated with DAO at the indicated concentrations or vehicle (0.1% DMSO) for 15 min or 60 min, acidic vesicles (red) were stained with the Lysotracker probe for 5 min. Fluorescence microscopy pictures (left panel) are representative of four independent experiments. Acidification of vesicles (right panel) was assessed by fluorescence measured by NOVOstar®. Acidification is expressed in correlation to Hoechst staining of each cell per sample with vehicle = 100%. Data are given as mean + S.E, n = 3. *p < 0.05, **p < 0.01, ***p < 0.001 vs vehicle control; ANOVA plus Bonferroni post hoc test.

Figure S3: Liposomal leakage test.

Liposomes (LUVs) composed of DOPC or DOPC/DOPE (1:1) containing HPTS/DPX were incubated with vehicle (DMSO, negative control) or DAO (10 µM) and the fluorescence was measured. Results are representative for n=3 independent experiments.

References

1. Bohnert, M., et al., *In vitro cytotoxicity of melleolide antibiotics: structural and mechanistic aspects.* Bioorg Med Chem Lett, 2011. **21**(7): p. 2003-6.
2. Bohnert, M., et al., *Cytotoxic and antifungal activities of melleolide antibiotics follow dissimilar structure-activity relationships.* Phytochemistry, 2014. **105**: p. 101-8.
3. Bohnert, M., et al., *Melleolides induce rapid cell death in human primary monocytes and cancer cells.* Bioorg Med Chem, 2014. **22**(15): p. 3856-61.
4. Misiek, M., et al., *Structure and cytotoxicity of arnamial and related fungal sesquiterpene aryl esters.* J Nat Prod, 2009. **72**(10): p. 1888-91.
5. Momose, I., et al., *Melleolides K, L and M, new melleolides from Armillariella mellea.* J Antibiot (Tokyo), 2000. **53**(2): p. 137-43.
6. Dorfer, M., et al., *Melleolides impact fungal translation via elongation factor 2.* Org Biomol Chem, 2019.17(19):4906-16
7. Konig, S., et al., *Melleolides from Honey Mushroom Inhibit 5-Lipoxygenase via Cys159.* Cell Chem Biol, 2019. **26**(1): p. 60-70 e4.
8. Chang, W.H., et al., *Armillaridin induces autophagy-associated cell death in human chronic myelogenous leukemia K562 cells.* Tumour Biol, 2016. **37**(10): p. 14291-14300.
9. Chen, Y.J., C.C. Chen, and H.L. Huang, *Induction of apoptosis by Armillaria mellea constituent armillarikin in human hepatocellular carcinoma.* Onco Targets Ther, 2016. **9**: p. 4773-83.
10. Yin, X., T. Feng, and J.-K. Liu, *Structures and cytotoxicities of three new sesquiterpenes from cultures of Armillaria sp.* Nat Prod and Bioprospect, 2012. **2**(6): p. 245-248.
11. Chen, C.C., et al., *Three New Sesquiterpene Aryl Esters from the Mycelium of Armillaria mellea.* Molecules, 2015. **20**(6): p. 9994-10003.
12. Chi, C.W., C.C. Chen, and Y.J. Chen, *Therapeutic and radiosensitizing effects of armillaridin on human esophageal cancer cells.* Evid Based Complement Alternat Med, 2013. **2013**: p. 459271.
13. Liu, T.P., et al., *Armillaridin, a Honey Medicinal Mushroom, Armillaria mellea (Higher Basidiomycetes) Component, Inhibits Differentiation and Activation of Human Macrophages.* Int J Med Mushrooms, 2015. **17**(2): p. 161-8.
14. Clarke, P.G., *Developmental cell death: morphological diversity and multiple mechanisms.* Anat Embryol (Berl), 1990. **181**(3): p. 195-213.
15. Galluzzi, L., et al., *Cell death modalities: classification and pathophysiological implications.* Cell Death Differ, 2007. **14**(7): p. 1237-43.
16. Kroemer, G. and M. Jaattela, *Lysosomes and autophagy in cell death control.* Nat Rev Cancer, 2005. **5**(11): p. 886-97.
17. Taylor, R.C., S.P. Cullen, and S.J. Martin, *Apoptosis: controlled demolition at the cellular level.* Nat Rev Mol Cell Biol, 2008. **9**(3): p. 231-41.
18. Mizushima, N., *Autophagy: process and function.* Genes Dev, 2007. **21**(22): p. 2861-73.
19. Levine, B. and G. Kroemer, *Autophagy in the pathogenesis of disease.* Cell, 2008. **132**(1): p. 27-42.
20. Festjens, N., T. Vanden Berghe, and P. Vandenabeele, *Necrosis, a well-orchestrated form of cell demise: signalling cascades, important mediators and concomitant immune response.* Biochim Biophys Acta, 2006. **1757**(9-10): p. 1371-87.
21. Golstein, P. and G. Kroemer, *Cell death by necrosis: towards a molecular definition.* Trends Biochem Sci, 2007. **32**(1): p. 37-43.
22. Vance, J.E., *Phospholipid synthesis and transport in mammalian cells.* Traffic, 2015. **16**(1): p. 1-18.
23. Emoto, K., et al., *Exposure of phosphatidylethanolamine on the surface of apoptotic cells.* Exp Cell Res, 1997. **232**(2): p. 430-4.
24. Dowhan, W. and M. Bogdanov, *Lipid-dependent membrane protein topogenesis.* Annu Rev Biochem, 2009. **78**: p. 515-40.

25. van den Brink-van der Laan, E., J.A. Killian, and B. de Kruijff, *Nonbilayer lipids affect peripheral and integral membrane proteins via changes in the lateral pressure profile.* Biochim Biophys Acta, 2004. **1666**(1-2): p. 275-88.
26. Verkleij, A.J., et al., *Non-bilayer structures in membrane fusion.* Ciba Found Symp, 1984. **103**: p. 45-59.
27. Bottinger, L., et al., *Phosphatidylethanolamine and cardiolipin differentially affect the stability of mitochondrial respiratory chain supercomplexes.* J Mol Biol, 2012. **423**(5): p. 677-86.
28. Birner, R., et al., *Roles of phosphatidylethanolamine and of its several biosynthetic pathways in Saccharomyces cerevisiae.* Mol Biol Cell, 2001. **12**(4): p. 997-1007.
29. Ichimura, Y., et al., *A ubiquitin-like system mediates protein lipidation.* Nature, 2000. **408**(6811): p. 488-92.
30. Rockenfeller, P., et al., *Phosphatidylethanolamine positively regulates autophagy and longevity.* Cell Death Differ, 2015. **22**(3): p. 499-508.
31. Menon, A.K. and V.L. Stevens, *Phosphatidylethanolamine is the donor of the ethanolamine residue linking a glycosylphosphatidylinositol anchor to protein.* J Biol Chem, 1992. **267**(22): p. 15277-80.
32. Falcieri, E., et al., *The protein kinase inhibitor staurosporine induces morphological changes typical of apoptosis in MOLT-4 cells without concomitant DNA fragmentation.* Biochem Biophys Res Commun, 1993. **193**(1): p. 19-25.
33. Green, D.R. and G. Kroemer, *The pathophysiology of mitochondrial cell death.* Science, 2004. **305**(5684): p. 626-9.
34. Hemmings, B.A., *Akt signaling: linking membrane events to life and death decisions.* Science, 1997. **275**(5300): p. 628-30.
35. Watanabe, T., et al., *Apoptosis Signal-regulating Kinase 1 (ASK1)-p38 Pathway-dependent Cytoplasmic Translocation of the Orphan Nuclear Receptor NR4A2 Is Required for Oxidative Stress-induced Necrosis.* J Biol Chem, 2015. **290**(17): p. 10791-803.
36. Dunai, Z.A., et al., *Staurosporine induces necroptotic cell death under caspase-compromised conditions in U937 cells.* PLoS One, 2012. **7**(7): p. e41945.
37. Mebarek, N., et al., *Polymeric micelles based on poly(methacrylic acid) block-containing copolymers with different membrane destabilizing properties for cellular drug delivery.* Int J Pharm, 2013. **454**(2): p. 611-20.
38. Campbell, W.G., *The chemistry of the white rots of wood: The effect on wood substance of Armillaria mellea (Vahl.) Fr., Polyporus hispidus (Bull.) Fr., and Stereum hirsutum Fr.* Biochem J, 1931. **25**(6): p. 2023-7.
39. Richard, C., *[Antibiotic activity of Armillaria mellea].* Can J Microbiol, 1971. **17**(11): p. 1395-9.
40. Donnelly, D.M., et al., *Antibacterial sesquiterpene aryl esters from Armillaria mellea.* J Nat Prod, 1985. **48**(1): p. 10-6.
41. Obuchi, T., et al., *Armillaric acid, a new antibiotic produced by Armillaria mellea.* Planta Med, 1990. **56**(2): p. 198-201.
42. Evidente, A., et al., *Herbicidal potential of ophiobolins produced by Drechslera gigantea.* J Agric Food Chem, 2006. **54**(5): p. 1779-83.
43. Chidley, C., et al., *The anticancer natural product ophiobolin A induces cytotoxicity by covalent modification of phosphatidylethanolamine.* Elife, 2016. **5**.
44. Morrison, R., et al., *Ophiobolin A, a sesterpenoid fungal phytotoxin, displays different mechanisms of cell death in mammalian cells depending upon the cancer cell origin.* International Journal of Oncology, 2017. **50**(3): p. 773-786.
45. Bury, M., et al., *Ophiobolin A induces paraptosis-like cell death in human glioblastoma cells by decreasing BKCa channel activity.* Cell Death Dis, 2013. **4**: p. e561.
46. Rodolfo, C., et al., *Ophiobolin A Induces Autophagy and Activates the Mitochondrial Pathway of Apoptosis in Human Melanoma Cells.* PLoS One, 2016. **11**(12): p. e0167672.
47. Bell, B.D., et al., *FADD and caspase-8 control the outcome of autophagic signaling in proliferating T cells.* Proc Natl Acad Sci U S A, 2008. **105**(43): p. 16677-82.
48. Yu, L., et al., *Regulation of an ATG7-beclin 1 program of autophagic cell death by caspase-8.* Science, 2004. **304**(5676): p. 1500-2.

49. Garscha, U., et al., *BRP-187: A potent inhibitor of leukotriene biosynthesis that acts through impeding the dynamic 5-lipoxygenase/5-lipoxygenase-activating protein (FLAP) complex assembly.* Biochem Pharmacol, 2016. **119**: p. 17-26.
50. MacDonald, R.C., et al., *Small-volume extrusion apparatus for preparation of large, unilamellar vesicles.* Biochim Biophys Acta, 1991. **1061**(2): p. 297-303.
51. Koeberle, A., et al., *Role of lysophosphatidic acid acyltransferase 3 for the supply of highly polyunsaturated fatty acids in TM4 Sertoli cells.* FASEB J, 2010. **24**(12): p. 4929-38.

Figure 1

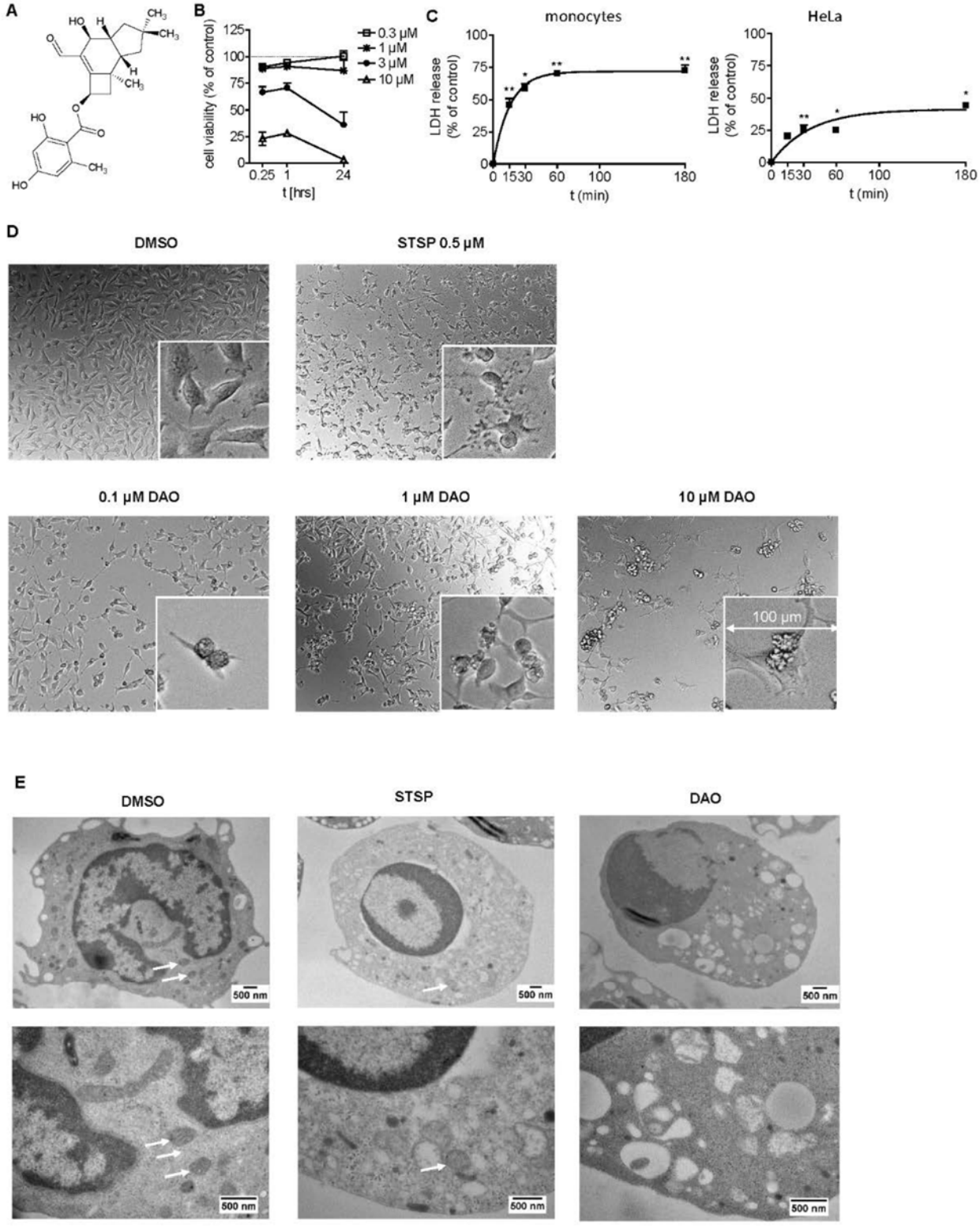
A
B
cell viability (% of control)
t [hrs]
0.3 µM
1 µM
3 µM
10 µM
C
monocytes
HeLa
LDH release (% of control)
t (min)
D
DMSO
STSP 0.5 µM
0.1 µM DAO
1 µM DAO
10 µM DAO
100 µm
E
DMSO
STSP
DAO
500 nm

Figure 2

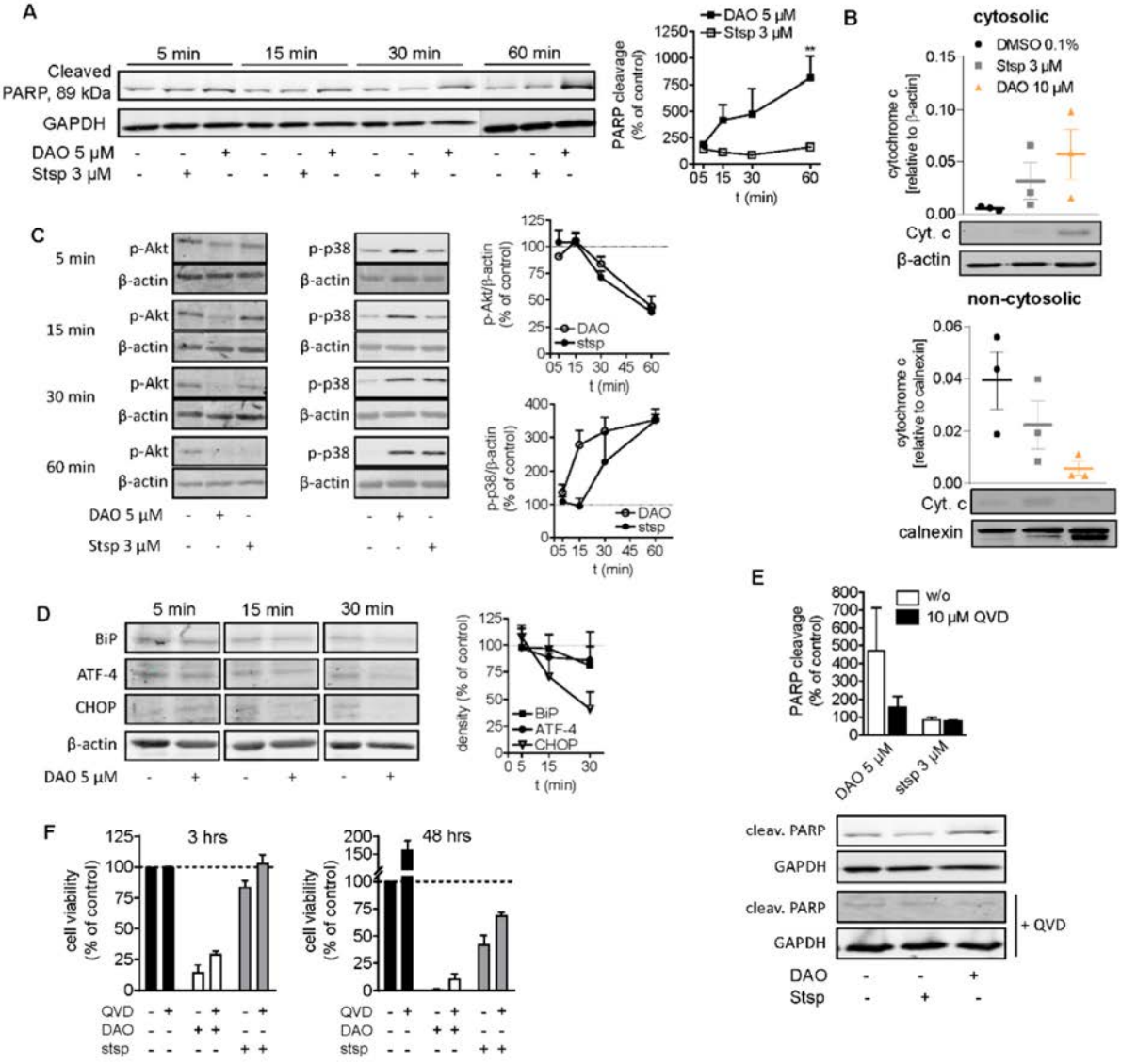
A
5 min
15 min
30 min
60 min
Cleaved PARP, 89 kDa
GAPDH
DAO 5 µM
Stsp 3 µM
PARP cleavage (% of control)
t (min)
B
cytosolic
DMSO 0.1%
Stsp 3 µM
DAO 10 µM
cytochrome c [relative to β-actin]
Cyt. c
β-actin
non-cytosolic
cytochrome c [relative to calnexin]
calnexin
C
p-Akt
p-p38
β-actin
p-Akt/β-actin (% of control)
p-p38/β-actin (% of control)
DAO
stsp
D
BiP
ATF-4
CHOP
density (% of control)
E
w/o
10 µM QVD
cleav. PARP
GAPDH
+ QVD
F
3 hrs
48 hrs
cell viability (% of control)
QVD
DAO
stsp

Figure 3

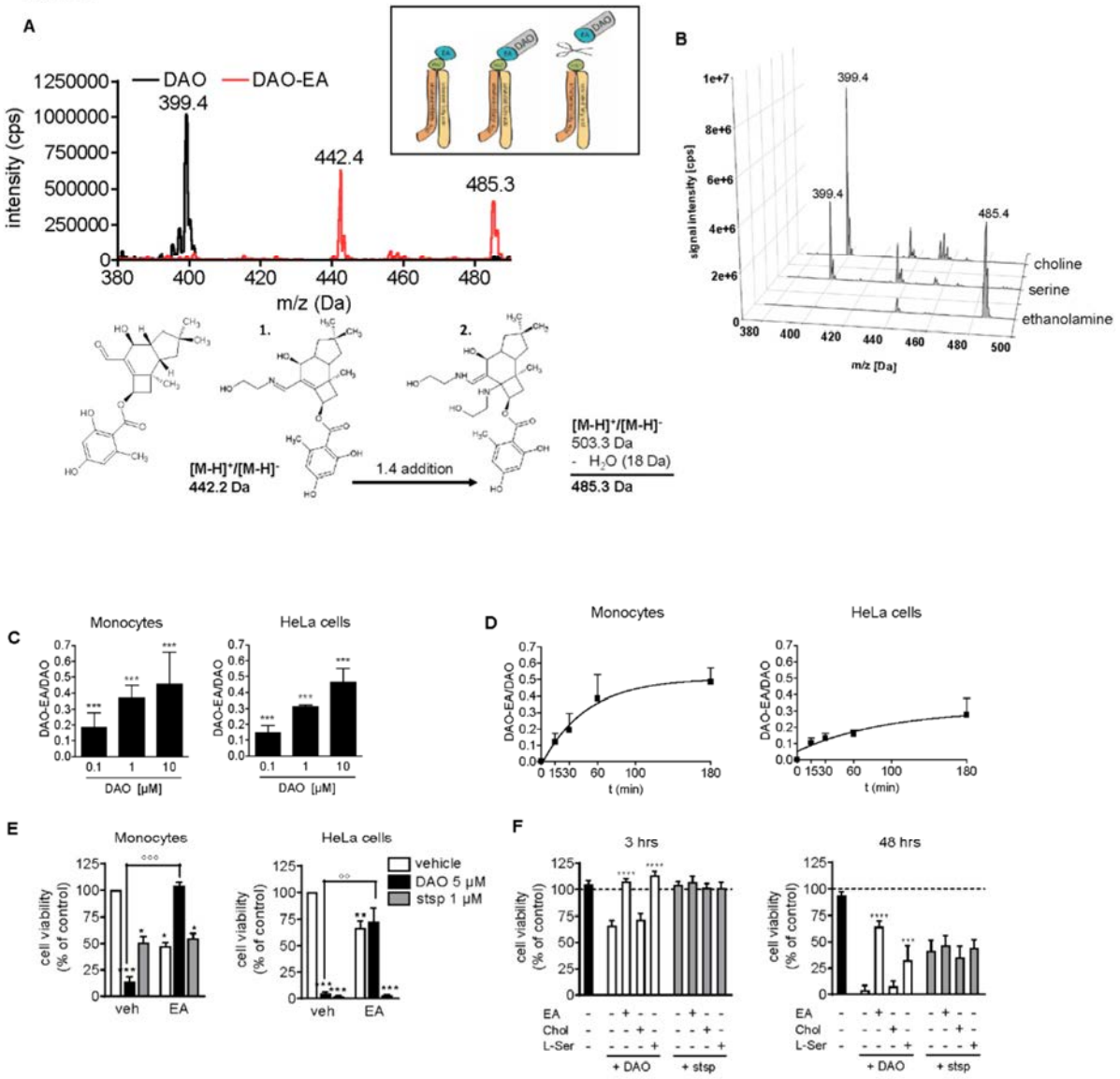
A
DAO
DAO-EA
399.4
442.4
485.3
intensity (cps)
m/z (Da)
1.
2.
[M-H]+/[M-H]-
442.2 Da
1.4 addition
[M-H]+/[M-H]-
503.3 Da
- H2O (18 Da)
485.3 Da
B
signal intensity [cps]
399.4
485.4
choline
serine
ethanolamine
m/z [Da]
C
Monocytes
HeLa cells
DAO-EA/DAO
DAO [µM]
D
Monocytes
HeLa cells
DAO-EA/DAO
t (min)
E
Monocytes
HeLa cells
cell viability (% of control)
vehicle
DAO 5 µM
stsp 1 µM
veh
EA
F
3 hrs
48 hrs
cell viability (% of control)
EA
Chol
L-Ser
+ DAO
+ stsp

Figure 4

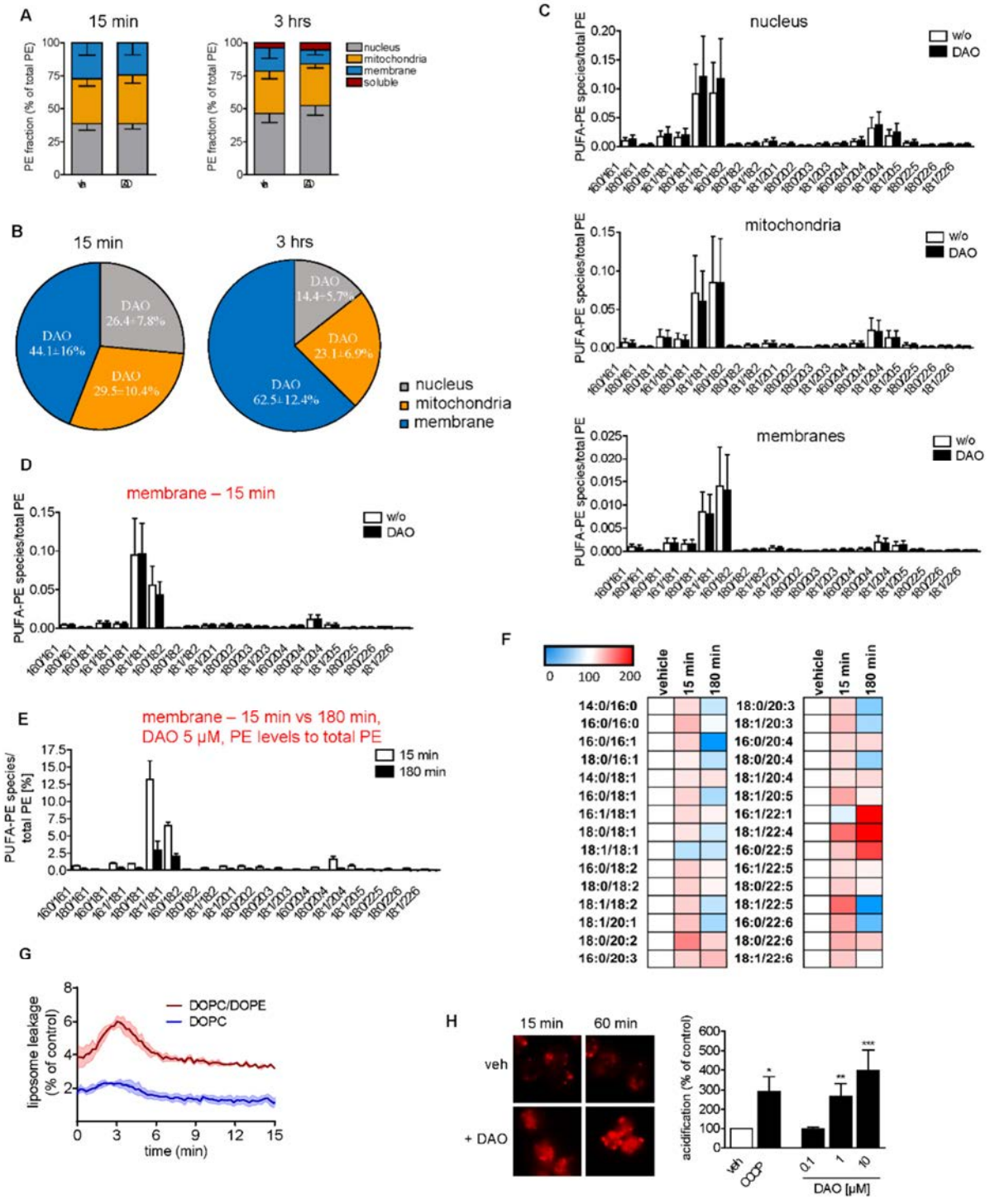
A
15 min
3 hrs
PE fraction (% of total PE)
nucleus
mitochondria
membrane
soluble
B
15 min
3 hrs
DAO 26.4±7.8%
DAO 44.1±16%
DAO 29.5±10.4%
DAO 14.4±5.7%
DAO 23.1±6.9%
DAO 62.5±12.4%
nucleus
mitochondria
membrane
C
nucleus
mitochondria
membranes
w/o
DAO
PUFA-PE species/total PE
D
membrane – 15 min
E
membrane – 15 min vs 180 min,
DAO 5 µM, PE levels to total PE
15 min
180 min
PUFA-PE species/ total PE [%]
F
vehicle
15 min
180 min
14:0/16:0
16:0/16:0
16:0/16:1
18:0/16:1
14:0/18:1
16:0/18:1
16:1/18:1
18:0/18:1
18:1/18:1
16:0/18:2
18:0/18:2
18:1/18:2
18:1/20:1
18:0/20:2
16:0/20:3
18:0/20:3
18:1/20:3
16:0/20:4
18:0/20:4
18:1/20:4
18:1/20:5
16:1/22:1
18:1/22:4
16:0/22:5
16:1/22:5
18:0/22:5
18:1/22:5
16:0/22:6
18:0/22:6
18:1/22:6
G
DOPC/DOPE
DOPC
liposome leakage (% of control)
time (min)
H
15 min
60 min
veh
+ DAO
acidification (% of control)
veh
CCCP
DAO [µM]

Supplemental Figure 1

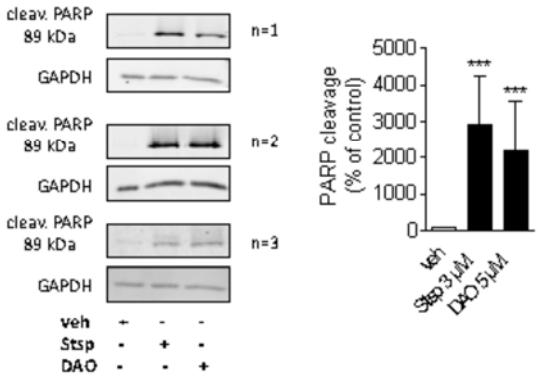

Supplemental Figure 2

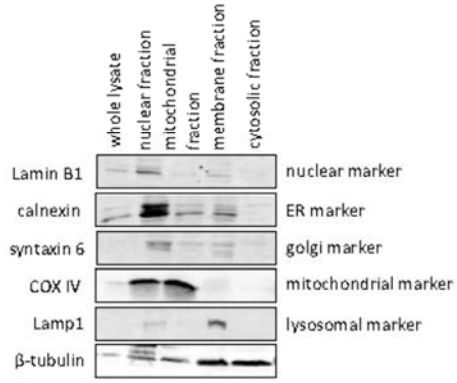

Supplemental Figure 3

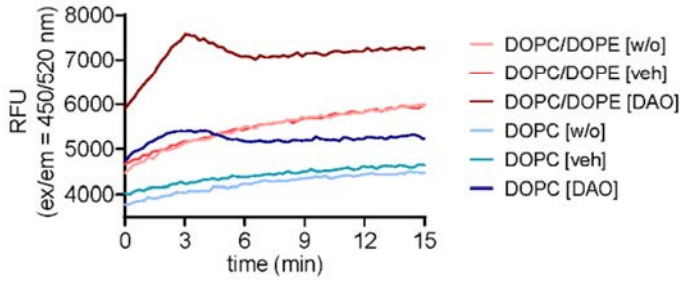

5. Diskussion

5.1. Vom Naturstoff zum Arzneimittel am Beispiel des Melleolids DAO

Die Verwendung eines Naturstoffs als Arzneimittel erfordert intensive Vorarbeit. Nach einem mehrjährigen Prozess, welcher sich von der Untersuchung physikochemischer Eigenschaften über Tierversuche bis hin zu klinischen Studien am Menschen erstreckt, kann der Naturstoff, formuliert in eine entsprechende Arzneiform, auf den Markt kommen. Doch vor all diesen Untersuchungen steht zunächst ein intensives Screening, in dem untersucht wird, wofür oder wogegen das neue Molekül überhaupt wirken kann. Sowohl Wirkziele für eine erwünschte Hauptwirkung, aber auch für mögliche Nebenwirkungen müssen bekannt sein. Wie findet man das molekulare Wirkziel eines neuen Naturstoffs?

5.1.1. Die Entdeckung des molekularen Wirkziels

In dieser Arbeit musste zunächst die Entscheidung für eine geeignete Methode getroffen werden. Mit der eingangs favorisierten Methode der **Drug Affinity Response Target Stability** (DARTS) wurden bereits Wirkmechanismen des Immunsuppressivums Rapamycin oder des COX-2 Inhibitors Celecoxib aufgeklärt (Lomenick et al., 2011b). Auch EF1α, das Wirkziel des Zytostatikums Didemnin wurde über DARTS gefunden (Lomenick et al., 2009). Die Methode basiert auf der Bindung kleiner Moleküle (SM - small molecule) an Zielproteine, welche dadurch unempfindlicher für eine nachfolgende Proteasebehandlung werden und somit identifiziert werden können. Der Vorteil dieser Methode ist, dass SM unmodifiziert angewendet werden können. Jedoch sind große Proteinmengen zur Wirkzielidentifizierung notwendig (Lomenick et al., 2009; Lomenick et al., 2011b). Nur so könnten von SMs selbst mit niedriger Affinität gebundene Proteine über eine Natriumdodecylsulfat-Polyacrylamid-Gelelektrophorese (SDS-PAGE) angereichert und analysiert werden (Lomenick et al., 2011a). Ein ungefährer Anhaltspunkt, z. B. in welcher Zellfraktion ein Wirkziel vermutet wird, erhöht die Erfolgsaussichten. Da dieser Anhaltspunkt genauso wenig gegeben war, wie ausreichend Testsubstanz DAO, musste eine andere Methode gewählt werden.

Bei der Methode des **aktivitätsbasierten Protein-Profilings** (ABPP) lassen sich Kulturen sowohl *in vivo* als auch *in vitro* untersuchen. Das ursprüngliche radioaktive Labeling von Proteinen (McFedries et al., 2013; Ostrowski und Barnard, 1961) ist in heutigen ABPP-Untersuchungen dreiteiligen Sonden, bestehend aus einem SM, einem „inerten“ Spacer und einem Marker wie Fluoreszenz- oder Biotinmarker, gewichen. Die Sondenbestandteile werden nach dem Proteinlabeling über bioorthogonale Reaktionen, heute mit der klassischen „Klickchemie“, zusammengefügt (Böttcher et al., 2010; Speers et al., 2003). Für einen *in vivo* Ansatz fehlten hier Kenntnisse über die Membrangängigkeit von Sondenbestandteilen im Modellorganismus *A. nidulans.*

Diese Arbeit behandelt deshalb einen klassischen, affinitätsbasierten *in vitro* Ansatz nachfolgend auch als **Pulldown-Assay** oder Targetfishing bezeichnet. Hierfür musste das SM DAO zunächst chemisch-synthetisch mit einem Spacer und Biotinmarker verbunden werden, um im Anschluss Proteine aus einem Zelllysat von *A. nidulans* über eine Streptavidin-Festphase aufreinigen zu können. Die Schwachstelle des *in vitro* Ansatzes ist, dass bei der Gewinnung eines Zelllysates Zellorganellen und –kompartimente geschädigt werden, was die Enzymaktivität beeinflussen kann (Bogyo et al., 2004). Um unspezifische Wirkziel-Wechselwirkungen mit DAO auszuschließen wurde eine Kontrollsonde entwickelt. Die Synthese der Sonden wird nachfolgend diskutiert.

5.1.2. Synthese einer Sonde für eine affinitätsgesteuerte Proteinaufreinigung

Die Leitstrukturen verschiedener Naturstoffe sind komplex, oft wenig erforscht und durch „Lehrbuchchemie“ selten zugänglich. Drei Hauptmerkmale unterscheiden Naturstoffe von einer *de novo* synthetisierten Substanz oft maßgeblich: Die Struktur ist meist komplex und sehr divers. Es gibt mehr sp^3-hybridisierte, gesättigte Kohlenstoffe als sp^2-hybridisierte. Naturstoffe haben meist mehrere Chiralitätszentren und eine komplexe Stereochemie (Guo, 2017).

A. mellea produziert ein komplexes Gemisch sehr ähnlicher Moleküle, die bis zu sechs, teilweise benachbarte Stereozentren enthalten können (Vgl. Abbildung 6). Diese Ähnlichkeiten machen eine saubere Isolation einzelner Melleolide sehr schwierig. Um die sauber aufgereinigten Melleolide nicht zu verschwenden, wurde von Synthesen mit ungeeigneten Modellsubstanzen wie Salicylsäurephenylester oder Salicylaldehyd auf Reaktionen im Mikromaßstab mit Kleinstmengen ausgewichen.

Durch eine Carbonat-katalysierte Ethersynthese nach Williamson mit Propargylbromid gelang am Salicylaldehyd die Einführung einer C-Dreifachbindung (Banday et al., 2010; Lingam et al., 2008), welche auf DAO nicht übertragbar war. Es konnte aber gezeigt werden, dass die Hydroxylgruppe der Reaktion am Modell zugänglicher ist, als ein Aldehyd (Purushothaman et al., 2013). Die Verwendung des reaktiveren Propargyliodids (Abbildung 8), welches über eine Finkelstein-Reaktion (Finkelstein, 1910) oder unter Verwendung von Propargylalkohol hergestellt wurde (Jammi et al., 2013), brachte keinen Umsatz. Ethersynthesen waren an der C5‘-Hydroxygruppe nicht möglich, ohne dass DAO-Molekül zu zerstören. Reaktionsprodukte aus DAO hatten häufig dieselbe Molekülmasse wie das zu erwartende Produkt. NMR-Analysen ergaben, dass aufgrund von Umlagerungen nicht die gewünschte Struktur entstand.

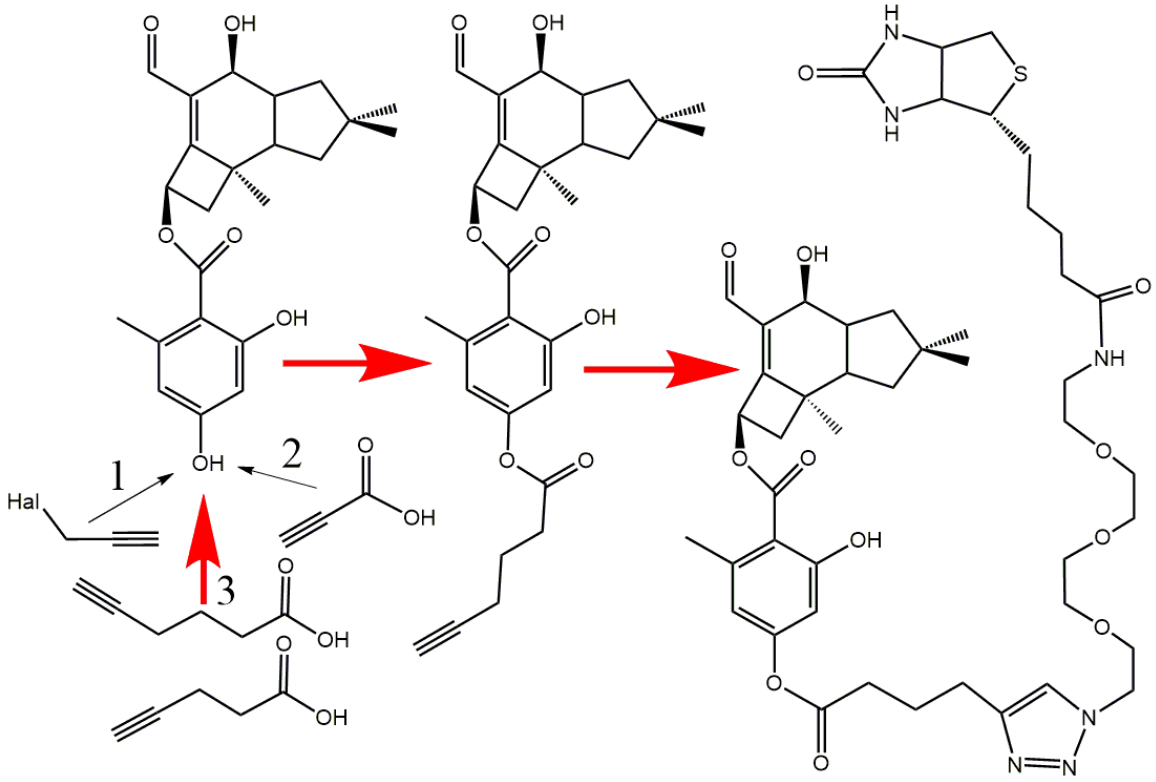

Abbildung 8. Reaktionsschema zur Sondensynthese. Versuch der Einführung einer C-Dreifachbindung über Propargyliodid oder -bromid (1), über Propargylsäure (2) und final über Pentin- und Hexinsäure. Erfolgreiche Syntheseroute in rot mit Cu(I)-katalysierter „Klick-Reaktion“ zum Biotin-gekoppelten Endprodukt.

In einem neuen Ansatz wurde die Einführung einer C-Dreifachbindung in das DAO-Molekül über eine Steglich-Veresterung dennoch erreicht. Die Bindung einer Carbonsäure an die freie, sterisch ungehinderte C5‘-OH Gruppe über Propargylsäure (Propiolsäure, Abbildung 8), führte nicht zum Ziel (Coles et al., 2018; Jolit et al., 2017). Mit demselben Reaktionsprinzip, aber längerkettiger und daher weniger reaktiver Pentin- und Hexinsäure, konnte das in Publikation 1 gezeigte Zwischenprodukt gebildet werden. Die hierbei verwendeten Kupplungsreagenzien wie die Carbodiimide Dicyclohexylcarbodiimid (DCC) oder 1-Ethyl-3-(3-dimethylamino-propyl)carbodiimid (EDC) aber auch Phosphoniumsalze wie Benzotriazol-1-yl-oxytripyrrolidino-phosphonium-hexafluorophosphat (PyBOP) sind klassische Edukte zur Knüpfung von Peptidbindungen in der Proteinsynthese, welche vor allem bei längeren Peptidketten zum Einsatz kommen (Al-Warhi et al., 2012). Anwendung finden sie aber auch für die Bildung von Estern oder Säure-Anhydriden aus Carbonsäuren. Die Verwendung eines Acylierungskatalysators wie 4-(Dimethylamino)-pyridin (DMAP) ermöglicht vor allem bei Esterbindungen höhere Ausbeuten mit weniger Nebenprodukten (Neises und Steglich, 1978).

Durch die erfolgreiche Funktionalisierung des DAOs war es möglich, über eine dipolare Huisgen-1,4-Cycloaddition („Klick-Reaktion“) unter Kupfer (I)-Katalyse einen Biotin-PEG_3-Azid Linker einzuführen (Rostovtsev et al., 2002). Nach Optimierung der Reaktionsbedingungen, insbesondere der Auswahl eines geeigneten Lösungsmittels, sowie der optimalen

Konzentration von Reduktionsmittel (Ascorbat) und Katalysator, konnten die laut Lehrbuch quantitativen Ausbeuten (hier 92 %) erreicht werden (Wu et al., 2004).

Analog wurde eine Sonde zur Verwendung als Negativkontrolle, basierend auf Butylparaben, synthetisiert. Die Sonde erfüllte im Nachgang ihre Funktion: da die Pulldown-Assays unterschiedliche Proteinbanden zeigten, waren die Sonden stabil. Der Spacer hatte ein optimales Verhältnis von Hydrophilie/Hydrophobie, um die Aktivität der SMs nicht zu stören.

Die Komplexität der Synthesestrategien zeigt, dass Naturstoffchemie selten nach Lehrbuchmethoden funktioniert und eine Analyse von Wirkzielen oder Struktur-Wirkungs-Beziehungen bereits an dieser Stelle scheitern kann, da sämtliche Folgeversuche auf dem Gelingen einer solchen Synthese aufbauen.

5.2. Melleolide im Vergleich zu anderen Antibiotika

5.2.1. Melleolide im Vergleich zu anderen Zytostatika

Wie bereits gezeigt wurde, sind einige Melleolide in der Lage, humane Zelllinien in ihrer Entwicklung zu inhibieren und das bis hin zum Zelltod. Um das Potenzial von DAO einordnen zu können, wurden eingangs die Wirkmechanismen etablierter Zytostatikagruppen erläutert.

Wirkmechanismen: In dieser Arbeit wurde festgestellt, dass Melleolide über eine kovalente Bindung von Cysteinen im aktiven Zentrum von 5-LO, vor allem von C159, die Bildung von Arachidonsäure und somit von Entzündungsmediatoren wie Leukotrienen inhibieren. Der in Vorarbeiten beobachtete, rasche Zelltod ist über diesen Mechanismus aber nicht erklärbar. Eine Inhibition der Proteinbiosynthese wird ausgeschlossen, da in Experimenten parallel zur Ermittlung der antifungalen Wirkmechanismen keine entsprechenden Wirkziele in humanen Zellen nachgewiesen werden konnten.
Bei einigen 2-Aminothiazolen wurde eine ähnliche Wirkung beobachtet. Diese binden neben C159 auch C418 der 5-LO und inhibieren diese ebenfalls (Kretschmer et al., 2017). Das in den USA als antiinflammatorisches Arzneimittel zugelassene Zileuton hemmt die 5-LO über einen gänzlich unterschiedlichen Mechanismus: Wie die sich noch in klinischen Studien befindenden Substanzen Atreleuton oder Setileuton reduziert Zileuton das im aktiven Zentrum der 5-LOX befindliche Fe^{3+}-nicht-Häm Eisen zu Fe^{2+} und inaktiviert so das Enzym (Sinha et al., 2019).

Es zeigte sich, dass DAO über das $\Delta^{2,4}$-ungesättigte Aldehyd kovalent an Phosphatidylethanolamin (PE) bindet und dieses in ein Imin überführt (Vgl. 4. Unveröffentlichte Ergebnisse). Diese Reaktion führt über die Bildung cytotoxischer Zwischenprodukte zur Destabilisierung der doppellagigen Phospholipid-Zellmembran und somit zum Zelltod durch Zelllyse. Bekannt ist ein ähnlicher Mechanismus bereits bei Ophiobolin A, einem Phytotoxin aus Pilzen der Gattung *Bipolaris* (Chidley et al., 2016). Auch bei Polygodial, einem Naturstoff aus *Warburgia spp.*, ist eine Zerstörung der Membranintegrität, basierend auf einem

ungesättigten Aldehyd bekannt (Kubo et al., 2001; Taniguchi et al., 1988). Der Wirkmechanismus ist hier allerdings sehr divers, so ist neben einer antimikrobiellen (Anke und Sterner, 1991) und antifungalen Aktivität (Lee et al., 1999) auch eine antientzündliche sowie antiallergische (da Cunha et al., 2001), Schmerzempfindlichkeit senkende (Mendes et al., 2000) und Gefäß relaxierende Wirkung bekannt (André et al., 1999). Die unspezifische Wirksamkeit der genannten Moleküle bedeutet auch für DAO eine hohe Reaktivität des $\Delta^{2,4}$- ungesättigten Aldehyds.

Nebenwirkungen: Den meisten Zytostatika ist gemein, dass sie sich in ihrer Wirkung gegen proliferierende Zellen richten. Da sich Krebszellen unkontrolliert und sehr schnell teilen (Lambert, 1913), ist die Wirkung gegen sie prinzipiell stärker. Gesunde und entartete Zellen unterliegen grundsätzlich denselben Mechanismen wie Zellzyklus, Stoffwechsel etc. Zytostatika können aufgrund dessen nicht ausschließlich gegen malignes Gewebe wirken, woraus sich viele Nebenwirkungen ergeben.
Der menschliche Körper reagiert auf eine Zytostatikabehandlung oftmals zuerst mit grippeähnlichen Symptomen wie Fieber mit Schwitzen oder Frösteln, sowie allergischen Reaktionen, Übelkeit und Erbrechen, was auf eine erste Immunantwort des Körpers hinweist. Da Zytostatika auch gesunde, sich schnell teilende Zellen bekämpften (Epithelzellen, Bindegewebszellen), sind spätere Nebenwirkungen einer Behandlung unter anderem Knochenmarksdepression, Schleimhautatrophie, Haarausfall, oder Reproduktionsprobleme (Ovulation, Spermatogenese) bedingt durch die Proliferationshemmung der Zellen (Carelle et al., 2002; Coates et al., 1983).
Außerdem bringen viele Zytostatika eine Organtoxizität mit sich. Am häufigsten betroffen sind die Nieren, aber auch Blase, Herz, Lunge, Haut, Leber und Nervensystem können durch bestimmte Wirkstoffe geschädigt werden (Malyszko et al., 2017; Siddik, 1986).
Da DAO in Reinsubstanz bisher weder an Menschen noch Tieren *in vivo* getestet wurde, kann hier nur spekuliert werden, in welchem Rahmen die Nebenwirkungen ausfallen würden. Fest steht, dass hinsichtlich der Destabilisierung der Zellmembranintegrität ein Einsatz zu therapeutischen Zwecken nicht möglich wäre, da die zu erwartenden Effekte nicht speziell auf Tumorzellen einzugrenzen wären. DAO wäre zu toxisch. Zellschädigungen wären in jedem Organ möglich, in welches der Wirkstoff gelangen kann. Reduziert auf die Interaktion des Michael-Akzeptors mit Cysteinen der 5-LO ist das Nebenwirkungspotenzial ebenfalls sehr groß, weshalb es auch dafür keine Studiendaten gibt (Hofmann et al., 2012; Maucher et al., 2017). In Zahlen ausgedrückt zeigte DAO bzw. Arnamial IC_{50}-Werte von 8,0 µM/15,4 µM gegen MCF7- und 16,9 µM/3,96 µM gegen Jurkat- Zelllinien (Bohnert et al., 2011). Zum Vergleich: bei Paclitaxel ist eine IC_{50} von ca. 0,7 µM gegen Jurkat Zellen bekannt (Myrick et al., 1999), was dem 24- bzw. 5,6-fachen von DAO und Arnamial entspricht. Die gebräuchliche Konzentration von Vinblastin in der Tumortherapie liegt bei ca. 0,12 µM (Ammon, 2014), die

IC_{50} folglich darunter.
Li et al. testeten 2016 verschiedene Melleolide gegen HepG2-Zellen. Alle Melleolide mit einem Aldehyd an C1 und einer β-Doppelbindung zeigten gleichermaßen Aktivität gegen Krebszellen und normale L02-Leberzellen (Li et al., 2016). Dies ist ebenfalls ein Argument gegen den Einsatz von Melleoliden als Zytostatikum.

Resistenzmechanismen: Zahlreiche Reviews geben einen guten Überblick über die Resistenzmechanismen von Zytostatika auf zellulärer Ebene (Dietel, 1991, 2007; Giaccone und Pinedo, 1996; Mansoori et al., 2017; Pan et al., 2016; Vendrik et al., 1992). Eine Resistenz kann sich basierend auf der Zellkinetik ergeben. Bei soliden, nicht aktiv proliferierenden Tumoren haben die meisten Zellen eine schlechte Ansprechrate auf zellzyklusspezifische Chemotherapeutika (Chauffert et al., 1998). Pharmakokinetische Hindernisse stellen Körperbarrieren wie die Blut-Hirn-Schranke dar, welche von Arzneimitteln nicht passiert werden können (Wilhelm et al., 2013). Auch Änderungen im Metabolismus von Wirkstoffen beispielsweise bei der Aktivierung von Prodrugs können Ursache einer plötzlichen Resistenz sein (Dumontet et al., 1999). Tumore können über den Verlust des Wirkziels oder die Überexpression anti-apoptotischer Proteine (p53, p21, bcl- 2) resistent werden (Torgovnick et al., 2018). Über den Verlust eines Carriers und eine dadurch bedingte verringerte Aufnahme eines Pharmakophors wie beispielsweise bei Methotrexat (Mosow, 1998) kann ebenso eine Resistenz erzeugt werden, wie durch einen verstärkten Efflux, beispielsweise von Vinca-Alkaloiden durch p-Glycoprotein (Sharom, 2007). Eine verstärkte Reparatur zytostatikabedingter DNA-Schäden und die Amplifikation von Zielgenen stellen weitere Resistenzmöglichkeiten dar (Mansoori et al., 2017).

Wie bei Chidley *et al*. beschrieben, führt bei Ophiobolin A die Abwesenheit von PE zu einer Resistenz der Zellen (Chidley et al., 2016). Wenn DAO dasselbe Wirkziel ansteuert, ist diese Resistenzentwicklung auch hier relevant. Aufgrund der hohen Reaktivität des Michael-Systems (Liebler, 2008; Wondrousch et al., 2010) sind aber auch weitere noch unbekannte Wirkungen zu erwarten, wogegen eine Resistenzausbildung schlecht vorherzugsagen ist. Ungeklärt ist, ob bezüglich der inhibierenden Wirkung auf 5-LO die vermehrte Freisetzung von Glutathion zu einer Inaktivierung des Michael-Systems führen könnte (Schwöbel et al., 2010). Des Weiteren ist noch unbekannt, welche weiteren Effekte der Auslösung einer Apoptose-reaktion in humanen Zellen zugrunde liegen, sodass weitere Resistenzentwicklungen aktuell nicht beurteilt werden können.

5.2.2. Melleolide im Vergleich zu anderen Antimykotika

Wie eingangs vermutet produzieren *Armillaria spp.* eine Vielzahl strukturell sehr ähnlicher Melleolide zum Zwecke der Verteidigung gegen, oder zur chemischen Kommunikation mit anderen bodenbesiedelnden Konkurrenten um Lebensraum und Nährstoffe.
Die Suche nach antifungalen Wirkstoffen ist auch heute noch von großer Bedeutung. Aufgrund der aktuellen Resistenzlage vieler pflanzen- und humanpathogener Pilze gegen Antimykotika, werden neue Leitstrukturen dringend benötigt (Gauwerky et al., 2009). Die potentesten Pathogene sind Vertreter der Arten *Cryptococcus, Candida* und *Aspergillus.* Diese stellen vor allem für immunsupprimierte Patienten eine lebensbedrohliche Gefahr dar (Brown et al., 2012).

Wirkmechanismen: Heute steht nur eine überschaubare Menge an Wirkstoffklassen zur Behandlung von Pilzinfektionen zur Verfügung. Deren Wirkmechanismen wurden eingangs bereits erläutert.
Mit DAO als Stellvertreter für $\Delta^{2,4}$-ungesättigte Melleolide mit einem Aldehyd an C1 wurde eine neue Leitstruktur eines antifungalen Stoffes identifiziert. Auch das molekulare Wirkziel dieser Strukturen stellt im Vergleich zu heute pharmazeutisch genutzten Wirkstoffen eine Neuheit dar. Wie eingangs erwähnt, wurde der eukaryotische Elongationsfaktor 2 (eEF2) als pilzliches Wirkziel von Sordarin bereits entdeckt. Allerding ergab sich u. a. aufgrund der kurzen Plasmahalbwertszeit bis heute keine Anwendung als Arzneimittel (Odds, 2001). Auch nachfolgende Untersuchungen zu potenteren Derivaten blieben erfolglos (Søe et al., 2007). Der Vergleich des EF2 aus *A. nidulans* zeigt zum humanen eEF2 in der Aminosäuresequenz eine Übereinstimmung von 67 %, unter Berücksichtigung ähnlich polarer Aminosäuren sogar 81 %. Diese Unterschiede könnten für eine pharmazeutische Anwendung antimykotischer Substanzen von Bedeutung sein und zukünftig bei DAO zum Tragen kommen.
Im Unterschied zu Sordarin scheint DAO den *in silico*-Vorhersagen zufolge eine völlig andere Bindestelle am eEF2 zu bevorzugen. In die modellierte Sordarin-Bindetasche von *A. nidulans* konnte Sordarin gut eingefügt werden, für DAO ergaben sich hier aber keine relevanten Bindungsmöglichkeiten. Eine entsprechende Konformationsänderung des eEF2, wie sie durch Sordarin hervorgerufen wird (Jørgensen et al., 2003), konnte durch DAO nicht dargestellt werden. Bisher ungeklärt ist der molekulare Mechanismus, über welche Wechselwirkung(en) $\Delta^{2,4}$-ungesättigte Melleolide an eEF2 binden. Für eine irreversible Bindung mit dem Wirkziel fehlt es an zugänglichen reaktiven Strukturen wie Schwefelatomen aus Cystein-Resten, so wie für 5-LO gezeigt. Interessant ist auch, dass die Bindung von DAO im eEF2 von *A. nidulans* zu einem größeren Teil auf der Interaktion des Orsellinsäureteils mit den zwei Aminosäuren Prolin P262 und Thyrosin Y249 beruht. Das für die Wirksamkeit wichtigere Pharmakophor, interagiert mit der Glutaminsäure E171. Wie bereits in einer Vorarbeit festgestellt, wird die molekulare

Struktur des Melleolids durch die Lage der Doppelbindung beeinflusst (Bohnert et al., 2014a). Eine $\Delta^{2,4}$-Doppelbindung scheint also den aromatischen Anteil in die Bindetasche zu dirigieren.

Nebenwirkungen: Aus der Tatsache, das sich humane und pilzliche Zellen als heterotrophe Organismen in Katabolismus und Anabolismus stark ähneln, resultieren eine Vielzahl an Nebenwirkungen (Musiol und Kowalczyk, 2012). Seit der Entdeckung der Azole 1944 wird die Wirkstoffklasse fortwährend entwickelt, um sowohl Resistenzen zu umgehen, als auch das Nebenwirkungsprofil zu verbessern (Allen et al., 2015) – zumindest hinsichtlich der Resistenzaussichten ohne große Erfolge.
Die strukturelle Ähnlichkeit pilzlichen Ergosterols und humanen Cholesterols sorgt auch für Probleme. Die Hemmung der pilzlichen Monooxygenasen geht mit einer Inhibition humaner CYP-Enzyme einher, welche vor allem bei Co-Medikationen zu starken Muskel- und Nierenschäden führt (Dybro et al., 2016). Polyene verursachen aufgrund einer nicht ausreichenden Selektivität Nebenwirkungen wie Blutbild-, Nieren- oder Leberschäden und gefährliche Wechselwirkungen mit anderen Arzneimitteln. (Kotler-Brajtburg et al., 1974; Laniado-Laborin und Cabrales-Vargas, 2009)
Viele der Nebenwirkungen lassen sich durch eine gezielte Weiterentwicklung der Wirkstoffe, z. B. hin zu selektiveren Molekülen umgehen (Mast et al., 2013). Auch durch die geeignete Auswahl der Formulierung des Arzneimittels lässt sich die Toxizität verringern (Aversa et al., 2017).

Bisher gab es mit Melleoliden noch keine *in vivo*-Tests an Lebewesen. Somit können mögliche Nebenwirkungen noch nicht vorausgesagt werden. Da sich die Anwendung von *A. mellea* in der TCM auf die Fruchtkörper beschränkt, sind auch hier keine verwertbaren Aussagen zu treffen. Es existieren lediglich Einzelfallberichte über Unverträglichkeiten zu den als Speisepilz verwendeten Fruchtkörpern. Ob diese Reaktionen auf Melleolide zurückgeführt werden können, ist fraglich, da der Pilz nicht grundsätzlich als giftig beschrieben wird (An et al., 2017). Prinzipiell ist eine schädigende Wechselwirkung von $\Delta^{2,4}$-ungesättigten Melleoliden mit Cystein-haltigen Proteinen aber denkbar, da der vorhandene Michael-Akzeptor sehr reaktiv gegen proteingebundene Schwefelatome wie in Cystein-Proteasen wirkt (Kitahata et al., 2017; König et al., 2018; Maucher et al., 2017).

Bei den meisten getesteten Hefen zeigten sich gegen Arnamial *in vivo* MICs im Bereich von 40-200 µg/ml. Für Azole wie Itraconazol, Polyene wie Amphotericin B oder Echinocandine wie Caspofungin sind deutlich geringere Literaturwerte von 0,03-8 µg/ml, 0.125-4 µg/ml oder 0,03-2 µg/ml zu finden (Cordeiro et al., 2013). Melleolide müssten für einen therapeutischen Effekt im Vergleich zu klassischen Antimykotika in viel höheren Mengen eingesetzt werden. Hierbei spielen jedoch auch die Aufnahme und Verteilung im Körper eine Rolle. Eine bessere Aufnahme und Verteilung als bei herkömmlichen Wirkstoffen wären vorteilhaft für

therapeutische Zwecke. Im wirksamen Bereich sind aber schon zytotoxische Effekte zu erwarten (Bohnert et al., 2011; Bohnert et al., 2014b).

Resistenzmechanismen: Die wenigen Angriffspunkte der Antimykotika ermöglichen es den Organismen in kürzester Zeit, Resistenzmechanismen auszubilden (Cowen, 2008). Ein möglicher Mechanismus ist hierbei die vermehrte Produktion des zellulären Wirkziels. *C. albicans* kann beispielsweise bei Azol-Exposition das Gen ERG11 überexprimieren, welches für die Bildung des Enzyms CYP51A verantwortlich ist (Perea et al., 2001). Auch Mutationen an ERG11 sind bekannt, welche zu einer Unempfindlichkeit gegenüber Fluconazol führen (Feng et al., 2010).
Bekannt ist aber auch die Modifikation der Aufnahme pilzlicher Toxine. ATP-abhängige ABC-Transportproteine kommen vielfach in *Candida spp*. oder *Aspergillus spp*. vor (Cowen et al., 2015) und sind häufig für eine Azolresistenz durch einen effektiven Efflux und daraus resultierende verringerte Toxin-Anreicherung verantwortlich (Coste et al., 2009). Durch eine Mutation im Fcy1 Gen zur Expression der Cytosin-Deaminase sorgt *C. glabrata* dafür, dass Prodrugs wie Flucytosin nicht in ihre aktive, wirksame Form umgewandelt werden (Edlind und Katiyar, 2010). Über die genannten Wege wird jeweils die effektive Wirkstoffkonzentration verringert (Sanglard, 2016). Im Falle der Zellwandbiosynthese ist auch eine Abweichung der Ergosterolproduktion über andere Biosyntheseenzyme, einem sogenannten metabolischen Bypass denkbar (Cowen et al., 2015; Sanglard, 2003, 2016; Sanglard et al., 1998).

Eine erworbene Resistenz konnte aufgrund der beschränkten Anwendungsmöglichkeiten für Melleolide noch nicht beobachtet werden. Jedoch stellt sich die Frage, warum *Armillaria* Organismen aus seinen Habitaten verdrängt, während z. B. Ascomyceten wie *Trichoderma* keine Reaktion auf $\Delta^{2,4}$-ungesättigte Melleolide zeigen. Der EF2 von *T. harzianum* zeigt im Vergleich zu *A. nidulans* eine genetische Übereinstimmung von 80 %. An der im Model vorhergesagten Stelle im Protein (Vgl. Publikation 1), besitzt *T. harzianum* wie die resistenten Hefen *C. glabrata* und *S. cerevisiae* ein Serin anstelle eines Threonins (^{170}S statt ^{170}T) bzw. Glutaminsäure (^{170}E) bei *A. nidulans*. Diese Abweichungen sind aber keiner spontan erworbenen Resistenz zuzuordnen, da der Prozess der Proteintranslation zu stark konserviert ist, also über evolutionär gesehen große Zeitspannen nicht oder nur minimal verändert worden (Justice et al., 1998).
Da beobachtet wurde, dass sich *A. nidulans* nach Toxin-Exposition wieder erholt, ist eine Überexpression von eEF2 vorstellbar. In einem Experiment sollte die Menge an Arnamial nach Exposition mit *A. nidulans* ermittelt werden. Es zeigte sich, dass innerhalb weniger Stunden kein Arnamial mehr vorhanden war (Daten nicht gezeigt). *A. nidulans* scheint also auch Mechanismen zur Detoxifizierung der Melleolide zu besitzen.

5.3. Zukünftige Anwendungen von Melleoliden

Melleolide als potenzielle Arzneimittel: Mit der Entdeckung konkreter Wirkziele der Melleolide und der damit verbundenen antifungalen und cytotoxischen Wirkung, wird die Verwendung dieser Naturstoffe als Arzneimittel zunehmend interessanter. Basierend auf der aktuellen Resistenzlage humanpathogener Pilze und der wachsenden Anzahl an Krebs erkrankender Menschen sind neue Arzneimittel auf diesen Gebieten sehr gefragt und notwendig (Cowen et al., 2015; Xu et al., 2019).

Die Nutzung von Melleoliden mit $\Delta^{2,4}$-ungesättigten Aldehyden als Antimykotikum ist besonders interessant, da die Blockade des Wirkziels eEF2 einen völlig neuen Ansatz in der antifungalen Therapie darstellt, welcher bisher von keiner auf dem Markt befindlichen Substanz adressiert wird (Dörfer et al., 2019). In der Behandlung entzündlicher Erkrankungen liefern Melleolide durch die Hemmung der 5-LO neben Zileuton eine neue Substanzgruppe mit einem neuen inhibitorischen Mechanismus an der 5-LO (Rossi et al., 2010). Da Entzündungen letztlich auch Verursacher maligner Tumore sein können, bieten die genannten Melleolide mit ihrer zytotoxischen Wirkung durch die Bindung an PE und die damit verbundene Reduktion der Zellmembranintegrität (siehe 4.1.) gleich zwei therapierelevante Wirkmechanismen im menschlichen Organismus.

Doch reicht es nicht, ein neues Wirkziel zu entdecken, um gleich ein Arzneimittel geschaffen zu haben. Arzneimittel müssen wichtige Anforderungen erfüllen, um überhaupt einen pharmazeutischen Nutzen erbringen zu können:
Die verwendete Substanz muss (im Körper) den Ort erreichen, an dem sie wirken soll. Zur Verteilung der Melleolide *in vivo* gibt es bisher keine Studien. Experimente an Mäusen wurden nur mit Rohextrakten durchgeführt (Zhang et al., 2019). Eine Verteilung von DAO oder Arnamial wurde bisher nicht ermittelt. Auch Metabolismus und Biotransformation spielen bei der Distribution eine wichtige Rolle. Der Wirkstoff darf vor Erreichen des Zielortes nicht ab-, umgebaut oder ausgeschieden werden. Im konkreten Fall bietet vor allem der ungesättigte Aldehyd im Molekül in C1 Position im Protoilluden-Teil des Moleküls eine gute Angriffsstelle für reduktive Angriffe. Die vorhandenen Hydroxylgruppen können für Wasseranlagerungen oder Wasserstoffbrückenbindungen zur Verfügung stehen und somit die Molekülbewegung *in vivo* beeinflussen.

Dem Erreichen des zellulären Wirkziels stehen zahlreiche Barrieren wie die Zellmembranen oder die pilzliche Zellwand entgegen. Aktuell existieren keine Kenntnisse über die Verteilung von Melleoliden in pilzlichen Zellen zur Inhibition des EF2 oder der Verteilung in humanen Zellen für antiinflammatorische oder antitumorale Wirkungen.

Ist eine Wirkung eingetreten, muss der Wirkstoff nach einer gewissen Zeit auch wieder abgebaut werden können. Ein Um- oder Abbau ist jetzt also erwünscht. Meist ist eine biotransformatorische Umwandlung vor allem von lipophilen Arzneistoffen die Voraussetzung für eine renale oder biliäre Ausscheidung. Gelingt dies nicht, kommt es zu einer Anreicherung der Arzneimoleküle hauptsächlich in Fettgeweben, was zu einer Anreicherung und Vergiftung führen kann (Mutschler, 2013). Auch irreversible Molekülinteraktionen zwischen Pharmakophor und Wirkziel können zu bleibenden Schäden für den Organismus führen.

Über diese Prozesse gibt es am Beispiel der Melleolide ebenso wenig Daten, wie über die Verträglichkeit. Ein Arzneimittel sollte nur wenige und ungefährliche Nebenwirkungen verursachen. Wechselwirkungen mit Nahrungsmitteln oder anderen Medikamenten sind unerwünscht. Wie bereits erwähnt ist bei den $\Delta^{2,4}$-ungesättigten Aldehyden von einer erhöhten Reaktivität auszugehen. Sollten Substanzen wie DAO oder Arnamial überhaupt unverändert ein Wirkziel erreichen ist fraglich, ob nicht aufgrund des Michael-Systems zahlreiche unerwünschte Reaktionen mit umliegenden Proteinen und Zellorganellen stattfinden, welche Nebenwirkungen mit sich ziehen können. *In puncto* Sicherheit erfordert eine pharmazeutische Anwendung am Menschen also weitere intensive Forschung.
Final sei noch erwähnt, dass eine großtechnische Herstellung der Naturstoffe notwendig ist, um eine Arzneimittelproduktion realisieren zu können. Die Ausbeute der Melleolide müsste selektiv optimiert werden können, um eine Totalsynthese zu umgehen. Bisher war nur eine Steigerung der Melleolid-Gesamtmenge möglich. Eine Isolierung sauberer Derivate wird dadurch aber nicht erleichtert. Der Gencluster zur Melleolid-Biosynthese ist mittlerweile bekannt, aber noch nicht vollständig charakterisiert. Proteine wie die Protoilluden-Synthase Pro1 und die Orsellinsäure-Synthase ArmB können heterolog produziert werden (Engels et al., 2011; Lackner et al., 2013). Wichtige modifizierende Enzyme, wie Halogenasen, liegen jedoch außerhalb des Genclusters oder sind, wie einige Methyltransferasen, ebenfalls nicht charakterisiert (Wick et al., 2016). Erst eine vollständige Charakterisierung ermöglicht eine biotechnologische Produktion. Hier schließt sich die Frage nach einem geeigneten Wirt an. Den Ergebnissen zufolge wären Melleolid-resistente Aspergillen oder Hefen denkbar.

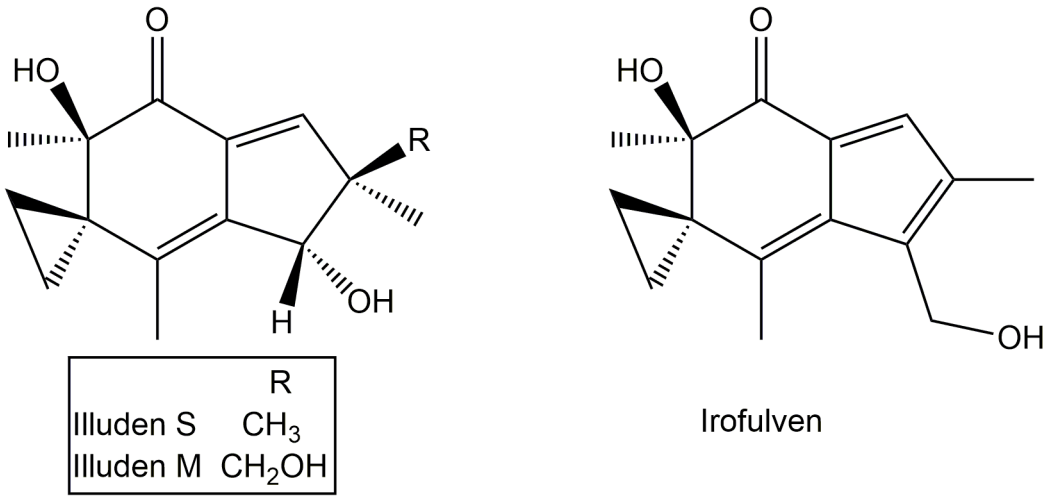

Abbildung 9. Weitere bioaktive Sesquiterpene aus Protoilluden. Links Illuden S und Illuden M aus Omphalotus olearius, rechts das daraus semisynthetisch erzeugte Irofulven.

Ein weiteres antibiotisch wirksames Sesquiterpen pilzlicher Herkunft hat es in der Entwicklung zum Arzneimittel in klinische Studien der Phase 2 geschafft. Ausgehend von den 1950 entdeckten Illudinen S und M aus *Omphalotus olearius* wurden weniger toxische Derivate entwickelt. Erfolgreich getestet werden konnte das Alkylans Irofulven. Die Substanz wurde an Patienten mit kleinzelligem Krebs (Dowell et al., 2001), Melanomen in Stadium IV (Pierson et al., 2002), Lungenkrebs (Sherman et al., 2004) sowie Prostata-, Brust-, Leberzell- oder Darmzellkarzinomen getestet (Baekelandt, 2002). Für einige wenige Krebs-Arten wie Ovarialkarzinome wurde Irofulven in Kombination mit anderen Zytostatika eine positive Wirkung zugeschrieben (Dings et al., 2008). Viele der vorausgenannten Karzinome sprachen gegen die Wirkung des Irofulvens nicht an. Ein therapeutischer Nutzen ergab sich deshalb und aufgrund der Toxizität der Substanz nicht. Es gibt jedoch Hoffnung auf die Entdeckung weiterer semisynthetischer Derivate mit einer höheren Tumorselektivität und geringerer Toxizität (Puyo et al., 2014).

Die Bestimmung einer neu entdeckten, bioaktiven Substanz muss jedoch nicht zwangsläufig in der Formulierung als Arzneimittel liegen. So könnten Melleolide zukünftig auch eine andere Anwendung finden.

Melleolide als molekulare Sonde zur Erforschung neuer SAR: Die Wirkung einiger Melleolide als Inhibitor von pilzlichem eEF2 oder von humanen 5-LO abhängigen Prozessen wurde in dieser Arbeit bereits ausführlich erläutert. So kann die Zukunft der Melleolide, vor allem aufgrund ihrer hohen Diversität und Selektivität auch in der Verwendung als molekulare Sonde zur Erforschung neuer SAR liegen. Ebenso könnten die durch Melleolide beeinflussten Prozesse aus anderen Blickwinkeln neu beobachtet und bewertet werden. Es ist anzunehmen, dass die Diversität der Melleolide mit der Verwendung als Sonde auch zur Entdeckung weiterer Wirkziele führt.

6. Ausblick

Um Melleolide in der Zukunft als Arzneimittel verwenden zu können, sind eine Vielzahl weiterer Untersuchungen, besonders hinsichtlich der Arzneimittelverteilung, der Rezeptoraffinität und des Nebenwirkungsprofils notwendig. Um einzelne Derivate zu sicheren Arzneimitteln zu machen, müssten sämtliche Wirkziele, auch die weniger selektiven, aufgeklärt und evaluiert werden. Dafür müssten die SAR noch weiter erforscht werden, z. B. durch die Synthese und Verwendung neuer Sonden. Kurz: es besteht Bedarf an selektiven und dennoch hoch aktiven Pharmakophoren. Vorstellbar wären hier vor allem antifungale Melleolide zur topischen Anwendung. So könnte man die Wirkung gegen Pilzzellen forcieren und umgeht einen Großteil der systemischen Nebenwirkungen an gesunden, humanen Zellen.

Eine weitere vorstellbare Verwendung von $\Delta^{2,4}$-ungesättigten Melleoliden liegt in der Forschung. Da EF2 als Wirkziel identifiziert wurde, ist nun ein wirkzielorientiertes Screening nach effektiveren Hemmstoffen der ribosomalen Translation möglich. So könnten stärker antifungale, aber gleichzeitig weniger cytotoxische Substanzen mit demselben Wirkziel gefunden werden.

Die Bedeutung der Melleolide für Pilze der Gattung *Armillaria* ist bisher völlig ungeklärt. Mit heutigen Mitteln können Effekte auf Zellen *in vivo/in vitro* nur nachgewiesen werden, wenn man messbare Mengen an Wirkstoffen im Experiment verwendet. Für die größten Organismen der Welt könnten Melleolide jedoch schon in Kleinstmengen eine ökologische Bedeutung haben. Die stark diversitätsorientierte Biosynthese der Sekundärstoffe könnte Quorum-Sensing-Funktionen erfüllen oder je nach Zusammensetzung des resultierenden Melleolid-Cocktails spezifische Reaktionen in anderen Organismen hervorrufen. Die chemische Kommunikation mit oder Inhibition von umgebenden Lebewesen bzw. Nahrungsmittelkonkurrenten in den Habitaten der *Armillarien* wird zukünftig Forschungsthema bleiben.

7. Zusammenfassung

Melleolide, Sekundärstoffe aus Vertretern der Basidiomyceten-Gattung *Armillaria,* besitzen eine hohe Bioaktivität. Die zugrundeliegenden Mechanismen der phytotoxischen, antifungalen, antibakteriellen und cytotoxischen Aktivität wurden bisher nie untersucht. Diese Arbeit setzt sich deshalb mit Struktur-Aktivitäts-Beziehungen und Wirkmechanismen ausgewählter Melleolid-Antibiotika auseinander.

Das Wirkziel für eine antifungale Wirkung wurde mittels einer chemisch synthetisierten Sonde basierend auf Dehydroarmillylorsellinat (DAO) im Modellorganismus *A. nidulans* identifiziert. Proteine, die an das Biotin-gekoppelte Melleolid banden, konnten an einer Streptavidin-Matrix affinitätschromatographisch aufgereinigt werden. Über MALDI-Massenspektrometrie und Western-Blotting wurde der pilzliche, eukaryotische Elongationsfaktor 2 (EF2) als Wirkziel von DAO für eine antifungale Wirkung gefunden und über Inhibitionsexperimente mit verschiedenen Hefen mit dem bereits bekannten EF2-Inhibitor Sordarin als Referenzsubstanz bestätigt. Der Wirkmechanismus von DAO konnte auf weitere Melleolide mit $\Delta^{2,4}$-ungesättigtem Aldehyd in Position C1 übertragen werden. Die Annahme unterschiedlicher Bindungsstellen im pilzlichen EF2-Protein konnte *in silico* an einem Modellprotein des EF2 von *A. nidulans* nachgestellt, und so eine putative DAO-Bindestelle identifiziert werden.
DAO interagiert in humanen Zellen mit 5-Lipoxygenase, einem Enzym der Entzündungskaskade. Durch eine Michael Addition basierend auf dem $\Delta^{2,4}$-ungesättigten Aldehyd bindet DAO selektiv und irreversibel an das Cystein 159 (C^{159}) am Eingang des katalytischen Zentrums der 5-LO, wodurch die Interaktion von 5-LO mit dem Helferprotein FLAP unterbunden und final die Leukotrien-Biosynthese reduziert wird.
Die beobachtete rasche Zytotoxizität humaner Krebszellen und Monozyten beruht auf einem weiteren Mechanismus. Die kovalente Bindung von DAO an die Kopfgruppe von Phosphatidyl-ethanolamin (PE) verursacht einen induzierten Zelltod. Es wurde herausgefunden, dass DAO bevorzugt mit dem PE aus Plasmamembran/Lysosomen-Fraktionen interagiert, was über die Verringerung des PE-Gehaltes zur Reduktion der Zellmembranpermeabilität und letztlich zu nekrotischen und apoptotischen Effekten führte.

In dieser Arbeit konnten also drei völlig unterschiedliche Wirkmechanismen von DAO bzw. $\Delta^{2,4}$-ungesättigten Melleoliden identifiziert werden, welche erste Erkenntnisse zum pharmazeutischen Einsatz der Melleolide liefern.

8. Summary

The basidiomycete genus *Armillaria* is known to produce highly bioactive secondary metabolites, known as melleolides. Studies showed phytotoxic, antifungal, antibacterial and cytotoxic activity but no pharmacological reasons for these effects. This work reveals structure-activity-relationships and the mode of action of selected melleolides.

The target for the antifungal effect in the model organism *A. nidulans* was found using a dehydroarmillylorsellinate (DAO)-based chemically synthesized molecular probe. Proteins binding to the biotin-coupled DAO were enriched by affinity chromatography using a streptavidin matrix. The fungal eukaryotic elongation factor 2 (EF2) was detected as a target by MALDI and Western Blotting. This finding was confirmed in growth experiments on different yeast strain in comparison with the previously known EF2-inhibitor sordarin. This mode of action was confirmed for other melleolides possessing an $\Delta^{2,4}$-unsaturated aldehyde in C1 position, like arnamial. In our experiments, DAO and sordarin showed different effects on the yeast strains used. By *in silico* protein modeling based on an *A. nidulans* EF2 protein model two differing binding pockets for these substances were found.

The cytotoxic effect of DAO in human cell lines could not be explained by EF2-inhibition. Instead we could identify 5-lipoxygenase (5-LO), as a target. The $\Delta^{2,4}$-unsaturated aldehyde selectively and irreversibly bound to the enzyme's cystein 159 (C^{159}) located at the entrance of 5-LO catalytic center, performing a Michael-addition. The interaction of DAO with C^{159} prevents 5-LO to bind FLAP, resulting in a reduced leukotriene biosynthesis.

This anti-inflammatory interaction is no declaration for the quick cell death we observed in former experiments on human cancer cell lines and monocytes. The induced cell death is the reason of DAO covalently binding to the head groups of phosphatidylethanolamines (PE). We found that DAO preferably binds PE from fractions of the plasma membrane and lysosomes leading to a diminished PE content. The DAO-PE interaction finally led to a reduction of the cell permeability resulting in necrotic and apoptotic effects in the cell.

In this work, three completely different mechanisms of action of DAO and related $\Delta^{2,4}$-unsaturated melleolides were identified, providing first important hints for possible future pharmaceutical applications of the melleolides.

9. Literaturverzeichnis

Abraham, W.R. (2001). Bioactive sesquiterpenes produced by fungi: are they useful for humans as well? *Curr Med Chem* **6** (*8)*, 583-606.

Al-Warhi, T.I., Al-Hazimi, H.M.A., and El-Faham, A. (2012). Recent development in peptide coupling reagents. *Journal of Saudi Chemical Society* **2** (*16)*, 97-116.

Alam, P., and Sharaf-Eldin, M.A. (2016). Limited production of plant derived anticancer drugs vinblastine and vincristine. *Planta Medica* **05** (*82)*, PC4.

Alberts, A.W., Chen, J., Kuron, G., Hunt, V., Huff, J., Hoffman, C., Rothrock, J., Lopez, M., Joshua, H., Harris, E.*, et al.* (1980). Mevinolin: a highly potent competitive inhibitor of hydroxymethylglutaryl-coenzyme A reductase and a cholesterol-lowering agent. *Proceedings of the National Academy of Sciences of the United States of America* **7** (*77)*, 3957-3961.

Allen, D., Wilson, D., Drew, R., and Perfect, J. (2015). Azole antifungals: 35 years of invasive fungal infection management. *Expert Review of Anti-infective Therapy* **6** (*13)*, 787-798.

Ammon, H.P.T. (2014). Hunnius Pharmazeutisches Wörterbuch, Vol 9 (Berlin: De Gruyter).

An, S., Lu, W., Zhang, Y., Yuan, Q., and Wang, D. (2017). Pharmacological basis for use of Armillaria mellea polysaccharides in Alzheimer's disease: antiapoptosis and antioxidation. *Oxid Med Cell Longevity*4184562/4184561-4184562/4184511.

Anderson, J.B., Bruhn, J.N., Kasimer, D., Wang, H., Rodrigue, N., and Smith, M.L. (2018). Clonal evolution and genome stability in a 2,500-year-old fungal individual. *Proceedings of the Royal Society B: Biological Sciences* **1893** (*285)*, 20182233.

André, E., Malheiros, Â., Cechinel-Filho, V., Yunes, R.A., and Calixto, J.B. (1999). Mechanisms underlying the relaxation caused by the sesquiterpene polygodial in vessels from rabbit and guinea-pig. *European Journal of Pharmacology* **1** (*386)*, 47-53.

Androulla, N.M., and Lefkothea, C.P. (2018). CAR T-cell therapy: A new era in cancer immunotherapy. *Current Pharmaceutical Biotechnology* **1** (*19)*, 5-18.

Anke, H., and Sterner, O. (1991). Comparison of the antimicrobial and cytotoxic activities of twenty unsaturated sesquiterpene dialdehydes from plants and mushrooms. *Planta Med* **04** (*57)*, 344-346.

Arnone, A., Cardillo, R., Di Modugno, V., and Nasini, G. (1989). Secondary mould metabolites. Part 29. Isolation and structure elucidation of candicansol, 3-epi-illudol and 1-O-acetyl-3-epi-illudol, novel sesquiterpenoids from *Clitocybe candicans*, and absolute configuration of 3-epi-illudol. *Journal of the Chemical Society, Perkin Transactions 1*(*11)*, 1995-2000.

Arnone, A., Nasini, G., Di Modugno, V., and Cardillo, R. (1988). Isolation and structure elucidation of melledonals D and E and Melleolides E-H, Novel Sesquiterpenoid Aryl Esters from clitocybe elegans and armillaria mellea. *Gazzetta chimica Italiana* **118** (*7)*, 517-521.

Aversa, F., Busca, A., Candoni, A., Cesaro, S., Girmenia, C., Luppi, M., Nosari, A.M., Pagano, L., Romani, L., Rossi, G.*, et al.* (2017). Liposomal amphotericin B (AmBisome®) at beginning of its third decade of clinical use. *Journal of Chemotherapy* **3** (*29)*, 131-143.

Baekelandt, M. (2002). Irofulven (MGI Pharma). *Current opinion in investigational drugs (London, England : 2000)* **10** (*3)*, 1517-1526.

Balandrin, M., Klocke, J., Wurtele, E., and Bollinger, W. (1985). Natural plant chemicals: sources of industrial and medicinal materials. *Science* **4704** (*228)*, 1154-1160.

Banday, A.H., Shameem, S.A., Gupta, B.D., and Kumar, H.M.S. (2010). D-ring substituted 1,2,3-triazolyl 20-keto pregnenanes as potential anticancer agents: Synthesis and biological evaluation. *Steroids* **12** (*75)*, 801-804.

Bartsch, V. (2004). Das Taxol Buch, 2. erweiterte Auflage edn (Stuttgart: Georg Thieme Verlag).

Baumgartner, K., Coetzee, M.P.A., and Hoffmeister, D. (2011). Secrets of the subterranean pathosystem of *Armillaria*. *Molecular Plant Pathology* **6** (*12)*, 515-534.

Boddy, L., Hynes, J., Bebber, D.P., and Fricker, M.D. (2009). Saprotrophic cord systems: dispersal mechanisms in space and time. *Mycoscience* **1** (*50)*, 9.

Bogyo, M., Baruch, A., Jeffery, D.A., Greenbaum, D., Borodovsky, A., Ovaa, H., and Kessler, B. (2004). Applications for chemical probes of proteolytic activity. *Current Protocols in Protein Science* **21** (*21)*, 17.

Bohnert, M., Miethbauer, S., Dahse, H.M., Ziemen, J., Nett, M., and Hoffmeister, D. (2011). In vitro cytotoxicity of melleolide antibiotics: structural and mechanistic aspects. *Bioorg Med Chem Lett* **7** (*21)*, 2003-2006.

Bohnert, M., Nützmann, H.-W., Schroeckh, V., Horn, F., Dahse, H.-M., Brakhage, A.A., and Hoffmeister, D. (2014a). Cytotoxic and antifungal activities of melleolide antibiotics follow dissimilar structure–activity relationships. *Phytochemistry* **1** (*105)*, 101-108.

Bohnert, M., Scherer, O., Wiechmann, K., König, S., Dahse, H.M., Hoffmeister, D., and Werz, O. (2014b). Melleolides induce rapid cell death in human primary monocytes and cancer cells. *Bioorg Med Chem* **15** (*22)*, 3856-3861.

Böttcher, T., Pitscheider, M., and Sieber, S.A. (2010). Naturstoffe und ihre biologischen Angriffsziele: proteomische und metabolomische Markierungsstrategien. *Angewandte Chemie* **15** (*122)*, 2740-2759.

Brown, G.D., Denning, D.W., Gow, N.A.R., Levitz, S.M., Netea, M.G., and White, T.C. (2012). Hidden killers: Human fungal infections. *Science Translational Medicine* **165** (*4)*, 165-177.

Cabral, M.E., Delgado, O.D., Sampietro, D.A., C.A., C., Figueroa, L.I.C., and Farina, J.I. (2010). Antifungal Activity and the Potential Correlation with Statin-Producing Ability: An Optimized Screening Applied to Filamentous Fungi from Las Yungas Subtropical Rainforest. *Research Journal of Microbiology* **9** (*5)*, 833-848.

Cacho, R.A., Jiang, W., Chooi, Y.-H., Walsh, C.T., and Tang, Y. (2012). Identification and Characterization of the Echinocandin B Biosynthetic Gene Cluster from *Emericella rugulosa NRRL 11440*. *Journal of the American Chemical Society* **40** (*134)*, 16781-16790.

Caputi, L., Franke, J., Farrow, S.C., Chung, K., Payne, R.M.E., Nguyen, T.-D., Dang, T.-T.T., Soares Teto Carqueijeiro, I., Koudounas, K., Dugé de Bernonville, T.*, et al.* (2018). Missing enzymes in the biosynthesis of the anticancer drug vinblastine in Madagascar periwinkle. *Science* **6394** (*360)*, 1235-1239.

Carelle, N., Piotto, E., Bellanger, A., Germanaud, J., Thuillier, A., and Khayat, D. (2002). Changing patient perceptions of the side effects of cancer chemotherapy. *Cancer* **1** (*95)*, 155-163.

Chang, W.-H., Huang, H.-L., Huang, W.-P., Chen, C.-C., and Chen, Y.-J. (2016). Armillaridin induces autophagy-associated cell death in human chronic myelogenous leukemia K562 cells. *Tumor Biology* **10** (*37)*, 14291-14300.

Chauffert, B., Dimanche-Boitrel, M.T., Garrido, C., Ivarsson, M., Martin, M., Martin, F., and Solary, E. (1998). New insights into the kinetic resistance to anticancer agents. *Cytotechnology* **1-3** (*27)*, 225-235.

Chen, C.-C., Cheng, J.J., and Shen, C.-C. (2011). Protoilludane norsesquiterpenoid esters and uses thereof. USA, US 2011/0262561 A1

Chen, C.-C., Kuo, Y.-H., Cheng, J.-J., Sung, P.-J., Ni, C.-L., Chen, C.-C., and Shen, C.-C. (2015). Three new sesquiterpene aryl esters from the mycelium of *Armillaria mellea*. *Molecules* **6** (*20)*, 9994-10003.

Chen, Y.-J., Chen, C.-C., and Huang, H.-L. (2016). Induction of apoptosis by *Armillaria mellea* constituent armillarikin in human hepatocellular carcinoma. *OncoTargets and therapy* **1** (*9)*, 4773-4783.

Chidley, C., Trauger, S.A., Birsoy, K., and O'Shea, E.K. (2016). The anticancer natural product ophiobolin A induces cytotoxicity by covalent modification of phosphatidylethanolamine. *eLife* **1** (*5)*, 14601.

Christianson, D.W. (2017). Structural and chemical biology of terpenoid cyclases. *Chemical Reviews* **17** (*117)*, 11570-11648.

Clive, D.L.J., Murthy, K.S.K., Wee, A.G.H., Prasad, J.S., Da Silva, G.V.J., Majewski, M., Anderson, P.C., Evans, C.F., and Haugen, R.D. (1990). Total synthesis of both (+)-compactin and (+)-mevinolin. A general strategy based on the use of a special titanium reagent for dicarbonyl coupling. *Journal of the American Chemical Society* **8** (*112)*, 3018-3028.

Coates, A., Abraham, S., Kaye, S.B., Sowerbutts, T., Frewin, C., Fox, R.M., and Tattersall, M.H.N. (1983). On the receiving end—patient perception of the side-effects of cancer chemotherapy. *European Journal of Cancer and Clinical Oncology* **2** (*19)*, 203-208.

Coles, N.T., Mahon, M.F., and Webster, R.L. (2018). 1,1-Diphosphines and divinylphosphines via base catalyzed hydrophosphination. *Chemical Communications* **74** (*54)*, 10443-10446.

Collins, C., Hurley, R., Almutlaqah, N., O'Keeffe, G., Keane, M.T., Fitzpatrick, A.D., and Owens, A.R. (2017). Proteomic characterization of *Armillaria mellea* reveals oxidative stress response mechanisms and altered secondary metabolism profiles. *Microorganisms* **3** (*5)*, 60-75.

Cordeiro, R.A., Teixeira, C.E.C., Brilhante, R.S.N., Castelo-Branco, D.S.C.M., Paiva, M.A.N., Giffoni Leite, J.J., Lima, D.T., Monteiro, A.J., Sidrim, J.J.C., and Rocha, M.F.G. (2013). Minimum inhibitory concentrations of amphotericin B, azoles and caspofungin against *Candida* species are reduced by farnesol. *Medical Mycology* **1** (*51)*, 53-59.

Coste, A., Ferrari, S., and Sanglard, D. (2009). Antifungal drug resistance mechanisms in fungal pathogens from the perspective of transcriptional gene regulation. *Federation of European Microbiological Society - Yeast Research* **7** (*9)*, 1029-1050.

Cowen, L.E. (2008). The evolution of fungal drug resistance: modulating the trajectory from genotype to phenotype. *Nature Reviews Microbiology* **3** (*6)*, 187.

Cowen, L.E., Sanglard, D., Howard, S.J., Rogers, P.D., and Perlin, D.S. (2015). Mechanisms of antifungal drug resistance. *Cold Spring Harbor Perspectives in Medicine* **7** (*5)*, a019752.

Cox, R.J. (2007). Polyketides, proteins and genes in fungi: programmed nano-machines begin to reveal their secrets. *Organic and Biomolecular Chemistry* **13** (*5)*, 2010-2026.

Crawford, J.M., Korman, T.P., Labonte, J.W., Vagstad, A.L., Hill, E.A., Kamari-Bidkorpeh, O., Tsai, S.C., and Townsend, C.A. (2009). Structural basis for biosynthetic programming of fungal aromatic polyketide cyclization. *Nature* **7267** (*461)*, 1139-1143.

da Cunha, F.M., Fröde, T.S., Mendes, G.L., Malheiros, A., Filho, V.C., Yunes, R.A., and Calixto, J.B. (2001). Additional evidence for the anti-inflammatory and anti-allergic properties of the sesquiterpene polygodial. *Life Sciences* **2** (*70)*, 159-169.

Denis, J.N., Greene, A.E., Guenard, D., Gueritte-Voegelein, F., Mangatal, L., and Potier, P. (1988). Highly efficient, practical approach to natural taxol. *Journal of the American Chemical Society* **17** (*110)*, 5917-5919.

Denning, D.W. (1997). Echinocandins and pneumocandins-a new antifungal class with a novel mode of action. *Journal of Antimicrobial Chemotherapy* **5** (*40)*, 611-614.

Dietel, M. (1991). What's new in cytostatic drug resistance and pathology. *Pathology - Research and Practice* **7** (*187)*, 892-905.

Dietel, M. (2007). Predictive pathology of cytostatic drug resistance and new anti-cancer targets. *Recent Results in Cancer Research* **1** (*176)*, 25-32.

Dings, R.P.M., Van Laar, E.S., Webber, J., Zhang, Y., Griffin, R.J., Waters, S.J., MacDonald, J.R., and Mayo, K.H. (2008). Ovarian tumor growth regression using a combination of vascular targeting agents anginex or topomimetic 0118 and the chemotherapeutic irofulven. *Cancer letters* **2** (*265)*, 270-280.

Domínguez, J.M., Gómez-Lorenzo, M.G., and Martín, J.J. (1999). Sordarin inhibits fungal protein synthesis by blocking translocation differently to fusidic acid. *Journal of Biological Chemistry* **32** (*274)*, 22423-22427.

Domínguez, J.M., and Martín, J.J. (1998). Identification of elongation factor 2 as the essential protein targeted by sordarins in *Candida albicans*. *Antimicrobial agents and chemotherapy* **9** (*42)*, 2279-2283.

Dörfer, M., Heine, D., König, S., Gore, S., Werz, O., Hertweck, C., Gressler, M., and Hoffmeister, D. (2019). Melleolides impact fungal translation via elongation factor 2. *Organic & Biomolecular Chemistry* **19** (*17)*, 4906-4916.

Dowell, J.E., Johnson, D.H., Rogers, J.S., Shyr, Y., McCullough, N., Krozely, P., and DeVore, R.F. (2001). A Phase II trial of 6-Hydroxymethylacylfulvene (MGI-114, Irofulven) in Patients with Advanced Non-Small Cell Cancer Previously Treated with Chemotherapy. *Investigational New Drugs* **1** (*19)*, 85-88.

Dumontet, C., Fabianowska-Majewska, K., Mantincic, D., Callet Bauchu, E., Tigaud, I., Gandhi, V., Lepoivre, M., Peters, G.J., Rolland, M.O., Wyczechowska, D*., et al.* (1999). Common resistance mechanisms to deoxynucleoside analogues in variants of the human erythroleukaemic line K562. *British Journal of Haematology* **1** (*106)*, 78-85.

Dybro, A.M., Damkier, P., Rasmussen, T.B., and Hellfritzsch, M. (2016). Statin-associated rhabdomyolysis triggered by drug-drug interaction with itraconazole. *British Medical Journal case reports* **1** (*2016)*, 1-3.

Edlind, T.D., and Katiyar, S.K. (2010). Mutational analysis of flucytosine resistance in *Candida glabrata*. *Antimicrobial agents and chemotherapy* **11** (*54)*, 4733-4738.

Engels, B., Heinig, U., Grothe, T., Stadler, M., and Jennewein, S. (2011). Cloning and characterization of an *Armillaria gallica* cDNA encoding protoilludene synthase, which catalyzes the first committed step in the synthesis of antimicrobial melleolides. *J Biol Chem* **9** (*286)*, 6871-6878.

Feng, L.J., Wan, Z., Wang, X.H., Li, R.Y., and Liu, W. (2010). Relationship between antifungal resistance of fluconazole resistant *Candida albicans* and mutations in *ERG11* gene. *Chin Med J (Engl)* **5** (*123)*, 544-548.

Ferguson, B.A., Dreisbach, T.A., Parks, C.G., Filip, G.M., and Schmitt, C.L. (2003). Coarse-scale population structure of pathogenic *Armillaria* species in a mixed-conifer forest in the Blue Mountains of northeast Oregon. *Canadian Journal of Forest Research* **4** (*33)*, 612-623.

Finkelstein, H. (1910). Darstellung organischer Jodide aus den entsprechenden Bromiden und Chloriden. *Berichte der deutschen chemischen Gesellschaft* **2** (*43)*, 1528-1532.

Firn, R.D., and Jones, C.G. (2003). Natural products-a simple model to explain chemical diversity. *Natural Product Reports* **4** (*20)*, 382-391.

Firn, R.D., and Jones, C.G. (2009). A Darwinian view of metabolism: molecular properties determine fitness. *Journal of Experimental Botany* **3** (*60)*, 719-726.

Gauwerky, K., Borelli, C., and Korting, H.C. (2009). Targeting virulence: A new paradigm for antifungals. *Drug Discovery Today* **3** (*14)*, 214-222.

Geissel, B., Loiko, V., Klugherz, I., Zhu, Z., Wagener, N., Kurzai, O., van den Hondel, C., and Wagener, J. (2018). Azole-induced cell wall carbohydrate patches kill *Aspergillus fumigatus*. *Nature Communications* **1** (*9)*, 3098.

Georgopapadakou, N.H. (2001). Update on antifungals targeted to the cell wall: focus on β-1,3-glucan synthase inhibitors. *Expert Opinion on Investigational Drugs* **2** (*10)*, 269-280.

Gershenzon, J., and Dudareva, N. (2007). The function of terpene natural products in the natural world. *Nature chemical biology*(*3)*, 408.

Giaccone, G., and Pinedo, H.M. (1996). Drug Resistance. *The Oncologist* **1** (*1)*, 82-87.

Gressler, M., Hortschansky, P., Geib, E., and Brock, M. (2015). A new high-performance heterologous fungal expression system based on regulatory elements from the *Aspergillus terreus* terrein gene cluster. *Frontiers in Microbiology*(*6)*, 184.

Guo, Z. (2017). The modification of natural products for medical use. *Acta Pharmaceutica Sinica B* **2** (*7)*, 119-136.

Hamedi, J., Khodagholi, F., and Hassani-Nasab, A. (2005). Increased erythromycin production by alginate as a medium ingredient or immobilization support in cultures of *Saccharopolyspora erythraea*. *Biotechnology Letters* **9** (*27)*, 661-664.

Hamilton-Miller, J.M.T. (1974). Fungal sterols and the mode of action of the polyene antibiotics. *Advances in Applied Microbiology* **1** (*17)*, 109-134.

Hanson, J.R. (2008). The chemistry of fungi (Cambridge: Royal Society of Chemistry Publishing).

Hauser, D., and Sigg, H.P. (1971). Isolierung und Abbau von Sordarin. 1. Mitteilung über Sordarin. *Helvetica Chimica Acta* **4** (*54)*, 1178-1190.

Hawksworth, D.L. (2001). The magnitude of fungal diversity: the 1.5 million species estimate revisited. *Mycological Research* **12** (*105)*, 1422-1432.

Heathcock, C.H., Hadley, C.R., Rosen, T., Theisen, P.D., and Hecker, S.J. (1987). Total synthesis and biological evaluation of structural analogues of compactin and dihydromevinolin. *Journal of Medicinal Chemistry* **10** (*30)*, 1858-1873.

Heijden, R.v.d., Jacobs, D.I., Snoeijer, W., Hallard, D., and Verpoorte, R. (2004). The *Catharanthus* alkaloids: pharmacognosy and biotechnology. *Curr Med Chem* **5** (*11)*, 607-628.

Heo, J.C., Woo, S.U., Son, M., Park, J.Y., Choi, W.S., Chang, K.T., Kim, S.U., Yoon, E.K., Kim, Y.H., Shin, H.M.*, et al.* (2007). Anti-tumor activity of *Gastrodia elata* Blume is closely associated with a GTP-Ras-dependent pathway. *Oncol Rep* **4** (*18)*, 849-853.

Herath, H.M.T.B., Jacob, M., Wilson, A.D., Abbas, H.K., and Nanayakkara, N.P.D. (2013). New secondary metabolites from bioactive extracts of the fungus *Armillaria tabescens*. *Natural product research* **17** (*27)*, 1562-1568.

Herreros, E., Martinez, C.M., Almela, M.J., Marriott, M.S., De Las Heras, F.G., and Gargallo-Viola, D. (1998). Sordarins: In vitro activities of new antifungal derivatives against pathogenic yeasts, *Pneumocystis carinii*, and Filamentous Fungi. *Antimicrobial agents and chemotherapy* **11** (*42)*, 2863-2869.

Hertweck, C. (2009). The biosynthetic logic of polyketide diversity. *Angewandte Chemie International Edition* **26** (*48)*, 4688-4716.

Hertweck, C., Luzhetskyy, A., Rebets, Y., and Bechthold, A. (2007). Type II polyketide synthases: gaining a deeper insight into enzymatic teamwork. *Natural Product Reports* **1** (*24)*, 162-190.

Hintikka, V. (1973). A note on the polarity of *Armillariella mellea*. *Karstenia* **13** (*1)*, 32-39.

Hirama, M., and Iwashita, M. (1983). Total synthesis of (+)-monacolin K (mevinolin). *Tetrahedron Letters* **17** (*24)*, 1811-1812.

Hofmann, B., Rödl, C.B., Kahnt, A.S., Maier, T.J., Michel, A.A., Hoffmann, M., Rau, O., Awwad, K., Pellowska, M., Wurglics, M.*, et al.* (2012). Molecular pharmacological profile of a novel thiazolinone-based direct and selective 5-lipoxygenase inhibitor. *British Journal of Pharmacology* **7** (*165)*, 2304-2313.

Holton, R.A., Somoza, C., Kim, H.-B., Liang, F., Biediger, R.J., Boatman, P.D., Shindo, M., Smith, C.C., Kim, S., Nadizadeh, H.*, et al.* (1994). The total synthesis of paclitaxel starting with camphor. In Taxane Anticancer Agents (Washington D. C.: American Chemical Society), pp. 288-301.

Holz, R.W. (1974). The effects of the polyene antibiotics nystatin and amphotericin B on thin lipid membranes. *Ann N Y Acad Sci* **0** (*235)*, 469-479.

Hood, I.A. (1991). *Armillaria* in planted hosts. In *Armillaria* root Disease, C.G. Shaw, and G.A. Kile, eds. (Washington D. C.: United States Department of Agriculture), pp. 122-154.

Hovey, M.T., Cohen, D.T., Walden, D.M., Cheong, P.H., and Scheidt, K.A. (2017). A carbene catalysis strategy for the synthesis of protoilludane natural products. *Angewandte Chemie International Edition* **33** (*56)*, 9864-9867.

Hüttel, W. (2017). Structural diversity in echinocandin biosynthesis: the impact of oxidation steps and approaches toward an evolutionary explanation. *Zeitschrift für Naturforschung* **1-2** (*72)*, 1-20.

Hüttel, W., Youssar, L., Grüning, B.A., Günther, S., and Hugentobler, K.G. (2016). Echinocandin B biosynthesis: a biosynthetic cluster from *Aspergillus nidulans* NRRL 8112 and reassembly of the subclusters *Ecd* and *Hty* from *Aspergillus pachycristatus* NRRL 11440 reveals a single coherent gene cluster. *BMC genomics* **17** (*0)*, 570-570.

Jammi, S., Mouysset, D., Siri, D., Bertrand, M.P., and Feray, L. (2013). Theoretical support for the involvement of a radical pathway in the formation of allenylzincs from propargyl iodides and dialkylzincs: influence of zinc coordination. *Journal of Organic Chemistry* **4** (*78)*, 1589-1603.

Jolit, A., Dickinson, C.F., Kitamura, K., Walleser, P.M., Yap, G.P.A., and Tius, M.A. (2017). Catalytic enantioselective nazarov cyclization. *European Journal of Organic Chemistry* **40** (*2017)*, 6067-6076.

Justice, M.C., Hsu, M.-J., Tse, B., Ku, T., Balkovec, J., Schmatz, D., and Nielsen, J. (1998). Elongation factor 2 as a novel target for selective inhibition of fungal protein synthesis. *Journal of Biological Chemistry* **6** (*273)*, 3148-3151.

Kitahata, S., Yakushiji, F., and Ichikawa, S. (2017). Impact of the structures of macrocyclic Michael acceptors on covalent proteasome inhibition. *Chemical science* **10** (*8)*, 6959-6963.

König, S., Romp, E., Krauth, V., Ruhl, M., Dörfer, M., Liening, S., Hofmann, B., Hafner, A.-K., Steinhilber, D., Karas, M.*, et al.* (2018). Melleolides from honey mushroom inhibit 5-Lipoxygenase via Cys159. *Cell chemical biology* **26** (*1)*, 60-70.

Korhonen, K. (1978). Infertility and clonal size in the *Armillariella mellea* complex. *Karstenia* **2** (*18)*, 31-42.

Korhonen, K., and Hintikka, V. (1974). Cytological evidence for somatic diploidization in dikaryotic cells of *Armillariella mellea*. *Archives of Microbiology* **1** (*95)*, 187.

Kotler-Brajtburg, J., Price, H.D., Medoff, G., Schlessinger, D., and Kobayashi, G.S. (1974). Molecular basis for the selective toxicity of amphotericin B for yeast and filipin for animal cells. *Antimicrobial agents and chemotherapy* **4** (*5)*, 377-382.

Kotlobay, A.A., Sarkisyan, K.S., Mokrushina, Y.A., Marcet-Houben, M., Serebrovskaya, E.O., Markina, N.M., Gonzalez Somermeyer, L., Gorokhovatsky, A.Y., Vvedensky, A., Purtov, K.V.*, et al.* (2018). Genetically encodable bioluminescent system from fungi. *Proceedings of the National Academy of Sciences* **50** (*115)*, 12728.

Kretschmer, S.B.M., Woltersdorf, S., Vogt, D., Lillich, F.F., Rühl, M., Karas, M., Maucher, I.V., Roos, J., Häfner, A.-K., Kaiser, A.*, et al.* (2017). Characterization of the molecular mechanism of 5-lipoxygenase inhibition by 2-aminothiazoles. *Biochemical Pharmacology*(*123)*, 52-62.

Kubo, I., Fujita, K.i., and Lee, S.H. (2001). Antifungal mechanism of polygodial. *Journal of Agricultural and Food Chemistry* **3** (*49)*, 1607-1611.

Kudo, F., Matsuura, Y., Hayashi, T., Fukushima, M., and Eguchi, T. (2016). Genome mining of the sordarin biosynthetic gene cluster from *Sordaria araneosa* Cain ATCC 36386: characterization of cycloaraneosene synthase and GDP-6-deoxyaltrose transferase. *J Antibiot (Tokyo)* **1** (*69)*, 541.

Kuehne, M.E., Matson, P.A., and Bornmann, W.G. (1991). Enantioselective syntheses of vinblastine, leurosidine, vincovaline and 20'-epi-vincovaline. *The Journal of Organic Chemistry* **2** (*56)*, 513-528.

Lackner, G., Bohnert, M., Wick, J., and Hoffmeister, D. (2013). Assembly of melleolide antibiotics involves a polyketide synthase with cross-coupling activity. *Chemistry and Biology* **9** (*20)*, 1101-1106.

Lackner, G., Misiek, M., Braesel, J., and Hoffmeister, D. (2012). Genome mining reveals the evolutionary origin and biosynthetic potential of basidiomycete polyketide synthases. *Fungal Genetics and Biology* **12** (*49)*, 996-1003.

Lambert, R.A. (1913). Comparative studies upon cancer cells and normal cells: II. The Character of growth in vitro with special reference to cell division. *The Journal of experimental medicine* **5** (*17)*, 499-510.

Lamour, A., Termorshuizen, A.J., Volker, D., and Jeger, M.J. (2007). Network formation by rhizomorphs of *Armillaria lutea* in natural soil: their description and ecological significance. *FEMS Microbiology Ecology* **2** (*62)*, 222-232.

Laniado-Laborin, R., and Cabrales-Vargas, M.N. (2009). Amphotericin B: side effects and toxicity. *Rev Iberoam Micol* **4** (*26)*, 223-227.

Lee, S.H., Lee, J.R., Lunde, C.S., and Kubo, I. (1999). *In vitro* antifungal susceptibilities of *Candida albicans* and other fungal pathogens to polygodial, a sesquiterpene dialdehyde. *Planta Medica* **03** (*65)*, 204-208.

Li, Z., Wang, Y., Jiang, B., Li, W., Zheng, L., Yang, X., Bao, Y., Sun, L., Huang, Y., and Li, Y. (2016). Structure, cytotoxic activity and mechanism of protoilludane sesquiterpene aryl esters from the mycelium of *Armillaria mellea*. *Journal of Ethnopharmacology* **1** (*184)*, 119-127.

Liang, H. (2008). Sordarin, an antifungal agent with a unique mode of action. *Beilstein journal of organic chemistry* **31** (*4)*, 1-14.

Liebler, D.C. (2008). Protein damage by reactive electrophiles: targets and consequences. *Chemical research in toxicology* **1** (*21)*, 117-128.

Lingam, V.S.P.R., Vinodkumar, R., Mukkanti, K., Thomas, A., and Gopalan, B. (2008). A simple approach to highly functionalized benzo[b]furans from phenols and aryl iodides via aryl propargyl ethers. *Tetrahedron Letters* **27** (*49)*, 4260-4264.

Liu, R., Luo, F., Liu, X., Wang, L., Yang, J., Deng, Y., Huang, E., Qian, J., Lu, Z., Jiang, X.*, et al.* (2016). Biological response modifier in cancer immunotherapy. In Progress in Cancer Immunotherapy, S. Zhang, ed. (Dordrecht: Springer Netherlands), pp. 69-138.

Lomenick, B., Hao, R., Jonai, N., Chin, R.M., Aghajan, M., Warburton, S., Wang, J., Wu, R.P., Gomez, F., Loo, J.A.*, et al.* (2009). Target identification using drug affinity responsive target stability (DARTS). *Proceedings of the National Academy of Sciences* **51** (*106)*, 21984-21989.

Lomenick, B., Jung, G., Wohlschlegel, J.A., and Huang, J. (2011a). Target identification using drug affinity responsive target stability (DARTS). *Current protocols in chemical biology* **4** (*3)*, 163-180.

Lomenick, B., Olsen, R.W., and Huang, J. (2011b). Identification of direct protein targets of small molecules. *ACS Chemical Biology* **1** (*6)*, 34-46.

Malyszko, J., Kozlowska, K., Kozlowski, L., and Malyszko, J. (2017). Nephrotoxicity of anticancer treatment. *Nephrology Dialysis Transplantation* **6** (*32)*, 924-936.

Mansoori, B., Mohammadi, A., Davudian, S., Shirjang, S., and Baradaran, B. (2017). The different mechanisms of cancer drug resistance: a brief review. *Advanced Pharmeutical Bulletin* **3** (*7)*, 339-348.

Marahiel, M.A. (2016). A structural model for multimodular NRPS assembly lines. *Natural Product Reports* **2** (*33)*, 136-140.

Marahiel, M.A., Stachelhaus, T., and Mootz, H.D. (1997). Modular peptide synthetases involved in nonribosomal peptide synthesis. *Chemical Reviews* **7** (*97)*, 2651-2674.

Martin, S.M., and Bushell, M.E. (1996). Effect of hyphal micromorphology on bioreactor performance of antibiotic-producing *Saccharopolyspora erythraea* cultures. *Microbiology* **7** (*142)*, 1783-1788.

Mast, N., Zheng, W., Stout, C.D., and Pikuleva, I.A. (2013). Antifungal azoles: structural insights into undesired tight binding to cholesterol-metabolizing CYP46A1. *Molecular Pharmacology* **1** (*84)*, 86-94.

Maucher, I.V., Rühl, M., Kretschmer, S.B.M., Hofmann, B., Kühn, B., Fettel, J., Vogel, A., Flügel, K.T., Manolikakes, G., Hellmuth, N.*, et al.* (2017). Michael acceptor containing drugs are a novel class of 5-lipoxygenase inhibitor targeting the surface cysteines C416 and C418. *Biochemical Pharmacology* **1** (*125)*, 55-74.

McFedries, A., Schwaid, A., and Saghatelian, A. (2013). Methods for the elucidation of protein-small molecule interactions. *Chemistry and Biology* **5** (*20)*, 667-673.

Mendes, G.L., Santos, A.R.S., Malheiros, A., Filho, V.C., Yunes, R.A., and Calixto, J.B. (2000). Assessment of mechanisms involved in antinociception caused by sesquiterpene polygodial. *Journal of Pharmacology and Experimental Therapeutics* **1** (*292)*, 164.

Meyers, M.A. (2007). *Veni, Vidi, Vinca*: The healing power of periwinkle. In Happy accidents-Serendipity in modern medical breakthroughs, M.A. Meyers, ed. (New York: Arcade Publishing), pp. 131-134.

Misiek, M., and Hoffmeister, D. (2012). Sesquiterpene aryl ester natural products in North *American Armillaria* species. *Mycological Progress* **1** (*11)*, 7-15.

Misiek, M., Williams, J., Schmich, K., Hüttel, W., Merfort, I., Salomon, C.E., Aldrich, C.C., and Hoffmeister, D. (2009). Structure and cytotoxicity of arnamial and related fungal sesquiterpene aryl esters. *Journal of Natural Products* **10** (*72)*, 1888-1891.

Mogil'naya, O.A., Ronzhin, N.O., Medvedeva, S.E., and Bondar', V.S. (2015). Total peroxidase and catalase activity of luminous basidiomycetes *Armillaria borealis* and *Neonothopanus nambi* in comparison with the level of light emission. *Applied Biochemistry and Microbiology* **4** (*51)*, 419-424.

Mosow, J.A. (1998). Methotrexate transport and resistance. *Leukemia and Lymphoma* **3-4** (*30)*, 215-224.

Musiol, R., and Kowalczyk, W. (2012). Azole antimycotics - A highway to new drugs or a dead end? *Curr Med Chem* **9** (*19)*, 1378-1388.

Mutschler, E. (2013). Mutschler Arzneimittelwirkungen : Lehrbuch der Pharmakologie, der klinischen Pharmakologie und Toxikologie, 10., vollständig überarbeitete und erweiterte Auflage edn (Stuttgart: WVG, Wissenschaftliche Verlagsgesellschaft).

Myrick, D., Blackinton, D., Klostergaard, J., Kouttab, N., Maizel, A., Wanebo, H., and Mehta, S. (1999). Paclitaxel-induced apoptosis in Jurkat, a leukemic T cell line, is enhanced by ceramide. *Leukemia Research* **6** (*23)*, 569-578.

Neises, B., and Steglich, W. (1978). Einfaches Verfahren zur Veresterung von Carbonsäuren. *Angewandte Chemie* **7** (*90)*, 556-557.

Nicolaou, K.C., and Guy, R.K. (1994). The total synthesis of paclitaxel by assembly of the ring system. In Taxane anticancer agents (Washington D. C.: American Chemical Society), pp. 302-312.

Odds, F.C. (2001). Sordarin antifungal agents. *Expert Opinion on Therapeutic Patents* **2** (*11)*, 283-294.

Oduro, K.A., Munnecke, D.E., Sims, J.J., and Keen, N.T. (1976). Isolation of antibiotics produced in culture by A mellea. *Trans Brit Mycol Soc* **2** (*66)*, 195-199.

Ohr, H.D., and Munnecke, D.E. (1974). Effects of methyl bromide on antibiotic production by *Armillaria mellea*. *Transactions of the British Mycological Society* **1** (*62)*, 65-73.

Ohr, H.D., Munnecke, D.E., and Bricker, J.L. (1973). The interaction of *Armillaria mellea* and *Trichoderma spp*. as modified by methyl bromide. *Phytopathlogy* **8** (*63)*, 965-973.

Oppolzer, W., and Nakao, A. (1986). Synthesis of (±)-6-protoilludene and (±)-3-EPI-6-protoilludene by intramolecular magnesium-ene- and ketene/alkene addition reactions. *Tetrahedron Letters* **45** (*27)*, 5471-5474.

Ostrowski, K., and Barnard, E.A. (1961). Application of isotopically-labelled specific inhibitors as a method in enzyme cytochemistry. *Experimental Cell Research* **2** (*25)*, 465-468.

Pan, S.-T., Li, Z.-L., He, Z.-X., Qiu, J.-X., and Zhou, S.-F. (2016). Molecular mechanisms for tumour resistance to chemotherapy. *Clinical and Experimental Pharmacology and Physiology* **8** (*43)*, 723-737.

Parrot, D., Peresse, T., Hitti, E., Carrie, D., Grube, M., and Tomasi, S. (2015). Qualitative and spatial metabolite profiling of lichens by a LC–MS approach combined with optimised extraction. *Phytochemical Analysis* **1** (*26)*, 23-33.

Peipp, H., and Sonnenbichler, J. (1992). Secondary fungal metabolites and their biological activities, II. Occurrence of antibiotic compounds in cultures of *Armillaria ostoyae* growing in the presence of an antagonistic fungus or host plant cells. *Biol Chem Hoppe Seyler* **8** (*373)*, 675-683.

Perea, S., López-Ribot, J.L., Kirkpatrick, W.R., McAtee, R.K., Santillán, R.A., Martínez, M., Calabrese, D., Sanglard, D., and Patterson, T.F. (2001). Prevalence of molecular mechanisms of resistance to azole antifungal agents in *Candida albicans* strains displaying high-level fluconazole resistance isolated from human immunodeficiency virus-infected patients. *Antimicrobial agents and chemotherapy* **10** (*45)*, 2676-2684.

Pérez-Sánchez, A., Uribe-Carvajal, S., Cabrera-Orefice, A., and Barrios-González, J. (2017). Key role of alternative oxidase in lovastatin solid-state fermentation. *Applied Microbiology and Biotechnology* **19** (*101)*, 7347-7356.

Petercord, R., Leonhard, S., Muck, M., Lemme, H., Lobinger, G., Immler, T., and Konnert, M. (2009). Klimaänderung und Forstschädlinge. *LWF aktuell* **1** (*72)*, 4-7.

Peters, G.J. (2014). Novel developments in the use of antimetabolites. *Nucleosides, Nucleotides and Nucleic Acids* **4-6** (*33)*, 358-374.

Petranyi, G., Ryder, N., and Stutz, A. (1984). Allylamine derivatives: new class of synthetic antifungal agents inhibiting fungal squalene epoxidase. *Science* **4654** (*224)*, 1239-1241.

Pierson, A.S., Gibbs, P., Richards, J., Russ, P., Eckhardt, S.G., and Gonzalez, R. (2002). A Phase II Study of Irofulven (MGI 114) in Patients with Stage IV Melanoma. *Investigational New Drugs* **3** (*20)*, 357-362.

Purtov, K.V., Petushkov, V.N., Baranov, M.S., Mineev, K.S., Rodionova, N.S., Kaskova, Z.M., Tsarkova, A.S., Petunin, A.I., Bondar, V.S., Rodicheva, E.K.*, et al.* (2015). The chemical basis of fungal bioluminescence. *Angewandte Chemie International Edition* **28** (*54)*, 8124-8128.

Purtov, K.V., Petushkov, V.N., Rodionova, N.S., and Gitelson, J.I. (2017). Why does the bioluminescent fungus *Armillaria mellea* have luminous mycelium but nonluminous fruiting body? *Biochemistry, Biophysics, and Molecular Biology* **1** (*474)*, 217-219.

Purushothaman, S., Prasanna, R., and Raghunathan, R. (2013). Regioselective synthesis of spiropyrrolidine/spiropyrrolizidine/spirothiazolidine-grafted macrocycles through 1,3-dipolar cycloaddition methodology. *Tetrahedron* **46** (*69)*, 9742-9750.

Puyo, S., Montaudon, D., and Pourquier, P. (2014). From old alkylating agents to new minor groove binders. *Critical Reviews in Oncology/Hematology* **1** (*89)*, 43-61.

Raabe, R. (1962). Host list of the root rot fungus, *Armillaria mellea*. *Hilgardia* **2** (*33)*, 25 - 88.

Rathinasamy, K., Jindal, B., Asthana, J., Singh, P., Balaji, P.V., and Panda, D. (2010). Griseofulvin stabilizes microtubule dynamics, activates p53 and inhibits the proliferation of MCF-7 cells synergistically with vinblastine. *BMC Cancer* **1** (*10)*, 213.

Ray, L., and Moore, B.S. (2016). Recent advances in the biosynthesis of unusual polyketide synthase substrates. *Natural Product Reports* **2** (*33)*, 150-161.

Ribera, J., Panzarasa, G., Stobbe, A., Osypova, A., Rupper, P., Klose, D., and Schwarze, F.W.M.R. (2019). Scalable biosynthesis of melanin by the basidiomycete *Armillaria cepistipes*. *Journal of Agricultural and Food Chemistry* **1** (*67)*, 132-139.

Riemsma, R., Forbes, C.A., Kessels, A., Lykopoulos, K., Amonkar, M.M., Rea, D.W., and Kleijnen, J. (2010). Systematic review of aromatase inhibitors in the first-line treatment for hormone sensitive advanced or metastatic breast cancer. *Breast Cancer Research and Treatment* **1** (*123)*, 9-24.

Rossi, A., Pergola, C., Koeberle, A., Hoffmann, M., Dehm, F., Bramanti, P., Cuzzocrea, S., Werz, O., and Sautebin, L. (2010). The 5-lipoxygenase inhibitor, zileuton, suppresses prostaglandin biosynthesis by inhibition of arachidonic acid release in macrophages. *British Journal of Pharmacology* **3** (*161)*, 555-570.

Rostovtsev, V.V., Green, L.G., Fokin, V.V., and Sharpless, K.B. (2002). A stepwise huisgen cycloaddition process: copper(I)-catalyzed regioselective "ligation" of azides and terminal alkynes. *Angewandte Chemie International Edition* **14** (*41)*, 2596-2599.

Sanglard, D. (2003). Resistance and tolerance mechanisms to antifungal drugs in fungal pathogens. *Mycologist* **2** (*17)*, 74-78.

Sanglard, D. (2016). Emerging threats in antifungal-resistant fungal pathogens. *Frontiers in Medicine* **11** (*3)*, 1-10.

Sanglard, D., Ischer, F., Calabrese, D., Micheli, M.d., and Bille, J. (1998). Multiple resistance mechanisms to azole antifungals in yeast clinical isolates. *Drug Resistance Updates* **4** (*1)*, 255-265.

Schäfer, B. (2010). Statine. Cholesterolsenker. *Chemie in unserer Zeit* **5** (*44)*, 344-364.

Schiff, P.B., Fant, J., and Horwitz, S.B. (1979). Promotion of microtubule assembly *in vitro* by taxol. *Nature* **5698** (*277)*, 665-667.

Schmidt-Dannert, C. (2015). Biosynthesis of terpenoid natural products in fungi. In Biotechnology of Isoprenoids, J. Schrader, and J. Bohlmann, eds. (Cham: Springer International Publishing), pp. 19-61.

Schmitt, C.L., and Tatum, M.L. (2008). The Malheur National Forest - Location of the world's largest living organism [The Humongous Fungus] U.S.D.o. Agriculture. 1-8

Schnabel, G., Rollins, A.P., and Henderson, G.W. (2011). Field evaluation of *Trichoderma spp.* for control of *Armillaria* root rot of peach. *Plant Health Progress* **1** (*12)*, 3.

Schroeckh, V., Scherlach, K., Nützmann, H.-W., Shelest, E., Schmidt-Heck, W., Schuemann, J., Martin, K., Hertweck, C., and Brakhage, A.A. (2009). Intimate bacterial–fungal interaction triggers biosynthesis of archetypal polyketides in *Aspergillus nidulans*. *Proceedings of the National Academy of Sciences* **34** (*106)*, 14558-14563.

Schwöbel, J.A.H., Wondrousch, D., Koleva, Y.K., Madden, J.C., Cronin, M.T.D., and Schüürmann, G. (2010). Prediction of Michael-type acceptor reactivity toward glutathione. *Chemical research in toxicology* **10** (*23)*, 1576-1585.

Sharom, F.J. (2007). ABC multidrug transporters: structure, function and role in chemoresistance. *Pharmacogenomics* **1** (*9)*, 105-127.

Shaw, C.G., and Kile, G.A. (1991). *Armillaria* root disease (Washington, D.C.: Forest Service, U.S. Dept. of Agriculture).

Sherman, C.A., Herndon, J.E., Watson, D.M., and Green, M.R. (2004). A phase II trial of 6-hydroxymethylacylfulvene (MGI-114, irofulven) in patients with relapsed or refractory non-small cell lung cancer. *Lung Cancer* **3** (*45)*, 387-392.

Siddik, Z.H. (1986). Minimising the organ toxic effects of chemotherapy. *European Journal of Cancer and Clinical Oncology* **8** (*22)*, 905-907.

Sinha, S., Doble, M., and Manju, S.L. (2019). 5-Lipoxygenase as a drug target: A review on trends in inhibitors structural design, SAR and mechanism based approach. *Bioorganic and Medicinal Chemistry* **17** (*27)*, 3745-3759.

Smith, E.F. (1894). Field notes, 1892. *The Journal of Mycology* **4** (*7)*, 373-377.

Søe, R., Mosley, R.T., Justice, M., Nielsen-Kahn, J., Shastry, M., Merrill, A.R., and Andersen, G.R. (2007). Sordarin derivatives induce a novel conformation of the yeast ribosome translocation factor eEF2. *Journal of Biological Chemistry* **1** (*282)*, 657-666.

Speers, A.E., Adam, G.C., and Cravatt, B.F. (2003). Activity-based protein profiling *in vivo* using a copper(I)-catalyzed azide-alkyne [3 + 2] cycloaddition. *Journal of the American Chemical Society* **16** (*125)*, 4686-4687.

Staunton, J., and Weissman, K.J. (2001). Polyketide biosynthesis: a millennium review. *Natural Product Reports* **4** (*18)*, 380-416.

Sturtevant, J. (2002). Translation elongation-3-like factors: are they rational antifungal targets? *Expert Opinion on Therapeutic Targets* **5** (*6)*, 545-553.

Sucher, A.J., Chahine, E.B., and Balcer, H.E. (2009). Echinocandins: the newest class of antifungals. *Ann Pharmacother* **10** (*43)*, 1647-1657.

Taniguchi, M., Yano, Y., Tada, E., Ikenishi, K., Oi, S., Haraguchi, H., Hashimoto, K., and Kubo, I. (1988). Mode of action of polygodial, an antifungal sesquiterpene dialdehyde. *Agricultural and Biological Chemistry* **6** (*52)*, 1409-1414.

Tarus, P.K., Lang'at-Thoruwa, C.C., Wanyonyi, A.W., and Chhabra, S.C. (2003). Bioactive metabolites from *Trichoderma harzianum* and *Trichoderma longibrachiatum*. *Bulletin of the Chemical Society of Ethiopia* **2** (*17)*, 185-190.

Torgovnick, A., Heger, J.M., Liaki, V., Isensee, J., Schmitt, A., Knittel, G., Riabinska, A., Beleggia, F., Laurien, L., Leeser, U.*, et al.* (2018). The Cdkn1a^{SUPER} mouse as a tool to study p53-mediated tumor suppression. *Cell Reports* **4** (*25)*, 1027-1039.e1026.

Vendrik, C.P.J., Bergers, J.J., De Jong, W.H., and Steerenberg, P.A. (1992). Resistance to cytostatic drugs at the cellular level. *Cancer Chemotherapy and Pharmacology* **6** (*29)*, 413-429.

Vermes, A., Guchelaar, H.-J., and Dankert, J. (2000). Flucytosine: a review of its pharmacology, clinical indications, pharmacokinetics, toxicity and drug interactions. *Journal of Antimicrobial Chemotherapy* **2** (*46)*, 171-179.

Vicente, M.F., Basilio, A., Cabello, A., and Peláez, F. (2003). Microbial natural products as a source of antifungals. *Clinical Microbiology and Infection* **1** (*9)*, 15-32.

Wani, M.C., Taylor, H.L., Wall, M.E., Coggon, P., and McPhail, A.T. (1971). Plant antitumor agents. VI. The isolation and structure of taxol, a novel antileukemic and antitumor agent from *Taxus brevifolia*. *Journal of the American Chemical Society* **9** (*93)*, 2325-2327.

Wick, J., Heine, D., Lackner, G., Misiek, M., Tauber, J., Jagusch, H., Hertweck, C., and Hoffmeister, D. (2016). A fivefold parallelized biosynthetic process secures chlorination of *Armillaria mellea* (honey mushroom) toxins. *Applied and Environmental Microbiology* **4** (*82)*, 1196-1204.

Wilhelm, I., Molnár, J., Fazakas, C., Haskó, J., and Krizbai, I.A. (2013). Role of the blood-brain barrier in the formation of brain metastases. *International journal of molecular sciences* **1** (*14)*, 1383-1411.

Williams, R.E.S., C. G., and Wargo, P.M.S., W. H. (1989). *Armillaria* root disease. *Forest Insect & Disease Leaflet* **1** (*78)*, 1-8.

Wilson, L., Creswell, K.M., and Chin, D. (1975). Mechanism of action of vinblastine. Binding of [acetyl-3H]-vinblastine to embryonic chick brain tubulin and tubulin from sea urchin sperm tail outer doublet microtubules. *Biochemistry* **26** (*14)*, 5586-5592.

Wondrousch, D., Böhme, A., Thaens, D., Ost, N., and Schüürmann, G. (2010). Local electrophilicity predicts the toxicity-relevant reactivity of Michael acceptors. *The Journal of Physical Chemistry Letters* **10** (*1)*, 1605-1610.

Woodward, R.B., Logusch, E., Nambiar, K.P., Sakan, K., Ward, D.E., Au-Yeung, B.W., Balaram, P., Browne, L.J., Card, P.J., and Chen, C.H. (1981). Asymmetric total synthesis of erythromcin. 1. Synthesis of an erythronolide A secoacid derivative via asymmetric induction. *Journal of the American Chemical Society* **11** (*103)*, 3210-3213.

Wu, P., Feldman, A.K., Nugent, A.K., Hawker, C.J., Scheel, A., Voit, B., Pyun, J., Fréchet, J.M.J., Sharpless, K.B., and Fokin, V.V. (2004). Efficiency and fidelity in a click-chemistry route to triazole dendrimers by the copper(I)-catalyzed ligation of azides and alkynes. *Angewandte Chemie International Edition* **30** (*43)*, 3928-3932.

Xiao, H., and Zhong, J.-J. (2016). Production of useful terpenoids by higher-fungus cell factory and synthetic biology approaches. *Trends in Biotechnology* **3** (*34)*, 242-255.

Xu, X., Qiu, G., Ji, L., Ma, R., Dang, Z., Jia, R., and Zhao, B. (2019). Research and development of anticancer agents under the guidance of biomarkers. *Cancer Translational Medicine* **1** (*5)*, 17-21.

Zhang, T., Du, Y., Liu, X., Sun, X., Cai, E., Zhu, H., and Zhao, Y. (2019). Study on antidepressant-like effect of protoilludane sesquiterpenoid aromatic esters from *Armillaria Mellea*. *Natural product research*1-4.

Zhu, J., Wang, M., Wen, W., and Yu, R. (2015). Biosynthesis and regulation of terpenoid indole alkaloids in *Catharanthus roseus*. *Pharmacognosy reviews* **17** (*9)*, 24-28.

Zonios, D.I., and Bennett, J.E. (2008). Update on azole antifungals. *Seminars in Respiratory and Critical Care Medicine* **02** (*29)*, 198-210.

10. Anhang

10.1.Eigenständigkeitserklärung

Ich versichere hiermit, die vorliegende Dissertation selbstständig und ohne Benutzung anderer als der angegebenen Quellen und Hilfsmittel angefertigt zu haben.
Die geltende Promotionsordnung der Fakultät für Biowissenschaften der Friedrich-Schiller-Universität Jena ist mir bekannt.
Personen, die mich bei der Auswahl und Auswertung des Materials sowie der Herstellung des Manuskriptes unterstützt haben, sind in der Danksagung der Dissertation oder den entsprechenden Manuskripten genannt.
Die Hilfe eines Promotionsberaters wurde nicht in Anspruch genommen. Niemand hat mittelbar oder unmittelbar geldwerte Leistungen für Arbeiten erhalten, welche im Zusammenhang mit der vorgelegten schriftlichen Abhandlung stehen.
Die Dissertation ist von mir in gleicher oder ähnlicher Form noch bei keiner anderen Hochschule eingereicht worden, auch nicht als Prüfungsarbeit für eine staatliche oder andere wissenschaftliche Prüfung.

Jena, den

_____

Maximilian Dörfer

10.2. Abkürzungsverzeichnis

$[M+H]^+$	positiv geladenes Ion der Masse M + 1
5-LO	5-Lipoxygenase
ACP	Acyl Carrier Protein
AT	Acyltransferase
cDNA	komplementäre DNA ohne Introns (complementary DNA)
DAO	Dihydroarmillylorsellinat
DC	Dünnschichtchromatografie
DH	Dehydratase
DNA	Desoxyribonukleinsäure (desoxyribonucleic acid)
DMAP	4-(Dimethylamino)-pyridin
DMAPP	Dimethylallylpyrophosphat
δ	chemische Verschiebung
E. coli	*Escherichia coli*
ER	Enoylreduktase
FLAP	5-Lipoxygenase aktivierendes Protein (5-lipoxygenase activating protein)
gDNA	genomische DNA (mit Introns)
HPLC	Hochleistungsflüssigchromatografie (high performance liquid chromatography)
IPP	Isopentenylpyrophosphat
J	Kopplungskonstante
KR	Ketoreduktase
KS	Ketoacylsynthase
LNKS	Lovastatin-nonaketid-synthase
MALDI	Matrixunterstützte Laserdesorption/Ionisation (Matrix-assisted laser desorption/ionization)
NMR	Magnetresonanzspektroskopie (Nuclear Magnetic Resonance)
NRPS	nichtribosomale Peptidsynthetase
PAGE	Polyacrylamid-Gelelektrophorese
PBS	Proteinbiosynthese
PCR	Polymerase Kettenreaktion (polymerase chain reaction)
PE	Phosphatidylethanolamin
PKS	Polyketidsynthase
PT	Produkttemplate
RNA	Ribonukleinsäure (ribonucleic acid)
ROS	Reaktive Sauerstoff-Spezies (reactive oxygen species)
SAR	Struktur-Aktivitäts-Beziehungen (structure-activity-relationships)
SDS	Sodiumdodecylsulfate (Natriumlauryl- bzw. –dodecylsulfat)
spp.	mehrere Arten einer Gattung (*species pluralis*)
TCM	Traditionelle Chinesische Medizin
TE	Thioesterase

10.3. Veröffentlichungen

10.3.1. Publikationen

Maximilian Dörfer, Daniel Heine, Stefanie König, Sagar Gore, Oliver Werz, Christian Hertweck, Markus Gressler, Dirk Hoffmeister. (2019) Melleolides impact fungal translation *via* elongation factor 2. Organic & Biomolecular Chemistry, Volume 17 (19), 4906-4916

Stefanie König, Erik Romp, Verena Krauth, Michael Rühl, **Maximilian Dörfer**, Stefanie Liening, Bettina Hofmann, Ann-Kathrin Hafner, Dieter Steinhilber, Michael Karas, Ulrike Garscha, Dirk Hoffmeister, Oliver Werz. (2019) Melleolides from Honey Mushroom Inhibit 5-Lipoxygenase via Cys159. Cell Chemical Biology, Volume 26 (1), 1-11

Maximilian Dörfer, Markus Gressler, Dirk Hoffmeister. (2019) Diversity and bioactivity of *Armillaria* sesquiterpene aryl ester natural products. Mycological Progress, Volume 18 (8), 1027-1037

Elena Geib, Florian Baldeweg, **Maximilian Dörfer**, Markus Nett, Matthias Brock. (2018) Cross-Chemistry Leads to Product Diversity from Atromentin Synthetases in Aspergilli from Section Nigri. Cell Chemical Biology, Volume 26 (2), 223-234

10.3.2. Poster

Dörfer, M., Heine, D., Hertweck, C., Hoffmeister, D. „Synthesis of a probe to identify the cellular target of melleolide antibiotics “, Leibniz Wirkstofftage/Leibniz meeting on bioactive compounds, April 2016, Jena.

Dörfer, M., König, S., Heine, D., Hertweck, C., Werz, O., Hoffmeister, D. „Investigations on the cellular targets of the melleolides “, 30. Irseer Naturstofftage, Februar 2018, Irsee.

10.4. Wissenschaftlicher Werdegang

Dörfer, Maximilian

geboren am 15.09.1989 in Gera

Akademische Ausbildung

12/14 – 03/19 **Promotionsstudium**

Friedrich-Schiller-Universität Jena

Wissenschaftlicher Angestellter in der AG von Herrn Prof. Dr. Dirk Hoffmeister am Lehrstuhl für Pharmazeutische Mikrobiologie in Assoziation mit dem Leibniz-Institut für Naturstoff-Forschung und Infektionsbiologie, Hans-Knöll-Institut

12/2014 **Approbation als Apotheker**

12/2014 **Diplomarbeit (Dipl. Pharm.)**

„Bakterielle Nanocellulose als Wirkstoffträger in zahnmedizinischen Anwendungen“

11/2014 **3. Staatsexamen**

Dritter Abschnitt der Pharmazeutischen Prüfung

02/14 - 12/14 **Diplomstudium**

Diplomarbeit am Lehrstuhl für pharmazeutische Technologie des Instituts für Pharmazie an der Friedrich-Schiller-Universität Jena unter der Leitung von Frau PD Dr. Dana Kralisch

03/2013 **Wahlpflichtfach Arbeit**

Aggregation von Erythrozyten unter Einfluss von Polymerbeschichteten Eisenoxid-Nanopartikeln

10/09 – 05/13 **Studium der Pharmazie**
an der Friedrich-Schiller-Universität Jena, erstes und zweites Staatsexamen

10.5. Danksagung

Am Ende dieser langen Durststrecke, dieser Geduldsprobe aber auch dieser großartigen Herausforderung, liegt es mir sehr am Herzen, mich bei all denen zu bedanken, die zum Gelingen dieser Arbeit beigetragen haben.

Zuerst geht mein Dank an meinen Doktorvater Prof. Dr. Dirk Hoffmeister. Danke für die Möglichkeit, dieses spannende Projekt fortführen zu dürfen. Du hast mir die anfänglichen Bedenken genommen, dass ein Pharmazeut nicht auch gut chemisch arbeiten kann und bald darauf mein Interesse für Pilze auf ein neues Level angehoben. Vielen Dank für die exzellente Betreuung, den regen wissenschaftlichen Austausch und dein Vermögen, dieses komplexe, interdisziplinäre Thema stets aus allen Blickwinkeln zu verstehen oder konstruktiv zu hinterfragen. Deine Tür stand mir immer offen, auch um an schlechteren Tagen wieder neue Motivation zu bekommen

Des Weiteren danke ich Prof. Dr. Oliver Werz, den Mitarbeitern des Lehrstuhles für pharmazeutische Chemie, vor allem Stefanie König für die angenehme Zusammenarbeit und die Einführung in die Welt des Target-Fishings.

Ein großes Dankeschön geht auch an Dr. Markus Greßler, der den Endspurt meiner Arbeit begleitete und mich mit völlig neuem Input in der Molekularbiologie versorgte. Danke auch, dass du in der Schlussphase noch einmal viele neue Ideen beigesteuert, dich am Ende aber auch um die zeitnahe Publikation meiner Ergebnisse mit eingebracht hast. Ohne dich würde ich jetzt noch an einer Monographie schreiben.

Ich danke allen Mitarbeitern der Arbeitsgruppe Biomolekulare Chemie am HKI in Jena unter der Leitung von Prof. Dr. Christian Hertweck. Die Arbeit am HKI, vor allem im ehemaligen Laborhaus 1 fühlte sich stets an, als sei man in der eigenen Arbeitsgruppe. Einen großen Anteil daran hatte Dr. Daniel Heine. Danke für die Betreuung meiner Synthesen und die Versorgung mit chemischem Know-How, aber auch für den Spaß im Labor. Ein weiteres Dankeschön an dieser Stelle auch an Dr. Florian Meyer, Jan Dworschak und Sabrina Boldt.
Vielen Dank Heike Heinecke für das Messen meiner NMR-Proben, aber auch für deine Motivation und für das ein oder andere Frühstück. Vielen Dank Andrea Perner für die Messung der HPLC-MS-Proben.

Ich danke Prof. Dr. Hans Peter Saluz, und Grit Mrotzek die Möglichkeit, in der Gruppe für Zell- und Molekularbiologie in endlosen Versuchen Ribosomen aufreinigen zu können.

Dank geht auch an Dr. Friedemann Gaube für die erneute Einführung ins Pflanzenreich. Unsere Praktika waren jedes Jahr aufs Neue eine Bereicherung für mich, der Plant-Harvesting-Day immer ein Highlight im Kalender.

Außerdem bedanke ich mich natürlich bei den Mitarbeitern der Arbeitsgruppe am Lehrstuhl für pharmazeutische Mikrobiologie. Dank euch war der Laboralltag nur selten grau – auch wenn es mal nicht so lief. Ein ganz besonderer Dank geht hierbei an Philip Brandt, du hast es dir nicht nehmen lassen, mich vom ersten Tag des Studiums bis fast zu meinem letzten an der Uni als Freund zu begleiten. Wir konnten uns gegenseitig immer wieder Mut machen - die Malle-Freitage waren dabei nur das „i“-Tüpfelchen auf dem gemeinsamen Leidensweg. Auch die interdisziplinären Kaffeepausen mit Eileen Brandenburger, Florian Baldeweg und Jakob Wurlitzer waren nicht nur persönlich, sondern auch hinsichtlich des Wissenszuwachses meiner Arbeit eine große Bereicherung. Auf viele Ideen kommt man einfach nicht am Schreibtisch. Danke auch an Tine Steinbach für die super Organisation in der AG und den Durchblick um universitären Bürokratie-Dschungel.
Vielen Dank auch an Sebastian Schober, Johannes Rassbach und Julia Greßler, für die Hilfe bei der Extraktion der Melleolide.

Ich danke all meinen Freunden in Jena und in der Heimat für euer Interesse an meinem Projekt und für den Ausgleich zur häufig doch herausfordernden Arbeit. Danke auch an die Jungs und Mädels vom Schwimmen & Wasserball. Sport war und bleibt immer mein wichtigstes Ventil zum Abschalten und Abreagieren.

Danke für die Unterstützung durch meine Schwiegereltern, Eltern und mein Bruderherz.

Last but not least: Der wohl größte Dank geht an meine Frau Juliane. Nachdem du mein ganzes Studium mit ertragen musstest und dadurch, wie du sagst, selbst zu einem halben Apotheker geworden bist, kam auch noch die Promotion. Du hast mir immer Freiräume erkämpft vor allem in den letzten Zügen meiner Arbeit stets den Rücken freigehalten. Vollzeit arbeiten, unsere kleine Tochter Ida betreuen, ein Haus sanieren und „nebenbei“ noch eine Dissertation schreiben. Ohne dich wäre mir längst die Decke auf den Kopf gefallen.